# Single cell analysis of iNKT cell heterogeneity, phenotype, and function




This thesis is submitted to the University of Dublin for the degree of

Doctor of Philosophy (Ph.D.)

By

Harry Kane

M.Sc.

2022

School of Biochemistry and Immunology

Trinity College Dublin

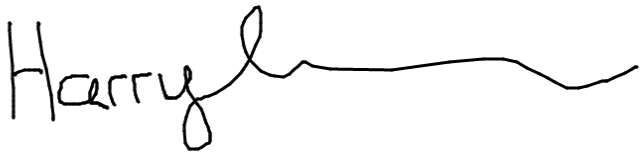
Supervisor: Professor Lydia Lynch

**Declaration**

I declare that this thesis has not been submitted as an exercise for a degree at this or any other university and it is entirely my own work.

I agree to deposit this thesis in the University's open access institutional repository or allow the Library to do so on my behalf, subject to Irish Copyright Legislation and Trinity College Library conditions of use and acknowledgment.

I consent to the examiner retaining a copy of the thesis beyond the examining period, should they so wish (EU GDPR May 2018).



Harry Kane

2022

This Thesis is Open Access

**Summary**

Innate T cells, including CD1d-restricted invariant natural killer T (iNKT) cells, are characterized by their rapid activation in response to non-peptide antigens, such as lipids. While the transcriptional profiles of naive, effector and memory adaptive T cells have been well studied, less is known about transcriptional regulation of different iNKT cell activation states. In this study, using single cell RNA-sequencing, we performed longitudinal analysis of activated iNKT cells and explored iNKT cell heterogeneity, generating a transcriptomic atlas of iNKT cell activation states. We found that transcriptional signatures of activation are highly conserved among heterogeneous iNKT cell populations, including NKT1, NKT2, and NKT17 subsets, and human iNKT cells. Strikingly, we found that regulatory iNKT cells, such as adipose iNKT cells, undergo blunted activation, are heterogeneous, and display enrichment of memory-like cMAF$^{+}$ and KLRG1$^{+}$ iNKT cell populations. Moreover, we identify a conserved cMAF-associated transcriptional network among NKT10 cells, providing novel insights into the biology of regulatory and antigen experienced iNKT cells.

**General Abstract**

Innate T cells, including CD1d-restricted invariant natural killer T (iNKT) cells, are characterized by their rapid activation in response to non-peptide antigens, such as lipids. While the transcriptional profiles of naive, effector and memory adaptive T cells have been well studied, less is known about transcriptional regulation of different iNKT cell activation states. In this study, using single cell RNA-sequencing, we performed longitudinal analysis of activated iNKT cells and explored iNKT cell heterogeneity, generating a transcriptomic atlas of iNKT cell activation states. We found that transcriptional signatures of activation are highly conserved among heterogeneous iNKT cell populations, including NKT1, NKT2, and NKT17 subsets, and human iNKT cells. Strikingly, we found that regulatory iNKT cells, such as adipose iNKT cells, undergo blunted activation, are heterogeneous, and display enrichment of memory-like cMAF$^{+}$ and KLRG1$^{+}$ iNKT cell populations. Moreover, we identify a conserved cMAF-associated transcriptional network among NKT10 cells, providing novel insights into the biology of regulatory and antigen experienced iNKT cells.

**Table of Contents**

Chapter 1: General Introduction.....16
1.1: General introduction to NKT cell biology.....17
1.2 iNKT cell development.....19
1.2.1 Early iNKT cells development and the CD44 NK1.1 model.....19
1.2.2 NKT1, NKT2 and NKT17 cells: a novel model branching model of iNKT cell development from an NKT2-like progenitor state.....21
1.2.3 Factors governing iNKT cell subset development and differentiation .....24
1.3 Steady State iNKT cell biology.....26
1.3.1 NKT1 cells.....26
1.3.2 NKT2 cells.....27
1.3.3 NKT17 cells.....29
1.3.4 iNKT cells in the lung and Peyer's patches.....31
1.3.5 iNKT cells in adipose tissue.....32
1.3.6 Human iNKT cells.....37
1.3.7 Homeostatic functions of iNKT cells.....39
1.4 Activated iNKT cells and the iNKT cell response to antigen.....42
1.4.1 Overview of the adaptive T cell response to antigen and activation .....42
1.4.2 Overview of the iNKT cell response to antigen and activation.....45
1.4.3 Framing iNKT cell activation and responses: Pathogen Immunity..49
1.4.4 Framing iNKT cell activation and responses: Tumor Immunity.....51
1.4.5 Memory-like KLRG1$^{+}$ iNKT cells.....53
1.4.6 Memory-like $NKT_{FH}$ cells.....54
1.4.7 iNKT cell anergy.....56
1.4.8 Regulatory iNKT cells.....59
1.5 iNKT cell immunometabolism.....63
1.5.1 Introduction to T cell metabolism.....63
1.5.2 iNKT cell metabolism during development and differentiation.....64

1.5.3 Activated iNKT cell metabolism.....66
1.6 Hypothesis.....69
1.7 Aims.....70
Chapter 2: Materials and Methods.....71
2.1 List of reagents, materials, instruments and software used.....72
Table 2.1.1 Reagents.....72
Table 2.1.2 Antibodies for flow cytometry.....73
Table 2.1.3 Instruments.....74
Table 2.1.4 scRNA-Seq batch guide.....75
Table 2.1.5 Software used.....75
Table 2.1.6 R package library.....76
Table 2.1.7 Module scores.....92
2.2 Animals.....100
2.3 *In vivo* stimulations.....100
2.4 Tissue processing.....100
2.5 *Ex vivo* stimulations and mitochondrial staining.....101
2.6 Flow cytometry and cell sorting.....101
2.7 scRNA-Seq sequencing and data pre-processing.....104
2.8 Downstream scRNA-Seq data analysis.....106
2.9 Bulk RNA-Seq and microarray analysis.....108
2.10 Statistics.....108
2.11 Data availability.....109
2.12 Explanation of bioinformatic terms, plots, and analyses.....109
Chapter 3: Transcriptional analysis of iNKT cell heterogeneity and early stage iNKT cell activation.....116
Introduction.....117
Hypothesis.....119
Aims.....119
3.1 Exploring splenic iNKT cell heterogeneity at steady state.....120
3.2 Exploring adipose iNKT cell heterogeneity at steady state.....124

3.3 Transcriptional analysis of adipose versus splenic iNKT cells at steady state.....130
3.4 Splenic iNKT cells undergo rapid and dramatic transcriptional remodeling after activation with αGalCer.....136
3.5 Granular analysis of splenic iNKT cell at 4 hours post-αGalCer.....143
3.6 NKT1, NKT2, and NKT17 cells share transcriptional signatures of activation, but NKT2 and NKT17 cells are distinguished by oxidative metabolic enrichment.....146
3.7 Exploring human iNKT cell heterogeneity at steady state.....157
3.8 Activated human iNKT cells undergo rapid and dramatic transcriptional remodeling.....163
3.9 Granular analysis of activated human iNKT cells.....170
3.10 Adipose iNKT cells display a blunted transcriptional response to stimulation with αGalCer.....174
3.11 Transcriptional analysis of adipose iNKT cell subset activation.....180
Discussion.....187
Chapter 4: Transcriptional analysis of downstream iNKT cell activation and memory-like iNKT cells.....193
Introduction.....194
Hypothesis.....196
Aims.....196
4.1 Activation with αGalCer induces extensive, rapid, and sustained transcriptional remodeling of splenic iNKT cells.....197
4.2 Granular analysis of splenic iNKT cells at 72 hours post-αGalCer.....203
4.3 Granular analysis of adipose iNKT cells at 72 hours post-αGalCer.....207
4.4 Comparative analysis of transcriptional remodeling among adipose and splenic iNKT cells at steady state, 4 hours post-αGalCer, 72 hours post-αGalCer.....212
4.5 Bulk transcriptional analysis of memory-like iNKT cells at 6 days post-αGalCer.....222

4.6 Prior activation with αGalCer induces long term transcriptional remodeling and an adipose-like activation scheme among splenic iNKT cells .....226
4.7 Granular analysis of resting splenic iNKT cells at 4 weeks post-αGalCer .....236
4.8 Granular analysis of reactivated splenic iNKT cells at 4 weeks post-αGalCer.....243
4.9 Transcriptional analysis and comparison of adipose and splenic iNKT cells at steady state and 4 weeks post-αGalCer.....251
4.10 Granular analysis of adipose iNKT cells at 4 weeks post-αGalCer. . .257
4.11 Characterization of the transcriptional phenotype of NKT10 cells.....263
Discussion.....272
Chapter 5: General Discussion.....279
References.....294

**Acknowledgments**

I would not have made it through this PhD without the help, guidance, friendship, and love of so many different people.

First and foremost, would like to thank my supervisor Dr Lydia Lynch. You have been such a fantastic and enthusiastic mentor, and have provided me with so many amazing opportunities, not least the chance to live and work in Boston, without which I never would have met Genna. It's not an exaggeration to say that doing a PhD with you has changed my life for the better.

To all of the folks in the Lynch lab, past and present – thank you for all of your help, advice, and company. It's been such a pleasure to work with all of you over the course of the PhD. I would especially like to thank Dr Nelson LaMarche, for his enthusiasm and hard work during our collaboration – it was really great to work with a fellow PhD student on all things iNKT cell related!

I would like to thank Dr Michael Brenner for co-funding our scRNA-Seq study, and for his help and advice with the project. I would also like to thank all of the Brenner lab folks for being very welcoming and kind, especially when I first arrived in Boston.

I would like to thank Dr Leandro Agudelo for his helpful advice on getting started with bioinformatics and data analysis, it was great to learn from and work with you!

I would like to thank Barry Moran and Adam Chicoine for their help with all things flow and sorting related, and the folks of the 10x core facility at BTM for making this scRNA-Seq project possible. Not only that, but you were all so nice to work with too!

I would like to thank all my family and friends for their love, support, and guidance over the course of the PhD. It's been some journey, and I can't wait to be able to spend time with you all soon.

A special thank you to Genna - I can’t express how lucky I am that this path brought us together. I couldn’t have done it without your love, advice, and support.

**Associated Publications**

1. Kane, H. and Lynch, L., 2019. Innate immune control of adipose tissue homeostasis. *Trends in immunology*, *40*(9), pp.857-872.

2. LaMarche, N.M., Kane, H., Kohlgruber, A.C., Dong, H., Lynch, L. and Brenner, M.B., 2020. Distinct iNKT cell populations use IFNγ or ER stress-induced IL-10 to control adipose tissue homeostasis. *Cell metabolism*, *32*(2), pp.243-258.

3. Kane, H., LaMarche, N.M., Scannail, Á.N. Brenner, M.B., and Lynch, L., 2021. Longitudinal analysis of invariant natural killer T cell activation reveals a cMAF-associated transcriptional state of NKT10 cells. *BioRxiv* (in revisions).

**List of Abbreviations**

NKT cell – Natural killer T cell

MAIT cell – Mucosal associated invariant T cell

TCR – T cell receptor

iNKT cell – Invariant natural killer T cell

MHC – Major histocompatibility complex

αGalCer – α-galactosylceramide

APC – Antigen presenting cell

DP – Double positive

DN – Double negative

NKTp cells – iNKT progenitor cells

RNA – Ribonucleic acid

scRNA-Seq – Single cell RNA-Sequencing

mTOR – Mammalian target of rapamycin

RICTOR – Rapamycin-insensitive companion of mTOR

RAPTOR – Regulatory-associated protein of mTOR

GZMB – Granzyme B

TBKBP1 – TBK-binding protein 1

ChIP-Seq – Chromatin immunoprecipitation assay with sequencing

ATAC-Seq – Assay for transposase-accessible chromatin

MLN – Mesenteric lymph node

ILN - Inguinal lymph node

IL-17RB – IL-17 receptor B

HMG – High mobility group

RHD – Rel homology domain

ZF – Zinc finger

bZIP – Basic leucine zipper

TRAF3IP3 – TRAF3-interacting protein 3

PMA – Phorbol 12-myristate 13-acetate

LtβR – lymphotoxin β receptor

ILC3 - Type 3 innate lymphoid cell

LPS – Lipopolysaccharide

UPR – Unfolded protein response

ER – Endoplasmic recticulum

PBMC – Peripheral blood mononuclear cell

Treg – Regulatory T cell

HFD – High fat diet

RYGB – Roux-en-Y gastric bypass

FGF-21 – Fibroblast growth factor 21

WAT – White adipose tissue

DIO – Diet induced obesity

DC – Dendritic cell

Ig – Immunoglobulin

MZB cell – Marginal zone B cell

PSC – Proximal signaling complex

$T_{CM}$ – Central memory T cell

$T_{SM}$ – Stem-like memory T cell

$T_{EM}$ – Effector memory T cell

$T_{RM}$ – Tissue-resident memory T cell

TPEX cell – Precursor exhausted T cell

GM-CSF – Granulocyte-macrophage colony-stimulating factor

TNF – Tumor necrosis factor

$NKT_{FH}$ cell - Follicular helper-like iNKT cell

$T_{FH}$ cell – Follicular helper T cell

S.pneumoniae – Streptococcus pneumoniae

TLR – Toll-like receptor

CPS – Pneumococcal capsular polysaccharide

A.fumigatus – Aspergillus fumigatus

CVB – Coxsackievirus B

MCMV – Murine cytomegalovirus

FV – Friend virus

EBV – Epstein-Barr virus

XIAP – X-linked inhibitor-of-apoptosis

HSC-iNKT – Hematopoietic stem cell-engineered iNKT cells

CAR – Chimeric antigen receptor

DC/Gal – αGalCer–loaded DCs

GZMA – Granzyme A

$NKT_{eff}$ – Effector iNKT cells

GSEA – Gene set enrichment analysis

EAE – Experimental autoimmune encephalitis

αGCPT – αGalCer-pretreated

$ApoE^{-/-}$ mice – Apolipoprotein E-deficient mice

TSC1 – Tuberous sclerosis 1

$Nur77^{tg}$ mice – Mice with overexpression of Nur77

iNKT10 cell – Induced NKT10 cell

CLN – Cervical lymph nodes

YY1 – Yin Yang 1

SRC – Spare respiratory capacity

PDK1 – Phosphoinositide-dependent kinase 1

PI3K – Phosphatidylinositol-3-kinase

FNIP1 – Folliculin-interacting protein 1

AMPK – AMP-activated protein kinase

2-DG – 2-deoxyglucose

$PLZF^{TG}$ – PLZF transgenic

ROS – Reactive oxygen species

FAO – Fatty acid oxidation

DMSO – Dimethylsulfoxide

RPMI – RPMI media

PBS – Phosphate-buffered saline

FBS – Fetal Bovine Serum

TMRM – Tetramethylrhodamine, Methyl Ester, Perchlorate

CD43-HG – CD43 Activation Glycoform

IP – Interpertioneal

(GEMs) – Gel Beads-in-emulsion

UMI – Unique molecular identifier

PCA – Principal component analysis

UMAP – Uniform manifold approximation and projection

RMA – Robust Multichip Average

TMM – Trimmed mean of M-values

LogCPM – Log2(counts per million)

RTEs – Recent thymic emigrants

KIR – Killer-cell inhibitory receptor

DEG – Differentially expressed gene

ISG – Interferon stimulated gene

MFI – Median fluorescence intensity

GRN – Gene regulatory network

# Chapter 1: General Introduction

### 1.1: General introduction to NKT cell biology

Natural killer T (NKT) cells, like mucosal associated invariant T (MAIT) cells and γδ T cells, are a conserved population of innate T lymphocytes[1]. NKT cells were initially defined by expression of the Vα14-Jα18 T cell receptor (TCR), rapid production of cytokines after activation, and co-expression of surface markers associated with both adaptive T cells and NK cells, such as CD3 and CD161 (NK1.1). This gave rise to the moniker “natural killer T cell”, as NKT cells were believed to represent a hybrid phenotype somewhere between that of an NK cell and a T cell[2–4]. NKT cells are now categorized based on the composition of their TCR, and their antigen specificity. Type I NKT cells express a semi-invariant TCR comprised of a single α chain paired with a limited number of β chains; murine type I NKT cells express a Vα14-Jα18 α chain paired with either a Vβ2, Vβ7, Vβ8.1, Vβ8.2 or Vβ8.3 β chain, while human type I NKT cells express a Vα24-Jα18 chain paired predominantly with Vβ11[5,6]. Due to this limited TCR diversity, type I NKT cells are typically referred to as invariant NKT (iNKT) cells. Type II NKT cells, by contrast, express a more diverse TCR and lack the conserved α chain present among iNKT cells[7].

In contrast to conventional adaptive $CD8^+$ and $CD4^+$ T cells, which recognize peptide antigens presented by major histocompatibility complex (MHC) class Ia and class II receptors[8], iNKT cells recognize glycolipid antigens, particularly species in which the carbohydrate moiety is connected to the lipid tail via an α-anomeric linkage (although glycolipids with β linkages can also be recognized)[9]. The prototypical iNKT cell ligand is α-galactosylceramide (αGalCer; KRN7000), which was initially derived from an extract of the Okinawan marine sponge *Agelas mauritianus* during a screen for compounds with anti-tumor activity in 1995[10,11]. αGalCer binds to the MHC class Ib receptor CD1d, forming a complex which can be presented by antigen presenting cells (APCs) to iNKT cells[12,13]. Ligation of the iNKT cell TCR with CD1d-αGalCer rapidly induces iNKT cell activation, triggering a potent cytokine response[14–17]. Activation of iNKT cells with αGalCer also induces potent anti-tumor responses

*in vivo*[10,17]. As a result, αGalCer is widely and commonly used to study iNKT cell activation and function. Moreover, conjugation of αGalCer, or synthetic αGalCer analogues such as PBS-57, to CD1d tetramers has enabled straightforward and robust identification of iNKT cells in applications like flow cytometry, while plate bound CD1d-αGalCer can be used to activate iNKT cells *in vitro*[5]. Other antigens capable of activating iNKT cells include glycolipids derived from microbes, such as α-glucosyldiacylglycerol produced by *Streptococcus pneumonia*, and endogenous lipid antigens produced by mammalian cells[9,18,19]. iNKT cells can also be directly stimulated by certain cytokines in the absence of TCR stimulation, including IL-2, IL-12 and IL-18[20,21], while other cytokines, such as IL-15, are capable of enhancing TCR-mediated iNKT cell activation[22].

The antigens recognized by type II NKT cells are less well defined than the antigens recognized by iNKT cells. Although type II NKT cells also recognize CD1d[23,24], they do not respond to αGalCer, and are instead suggested to recognize a broad range of other lipid species, including sulfatides and phospholipids such as lysophosphatidylcholine[25,26]. The diverse and relatively undefined nature of type II NKT cell antigens makes the analysis of these cells more difficult than iNKT cells, as there is no universal tetramer for identification of type II NKT cells, and many available tetramers exhibit high background staining and poor resolution. Furthermore, there is no potent consensus antigen equivalent to αGalCer for activation of type II NKT cells[7,27]. Most studies of type II NKT cells also require prior depletion of iNKT cells, or specific transgenic mouse models expressing altered TCR repertoires, such as Traj18$^{-/-}$ or Jα18$^{-/-}$4get mice, as iNKT cells are much more frequent than type II NKT cells in mice[27,28]. By comparison, type II NKT cells can comprise a significant proportion of the total NKT cell pool in humans[29]. NKT cells are generally less frequent in humans than in mice[30], as MAIT and γδ T cells tend to predominate the human innate T cell repertoire[31,32], although interestingly NKT cells are enriched in human adipose tissue[33]. In this thesis, I will henceforth focus on

iNKT cells, owing to their more defined antigen status and the reagents available for analysis of iNKT cell activation and function.

### 1.2 iNKT cell development

Most iNKT cells develop in the thymus from the same bone marrow-derived $CD8^+$ $CD4^+$ (double positive; DP) progenitor cells that give rise to adaptive T cells. However, while adaptive T cells are positively selected through interaction with specialized cortical epithelial cells, iNKT cells undergo positive selection via interactions with other DP thymocytes[34,35]. Interestingly, a minority of iNKT cells have been found to develop from $CD8^-$ $CD4^-$ (double negative; DN) progenitors and bypass the classic DP stage, indicating that there are multiple routes by which progenitor cells can become committed to the iNKT lineage[36]. Following lineage commitment, nascent iNKT cells pass through a series of different developmental stages[37].

#### 1.2.1 Early iNKT cells development and the CD44 NK1.1 model

After positive selection, DP iNKT cells downregulate CD8 and enter Stage 0 of iNKT cell development. Stage 0 iNKT cells upregulate CD69, which retains these immature cells in the thymus[38], and express the sialoglycoprotein CD24[39]. Stage 0 iNKT cells also upregulate expression of the transcription factors EGR1 and EGR2, which further progress iNKT cell development by binding to and activating the *Zbtb16* promoter[40]. *Zbtb16* encodes PLZF, which is a critical lineage-defining transcription factor for iNKT cells. A key characteristic of mature iNKT cells is that they are ‘poised’ and exhibit a rapid primary response to antigen similar to the secondary response of adaptive memory T cells. However, unlike adaptive memory T cells, iNKT cells do not require prior antigen exposure, activation and differentiation, and emerge from the thymus as poised memory/effector cells[41,42]. Notably, PLZF is believed to orchestrate the establishment of this “poised” memory/effector phenotype in

iNKT cells, as ectopic expression of PLZF in adaptive T cells results in the spontaneous acquisition of memory/effector characteristics[43]. PLZF is essential for normal iNKT development, as mice lacking PLZF demonstrate severely reduced frequencies of iNKT cells across all tissues, and thymic PLZF$^{-/-}$ iNKT cells fail to expand following positive selection[41,42,44].

Induction of PLZF initiates the progression of nascent iNKT cells through several further developmental stages in which the cells blast, proliferate, and undergo differentiation and maturation. Traditionally, iNKT cell development after Stage 0 has been defined in terms of three further stages delineated by the surface markers CD44 and NK1.1. Stage 1 iNKT cells are CD44$^{-}$ NK1.1$^{-}$, Stage 2 iNKT cells are CD44$^{+}$ NK1.1$^{-}$, and Stage 3 iNKT cells express both CD44 and NK1.1[39,45]. Microarray analysis has demonstrated that Stage 1, 2, and 3 iNKT cells are transcriptionally distinct, with Stage 1 and Stage 2 iNKT cells demonstrating enrichment of genes associated with stemness and proliferation, while Stage 3 cells express granzymes and cytotoxicity receptors, similar to most mature iNKT cells[45,46]. Interestingly, transcriptomic analysis of thymic iNKT cells by Cohen *et al.* (2013) found that the greatest gene expression changes in iNKT cell development occur during commitment of DP progenitors to the iNKT cell lineage, and then during terminal differentiation of Stage 1 and Stage 2 iNKT cells into Stage 3 iNKT cells[45]. Work by Bendelac *et al.* (1994) and Pellicci *et al.* (2002) has shown that most iNKT cells exit the thymus during Stage 2, and undergo terminal differentiation in the peripheral tissues[47,48]. As studies by Thomas *et al.* (2011) and Lynch *et al.* (2015) have shown that iNKT cells are predominantly tissue resident, egress of most iNKT cells from the thymus at Stage 2 suggests that individual tissues may play an important role in establishing the final phenotype of mature iNKT cells[49–52]. By contrast, thymic Stage 3 iNKT cells are thought to comprise a long-lived resident population, and work by Drennan *et al.* (2009) has shown that expression of CXCR3 may be crucial for their retention in the thymus[53,54].

### 1.2.2 NKT1, NKT2 and NKT17 cells: a novel model branching model of iNKT cell development from an NKT2-like progenitor state

One of the major assumptions of the CD44 NK1.1 model of iNKT cell development is that Stage 2 iNKT cells are immature, and eventually undergo differentiation into Stage 3 iNKT cells. However, this assumption has been challenged by the discovery and characterization of iNKT cell subsets, which demonstrated that iNKT cells are, in fact, heterogeous[55–57]. The main iNKT cell subsets present in mice are known as NKT1, NKT2, and NKT17 cells, and they broadly correspond to adaptive Th1, Th2, and Th17 effector T cells[58–60]. Analysis of thymic iNKT cells has shown that Stage 3 iNKT cells are almost exclusively NKT1 cells, whereas Stage 2 iNKT cells are enriched for NKT2 and NKT17 cells[60]. However, if NKT2 and NKT17 cells represent distinct iNKT cell lineages, and do not eventually differentiate into NKT1 cells, this indicates that the CD44 NK1.1 model is not completely correct. Therefore, an alternative model of iNKT development has been proposed in which NKT1, NKT2, and NKT17 cell subsets instead differentiate from a common progenitor population[46,61–65].

Notably, since this new model was originally conceived, several studies have used modern sequencing technology and fate mapping to analyze iNKT cell development in unparalleled detail[46,61,63–67], largely resulting in validation of the common progenitor model and the identification of an NKT2-like progenitor population that can give rise to NKT1, NKT2, and NKT17 cells. Studies by Lee *et al.* (2013; 2016), Engel *et al.* (2016), Georgiev *et al.* (2016), and Wang *et al.* (2018) have collectively shown that thymic NKT2 cells are heterogeneous, and segregate into two distinct populations. One of these populations was found to express IL-4 and the maturity marker CD44, consistent with a true functional NKT2 cell subset, while the other NKT2-like population largely lacked expression of CD44 and displayed enrichment of genes associated with proliferation and the cell cycle, indicative of a candidate progenitor population[46,60,61,66]. Furthermore, fate mapping revealed that these CD44$^{low}$

NKT2-like cells, dubbed NKTp cells, differentiated into *bona fide* NKT1, NKT2, and NKT17 cells, characteristic of a mulitpotent progenitor population[60,66]. Therefore, this work suggests that all iNKT cells differentiate from a common NKT2-like progenitor state. Further evidence supporting this conclusion also emerged from work by O'Brien *et al.* (2016), who used an IL-13 reporter mouse model to show that all iNKT cells express IL-13 during development, consistent with a Th2-like or NKT2-like progenitor state[63].

Recently, validation of the common progenitor model has also come from single cell ribonucleic acid (RNA)-Sequencing (scRNA-Seq) of thymic iNKT cells. Pioneering scRNA-Seq by Engel *et al.* (2016) found that some NKT2-like cells in the thymus expressed *Tbx21* (T-bet), an NKT1 cell marker, suggesting that NKT2-like cells could give rise to NKT1 cells[46]. More recently, 10x scRNA-Seq and pseudotemporal analysis of thymic iNKT cells by Krovi *et al.* (2020) and Baranek *et al.* (2020) identified an intermediate NKT2-like state from which both NKT1 and NKT17 cells could develop, illustrating the branching developmental trajectory central to the common progenitor model[64,65]. Therefore, while the CD44 NK1.1 model correctly identified Stage 3 or NKT1 cells as a terminally differentiated end state for iNKT cell development, recent analysis has shown that nascent iNKT cells can differentiate along several different branching trajectories and pass through an immature NKT2-like state (Figure 1.1).

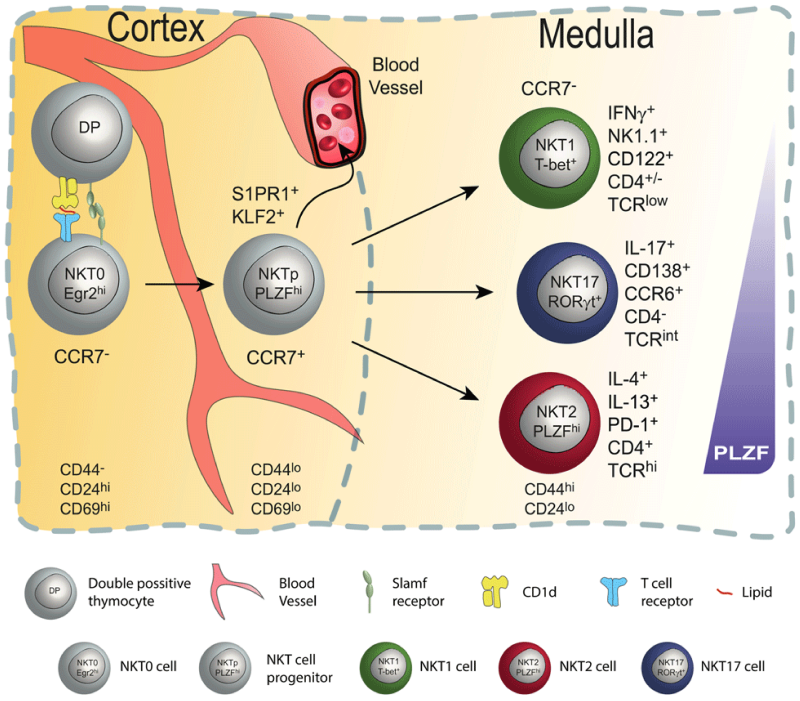



**Figure 1.1: The common progenitor model of iNKT cell development.** Following positive selection through cognate interactions with other DP thymocytes, nascent iNKT cells upregulate expression of PLZF, blast, proliferate, and become committed to the iNKT cell lineage. Progression through early iNKT cell development leads to the generation of a multipotent progenitor iNKT cell state, termed NKTp cells, which express CCR7 and LEF1. At this stage, NKTp cells may exit the thymus to complete maturation in other tissues or can continue to differentiate in the thymus. NKTp cells then differentiate into mature, functionally distinct $CD44^+$ NKT1, NKT2, or NKT17 cells along a branching differentiation trajectory. Adapted from Hogquist *et al*. (2020)[68].

### 1.2.3 Factors governing iNKT cell subset development and differentiation

Ever since the discovery of NKT1, NKT2, and NKT17 cells, there has been much interest in elucidating the factors and signals that regulate NKTp cell commitment towards an NKT1, NKT2, or NKT17 cell lineage. Several studies have identified a possible role for TCR signal strength in iNKT cell differentiation[69,70]. Analysis of YYAA and SKG mice by Tuttle *et al.* (2018), two strains that have mutations in the TCR signal transducing tyrosine kinase ZAP70[71,72], revealed reduced frequencies of NKT2 and NKT17 cells versus NKT1 cells, suggesting that increased TCR signal strength might promote the differentiation of NKT2 and NKT17 cells[69]. Similar results were obtained by Zhao *et al.* (2018), who showed that that NKT1 cells display enrichment of numerous negative regulators of TCR signaling, including *Ptpn22*, *Pag1*, and *Ptpn6*, whereas NKT2 and NKT17 cells display enrichment of markers associated with increased TCR signaling, including *Pdcd1*, *Icos*, and *Egr2*[70]. iNKT cell subsets also display differential TCR expression in the order of NKT2 > NKT17 > NKT1[67,69], suggestive of differential sensitivity to TCR stimulus. Moreover, work by Georgiev *et al.* (2016) identified differential expression of the TCR regulatory components *Fcer1g*, *Cd247*, and *Blk* among NKT1, NKT2 and NKT17 cells[67], suggesting that iNKT cell subsets may use and be regulated by distinct TCR signaling apparatus. Interestingly, a study by Park *et al.* (2019) has shown that PLZF expression may also regulate iNKT cell subset differentiation. Analysis of PLZF$^{GFPcre}$ mice, which express a hypomorphic *Zbtb16* allele and show greatly reduced PLZF expression, demonstrated significantly reduced frequencies of NKT2 and NKT17 cells, whereas the frequency of NKT1 cells was greatly increased[73]. Notably, NKT1, NKT2 and NKT17 cells also demonstrate baseline differences in PLZF expression following the same NKT2 > NKT17 > NKT1 pattern as TCR expression[60,73]. Since PLZF is induced following TCR stimulation in iNKT cells, both during iNKT cell development and following activation of mature iNKT cells[41,74], it is

possible the the influence of PLZF on iNKT cell lineage differentiation may be downstream of TCR-mediated effects.

In addition to TCR stimulus and PLZF expression, many other developmental factors have been shown to influence iNKT cell subset differentiation. Most notably, a suite of studies has suggested that NKT17 cells display a highly distinctive developmental program compared to NKT1 and NKT2 cells. For example, a study by Uddin *et al.* (2016) found that deletion of the transcription factor BCL11B in post-selected DP thymocytes resulted in specific depletion of NKT1 and NKT2 cells, but not NKT17 cells. BCL11B, which regulates glycolipid processing and presentation, was required for the effector functions of NKT2 and NKT1 cells and suppressed the expression of NKT17-associated genes[75]. Other factors described as being important regulators of NKT17 versus NKT1 and NKT2 cell development include cMAF, RUNX1, SOX4, SOX13, BATF, NKAP, TH-POK, SerpinB1, and TGF-β[67,76–80]. NKT1, NKT2 and NKT17 cells have also been shown to display differential developmental requirements for mammalian target of rapamycin (mTOR), a key regulator of cellular metabolism and growth[81–83], based on studies involving the mTOR binding proteins rapamycin-insensitive companion of mTOR (RICTOR) and regulatory-associated protein of mTOR (RAPTOR). Deletion of RICTOR and loss of mTORC2 complex activity produced a specific depletion of NKT17 but not NKT1 or NKT2 cells, whereas deletion of RAPTOR and loss of mTORC1 complex activity resulted in a loss of NKT1 and NKT2 but not NKT17 cells[84–86]. Moreover, analysis of *Pten*$^{-/-}$ mice, which display greatly increased mTORC2 activity, also showed a dramatically increased frequency of NKT17 cells, but this effect was lost in *Pten*$^{-/-}$ *Rictor*$^{-/-}$ mice, indicating that NKT17 cells are specifically reliant on mTORC2 for their development and survival[85,86]. Overall, this work suggests that NKT17 cells follow a distinct developmental trajectory to NKT1 and NKT2 cells.

### 1.3 Steady State iNKT cell biology

After progressing through development iNKT cells upregulate expression of pro-migratory genes associated with the KLF2 regulon, including *Klf2*, *Emp3*, and *S100a6*, which enables these cells to mobilize and leave the thymus[65,87]. Following thymic egress, distinct patterns of chemokine receptor expression promote differential accumulation of iNKT cell subsets across various tissues, a process which may also be influenced by the homeostatic requirements of NKT1, NKT2, and NKT17 cells[46,58–60,88,89]. As previously mentioned, most iNKT cells are thought to undergo terminal differentiation and maturation in the tissues where they take up residency, which can confer unique tissue-specific phenotypes[49–52]. For example, iNKT cells in adipose tissue, where they are enriched and can constitute 15-20% of total T cells[90], are highly unusual, and biased towards production of IL-10 rather than IFNγ[49,91]. Other tissues harboring potentially unique iNKT cell populations include Peyer's patches and the lung[52,92]. Therefore, the iNKT cell repertoire is thought to be highly heterogeneous at steady state and varies on both a subset and a tissue level.

#### 1.3.1 NKT1 cells

NKT1 cells are typically defined as T-bet$^{+}$ PLZF$^{low}$ TCR$^{low}$ CD3$^{low}$ NK1.1$^{+}$ iNKT cells that produce copious amounts of IFNγ upon activation, and can co-express Th2 cytokines in some tissues[17,59,60,67,69,93,94]. NKT1 cells are generally considered to be the main cytotoxic iNKT cell subset, as NKT2 and NKT17 cells typically lack expression of Granzyme B (GZMB) and do not express many of the cytotoxicity receptors found in NKT1 cells[46,58,61,67,95,96]. NKT1 cells are also the predominant iNKT cell subset present in C57BL/6 mice, which is a commonly used mouse model for the study of iNKT cells[60]. Tissue-wise, NKT1 cells are particularly enriched in the liver, where they can constitute more than 90% of all iNKT cells, and they also comprise a majority of iNKT cells in the spleen and the lamina propria[59]. Transcriptomic analysis of NKT1 cells has

identified enrichment of genes associated with the pro-survival IL-2/IL-15 pathway, such as *Il2rb*, *Stat4*, *Bcl2*, *Sgk1* and *Nr3c1*, and genes associated with regulation of apoptosis, such as *Dapk2*, *Cdh1*, *Tnfsf10*, *Tnfrsf1a*, *Tjp1*, *Ppp3cc* and *Camk2b*, suggesting that NKT1 cells are a long-lived effector population[46]. IL-15 is thought to play a key role in NKT1 cell homeostasis. Gordy *et al.* (2011) found that IL-15 signaling promoted expression of granzymes, T-bet and IFNγ in NKT1 cells, demonstrating that IL-15 is important for the characteristic Th1-like and cytotoxic NKT1 cell phenotype[88]. A study by Zhu *et al.* (2018) also showed that IL-15 signaling was important for regulation of autophagy in NKT1 cells through TBK-binding protein 1 (TBKBP1). TBKBP1 deficiency resulted in accumulation of reactive oxygen species and reduced expression of the anti-apoptotic protein BCL2, leading to a reduced frequency of NKT1 cells and a loss of T-bet expression[97]. Several studies have also profiled the regulatory landscape of NKT1 cells. Chromatin immunoprecipitation assay with sequencing (ChIP-Seq) by Engel *et al.* (2016), and assay for transposase-accessible chromatin using sequencing (ATAC-Seq) by Murray *et al.* (2021) demonstrated that Runx, Ets, and Tbox transcription factors, such as T-bet, are likely to be critical regulators of NKT1 cells[46,92]. Chemokine receptor and homing molecules enriched among NKT1 cells include CXCR3[67], which is important for retention of resident NKT1 cells in the thymus[54], CD49A, ITGB1, ITGA1, and CCR5[46].

### 1.3.2 NKT2 cells

NKT2 cells are enriched in BALB/c mice and constitute a large proportion of iNKT cells present in the mesenteric lymph nodes (MLNs), inguinal lymph nodes (ILNs), and the lungs[51,59,98]. First identified by Terashima *et al.* (2008) as a subset of pulmonary iNKT cells that expressed IL-17 receptor B (IL-17RB)[57], NKT2 cells are characterized as PLZF$^{high}$ T-bet$^{-}$ RORγT$^{-}$ NK1.1$^{-}$ GATA3$^{high}$ TCR/CD3$^{high}$ CD4$^{+}$ iNKT cells that produce Th2 cytokines such as IL-4 and IL-13[61,93,99]. Transcriptomic analysis of NKT2 cells has historically been

complicated by the presence of NKTp cells, especially since many transcriptomic studies have focused on thymic iNKT cells[46,61,92]. Nevertheless, NKT2 cells have been shown to display enrichment of many stem-like markers, including *Slamf6*, *Tcf7*, *Id3, Lef1,* and *Ccr7*, similar to naive and stem-like memory adaptive T cells[46,61,100–102]. *In silico* analysis of thymic NKT2 cells by Engel *et al.* (2016) using ChIP-Seq identified enrichment of a wide range of different transcription factor binding motifs, including KLF, SOX, TCF, GATA and IRF family members[46], while ATAC-Seq analysis of NKT2 cells by Murray *et al.* (2021) identified enrichment of high mobility group (HMG) box protein motifs associated with stem-like markers such as TCF1 (*Tcf7*) and LEF1, suggesting that TCF family transcription factors play an important role in NKT2 cell biology[92]. Interestingly, Rel homology domain (RHD) and zinc finger (ZF) motifs, which includes binding sites for NFAT and EGR1, were also enriched among NKT2 cells, reflecting previous observations that NKT2 cells are $TCR^{high}$ and demonstrate expression of markers associated with TCR stimulation and activation at steady state[67,69,70]. Assessment of chemokine receptor expression among NKT2 cells by Engel *et al.* (2016)[46] revealed increased expression of CCR4, which has previously been associated with Th2 cells[103], and CCR9, which typically promotes homing of T cells to the gut[104].

Several factors have been proposed to regulate NKT2 cell homeostasis and function. A potential role for IL-6 has been suggested by Engel *et al.* (2016), since NKT2 cells display enrichment of *Il6ra*, and IL-6 has previously been shown to promote IL-4 production and Th2 cell differentiation via an NFATc2-dependent mechanism[46,105]. Moreover, work by Georgiev *et al.* (2016) has shown that IL6Rα is strongly expressed by thymic NKT2 cells from BALC/C mice[67]. NKT2 cells can also express IL-17RB, which is a receptor for the Th2-promoting cytokine IL-25 (also known as IL-17E)[57,98]. IL-25 is thought to promote Th2 functionality in NKT2 cells, and depletion of $IL\text{-}17RB^{+}$ NKT cells has been shown to attenuate IL-25-induced airway hypersensitivity in mice[57].

Interestingly, work by Watarai *et al.* (2012) found that IL-25 selectively induces expression of the basic leucine zipper (bZIP) transcription factor E4BP4 (encoded by *Nfil3*) in $CD4^+$ $IL\text{-}17RB^+$ iNKT cells, and E4BP4 expression was required for the production of several different Th2 cytokines, including IL-13[98]. Another factor shown to regulate NKT2 cells is TRAF3-interacting protein 3 (TRAF3IP3). Deletion of TRAF3IP3 resulted in a reduction in the frequency of NKT2 cells, and fewer $IL\text{-}4^+$ iNKT cells after Phorbol 12-myristate 13-acetate (PMA)/Ionomycin stimulation. Mechanistically, Zhang *et al.* (2019) found that TRAF3IP3 promoted MEK1 recruitment downstream of lymphotoxin β receptor (LtβR) signaling[106], implicating the LtβR pathway as a possible regulator of NKT2 cell homeostasis.

### 1.3.3 NKT17 cells

NKT17 cells are usually the rarest of the three main iNKT cell subsets, typically comprising less than 5% of the total iNKT cell population. However, NKT17 cells are also enriched in the lungs, the skin, the peripheral lymph nodes, and the thymus of BALB/c mice[51,55,59,60,93]. Initially identified as an $NK1.1^-$ $CD4^-$ iNKT cell population that produced IL-17[56,107], NKT17 cells display intermediate expression of TCR, PLZF, and CD3, and they also constitutively express RORγT, which is the defining transcription factor of the NKT17 cell lineage[46,61,69,93]. Transcriptional characterization of NKT17 cells by studies such as Lee *et al.* (2016) and Engel *et al.* (2016) has shown that NKT17 cells share expression of many of the same key genes as γδ17 cells, type 3 innate lymphoid cells (ILC3s) and Th17 cells, including *Sdc1*, *Il1r1*, *Il23r*, *Aqp3*, and *Nr1d1*[46,61]. Interestingly, cross comparison of NKT1, NKT2, and NKT17 cells from spleen, thymus, liver and lung by Murray *et al.* (2021) has illustrated that NKT17 cells from different tissues, are more similar to each other than to NKT1 or NKT2 cell subsets from the same tissue, and the same was also true for NKT2 and NKT1 cell populations from different tissues[92]. This suggests that iNKT cell subset biology generally predominates over transcriptional effects

mediated by tissue residency[61,92]. Overall, NKT17 cells are thought to be more transcriptionally similar to NKT2 cells than to NKT1 cells[92].

Whereas IL-15 has been identified as a key survival factor for NKT1 cells, NKT17 cells are thought to be uniquely dependent on IL-7. Webster *et al.* (2014) demonstrated that *in vivo* treatment of mice with IL-7 selectively expanded NKT17 cells, and NKT17 cells displayed significantly increased expression of IL-7R (CD127) compared to other iNKT cells[89]. Moreover, iNKT cells from IL-7$^{-/-}$ mice failed to produce IL-17 while remaining IFNγ and IL-4 competent, and RORγT$^{+}$ iNKT cells were selectively depleted in IL-7$^{-/-}$ mice. Therefore, this study demonstrates that IL-7 plays a crucial role in NKT17 cell homeostasis. Other factors thought to regulate NKT17 cells include IL-23 and IL-1β[108], similar to γδ17 cells and other IL-17 producing populations[109,110], and a study by Cameron *et al.* (2018) has shown that NKT17 cells can respond to lipopolysaccharide (LPS), both alone and in combination with TCR stimulation[93]. Another possible regulator of NKT17 cell homeostasis is the serine protease SerpinB1. Work by Georgiev *et al.* (2016) found that knockout of SerpinB1 expression led to a significant increase in the frequency of NKT17 cells in the thymus and lungs of C57BL/6 mice, indicating that SerpinB1 negatively regulates NKT17 cells. Analysis of chemokine receptor and homing molecule expression in NKT17 cells by Engel *et al. (*2016) demonstrated enrichment of CCR6[46], which is known to be expressed in Th17 cells and promotes migration to the lung, the skin, and the gut[111,112], as well as the β4 and β5 integrin subunits ITGA4 and ITGA5[46]. ChIP-Seq and ATAC-Seq analysis of NKT17 cells by Engel *et al.* (2016) and Murray *et al.* (2021) revealed enrichment of binding motfis for many nuclear receptors, including RORγT (*Rorc*) and Rev-Erb (*Nr1d1*)[46,92], suggesting a key role for nuclear receptors in NKT17 cell biology.

### 1.3.4 iNKT cells in the lung and Peyer's patches

Since iNKT cells are predominantly tissue resident, the tissue in which they reside can have a significant impact on their phenotype and function. One tissue which has been shown to strongly influence resident iNKT cells is the lung. RNA-Seq analysis of pulmonary iNKT cells by Murray *et al.* (2021) found that lung iNKT cells displayed enrichment of a unique gene signature which was not present in either splenic or thymic iNKT cells, including the immune checkpoint CTLA-4, the activation and tissue residency marker CD69, and the activation marker NUR77 (*Nr4a1*)[92]. Moreover, ATAC-Seq of pulmonary, splenic and thymic iNKT cells revealed lung-specific enrichment of bZIP, AP1 and ATF, and RHD motifs, suggestive of a unique regulatory profile among pulmonary iNKT cells[92]. Moreover, cross comparison of iNKT cells with NK cells, γδ T cells and adaptive $CD4^+$ T cells in the lung and the spleen demonstrated common enrichment of lung-specific gene and chromatin signatures among all pulmonary immune cells versus all splenic immune cells[92]. Therefore, this work suggests that pulmonary iNKT cells exhibit a distinct gene expression and chromatin profile, similar to other immune cells in the lung.

iNKT cells resident in Peyer's patches, the aggregated lymphoid follicles present in the gut[113], have also been shown to demonstrate a unique phenotype and transcriptional profile. Clancy-Thompson *et al.* (2019) identified a population of iNKT cells present in murine Peyer's patches which were predominantly T-$bet^+$, indicative of an NKT1 cell phenotype, but produced IL-4 and not IFNγ after oral administration of αGalCer[52]. Adoptive transfer experiments revealed that exogenous iNKT cells did not populate Peyers patches in irradiated $Jα18^{-/-}$ mice, suggesting that that the iNKT cells present in Peyer's patches are unique, and highly resident. Transcriptional analysis of Peyer's patches versus splenic iNKT cells revealed enrichment of *Cd69*, *Gzmb*, *Gzma*, *Ccr9*, *Ahr*, *Ifngr1* and *Ctla4* among Peyer's patches iNKT cells, with gene module analysis demonstrating increased expression of programs

associated with cytotoxicity, IFN signaling, and tissue residency[52]. Interestingly, enrichment of *Ctla4* and *Cd69* is reminiscent of pulmonary iNKT cells[92], suggesting that there may be conserved gene signatures enriched among iNKT cells from non-lyphoid organs versus iNKT cells from lymphoid organs, which also has recently been demonstrated for γδ T cells[109].

### 1.3.5 iNKT cells in adipose tissue

Adipose iNKT cells, like iNKT cells in the lung and Peyer's patches, are a highly tissue resident population. However, even among tissue resident iNKT cells, adipose iNKT cells are highly unusual. Unlike most iNKT cells, adipose iNKT cells are less biased towards production of IFNγ after stimulation with αGalCer, but instead demonstrate significantly increased production of IL-2, IL-10, IL-4 and IL-13[49,90,91]. This identifies adipose iNKT cells as a unique population that is enriched for regulatory iNKT cells at steady state. Interestingly, stimulation of adipose iNKT cells with PMA and Ionomycin is sufficient to induce IFNγ production, suggesting that the capacity of adipose iNKT cells to produce IFNγ is actively suppressed under physiological conditions[49]. Adipose iNKT cells also show increased expression of KLRG1, CD69 and PD-1, and display a distinct transcriptional profile, including steady state enrichment of the activation marker *Nr4a1*, similar to pulmonary iNKT cells[49,92]. Most notably, Lynch *et al.* (2015) found that adipose iNKT cells lack expression of PLZF, which is widely expressed by iNKT cells in other tissues[49]. $PLZF^{+/-}$ mice, which have a partial deficiency in *Zbtb16* expression, also display significantly fewer iNKT cells in the spleen and liver but not in adipose tissue, and adipose iNKT cells are less depleted than splenic or hepatic iNKT cells in $PLZF^{-/-}$ mice[49].

Interestingly, Lynch *et al.* (2015) confirmed that adipose iNKT cells express PLZF during development using a PLZF-Cre $Rosa26^{fl/fl}$ mouse model. In this model, all cells that express PLZF (and therefore Cre) are permanently

tdTomato$^{+}$, and Lynch *et al.* (2015) found that adipose tissue iNKT cells were indeed tdTomato$^{+}$, demonstrating that adipose iNKT cells previously expressed PLZF, but subsequently downregulated PLZF expression[49]. This suggested that the PLZF$^{low}$ phenotype of adipose iNKT cells is induced at some point after PLZF is expressed during iNKT cell development, possibly in the adipose tissue itself. By contrast, a study by Vieth *et al.* (2017) found that genetic modification of the iNKT cell TCR could specifically promote the development of adipose-like iNKT cells in the thymus. While disruption of the hydrophobic pocket in the iNKT cell TCR via substitution of alanine for phenylalanine (F108A) blocked CD1d recognition and attenuated iNKT cell development, substitution of tyrosine at the same location (F108Y) resulted in increased numbers of adipose iNKT cells but fewer iNKT cells in the spleen or liver[114]. Moreover, FY108 thymic iNKT cells displayed reduced PLZF expression and increased PD-1 expression, suggesting that the FY108 mutation induces acquisition of an adipose iNKT cell-like phenotype in the thymus[114]. Therefore, this model raised the possibility that PLZF$^{low}$ adipose iNKT cells could be specifically selected in the thymus as a result of differential TCR-CD1d interaction(s).

Recent work by LaMarche *et al.* (2020), however, has suggested that the adipose iNKT cell phenotype is actively established in the adipose tissue, rather than during thymic development. Adipose iNKT cells from neonatal mice were found to display enrichment of a PLZF$^{high}$ Tbet$^{-}$ RORγT$^{-}$ iNKT cell population, similar to NKTp cells or NKT2 cells, but noticeably this population was absent among adipose iNKT cells from adult mice, suggesting that immature PLZF$^{high}$ iNKT cells migrate to adipose tissue and then subsequently downregulate expression of PLZF[115]. Moreover, LaMarche *et al.* (2020) confirmed that adipose tissue residency induced downregulation of PLZF using an adoptive transfer model. Adoptively transferred splenic iNKT cells, which expressed PLZF, specifically downregulated PLZF expression in the adipose tissue but not spleens of recipient mice[115]. Therefore, this work

demonstrated that adipose iNKT cells express PLZF during development but then subsequently downregulate PLZF after migrating to adipose tissue, implicating signals in the adipose tissue microenvironment as the molecular cue(s) for downregulation of PLZF. Notably, adipocytes are known to express CD1d, and have been shown to present ligands to iNKT cells[116,117], so it is possible that TCR-ligand-CD1d interactions in the adipose tissue might play an important role in establishing the adipose iNKT cell phenotype, analogous to how Vieth *et al.* (2017) found that modified TCR-ligand-CD1d interactions could promote an adipose-like iNKT cell phenotype in the thymus.

Further evidence for the role of the adipose tissue microenvironment in establishment of the adipose iNKT cell phenotype has come from studies of the transcription factor E4BP4. Lynch *et al.* (2015) found that adipose iNKT cells constitutively express E4BP4 at steady state, whereas iNKT cells in other organs such as the spleen, thymus and liver do not, and transfection of splenic iNKT cells with E4BP4 induced production of IL-10[49], implicating E4BP4 as a key regulator of IL-10 production in adipose iNKT cells. This was further elaborated on by LaMarche *et al.* (2020) with the finding that free fatty acids can induce expression of E4BP4 in iNKT cells through the IRE1a-XBP1s arm of the unfolded protein response (UPR). Culture of splenic iNKT cells in media supplemented with the C-16 saturated fatty acid palmitate or tunicamycin, a specific small molecule activator of endoplasmic recticulum (ER) stress and the UPR[118], induced *Nfil3* and *Il10* expression, and culture of splenic iNKT cells with the organic (lipid) phase of adipose-conditioned media was also sufficient to induce *Nfil3* expression. Moreover, scRNA-Seq and flow cytometry analysis of adipose iNKT cells revealed increased expression of *Xbp1* and increased lipid content relative to splenic iNKT cells[115]. Therefore, this work implicates lipids in the adipose microenvironment as regulators of E4BP4 expression in adipose iNKT cells, and consequently production of IL-10 (Figure 1.2). Notably, in agreement with this finding, Vieth *et al.* (2017) found that FY108 thymic

iNKT cells did not express E4BP4, despite displaying other features consistent with an adipose iNKT cell phenotype[114].

Overall, the transcriptional state of adipose iNKT cells has been most clearly distinguished by their lack of PLZF expression and unique enrichment of E4BP4. However, to date, most studies of adipose iNKT cells have focused on this population as a bulk cohort of cells, and it was unknown exactly if and what iNKT cell subsets might be present in adipose tissue. Work by Lynch *et al.* (2015) showed that most adipose iNKT cells express T-bet, suggesting broad enrichment of NKT1 cells, with a minority of cells expressing RORγT, indicative of an NKT17 cell phenotype[49]. Most adipose iNKT cells also express GATA3[49], which is often associated with Th2 cells and NKT2 cells[46,61], although work by Cameron *et al.* (2018) has shown that NKT1, NKT2 and NKT17 cells all express GATA3, and GATA3 may not be sufficient to distinguish iNKT cell subsets[93]. Adipose iNKT cells do express several markers that could potentially distinguish iNKT cell subsets, including KLRG1, ICOS, and PD-1, and unlike thymic and splenic iNKT cells, a large population of adipose iNKT cells are NK1.1$^{-}$, suggesting that NK1.1 might demarcate different adipose iNKT cell subsets[49]. During my PhD program, and as part of the *Cell Metabolism* publication by LaMarche *et al.* (2020), I performed analysis of adipose iNKT cell subsets, the results of which will be discussed in Chapter 3 of this thesis.

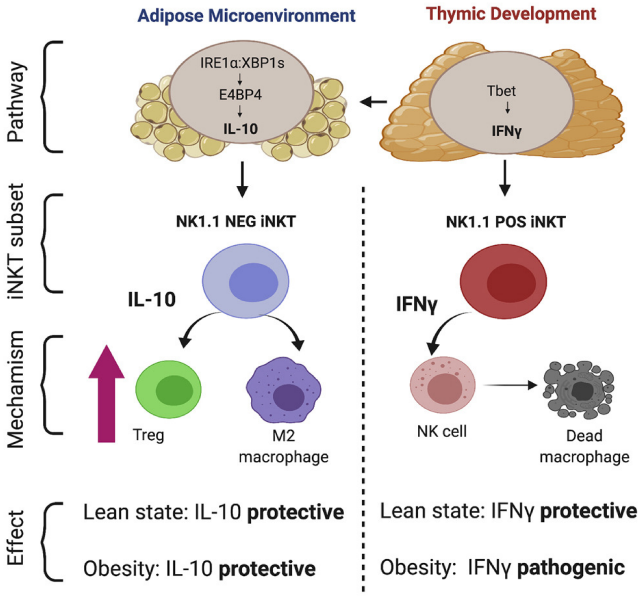



**Figure 1.2: The heterogeneous phenotype of adipose iNKT cells.** Adipose NK1.1$^{-}$ iNKT cells correspond to the classic regulatory adipose iNKT cell phenotype and display an increased capacity for production of IL-10 and IL-2. This enables adipose NK1.1$^{-}$ iNKT cells to suppress adipose tissue inflammation, support adipose Treg homeostasis, and polarize adipose tissue macrophages towards an M2-like phenotype. During diet induced obesity or high fat diet, adipose NK1.1$^{-}$ iNKT cells play a protective role. Expression of IL-10 is induced by the transcription factor E4BP4, which becomes upregulated downstream of lipid-induced ER stress, activation of the unfolded protein response, and signaling through the IRE1α-XBP1s pathway. The NK1.1$^{-}$ iNKT cell population includes both NKT1 and NKT17 cells. NK1.1$^{+}$ iNKT cells are similar to NKT1 cells in other tissues and produce IFNγ. In lean adipose tissue, NK1.1$^{+}$ iNKT cells can contribute to adipose tissue homeostasis by transactivating NK cells and promoting the clearance of adipose tissue macrophages. During diet induced obesity or high fat diet, however, production of IFNγ by NK1.1$^{+}$ iNKT cells may contribute to adipose tissue inflammation. Adapted from LaMarche *et al*. (2020)[115].

### 1.3.6 Human iNKT cells

While murine iNKT cells demonstrably segregate into distinct NKT1, NKT2 and NKT17 cell lineages, human iNKT cells are generally subdivided based on their expression of CD4 and CD8. Unlike murine iNKT cells, which generally do not express CD8[119,120], human iNKT cells can express CD8, and analysis of human iNKT cells has revealed $CD4^+$, $CD8^+$ and $CD4^-$ $CD8^-$ (DN) iNKT cell populations[121–128]. Most analyses of human iNKT cells have focused on iNKT cells present among peripheral blood mononuclear cells (PBMCs), although iNKT cells have also been identified in human adipose tissue, and work by Lynch *et al.* (2009) has shown that iNKT cells are enriched in the omentum relative to the blood[33]. Functionally, $CD4^+$ iNKT cells are thought to be more biased towards a Th2-like phenotype, whereas $CD8^+$ iNKT cells may be more Th1-like[122,125,128]. However, $CD4^+$, $CD8^+$ and DN human iNKT cells have all been shown to co-produce IFNγ and IL-4, indicating most human iNKT cells may be phenotypically similar to murine NKT1 cells[125].

Interestingly, human iNKT cell populations have been shown to display differences in their capacity to expand following mitogenic stimulus, as studies by O'Reilly *et al.* (2011), Andrews *et al.* (2020), and Trujillo-Ocampo *et al.* (2020) found that *in vitro* culture of iNKT cells preferentially promotes the expansion of $CD4^+$ iNKT cells[124,125,127]. *In vitro* culture of iNKT cells can also promote the induction of regulatory human iNKT cells. Monteiro *et al.* (2010) and O'Reilly *et al.* (2011) identified increased expression of the regulatory T cell (Treg) markers FOXP3 and CD25 among expanded $CD4^+$ iNKT cells[125,129], and increased CD25 expression was also observed among expanded $CD4^+$ iNKT cells by Trujillo-Ocampo *et al.* (2020)[127]. This aligns with functional analyses by Gumperz *et al.* (2002) and Sag *et al.* (2014) demonstrating that a subset of $CD4^+$ human iNKT cells produce IL-10 after activation[91,122], similar to Tregs. While historically relatively few studies performed transcriptional analysis of human iNKT cells, several recent studies utilizing scRNA-Seq have emerged over the last 2-3 years. A scRNA-Seq cell atlas of developing thymic

cells produced by Park *et al.* (2020) identified a population of NKT cells, and profiling of gene signatures associated with NKT cells versus other T cell subsets identified enrichment of *EOMES*, *IFNG*, *TBX21*, and *NKG7*, suggesting that these are key markers associated with the human NKT cell lineage[130]. Notably, a recent study by Shimizu et al. (2019) found that EOMES is also important in murine iNKT cell development, implicating EOMES as a conserved transcriptional regulator of iNKT cell development[131]. A transcriptomic atlas of human liver identified a population of NKT cells expressing *CD8A* and *CCL5*, with some cells expressing *CD56*; this suggests that human liver is enriched for $CD8^+$ NKT cells, consistent with their more Th1-like profile and the analogous enrichment of NKT1 cells in murine liver[54,59,122,125,128,132]. Separately, the overall transcriptional relatedness of iNKT cells to other immune cell populations, including adaptive T cells, NK cells, γδ T cells, and MAIT cells, was assessed by Gutierrez-Arcelus *et al*. (2019)[133].

More in depth transcriptional characterization of iNKT cells alone has been performed by Erkers *et al.* (2020) and Zhou *et al.* (2020)[134,135]. scRNA-Seq analysis of PBMC iNKT cells at steady state or stimulated *in vitro* with anti-CD3/CD28 by Erkers *et al.* (2020) revealed two distinct populations of activated iNKT cells. One population expressed markers similar to NK cells, including *KLRG1*, *KLRK1*, *GNLY*, *GZMA*, *CCL5* and *PRF1*, genes, while the second population expressed genes associated with adaptive effector T cells and memory T cells, such as *IL2*, *IFNG*, *IL4*, *IL17A*, *BCL6*, *CD40LG* and *CD44*[134]. This work suggests that there are distinct cytotoxic and helper or memory-like arms to the human iNKT cell response, although Erkers *et al,* (2020) did not identify differential expression of CD4 or CD8[134]. Analysis of PBMC iNKT cells by Zhou *et al.* (2020) using scRNA-Seq also identified different functional subpopulations among iNKT cells stimulated with PMA and Ionomycin[135]. While most activated iNKT cells expressed *IFNG*, one distinct population co-expressed *IL4*, *IL13*, *IL10* and *IL2*, whereas a second population demonstrated enrichment of *GZMB*, *GZMH*, and *GNLY,* similar to the previous

study by Erkers *et al.* (2020)[134]. Notably, Zhou *et al.* (2020) also did not report differential CD8 or CD4 expression among iNKT cells, and so the transcription profiles of $CD4^+$, $CD8^+$ and DN cells remain undefined[135]. During my PhD program, I performed re-analysis of published human iNKT cell scRNA-Seq data from Erkers *et al.* (2020), Zhou *et al.* (2020), and Gutierrez-Arcelus *et al*. (2019)[133] to investigate the biology of human iNKT cells, the results of which will be discussed in Chapter 3 of this thesis.

### 1.3.7 Homeostatic functions of iNKT cells

iNKT cells are thought to contribute to a wide range of unconventional homeostatic functions distinct from their roles during immune responses. One notable example is the regulation of adipose tissue homeostasis and body weight by adipose iNKT cells. Studies by Lynch *et al*. (2012), Ji *et al.* (2012), Schipper *et al.* (2012), and Huh *et al.* (2017) have shown that $CD1d^{-/-}$ and $J\alpha18^{-/-}$ mice, which lack iNKT cells, display increased weight gain compared to WT control mice during high fat diet (HFD), and demonstrate metabolic defects such as increased lipid accumulation in the liver and insulin resistance[90,117,136,137]. iNKT cells also become depleted in murine adipose tissue during HFD, and in the circulation during human obesity[90]. Moreover, activation of iNKT cells with αGalCer has been shown to induce adaptive thermogenesis and weight loss in obese mice, coinciding with an expansion of adipose iNKT cells, while the frequency of iNKT cells is increased in the circulation of obese human patients who undergo Roux-en-Y gastric bypass (RYGB) surgery[90,138]. Collectively, therefore, these studies implicate iNKT cells as important regulators of systemic metabolism and weight control, with a particular link to the unique population of iNKT cells enriched in adipose tissue. While a majority of studies in the literature have suggested that iNKT cells play a beneficial role in systemic metabolism, including Lynch *et al*. (2012), Ji *et al.* (2012), Schipper *et al.* (2012), Lynch *et al.* (2015), Lynch *et al.* (2016), Huh *et al.* (2017), and Arora *et al.* (2021)[49,90,117,136–139], it should be noted that several

studies, such as Wu *et al.* (2012) and Satoh *et al.* (2016), have reported that iNKT cells can be detrimental to metabolic health, and may contribute to adipose tissue inflammation during HFD and obesity[140,141]. However, a solution for these apparently contradictory lines of evidence has recently been proposed by LaMarche *et al.* (2020), with the finding that adipose iNKT cell subsets can differentially regulate adipose tissue homeostasis (Figure 1.2)[115].

iNKT cells regulate adipose tissue homeostasis and systemic metabolic homeostasis through several different mechanisms. For example, adipose iNKT cells can directly secrete IL-10, IL-4, IL-13, and IL-2, which can polarize adipose tissue macrophages towards an alternatively activated, M2-like phenotype, expand adipose Tregs, and suppress inflammation in the adipose tissue microevironment[49,90,91,117,136,137]. Recent work by Arora *et al.* (2021) has also shown that activated iNKT cells promote the clearance of senescent preadipocytes in adipose tissue during HFD through targeted cytotoxicity[139], and LaMarche *et al.* (2020) found that iNKT cells could promote NK cell cytotoxicity against adipose tissue macrophages[115], identifying a role for adipose iNKT cells in regulation of preadipocyte and macrophage homeostasis in adipose tissue. Moreover, Lynch *et al.* (2016) demonstrated that adipose iNKT cells can promote production of the thermogenic hormone fibroblast growth factor 21 (FGF21) by adipocytes, inducing the beiging of white adipose tissue (WAT)[138]. Conversely, Wu *et al.* (2012) and Satoh *et al.* (2016) found that iNKT cells can produce pro-inflammatory cytokines during HFD, driving increased inflammation in adipose tissue[140,141]. However, LaMarche *et al.* (2020) showed that adipose iNKT cells can be separated into two functional cohorts based on NK1.1 expression. $NK1.1^{+}$ iNKT cells primarily produced IFNγ, whereas $NK1.1^{-}$ iNKT cells mainly produced Th2 and immunoregulatory cytokines. While $NK1.1^{+}$ and $NK1.1^{-}$ cells were capable of positively regulating adipose tissue homeostasis, either through NK cell trans-activation ($NK1.1^{+}$), or suppression of inflammation ($NK1.1^{-}$), only $NK1.1^{-}$ cells were able to improve metabolic homeostasis after adoptive transfer into mice fed a HFD[115].

Therefore, this work suggests that NK1.1$^{-}$ iNKT cells are beneficial during HFD, whereas NK1.1$^{+}$ iNKT cells, although normally beneficial during homeostasis, may promote inflammation during HFD or diet induced obesity (DIO) through production of IFNy.

While regulation of adipose tissue is perhaps one of the most prominent examples of the unconventional role of iNKT cells in homeostasis, iNKT cells have been shown to perform many other homeostatic functions. For example, Lee *et al.* (2013) found that NKT2 cells produce IL-4 at steady state in the thymic medulla, which was important for several different effects, including conferral of an EOMES$^{+}$ memory-like phenotype to CD8$^{+}$ T cells, increasing production of IgE by B cells, and inducing CCL17 and CCL22 production by dendritic cells (DCs)[60]. In another example, Arora *et al.* (2021) found that activation of iNKT cells during lung injury decreased lung fibrosis through elimination of senescent epithelial and mesenchymal cells, promoting tissue repair[139]. Further published examples of homeostatic iNKT cell functions include tissue repair and resolution of inflammation in the liver (Liew *et al*.; 2017)[142], formation of fat associated lymphoid clusters (FALCs) in visceral adipose tissue (Bénézech *et al*.; 2016)[143], regulation of the immunoglobulin (Ig)A repertoire and induction of regulatory T cells within the gut (De Guinoa *et al*.; 2018)[144], and regulation of marginal zone B cells (MZBs) in lymph nodes (Wen *et al*.; 2011)[145]. Therefore, iNKT cells regulate homeostasis through a diverse set of functions and roles across different tissues.

## 1.4 Activated iNKT cells and the iNKT cell response to antigen

The iNKT cell response to antigen is multifaceted, and can be broken down into several different phases, beginning with rapid activation and cytokine production, followed by proliferation and expansion, and then differentiation of novel memory-like or “trained” iNKT cell populations, as well as long term changes in the responsiveness of iNKT cells to antigen[146]. A defining feature of iNKT cells is that they do not need to undergo differentiation to mount an effector response. By contrast, naive adaptive T cells are quiescent, and must undergo dramatic phenotypic and transcriptional remodeling to differentiate into highly activated effector T cells[147]. This represents a fundamental difference between the adaptive T cell response to antigen, and the response of iNKT cells to antigen. However, like adaptive T cells, iNKT cells undergo expansion after antigenic stimulation, and the induction of memory-like iNKT cell subsets after activation is similar to the differentiation of adaptive memory T cells[146,147]. Therefore, iNKT cell activation is similar to adaptive T cell activation in some respects, but also distinct in fundamental aspects, most prominently the timing and kinetics of the effector response.

### 1.4.1 Overview of the adaptive T cell response to antigen and activation

Naive $CD8^+$ and $CD4^+$ T cell activation begins upon recognition of cognate antigen presented by APCs via MHC class I or II receptors in tandem with ligation of costimulatory molecules such as CD28, as signaling through the TCR alone results in a non-responsive state (anergy) in which T cells fail to respond and are then refractory to further stimulation. TCR ligation and co-stimulation triggers the formation of the proximal signaling complex (PSC), resulting in propagation of the TCR signal into distal signaling pathways[148]. Signal transduction downstream of the PSC, assisted by calcium and integrin/cytoskeletal signaling events, then induces transcription factors that promote T cell activation, including NF-κB, NFAT, AP1 and IRF4[149,150]. T cell

activation also triggers rapid expression of IL-2 and its receptor IL-2Rα. IL-2 signaling induces activation of STAT5 and AP1, and plays a critical role in driving the growth, proliferation, and expansion of nascent activated T cells[151]. The cascade of transcriptional events induced by T cell activation promotes extensive genome-wide chromatin reorganization, facilitating transcriptional and proteomic remodeling of the activated T cell over a period of ~16-24 hours[149,151–155]. After this initial period of activation, nascent activated T cells blast, proliferate, undergo clonal expansion, and acquire effector functionality in response to polarizing cytokine signals, resulting in the emergence of effector T cell populations by ~72-120 hours post-activation[154–157], while some activated T cells differentiate into memory T cells[158,159]. Notably, the entire process of T cell activation, proliferation and differentiation necessitates substantial changes in cellular metabolism, as activated T cells must fuel anabolic pathways and fulfill energetic requirements (see section 1.5)[156,160–163]. After differentiation, clonal effector T cells traffic to sites of infection or inflammation, where antigen re-encounter induces reactivation, allowing effector T cells to engage in cytokine production and kill target cells. As the immune response subsides after pathogen clearance or resolution of inflammation, most effector T cells undergo apoptosis[147,164], leaving behind a cohort of memory T cells.

Many different memory T cells populations have been described, most notably central memory, resident memory, effector memory, and stem-like memory T cells ($T_{CM}$, $T_{RM}$, $T_{EM}$, and $T_{SM}$ cells respectively)[165,166]. Broadly speaking, $T_{SM}$ and $T_{CM}$ cells are more stem-like, displaying a greater capacity for self-renewal, and can differentiate into $T_{EM}$ and effector T cells after reactivation. $T_{EM}$ cells, by contrast, are more terminally differentiated and effector-like than $T_{SM}$ and $T_{CM}$ cells and show a greater capacity for cytotoxicity. $T_{RM}$ cells are tissue resident and remain at local sites where they are poised to respond to secondary infection. Like $T_{EM}$ cells, $T_{RM}$ cells are thought to be more effector-like than $T_{SM}$ and $T_{CM}$ cells, and are thus are considered to be more terminally

differentiated[166]. Therefore, memory T cells exist on a spectrum, and several studies have shown that effector T cell responses can be sustained from long lived stem-like memory T cell populations[100,101]. A suite of transcription factors has been shown to govern the phenotype of memory T cells. Stem-like memory T cells show enrichment for TCF7 (also known as TCF1), BACH2, EOMES, BCL6, ZEB1, ID3, STAT3, and FOXO1, whereas more terminally differentiated effector-like cells show enrichment of T-bet, STAT4, BLIMP1, ID2, and ZEB2, and express the surface receptor KLRG1[166,167]. A general feature of memory T cells is that they display a “poised” chromatin state, by which they can more easily re-differentiate into an effector T cell[168]. Therefore, activation can induce long term transcriptional remodeling of adaptive T cells.

While acute immune activation and resolution is thought to promote the differentiation of memory T cells, chronic activation can promote T cell exhaustion. Exhausted T cells are characterized by their impaired functional capacity, increased expression of PD-1, CTLA-4, and TIM-3, and increased expression of NR4A, NFAT and TOX family transcription factors[166,169–172]. Like memory and effector T cells, exhausted T cells are thought to exist on a gradient. Phenotypic studies have defined two T cell exhaustion states, precursor exhausted T (TPEX) cells and terminally exhausted T cells[100,101,169,173]. TPEX cells show enrichment of some stem-like markers, such as TCF7, SLAMF6 and ID3, and express some immune checkpoint receptors, including PD-1 and CTLA-4. By contrast, terminally exhausted T cells lack expression of stemness markers, show further enrichment of PD-1 and CTLA-4, express terminal exhaustion markers, such as TIM-3, and are strongly functionally impaired. TPEX cells can give rise to exhausted T cells, and therefore may be considered a reservoir for terminally exhausted T cells, analogous to how stem-like memory T cells can act as a reservoir for effector T cells[100,166,174,175]. Interestingly, however, recent studies using checkpoint inhibitors have shown that TPEX cells can give rise to effector T cells after immune checkpoint blockade[101,176,177], suggesting that the exhausted

phenotype of TPEX cells may be reversible, allowing these cells to function like $T_{SM}$ cells.

### 1.4.2 Overview of the iNKT cell response to antigen and activation

In the first instance, activation of iNKT cells triggers a rapid cytokine response[15]. This represents a critical difference between iNKT cells and adaptive T cells, as while naive adaptive T cells must undergo differentiation to acquire effector functionality, activated iNKT cells can immediately produce cytokines upon antigen encounter. Moreover, adaptive T cells must be programmed by cytokine signals to assume a particular phenotype, e.g. Th1, Th2, or Th17, whereas NKT1, NKT2, and NKT17 cells emerge during thymic development. The rapid cytokine response of iNKT cells is facilitated by constitutive expression of cytokine mRNAs at steady state, enabling immediate translation of cytokines upon activation[178,179]. The ensemble of cytokines and secreted factors produced varies between different iNKT cell subsets and across iNKT cells in different tissues, but typical cytokines include IFNy, IL-2, IL-4, IL-13, IL-17A, GZMB, granulocyte-macrophage colony-stimulating factor (GM-CSF), and tumor necrosis factor (TNF)α[17,49,60].

Kinetically, iNKT cells rapidly produce a burst of cytokines within ~4-5 hours[17], but iNKT cell cytokine production can continue for several days[15,142,146,180]. Thereafter, the iNKT cell cytokine response gradually diminishes in the absence of further stimulation[15]. The cytokines produced by iNKT cells can transactivate other cells, including NK cells, adaptive T cells, neutrophils, macrophages, DCs, and B cells[14,115,181–191], enabling iNKT cells to orchestrate and potentiate immune responses. Cytokines produced by other immune cells can also signal to iNKT cells, leading to cross talk[192–194]. Activated iNKT cells upregulate expression of T cell activation markers such as PD-1, CD69, Nur77, CD25, and ICOS, and upregulate PLZF, although the kinetics of PLZF upregulation remain undefined, while expression of NK1.1 is reduced among

activated iNKT cells[59,74,91,195–197]. Activation of iNKT cells also triggers TCR downregulation by 6-8 hours post-activation, which creates a “blind spot” during which iNKT cells cannot be detected *in vivo*, until iNKT cells re-upregulate their TCR around 24-48 hours post-activation[198–200]. Transcriptional characterization of activated iNKT cells has been limited to date, and the gene programs underpinning iNKT cell effector function are not well defined.

Antigenic stimulation also induces iNKT cell proliferation, resulting in a massive expansion of iNKT cells within 2-3 days; for example, the number of murine splenic iNKT cells increases by ~10-15 fold after *in vivo* stimulation with αGalCer[198,200]. Expanded iNKT cells retain their ability to produce cytokines in response to further stimulation[93], and display enrichment of PLZF relative to resting iNKT cells[74], but their phenotype has not been explored in detail. After 72 hours the expanded pool of iNKT cell starts to contract as most of the expanded iNKT cells undergo apoptosis, leading to a return to baseline iNKT cell frequencies within 1-2 weeks[198,200]. Novel memory-like or “trained” iNKT cell populations also start to appear 3-7 days post-activation. These include follicular helper-like iNKT ($NKT_{FH}$) cells, which are similar to adaptive follicular helper T ($T_{FH}$) cells[92,201–205], and $KLRG1^+$ iNKT cells, which may be functionally similar to adaptive effector $CD8^+$ T cells[92,206].

Interestingly, while $NKT_{FH}$ and $KLRG1^+$ cells are most numerous at ~5-7 days post-activation, and their frequency declines thereafter, work by Shimizu *et al.* (2014, 2019), and Murray *et al.* (2021) has demonstrated long term persistence of these populations up to 30 days post-activation[92,131,206], suggesting that there is lasting modification of the iNKT cell repertoire after activation, which could constitute a form of immunological memory or trained immunity[207]. Numerous studies have also found that αGalCer can induce iNKT cell anergy, as secondary activation of iNKT cells previously stimulated with αGalCer has been shown to produce a muted, tolerogenic response, potentially similar to exhausted T cells[195,208]. The mechanism(s) underpinning this phenomenon are unclear. Prior activation of iNKT cells with αGalCer has

also been shown to promote the expansion of iNKT cells that produce IL-10, known as NKT10 cells, which are typically rare outside of adipose tissue. Therefore, the response of iNKT cell to antigens such as αGalCer presents an interesting dichotomy, whereby iNKT cells are “stunned” by αGalCer (Sullivan *et al*; 2005) and this can result in either activation or anergy[209]. Overall, the iNKT cell response to antigen and activation is multifaceted, reflective and mirrors the heterogeneity of iNKT cells at steady state (Figure 1.3).

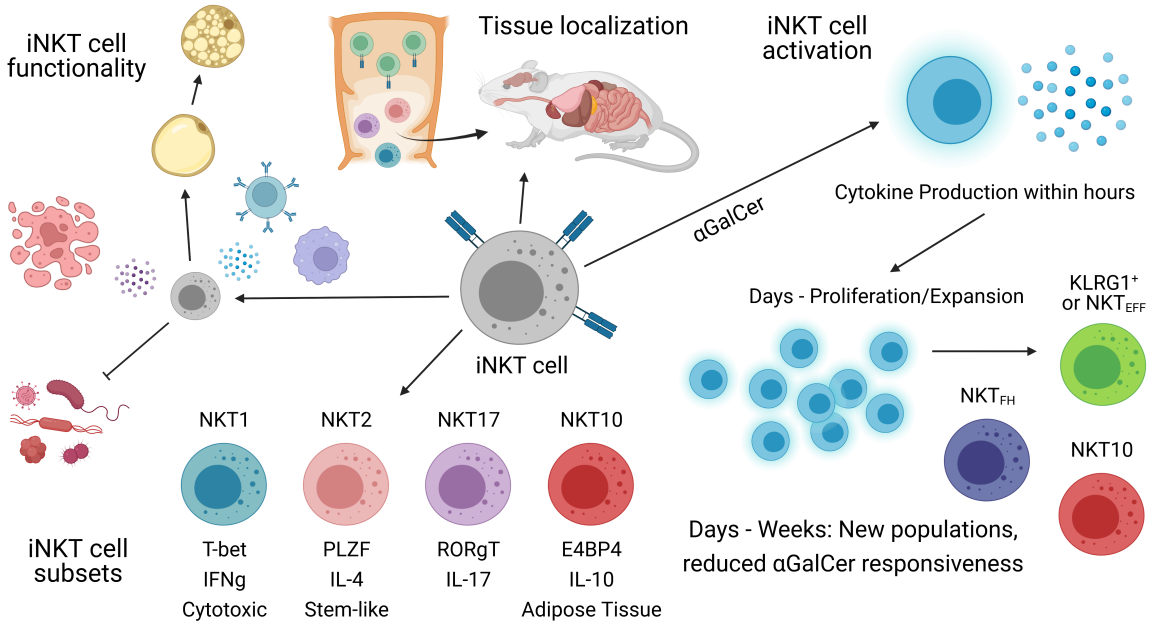



**Figure 1.3: iNKT heterogeneity and the multifaceted iNKT response to antigenic stimulation.** iNKT cells exhibit multiple levels of heterogeneity, both at steady state and during immune responses. A branching thymic developmental pathway generates phenotypically distinct iNKT cell subsets, including NKT1, NKT2, and NKT17 cells. iNKT cells also differentially populate individual tissues and organs, which can strongly influence their function. For example, regulatory NKT10 cells are enriched in adipose tissue. Functionally, iNKT cells can direct, potentiate, and participate in diverse immune responses against tumors, bacteria, fungi, and viruses. The response of iNKT cells to lipid antigens, such as αGalCer, is also multifaceted. TCR ligation initially triggers rapid cytokine production within minutes to hours. Later, over several days, iNKT cells proliferate, producing an expanded pool of effector cells. Most of these cells eventually undergo apoptosis, but memory-like or “trained” iNKT cells, such as $NKT_{FH}$ and $KLRG1^{+}$ iNKT cells, can persist for months after activation. Activation can also render iNKT cells anergic to further antigenic stimulation, and secondary iNKT cell activation is associated with an increase in the frequency of regulatory NKT10 cells.

### 1.4.3 Framing iNKT cell activation and responses: Pathogen Immunity

iNKT cells play an important role in the immune response to bacterial pathogens. For example, a study by Kawakami *et al.* (2003) found that Jα18$^{-/-}$ mice infected with *Streptococcus pneumoniae* (*S.pneumoniae*) showed increased bacterial burden in the lungs, and impaired recruitment of neutrophils, suggesting that iNKT cells play an important role in the immune response to *S.pneumoniae*[210]. Subsequent work by Nakamatsu *et al.* (2007) found that transfer of liver mononuclear cells (which are ~20-40% iNKT cells in C57BL/6 mice) from WT but not Jα18$^{-/-}$ or IFNγ$^{-/-}$ mice was able to restore neutrophil recruitment and reduce bacterial burden. Furthermore, treatment of infected mice with αGalCer enhanced bacterial clearance and neutrophil recruitment, and this effect was dependent on IFNγ[211], demonstrating that production of IFNγ by activated iNKT cells is important for bacterial clearance from the lung. Mechanistically, work by Kinjo *et al.* (2011) and Girardi and Yu *et al.* (2011) found that iNKT cells can directly recognize pneumococcal glycolipids through their TCR[212,213], while a study by Bridl *et al.* (2011) found that iNKT cell activation is enhanced by IL-12 released from APCs in response to toll-like receptor (TLR) ligands present on *S.pneumoniae*[214]. Therefore, iNKT cells can become activated following direct recognition of bacterial antigens, or through downstream cytokine signals from other immune cells during bacterial infection.

iNKT cells have also been shown to promote adaptive immune responses to S.*pneumoniae* through the action of $NKT_{FH}$ cells. Work by Bai *et al.* (2013) and Cavallari *et al*. (2014) found that immunization of mice with liposomes containing pneumococcal capsular polysaccharide (CPS) and the αGalCer analogue PBS57 was sufficient to induce $NKT_{FH}$ cell development, and mice treated with these liposomes showed a CD1d-dependent enhancement of IgG1 production[204,215]. This indicates that iNKT cells can induce humoral antibody responses against bacterial pathogens, collectively defining a broad role for iNKT cells across different stages of the immune response towards

*S.pneumoniae*. Interestingly, bacterial infection can impart lasting effects upon the responsiveness of iNKT cells to antigen. Work by Choi *et al.* (2008) and Kim *et al.* (2008) showed that iNKT cells from mice infected by one of several different bacteria, including *Escherichia Coli*, *Listeria Monocytogenes*, and *Mycobacterium Bovis*, demonstrated blunted secondary activation after *in vivo* stimulation with αGalCer[216,217], suggesting that bacterial infection can render iNKT cells anergic, similar to prior activation with αGalCer.

iNKT cells can also participate in immune responses against fungal pathogens. For example, iNKT cells have been documented to play an important role in combating infection by *Aspergillus fumigatus* (*A.fumigatus*), a saprophytic fungus implicated in opportunistic invasive fungal infections. Cohen *et al.* (2011) found that $CD1d^{-/-}$ mice displayed poor control of *A.fumigatus* infection compared to WT mice, suggesting that iNKT cells are important for mounting an effective response to *A.fumigatus*[218]. Surprisingly, although CD1d recognition was required for iNKT cell responses against *A.fumigatus*, Cohen *et al.* (2011) found that iNKT cells were not activated by fungal lipid-TCR interactions, but rather by IL-12 produced by APCs in response to Dectin-1-MyD88 signaling. A similar mechanism was also identified for other fungal pathogens, including *Candida albicans*, *Histoplasma capsulatum* and *Alternaria alternata*, suggesting that this may be a conserved mechanism by which iNKT cells become activated in response to fungal pathogens[218].

iNKT have also been linked with immune responses against many different viruses, including human immunodeficency virus, hepatitis B virus, respiratory syncytial virus, encephalomyocarditis virus, herpes simplex virus, coxsackievirus B (CVB), lymphocytic choriomeningitis virus, H1N1 swine influenza, and influenza A virus[219–229], as well as the murine model viruses murine cytomegalovirus (MCMV) and Friend retrovirus (FV)[185,230,231]. Other evidence for the role of iNKT cells in anti-viral immunity has been gleaned from rare cases in which humans display inborn defects in their innate immune system. For example, patients with mutations in the adapter protein SAP (also

known as SH2D1A) are deficient in iNKT cells, and they display a strikingly increased susceptibility to Epstein-Barr virus (EBV) infection[232]. Interestingly, a similar phenotype has also been described for patients with mutations in X-linked inhibitor-of-apoptosis (XIAP)[233], indicating that iNKT cells may be key mediators of the immune response against EBV. Overall, this work indicates that iNKT cells play an important role in immunity against a wide variety of different pathogens, including bacteria, fungi and viruses.

### 1.4.4 Framing iNKT cell activation and responses: Tumor Immunity

Ever since Kobayashi *et al.* (1995) first identified αGalCer in a screen for compounds with anti-tumor activity[10] there has been interest in utilizing iNKT cells for therapeutic interventions in cancer. However, clinical trials involving αGalCer have largely been disappointing to date[234,235], which may be due in part to the low frequency of iNKT cells present at baseline in many individuals, as well as the persistent problem of iNKT cell anergy after αGalCer exposure[236]. However, despite these setbacks, interest in the anti-tumor potential of iNKT cells has persisted, and there are ongoing studies investigating novel approaches for iNKT cell utilization in cancer treatment, including hematopoietic stem cell-engineered iNKT cells (HSC-iNKTs) and chimeric antigen receptor (CAR) iNKT cells[237,238].

iNKT cells are generally thought to play a protective role during cancer. Work by Kobayashi *et al.* (1995), Cui *et al.* (1997), Kawano *et al.* (1998), Nakagawa *et al.* (1998, 2001), Smyth *et al.* (2000, 2002), Crowe *et al.* (2002), Hayakama *et al.* (2001; 2003), Amborsino *et al.* (2007), Shimuzu *et al.* (2007), and Paget *et al.* (2012) has demonstrated that *in vivo* activation of iNKT cells with αGalCer or IL-12 can promote tumor rejection across a wide variety of different murine cancer models, either through transactivation of other immune cells, including NK cells, $CD8^+$ T cells and γδ T cells, and/or direct killing of tumor cells. Moreover, mice lacking iNKT cells were found to be more susceptible to

spontaneous tumor development in spontaneous cancer models and to developing tumors after treatment with carcinogenic agents[10,13,187,239–252]. This indicates that iNKT cells are capable of mounting potent anti-tumor responses, and that iNKT cells play a role in tumor immunosurveillance. Several studies have also shown that human iNKT cells can kill tumor cells via a CD1d-dependent mechanism[253–255]. Moreover, reduced frequencies of iNKT cells in the peripheral blood of cancer patients has been correlated with poorer outcomes in several malignancies, including acute myeloid leukaemia and head and neck squamous cell carcinoma[256,257], while accumulation of iNKT cells in colorectal carcinoma was associated with prolonged survival[258,259]. Therefore, current evidence suggests that iNKT cells largely play a beneficial role in anti-tumor immunity in humans and mice.

Interestingly, however, a recent report by Wang *et al.* (2017) identified a subset of iNKT cells in intestinal polyps that could suppress Th1 immune responses and support Treg accumulation. Using an $APC^{Min/+}$ mouse model, in which mice spontaneously develop mammary and intestinal adenomas[260], Wang *et al.* (2017) found that iNKT cells present in intestinal polyps demonstrated an unusual phenotype characterized by enhanced production of IL-10 and IL-17A[261]. These polyp iNKT cells were $PLZF^{low}$, showed reduced expression of NK1.1 and CD4 compared to splenic iNKT cells, and were $CD69^{+}$, suggesting that they might be similar to adipose iNKT cells[49,261]. Like adipose iNKT cells, polyp iNKT cells were found to regulate Tregs, as polyps from $Apc^{Min/+}Ja18^{-/-}$ had fewer Tregs, and $Apc^{Min/+}Ja18^{-/-}$ Tregs showed reduced expression of FOXP3, CD25 and CD69[261]. Depletion of polyp iNKT cells was associated with a global increase in expression of inflammatory genes such as *Ifng* and *Nos2*, and a switch from an M2-like to M1-like phenotype among polyp macrophages. Subsequent work from the same group found that a combination of αGalCer and anti-PD-1 therapy significantly reduced the number of polyps in the small and large intestine, and this was associated enrichment of $T\text{-}bet^{+}$ iNKT cells[262]. Therefore, the immunosuppressive and pro-

tumor role of iNKT cells in this cancer model may be limited to the PLZF$^{low}$ iNKT cell population. Enrichment of immunosuppressive tumor-associated iNKT cells has also been identified in the context of glioma by Tang *et al.* (2014). *In vitro* culture of human PMBC iNKT cells with primary glioma cells induced a population of iNKT cells that co-produced IL-10 and IL-6, and showed reduced expression of IFNy, perforin and FASL compared to control iNKT cells[263]. Therefore, some iNKT cells may potentially contribute to the suppression of immune responses during cancer.

### 1.4.5 Memory-like KLRG1$^+$ iNKT cells

Long lived memory-like KLRG1$^+$ iNKT cells were first identified in a study by Shimizu *et al.* (2014). Immunization of mice with αGalCer–loaded DCs (DC/Gal) produced an expansion of KLRG1$^+$ iNKT cells in the lungs of mice after 7 days, while KLRG1$^+$ iNKT cells were almost completely absent in naive mice. KLRG1$^+$ iNKT cells were also detectable in the spleen and the liver after DC/Gal immunization and were found to persist in the lung for at least 8-9 months, demonstrating that KLRG1$^+$ iNKT cells are a long lived population of memory-like iNKT cells[206]. Phenotyping of KLRG1$^+$ iNKT cells revealed that these cells were CD27$^-$ CD44$^+$ CD122$^+$ NK1.1$^+$ NKG2D$^+$ CD49d$^+$ granzyme A (GZMA)$^+$, and showed enrichment of *Ifng*, *Fasl*, *Ccl3*, *Ccl4*, *Tbx21*, *Eomes*, and *Runx3*, while expression of *Il4* was lower in KLRG1$^+$ iNKT cells than naive iNKT cells. Functionally, KLRG1$^+$ iNKT cells were found to produce IFNy in response to B16 tumor challenge, and DC/Gal immunization reduced B16 lung metastasis burden in tumor-bearing mice, suggesting that KLRG1$^+$ iNKT cells might display anti-tumor activity[206].

Recent studies by Shimizu *et al.* (2019) and Murray *et al.* (2021) have further investigated the origin and phenotype of KLRG1$^+$ iNKT cells. Having previously detected enrichment of *Eomes* in KLRG1$^+$ iNKT cells, Shimizu *et al.* (2019) found that DC/Gal immunization of CD4-Cre *Eomes*$^{fl/fl}$ mice but not WT mice

failed to generate KLRG1$^+$ iNKT cells, indicating that EOMES is required for the differentiation of KLRG1$^+$ iNKT cells[131]. Separately, Murray *et al.* (2021) used a T-bet tdtomato reporter mouse model[264] to demonstrate that ~96% of non-NKT$_{FH}$ splenic iNKT cells at 6 days post-αGalCer (termed NKT$_{eff}$ cells), which were strongly enriched for KLRG1$^+$ iNKT cells, had previously expressed T-bet[92], suggesting that some NKT1 cells may differentiate into KLRG1$^+$ iNKT cells after activation with αGalCer. Bulk RNA-Seq gene set enrichment analysis (GSEA)[265] of NKT$_{eff}$ cells identified enrichment of gene signatures associated with CD8$^+$ effector T cells, matching previous analysis of KLRG1$^+$ iNKT cells by Shimizu *et al.* (2014)[206], and ATAC-Seq analysis showed that accessible chromatin regions in NKT$_{eff}$ cells were enriched for T-bet, Runt, and Ets domain-associated motifs, similar to NKT1 cells. Among NKT1, NKT2 and NKT17 cells, NKT$_{eff}$ cells were most transcriptionally similar to NKT1 cells, then NKT2 cells, and were least similar to NKT17 cells[92]. Murray *et al.* (2021) also found increased ATAC-seq signals within loci for genes encoding GZMA, GZMB, KLRG1, CX3CR1 and SPRY2 among NKT$_{eff}$ cells[92]. Interestingly, there is also evidence to suggest that KLRG1$^+$ iNKT cells are present in humans, as Erkers *et al.* (2020) identified enrichment of *KLRG1* among a majority of PBMC steady state iNKT cells and among some iNKT cells activated with anti-CD3/CD28. Furthermore, iNKT cells expressing KLRG1 displayed co-enrichment of NK cell receptors and cytotoxic cell markers previously identified in murine KLRG1$^+$ iNKT cells, including *GZMA*, and *KLRK1* (NKG2D)[134]. Overall, work in both mice and humans has identified a Th1-like KLRG1$^+$ iNKT cell subset which is phenotypically similar to CD8$^+$ effector T cells and NK cells and constitutes a memory-like population induced after antigen challenge in mice.

### 1.4.6 Memory-like NKT$_{FH}$ cells

NKT$_{FH}$ cells are typically defined as BCL6$^+$ PD-1$^+$ CXCR5$^+$ ICOS$^{high}$ iNKT cells that produce IL-21[201,203,204,266]. Coquet *et al.* (2007; 2008) showed that there

was an NK1.1$^{-}$ population of murine iNKT cells that produced the $T_{FH}$ cytokine IL-21 after 2-3 days of TCR stimulation, suggesting that activation might induce a $T_{FH}$ cell-like population of iNKT cells[107,267,268]. Subsequent studies by Chang *et al.* (2011) and Tonti *et al.* (2012) identified enrichment of PD-1$^{+}$ CXCR5$^{+}$ ICOS$^{high}$ BCL6$^{+}$ iNKT cells in the spleen and lymph nodes after treatment with αGalCer, which were termed $NKT_{FH}$ cells. $NKT_{FH}$ cells were not present in naive mice but appeared as early as 3 days after challenge with αGalCer, and were most enriched 5-7 days after challenge. Notably, $NKT_{FH}$ cells did not develop in mice lacking BCL6 or CD28[201,266], indicating that TCR stimulation and BCL6 expression were required for $NKT_{FH}$ cell differentiation. Chang *et al.* (2011) also profiled T cells from human tonsils (removed after routine tonsillectomy) and found that ~10% of iNKT cells expressed PD-1 and CXCR5, suggesting that $NKT_{FH}$ cells are also present in humans[201]. Similar to the early observations by Coquet *et al.* (2007; 2008), Chang *et al.* (2011) found that most $NKT_{FH}$ cells lacked expression of NK1.1[107,201,267]. $NKT_{FH}$ cells were also predominantly CD4$^{+}$, showed enrichment for the inhibitory receptor BTLA, and had reduced expression of IL-7R, while human $NKT_{FH}$ cells were enriched for expression of the differentiation marker CD57[201]. Functionally, King *et al.* (2012) used *Il21* deficient iNKT cells to determine that $NKT_{FH}$ cells were an important source of IL-21 during immune responses derived from immunization with lipid antigen[269]. Like $T_{FH}$ cells, $NKT_{FH}$ cells have been shown to direct B cell responses through cognate interactions, and can promote the formation of early germinal centers[201,269]. $NKT_{FH}$ cells also appear to be a long-lived memory-like population of memory-like iNKT cells, as work by Chen *et al.* (2018) found that re-stimulation of $NKT_{FH}$ cells can induce IL-21 production up to 60 days after initial immunization and activation of iNKT cells[203].

Recently, Murray *et al.* (2021) performed bulk RNA-Seq and ATAC-Seq of murine splenic $NKT_{FH}$ cells isolated 6 days after *in vivo* stimulation with αGalCer. Comparison with steady state NKT1, NKT2 and NKT17 cells revealed that $NKT_{FH}$ cells were transcriptionally distinct from all three subsets,

although $NKT_{FH}$ cells displayed the most transcriptional overlap with NKT2 cells, then NKT1 cells, and were least similar to NKT17 cells. Profiling of accessible chromatin regions in $NKT_{FH}$ cells showed increased accessibility at loci encoding IL-21 and PD-1, aligning with previous work on $NKT_{FH}$ cells[201–203,205,269], and accessible chromatin regions in $NKT_{FH}$ cells showed enrichment for RHD domain transcription factor motifs, especially NFAT, and bZIP motifs associated with AP1 family transcription factors[92]. Murray *et al.* (2021) also profiled the origin of $NKT_{FH}$ cells using T-bet fate mapping. Although differentiated $NKT_{FH}$ cells lacked expression of T-bet, analysis of iNKT cells from T-bet tdtomato reporter mice[264] revealed that ~75% of $NKT_{FH}$ cells had previously expressed T-bet, suggesting that $NKT_{FH}$ cells can arise from both NKT1 cells and $Tbet^{neg}$ populations, such as NKT2 or NKT17 cells[92]. Similarly, Rampuria *et al.* (2015) found that $NKT_{FH}$ cells could differentiate from adoptively transferred steady state $PD\text{-}1^{-}$ iNKT cells after *in vivo* activation with αGalCer[202], confirming that $NKT_{FH}$ cells arise from non-$NKT_{FH}$ cells. Therefore, $NKT_{FH}$ cells are an inducible memory-like population of iNKT cells that differentiate from non-$NKT_{FH}$ cells.

### 1.4.7 iNKT cell anergy

While initial stimulation of iNKT cells with αGalCer elicits a potent effector response, numerous studies have documented that subsequent stimulation with αGalCer fails to recapitulate this initial effector response. iNKT cells previously exposed to αGalCer demonstrate reduced cytokine production and proliferation in response to secondary αGalCer stimulation, and there is a shift towards production of regulatory cytokines such as IL-10[91,195,208]. This phenotype was first reported by Burdin *et al.* (1999) and Singh *et al.* (1999), who found that found that immunization or repeated *in vivo* activation of iNKT cells with αGalCer promoted increased production of IL-4 and IL-10, and reduced production of IFNγ by splenic iNKT cells and conventional T cells[16,191]. Similarly, immunization of mice with αGalCer was found to protect against the

development of type 1 diabetes[189,270–272] and experimental autoimmune encephalitis (EAE)[273–275]. Interestingly, Parekh *et al.* (2005) found that while αGalCer-pretreated (αGCPT) iNKT cells were hyporesponsive to secondary αGalCer stimulation, stimulation of αGCPT iNKT cells with PMA and Ionomycin produced an effector cytokine response similar to steady state iNKT cells. Moreover, supplemental administration of exogenous IL-2 in the presence of αGalCer was sufficient to rescue activation-induced proliferation and expansion of αGCPT iNKT cells[208]. Therefore, this work suggested that the altered secondary response of αGCPT iNKT cells to αGalCer is at least partially because αGCPT iNKT cells are refractory to TCR stimulation, although Parekh *et al.* (2005) did not address IL-10 production by αGCPT iNKT cells.

The phenotype of tolerogenic αGCPT iNKT cells has been further explored by Iyoda *et al.* (2010) and Sag *et al*. (2014)[91,195]. αGCPT iNKT cells show increased expression of PD-1 relative to steady state iNKT cells; while Chang *et al.* (2008) suggested that PD-1 is important for limiting αGCPT function, Iyoda *et al.* (2010) did not find a role for PD-1 in αGCPT anergy[195,276]. αGCPT iNKT cells demonstrate reduced upregulation of CD25, Nur77 and CD69 upon reactivation, and show reduced expression of cytokines such as IFNγ, while producing more IL-10[91,195,208]. Sag *et al.* (2014) found that αGCPT cells showed enrichment of Treg markers, including CD4, NRP1, CTLA-4, and FR4, while displaying reduced expression of NK1.1 and CD122[91]. Interestingly, αGCPT iNKT cells also demonstrate increased expression of CXCR5, ICOS, CD49d and KLRG1, suggestive of $NKT_{FH}$ and $KLRG1^{+}$ iNKT cell enrichment. Sag *et al.* (2014) also profiled the activation and proliferation kinetics of αGCPT iNKT cells and examined their cytotoxic capacity. While Parekh *et al.* (2005) showed that αGCPT iNKT cells proliferate and expand less after αGalCer challenge, Sag *et al.* (2014) unexpectedly found that αGCPT iNKT cells proliferate more than steady state iNKT cells at rest, similar to the phenotype of adipose iNKT cells as described by LaMarche *et al.* (2020)[91,115,208]. While Parekh *et al.* (2005)

found that αGCPT iNKT cells were less able to control the growth and metastasis of B16 tumors, direct assessment of αGCPT iNKT cell cytotoxicity by Sag *et al*. (2014) showed that αGCPT iNKT cells do not show greatly decreased cytotoxic capacity compared to that of steady state iNKT cells, suggesting that the reduced ability of αGCPT iNKT cells to control tumor metastases might be primarily due to reduced expression of IFNγ and decreased transactivation of other immune cell populations, such as NK cells[91], especially since B16 tumor cells do not express CD1d[277].

While iNKT cell anergy has been most studied in the context of prior activation of iNKT cells with αGalCer, iNKT cells can also become anergic under other circumstances. For example, a study by Braun *et al.* (2010) found that iNKT cells from apolipoprotein E-deficient ($apoE^{-/-}$) mice demonstrated reduced expansion and cytokine production after *in vivo* αGalCer administration, and showed increased expression of PD-1, similar to αGCPT iNKT cells[278]. Braun *et al.* (2010) also showed that $apoE^{-/-}$ iNKT cell anergy was not due to defects in antigen presentation, and addition of exogenous IL-2 with αGalCer was sufficient to rescue $apoE^{-/-}$ iNKT cell proliferation, matching previous findings in αGCPT iNKT cells[208,278]. Conversely, loss of αGalCer-induced anergy was observed in iNKT cells from mice deficient in tuberous sclerosis 1 (TSC1), which is a negative regulator of mTOR signaling. Wu *et al.* (2014) found that iNKT cells from $Tsc1^{-/-}$ mice were resistant to αGalCer-induced anergy and showed significantly increased expansion and cytokine production in response to secondary antigen challenge compared to WT mice. Moreover, αGCPT $Tsc1^{-/-}$ iNKT cells showed reduced expression of PD-1 compared to WT αGCPT iNKT cells, and superior control of B16F10 melanoma metastases[279]. Therefore, this work showed that loss of mTOR inhibition could overcome or prevent anergy in αGCPT iNKT cells, while also implicating mTOR as a key regulator of iNKT cell activation.

Recently, a study by Kumar *et al.* (2020) linked sustained overexpression of Nur77 ($Nur77^{tg}$) with reduced responsiveness of iNKT cells to αGalCer. $Nur77^{tg}$

iNKT cells showed increased steady state expression of PD-1, and were capable of recognizing αGalCer, but showed reduced expression of CD69 and reduced cytokine production after activation[280]. Notably, Nur77 has been found to promote tolerance and exhaustion in conventional T cells, especially in combination with TOX and NFAT transcription factors, suggesting that Nur77 could play a similar role in iNKT cells[170,172]. iNKT cells are known to upregulate Nur77 after activation[59], and Lynch *et al*. (2015) found that adipose iNKT cells demonstrate constitutive enrichment of Nur77 at steady state[49], correlating with the reduced cytokine response of adipose iNKT cells after αGalCer. Interestingly, Kumar *et al.* (2020) also found that a subset of $Nur77^{tg}$ iNKT cells expressed FOXP3, which is suggestive of a regulatory iNKT cell phenotype[280].

### 1.4.8 Regulatory iNKT cells

While regulatory iNKT cells are typically rare under steady state conditions, except in adipose tissue[49,91], they represent a conserved population of iNKT cells present in both mice and humans and have been identified across many different organs in mice, including the spleen, liver, adipose tissue and lungs[91,281]. Several reports have also identified increased production of IL-10 by iNKT cells previously stimulated with αGalCer *in vivo* or *in vitro*, indicating that regulatory iNKT cells become enriched after αGalCer activation[16,91,93]. Moreover, induced NKT10 cells (iNKT10) cells are long lived[91], and therefore could be considered a memory-like population, similar to $NKT_{FH}$ or $KLRG1^{+}$ iNKT cells. Interestingly, there is evidence that regulatory iNKT cells may be diverse, as different reports have variously identified E4BP4, FOXP3, and YY1 as markers and/or regulators of NKT10 cells[49,115,129,281]. Functionally, NKT10 cells have been implicated in a suite of disease models, including type I diabetes[189,271,272], EAE[273–275,282], alcoholic hepatosteatosis[283], colorectal cancer[261], and DIO[90,115], suggesting that regulatory iNKT cells may play an important role in the context of disease and iNKT cell responses.

While Lynch *et al.* (2015) and LaMarche *et al.* (2020) profiled the phenotype of regulatory cells in adipose tissue, Sag *et al.* (2014) profiled regulatory cells outside of adipose tissue, before and after αGalCer stimulation. Approximately 0.5-2% of iNKT cells in the spleen were found express IL-10 after a single stimulation with αGalCer or PMA/Ionomycin, and NKT10 cells were also identified among $CD4^+$ iNKT cells from human PBMCs at a frequency of <1%[91], matching previous work by Gumperz *et al.* (2002) showing that a subset of human $CD4^+$ iNKT cells can produce IL-10[122]. By contrast, ~5-6% of murine αGCPT iNKT cells produced IL-10 after secondary αGalCer stimulation[91]. Phenotypically, NKT10 cells were $NK1.1^-$ $NRP1^+$ $PD\text{-}1^+$ $SLAMF6^+$ $FR4^{high}$, suggesting that they might be similar to Tregs or NKT2 cells, and NKT10 cells also expressed CD49d, similar to memory-like $KLRG1^+$ iNKT cells[91,206]. Sag *et al.* (2014) found that NKT10 cells did not produce IL-17A, did not express BCL6, and did not express FOXP3[91], similar to the phenotype of adipose iNKT cells described by Lynch *et al.* (2015) and LaMarche *et al.* (2020)[49,115]. Therefore, this work suggested that regulatory NKT10 cells are a distinct iNKT cell subset which is present at low frequencies outside of adipose tissue under steady state conditions but expands after αGalCer treatment. Interestingly, a study by Cameron *et al.* (2018) found that thymic iNKT cells cultured *in vitro* for 48-72 hours with DC/Gal could co-produce IL-10 with IFNγ, IL-4 or IL-17A after re-stimulation with PMA/Ionomycin[93], suggesting that NKT17 cells and other iNKT cell populations might acquire the ability to produce IL-10 after chronic stimulation, or during the proliferative, expanded phase of iNKT cell activation 48-72 hours post-αGalCer. However, it remains to be seen whether this finding translates to iNKT cells *in vivo*.

While Sag *et al.* (2014) and others did not identify FOXP3 expression among NKT10 cells[49,91,115], several other studies have identified $FOXP3^+$ iNKT cells[125,129,284]. Monteiro *et al.* (2010) and O'Reilly *et al.* (2011) identified enrichment of $FOXP3^+$ $CD4^+$ human iNKT cells after *in vitro* expansion[125], while Engelmann and Farkas *et al.* (2011) found that a small subset (<3%) of iNKT

cells from human PBMCs expressed FOXP3, the expression of which was increased upon activation with either anti-CD3 or αGalCer[284]. Monteiro *et al.* (2010) identified a population of FOXP3$^+$ CD25$^+$ iNKT cells in the cervical lymph nodes (CLNs) of mice immunized with αGalCer, which was associated with protection from development of EAE[129]. These FOXP3$^+$ CD25$^+$ iNKT cells could be differentiated *in vitro* from steady state iNKT cells upon stimulation with anti-CD3 in the presence of IL-2 and TGF-β for 72 hours. Phenotypically, FOXP3$^+$ iNKT cells displayed enrichment of Treg markers such as CTLA-4 and GITR, were NK1.1$^-$, and a minority expressed CD4[129]. Interestingly, Monteiro *et al.* (2010) found that FOXP3$^+$ iNKT cells did not emerge *in vivo* or differentiate *in vitro* in the absence of TGF-β, suggesting that TGF-β is an essential regulator of FOXP3$^+$ iNKT cells. Functionally, the authors of this study did not demonstrate IL-10 production by FOXP3$^+$ iNKT cells but did show that FOXP3$^+$ iNKT cells could inhibit the proliferation of CD4$^+$ T cells after *in vitro* activation with anti-CD3, via a contact-dependent GITR-mediated mechanism[129]. Therefore, this study suggests that regulatory iNKT cells can express FOXP3, although it is unclear if FOXP3$^+$ iNKT cells produce IL-10.

Lack of expression of the transcriptional repressor Yin Yang 1 (YY1) has also recently been linked with regulatory NKT10 cells. Darcy *et al.* (2020) identified a conserved population of YY1$^{low}$ iNKT cells, which were PLZF$^{low}$ T-bet$^{low}$ RORγT$^-$ CD44$^+$ and present in spleen, liver, adipose tissue and lung at steady state. Functionally, YY1$^{low}$ iNKT cells produced little IFNγ and IL-4 upon *in vivo* stimulation with αGalCer, and instead showed increased production of IL-10, and had preformed *Il10* mRNA at steady state, similar to how other iNKT cells express *Ifng* and *Il4* mRNA at steady state[178,179], suggesting that YY1$^{low}$ iNKT cells are a regulatory NKT10 population[281]. However, while YY1$^{low}$ iNKT cells expressed PD-1, similar to other reported NKT10 cell populations, YY1$^{low}$ iNKT expressed low levels of NRP1, CD49d and ICOS, unlike iNKT10 cells induced after αGalCer immunization[91], suggesting that YY1$^{low}$ iNKT cells are a distinct population of NKT10 cells. Interestingly, Darcy *et al.* (2020) identified

enrichment of YY1$^{low}$ iNKT cells in CT26 colon cancer, B16F10 melanoma and D4M3A melanoma tumors, indicating that YY1$^{low}$ iNKT cells accumulate in murine tumors, although the authors could not detect IL-10 expression among these tumor-infiltrating YY1$^{low}$ iNKT cells[281]. Notably, the phenotype of YY1$^{low}$ iNKT cells bears a strikingly resemblance to the tumor-associated polyp iNKT cells previously identified by Wang *et al.* (2017)[261].

## 1.5 iNKT cell immunometabolism

Cellular metabolism plays a critical role in fueling and regulating immune responses[285] and has been shown to delineate different immune populations[156]. Since cellular metabolism plays an important role in modulating the phenotype and function of adaptive T cells[152,156,160,163], NK cells[162,286–289], γδ T cells[109], and MAIT cells[83,290], it is worth considering how cellular metabolism impacts upon the development, differentiation, and response of iNKT cells to antigen.

### 1.5.1 Introduction to T cell metabolism

Adaptive $CD4^+$ and $CD8^+$ cells utilize distinct metabolic programs at different stages of their life cycle. Naive T cells are relatively metabolically quiescent, and mainly rely on oxidative phosphorylation for survival and homeostasis. Activation of naive T cells triggers metabolic remodeling towards an aerobic glycolytic phenotype, whereby activated T cells rapidly upregulate glycolysis, amino acid uptake and metabolism, and polyamine metabolism, and substantially increase their metabolic rate[152,156,161,162,291]. Activated T cells also shunt metabolic intermediates into anabolic pathways such as lipid synthesis, protein translation, and nucleic acid production to facilitate growth, proliferation, and transcriptional and epigenetic reprogramming. Metabolic remodeling of activated T cells occurs over several days and is essential for the generation of clonal effector T cells capable of cytokine production, targeted cytotoxicity, and migration to sites of inflammation and infection[147,156,285,292]. Metabolic remodeling also characterizes the generation of memory T cell phenotypes. Although less metabolically active than effector T cells, memory T cells are more metabolically active than naive T cells, demonstrating increased fatty acid oxidation and fatty acid synthesis, and they display a higher spare respiratory capacity (SRC)[292,293]. Another important feature of memory T cells is that they are metabolically “poised” to undergo secondary activation, leading to rapid and robust generation of effector T cells

following secondary antigen encounter[292]. Notably, $T_{CM}$, $T_{RM}$, $T_{EM}$, and $T_{SM}$ memory T cells subsets demonstrate distinct metabolic profiles[294], as do Th1, Th2, Th17 and Treg populations[285,295], indicating that cellular metabolism is closely linked to T cell identity and functionality. T cell metabolism is also severely blunted during T cell exhaustion; for example, increased expression of the inhibitory receptors PD-1 and CTLA-4 on exhausted T cells has been shown to inhibit glycolysis and glutaminolysis[292,296,297].

### 1.5.2 iNKT cell metabolism during development and differentiation

Cellular metabolism regulates iNKT cell development in the thymus, after positive selection. Studies by Shin *et al.* (2014) and Zhang *et al.* (2014) have shown that the deletion of RAPTOR, which ablates mTORC1 activity, is sufficient to block iNKT cell development at Stage 1/Stage 2[84,298]. Mechanistically, Shin *et al.* (2014) proposed that this requirement for mTORC1 may be linked to PLZF activity. While PLZF levels were not decreased in *Raptor*$^{-/-}$ iNKT cells, localization of PLZF to the nucleus was blocked[298]. This suggests that cellular metabolism is switched on early in iNKT cell development and helps to initiate progression of iNKT cells through development by enabling translocation of PLZF to the nucleus. Early stage iNKT cells also express the transcription factor MYC, which plays a key role in metabolic activation of adaptive naive T cells[152,299]. Mycko *et al.* (2009) found that loss of *Myc* blocked iNKT cell development at Stage 1, indicating that early expression of MYC is important for normal iNKT cell development, although notably MYC was not required for iNKT cell proliferation[299]. Phosphoinositide-dependent kinase 1 (PDK1), a major activator of the Phosphatidylinositol-3-kinase (PI3K) pathway, has also been shown regulate early stage iNKT cell metabolism. Finlay *et al.* (2010) demonstrated that PDK1 deletion resulted in a severe global reduction in the frequency of iNKT cells, and inhibition of iNKT cell proliferation and metabolic activation. While PDK1$^{-/-}$ iNKT cells displayed normal expression of PLZF, they showed a reduction in

cell size, and reduced expression of CD71 and CD98, two key nutrient receptors that regulate the uptake of iron and L-amino acids[300]. Collectively, therefore, these studies indicate that normal regulation of cellular metabolism is essential for the development and proliferation of early stage iNKT cells.

Similarly, cellular metabolism has been shown to regulate downstream iNKT cell development and differentiation. A study by Park *et al.* (2014) demonstrated that deletion of Folliculin-interacting protein 1 (Fnip1), an adapter protein for the mTOR inhibitor AMP-activated protein kinase (AMPK), resulted in arrest at Stage 2 of iNKT cell development. Fnip$^{-/-}$ iNKT cells failed to downregulate PLZF, and displayed hyperactive mTOR, suggesting that iNKT cells must downregulate mTOR to exit development[301]. Interestingly, cellular metabolism may also differentially regulate iNKT cell subsets and their development. A study by Raynor *et al.* (2020) found that deletion of *Mst1*, a serine threonine kinase in the Hippo pathway, inhibited the differentiation of NKT1 cells, but not NKT2 and NKT17 cell differentiation. Mechanistically, MST1 acted downstream of IL-15, and functioned to downregulate mitochondrial metabolism during iNKT cell development[302]. Therefore, this study suggests that while NKT1 cells may downregulate mitochondrial metabolism during differentiation, NKT2 and NKT17 cells may not. In support of this finding, a recent study by Zhao *et al*. (2021) showed that oxidative phosphorylation was enhanced among NKT2 versus NKT1 cells in the thymus, and NKT2 but not NKT1 cells displayed an enhanced mitochondrial phenotype[303]. This suggests that iNKT cell subsets may acquire distinct metabolic phenotypes in the thymus, as has recently been shown for γδ T cells[109], and that oxidative metabolism may delineate NKT1, NKT2, and NKT17 cell subsets.

### 1.5.3 Activated iNKT cell metabolism

Metabolism continues to impact iNKT cell phenotype and function after these cells leave the thymus. A study by Fu *et al.* (2019) assessed the metabolic phenotype of iNKT cells from spleen and liver. iNKT cells showed a reduced respiratory capacity compared to naive conventional $CD4^+$ T cells, which are known to primarily rely on oxidative phosphorylation, but displayed an increased rate of glycolysis that was further increased after activation with anti-CD3/CD28[94]. Treatment of iNKT cells with 2-deoxyglucose (2-DG), a potent inhibitor of glycolytic flux, or incubation of iNKT cells in glucose free media during αGalCer stimulation resulted in significantly decreased production of IFNγ, which was only partially rescued by addition of pyruvate (which feeds into the citric acid cycle and oxidative phosphorylation downstream of glycolysis). Production of IL-4, while also decreased after 2-DG treatment, was less affected than IFNγ production[94], and the authors did not examine production of IL-17. Therefore, these data suggest that splenic and hepatic iNKT cells primarily utilize glycolysis to fuel production of IFNγ, whereas production of IL-4 appears to be only partially dependent on glycolysis. Given that iNKT cells in the spleen and the liver are predominantly NKT1 cells[59], these findings are likely to be reflective of NKT1 cell metabolism. Splenic iNKT metabolism was also investigated by Kumar *et al.* (2019). Profiling of iNKT cells and $CD4^+$ conventional T cells in the spleen revealed that iNKT cells take up less glucose than conventional cells, and metabolic tracing with [U-13C]-glucose using PLZF transgenic ($PLZF^{TG}$) $CD4^+$ T cells, which have been shown to display iNKT cell-like functionality[43], revealed that $PLZF^{TG}$ cells preferentially metabolize glucose using the pentose phosphate pathway and mitochondria, rather than converting glucose into lactate[304]. In agreement with Fu *et al.* (2019), incubation of iNKT cells in the presence of reduced glucose concentrations inhibited cytokine production in response to stimulation with αGalCer, indicating that iNKT cells utilize glucose to fuel cytokine production[94,304].

Notably, when Kumar *et al.* (2019) profiled glucose dependency among iNKT cells they found that production of IFNγ, IL-4 and IL-17A was decreased, including production of IL-4 by IFNγ$^{neg}$ iNKT cells, indicating that NKT1, NKT2 and NKT17 cells utilize glucose metabolism, although glucose did not impact on iNKT cell survival[304]. Therefore, collectively, these two studies implicate glucose as an important fuel for iNKT cell effector function, including among different iNKT cell subsets, although there is some evidence that IFNγ production may be more dependent on glucose. This is similar to what has been found for other innate T cells. Work by Lopes *et al.* (2021) in γδ T cells found that glucose was important for IFNγ production by γδ1 cells, while γδ17 cells were enriched for oxidative phosphorylation, and showed enrichment of genes associated with lipid metabolism[109]. Similarly, analysis by Zinser *et al*. (2018) and O'Brien *et al.* (2019) demonstrated that human MAIT cells utilize glycolysis for production of IFNγ and GZMB[83,290], linking glucose metabolism with Th1 and cytotoxic effector function. Interestingly, iNKT cell subsets also segregate according to their reactive oxygen species (ROS) profile. ROS, including the superoxide anion ($O2^{-}$) and hydrogen peroxide ($H_2O_2$), are produced during normal mitochondrial metabolism, and can act as signaling molecules at lower concentrations. However, uncontrolled ROS production can drive cellular dysfunction and induce cell death[305]. A study by Kim *et al.* (2017) found that NKT1 and NKT17 cells were enriched for ROS, while NKT2 cells showed lower levels of ROS. Moreover, treatment with antioxidants led to reduced frequencies of IFNγ$^{pos}$ and IL-17$^{pos}$ iNKT cells, whereas the frequency of IL-4$^{pos}$ iNKT cells was increased[197]. Therefore, this work suggests that ROS positively regulates production of Th1 and Th17 but not Th2 cytokines by iNKT cells. Kim et al. (2017) also found that ROS displayed a relationship with PLZF expression. Ectopic expression of PLZF in CD4$^{+}$ T cells increased ROS levels, and PLZF$^{low}$ adipose iNKT cells displayed reduced levels of cellular ROS[197]. Therefore, this suggested that ROS levels correlated with PLZF expression, although the authors did not address why PLZF$^{high}$ NKT2 cells were ROS$^{low}$.

While most studies of cellular metabolism in iNKT cells have focused on murine iNKT cells, studies investigating human iNKT cell metabolism are beginning to emerge. A recent report by Khurana *et al.* (2021) found that human iNKT cells were less reliant on glucose and glutamine than activated conventional T cells for production of GZMB and IFNγ, and iNKT cells showed reduced expression of glycolytic genes after stimulation with anti-CD3/CD28 compared to conventional T cells, similar to report by Kumar *et al.* (2019)[304,306]. Activated iNKT cells showed enrichment of genes associated with mitochondrial metabolism and fatty acid oxidation (FAO) compared to activated conventional T cells, and treatment with etomoxir, a pharmacological inhibitor of the critical fatty acid β-oxidation enzyme CPT1A, reduced oxidative metabolism in iNKT cells but not conventional T cells[306]. Therefore, these data suggest that human iNKT cells are more reliant on oxidative and lipid metabolism than conventional effector T cells. A similar study by Fu *et al.* (2020) found that murine iNKT cells increase cholesterol biosynthesis after activation with anti-CD3/CD28 or PBS-57 loaded CD1d tetramer, and this was mediated by PPARγ and PLZF through enhanced transcription of *Srebf1*[307], an important metabolic transcription factor that has been shown to regulate metabolic reprogramming and effector function in NK cells[289]. Fu *et al.* (2020) found that cholesterol biosynthesis was important for production of IFNγ by iNKT cells, as treatment with Tofa, an inhibitor of fatty acid synthesis, blocked IFNγ production, and treatment with cholesterol restored IFNγ production[307]. Therefore, collectively, these studies from Khurana *et al.* (2021) and Fu *et al.* (2020) implicate a role for lipid metabolism in the effector function of activated iNKT cells.

### 1.6 Hypothesis

Studies to date have shown that iNKT cells are phenotypically diverse, and upon exposure to antigen pass through several distinct phases of activation, culminating in the generation of memory-like or “trained” iNKT cell populations. This suggests that iNKT cells must undergo dramatic transcriptional remodeling during activation, as has been shown for adaptive T cells. However, transcriptional resources for the study of activated iNKT cells are lacking compared to adaptive T cells. There is also evidence that the activation of iNKT cells can induce functional anergy and promote the differentiation of memory-like regulatory NKT10 cells, while iNKT cells from adipose tissue are constitutively enriched for NKT10 cells and produce fewer cytokines than iNKT cells from other organs upon activation with αGalCer. This suggests that common pathways or gene signatures may underpin the tolerogenic phenotype of adipose iNKT cells and αGCPT iNKT cells. However, the transcriptional signatures of adipose and αGCPT iNKT cells have not been compared. Furthermore, it is unknown whether the phenotypes of NKT10 cells in adipose tissue and memory-like iNKT cells induced after αGalCer are similar, and the relationship between memory-like NKT10 cells and other memory-like iNKT cell populations, such as $NKT_{FH}$ cells and $KLRG1^{+}$ iNKT cells, remains unclear.

We propose that leveraging scRNA-Seq will enable integrated analysis of iNKT cells during different phases of *in vivo* activation, memory-like iNKT cells, adipose iNKT cells, and regulatory αGCPT iNKT cells, while also allowing us to capture information on iNKT cell subsets, including NKT1, NKT2, NKT17, and NKT10 cells. Furthermore, using scRNA-Seq will allow for comparison of our data with other transcriptomic resources available for iNKT cells, including recent scRNA-Seq of human iNKT cells by Erkers *et al.* (2020), Zhou *et al.* (2020) and Gutierrez-Arcelus *et al*. (2019), as well as bulk RNA-Seq and microarray resources published by Murray *et al*. (2021) and Sag *et al.* (2014).

Using these data, we will generate a transcriptomic atlas of iNKT cells, and address outstanding questions about the iNKT cell response to antigen.

### 1.7 Aims

We will perform scRNA-Seq of iNKT cells from spleen and adipose tissue at steady state, 4 hours post-αGalCer, 72 hours post-αGalCer, and 4 weeks post-αGalCer, and analyze these data in combination with reanalysis of published transcriptomic iNKT cell data, focusing in particular on the following:

- The composition of the splenic and adipose iNKT cell repertoire before (steady state) and after antigen exposure (4 weeks post-αGalCer)
- The transcriptional signatures of murine and human iNKT cell activation, including iNKT cell subsets, e.g. NKT1, NKT2, and NKT17 cells, expanded iNKT cells at 72 hours post-αGalCer, and reactivated iNKT cells after secondary αGalCer stimulation
- The phenotype of memory-like iNKT cell populations, including $KLRG1^{+}$ iNKT cells, $NKT_{FH}$ cells, and NKT10 cells

# Chapter 2: Materials and Methods

## 2.1 List of reagents, materials, instruments and software used

### Table 2.1.1 Reagents

| Reagent | Company | Location |
|---|---|---|
| RPMI Media (RPMI) | Thermofisher Scientific | Waltham, MA, USA |
| α-galactosylceramide (αGalCer) | Avanti Polar Lipids | Alabaster, AL, USA |
| Dimethylsulfoxide (DMSO) | Sigma Aldrich | St. Louis, MO, USA |
| Phosphate-buffered saline (PBS) | Sigma Aldrich | St. Louis, MO, USA |
| Collagenase type II | Worthington Biochemical Corporation | Lakewood, NJ, USA |
| ACK Lysing Buffer | VWR | Radnor, PA, USA |
| RBC Lysis Buffer | Biolegend | San Diego, CA, USA |
| Cell Stimulation Cocktail | Biolegend | San Diego, CA, USA |
| Brefeldin A | Biolegend | San Diego, CA, USA |
| Oligomycin | Sigma Aldrich | St. Louis, MO, USA |
| L-glutamine | Thermofisher Scientific | Waltham, MA, USA |
| Penicillin | Thermofisher Scientific | Waltham, MA, USA |
| Streptomycin | Thermofisher Scientific | Waltham, MA, USA |
| Fetal Bovine Serum (FBS) | Thermofisher Scientific | Waltham, MA, USA |
| Tetramethylrhodamine, Methyl Ester, Perchlorate (TMRM) | Thermofisher Scientific | Waltham, MA, USA |
| Mitotracker Green FM | Thermofisher Scientific | Waltham, MA, USA |
| Fixable Viability Dye eFluor 780 | Thermofisher Scientific | Waltham, MA, USA |
| Fixable Viability Dye eFluor 455UV | Thermofisher Scientific | Waltham, MA, USA |
| Zombie Aqua | Biolegend | San Diego, CA, USA |
| Zombie Yellow | Biolegend | San Diego, CA, USA |
| True-Nuclear Transcription Factor Buffer Set | Biolegend | San Diego, CA, USA |
| Foxp3/Transcription Factor Fixation/Permeabilization Kit | Thermofisher Scientific | Waltham, MA, USA |
| Cytofix/Cytoperm Fixation/ | BD Biosciences | Franklin Lakes, NJ, |

| | | |
|---|---|---|
| Permeabilization Kit | | USA |
| TotalSeq-A0301 anti-mouse Hashtag 1 Antibody | Biolegend | San Diego, CA, USA |
| TotalSeq-A0302 anti-mouse Hashtag 2 Antibody | Biolegend | San Diego, CA, USA |
| TotalSeq-A0303 anti-mouse Hashtag 3 Antibody | Biolegend | San Diego, CA, USA |
| TotalSeq-A0304 anti-mouse Hashtag 4 Antibody | Biolegend | San Diego, CA, USA |
| PBS57-loaded CD1d tetramer | NIH Tetramer Core Facility/Emory Vaccine Center | Atlanta, GA, USA |

## Table 2.1.2 Antibodies for flow cytometry

| **Antigen** | **Antibody Clone** | **Company** | **Location** |
|---|---|---|---|
| Purified anti-mouse CD16/32 Antibody | 93 | Biolegend | San Diego, CA, USA |
| CD3 | 17A2 | Biolegend | San Diego, CA, USA |
| CD19 | 6D5 | Biolegend | San Diego, CA, USA |
| CD11b | M1/70 | Biolegend | San Diego, CA, USA |
| CD45 | 30-F11 | Biolegend | San Diego, CA, USA |
| TCRβ | H57-597 | Biolegend | San Diego, CA, USA |
| CD8A | 53-6.7 | Biolegend | San Diego, CA, USA |
| KLRG1 | 2F1/KLRG1 | Biolegend | San Diego, CA, USA |
| IL-17A | TC11-18H10.1 | Biolegend | San Diego, CA, USA |
| IL-4 | 11B11 | Biolegend | San Diego, CA, USA |
| IFNγ | XMG1.2 | Biolegend | San Diego, CA, USA |
| CD43 Activation Glycoform (CD43- | S11 | Biolegend | San Diego, CA, USA |

| | | | |
|---|---|---|---|
| HG) | | | |
| ICOS | C398.4A | Biolegend | San Diego, CA, USA |
| cMAF | sym0F1 | Thermofisher Scientific | Waltham, MA, USA |
| RORγT | B2D | Thermofisher Scientific | Waltham, MA, USA |
| CD8A | 53-6.7 | Thermofisher Scientific | Waltham, MA, USA |
| IL-10 | JES5-16E3 | Thermofisher Scientific | Waltham, MA, USA |
| IL-13 | eBio13A | Thermofisher Scientific | Waltham, MA, USA |
| CD11b | M1/70 | Thermofisher Scientific | Waltham, MA, USA |
| F4/80 | BM8 | Thermofisher Scientific | Waltham, MA, USA |
| CD19 | 1D3 | Thermofisher Scientific | Waltham, MA, USA |
| IFNγ | XMG1.2 | BD Biosciences | Franklin Lakes, NJ, USA |

## Table 2.1.3 Instruments

| **Instrument** | **Company** | **Location** |
|---|---|---|
| FACS Canto II | BD Biosciences | Franklin Lakes, NJ, USA |
| LSR Fortessa | BD Biosciences | Franklin Lakes, NJ, USA |
| FACS Aria Fusion Cell Sorter | BD Biosciences | Franklin Lakes, NJ, USA |
| 10x Chromium Controller | 10x Genomics | Pleasanton, CA, USA |
| NextSeq 500 System | Illumina | San Diego, CA, USA |

## Table 2.1.4 scRNA-Seq batch guide

| Sample ID | Batch key | Lane key | Hashtag_ID | Accession code |
|---|---|---|---|---|
| Steady state adipose iNKT cells | 1 | 1 | NA | GSE142845 |
| Adipose iNKT cells at 4 hours post-αGalCer | 1 | 2 | NA | GSE190201 |
| Steady state splenic iNKT cells | 1 | 3 | Hashtag 1 | GSE142845 |
| Splenic iNKT cells at 4 hours post-αGalCer | 1 | 3 | Hashtag 2 | GSE142845 |
| Adipose iNKT cells at 72 hours post-αGalCer | 2 | 4 | NA | GSE190201 |
| Splenic iNKT cells at 72 hours post-αGalCer | 2 | 5 | NA | GSE190201 |
| Adipose iNKT cells at 4 weeks post-αGalCer | 3 | 6 | Hashtag 2 | GSE190201 |
| Resting splenic iNKT cells at 4 weeks post-αGalCer | 3 | 6 | Hashtag 3 | GSE190201 |
| Reactivated splenic iNKT cells at 4 hours post-αGalCer | 3 | 6 | Hashtag 4 | GSE190201 |

## Table 2.1.5 Software used

| **Software** | **Version** | **Source** | **Location** |
|---|---|---|---|
| FlowJo | 10.0.7r2 | BD Biosciences | Franklin Lakes, NJ, USA |
| Cell Ranger | 3.0.2 | 10x genomics | Pleasanton, CA, USA |
| R | 4.1.2 | R Project for Statistical Computing | Vienna, Austria |
| R Studio | 1.4.1712 | RStudio PBC | Boston, MA, USA |

## Table 2.1.6 R package library

| Package | Version |
|---|---|
| abind | 1.4-5 |
| affy | 1.70.0 |
| affyio | 1.62.0 |
| anndata | 0.7.5.3 |
| annotate | 1.70.0 |
| AnnotationDbi | 1.53.2 |
| AnnotationHub | 3.0.2 |
| ape | 5.6-1 |
| aplot | 0.1.2 |
| askpass | 1.1 |
| assertthat | 0.2.1 |
| babelgene | 21.4 |
| babelwhale | 1.0.3 |
| backports | 1.4.1 |
| base | 4.1.2 |
| base64enc | 0.1-3 |
| beachmat | 2.7.9 |
| beeswarm | 0.4.0 |
| BH | 1.78.0-0 |
| Biobase | 2.51.0 |
| BiocFileCache | 1.99.8 |
| BiocGenerics | 0.37.6 |
| BiocIO | 1.2.0 |
| BiocManager | 1.30.16 |
| BiocNeighbors | 1.9.6 |
| BiocParallel | 1.25.5 |
| BiocSingular | 1.7.2 |
| BiocVersion | 3.13.1 |

| | |
|---|---|
| biomaRt | 2.48.2 |
| Biostrings | 2.59.4 |
| bit | 4.0.4 |
| bit64 | 4.0.5 |
| bitops | 1.0-7 |
| blob | 1.2.2 |
| boot | 1.3-28 |
| brew | 1.0-7 |
| brio | 1.1.3 |
| broom | 0.7.12 |
| bslib | 0.3.1 |
| cachem | 1.0.6 |
| Cairo | 1.5-14 |
| callr | 3.7.0 |
| car | 3.0-12 |
| carData | 3.0-5 |
| Caret | 6.0-90 |
| carrier | 0.1.0 |
| caTools | 1.18.2 |
| cellranger | 1.1.0 |
| circlize | 0.4.14 |
| class | 7.3-20 |
| cli | 3.2.0 |
| clipr | 0.7.1 |
| clue | 0.3-60 |
| cluster | 2.1.2 |
| clusterProfiler | 3.99.2 |
| codetools | 0.2-18 |
| colorspace | 2.0-2 |
| commonmark | 1.7 |

| | |
|---|---|
| compiler | 4.1.2 |
| ComplexHeatmap | 2.7.11 |
| conflicted | 1.1.0 |
| conquer | 1.2.2 |
| corrgram | 1.14 |
| corrplot | 0.92 |
| cowplot | 1.1.1 |
| cpp11 | 0.4.2 |
| crayon | 1.5.0 |
| credentials | 1.3.2 |
| crosstalk | 1.2.0 |
| curl | 4.3.2 |
| data.table | 1.14.2 |
| datasets | 4.1.2 |
| DBI | 1.1.2 |
| dbplyr | 2.1.1 |
| DelayedArray | 0.17.13 |
| DelayedMatrixStats | 1.13.7 |
| deldir | 1.0-6 |
| desc | 1.4.0 |
| DescTools | 0.99.44 |
| devtools | 2.4.3 |
| dials | 0.1.0 |
| DiceDesign | 1.9 |
| dichromat | 2.0-0 |
| diffobj | 0.3.5 |
| digest | 0.6.29 |
| dittoSeq | 1.4.1 |
| DO.db | 2.9 |
| doParallel | 1.0.17 |

| | |
|---|---|
| DOSE | 3.17.2 |
| downloader | 0.4 |
| dplyr | 1.0.8 |
| dqrng | 0.3.0 |
| DropletUtils | 1.12.1 |
| DT | 0.20 |
| dtplyr | 1.2.1 |
| dynparam | 1.0.2 |
| dynutils | 1.0.9 |
| dynwrap | 1.2.2 |
| e1071 | 1.7-9 |
| edgeR | 3.33.7 |
| egg | 0.4.5 |
| ellipse | 0.4.2 |
| ellipsis | 0.3.2 |
| enrichplot | 1.11.3 |
| evaluate | 0.15 |
| Exact | 3.1 |
| expm | 0.999-6 |
| fansi | 1.0.2 |
| farver | 2.1.0 |
| fastmap | 1.1.0 |
| fastmatch | 1.1-3 |
| fgsea | 1.17.0 |
| filelock | 1.0.2 |
| fitdistrplus | 1.1-6 |
| fmsb | 0.7.2 |
| FNN | 1.1.3 |
| fontawesome | 0.2.2 |
| forcats | 0.5.1 |

| | |
|---|---|
| foreach | 1.5.2 |
| foreign | 0.8-82 |
| formatR | 1.11 |
| fs | 1.5.2 |
| furrr | 0.2.3 |
| futile.logger | 1.4.3 |
| futile.options | 1.0.1 |
| future | 1.24.0 |
| future.apply | 1.8.1 |
| gargle | 1.2.0 |
| generics | 0.1.2 |
| GENIE3 | 1.14.0 |
| GenomeInfoDb | 1.27.13 |
| GenomeInfoDbData | 1.2.6 |
| GenomicRanges | 1.43.4 |
| gert | 1.5.0 |
| GetoptLong | 1.0.5 |
| GGally | 2.1.2 |
| ggbeeswarm | 0.6.0 |
| ggforce | 0.3.3 |
| ggfun | 0.0.5 |
| ggHoriPlot | 1.0.0 |
| ggiraph | 0.8.1 |
| ggiraphExtra | 0.3.0 |
| ggplot2 | 3.3.5 |
| ggplotify | 0.1.0 |
| ggpmisc | 0.4.5 |
| ggpp | 0.4.3 |
| ggpubr | 0.4.0 |
| ggradar | 0.2 |

| | |
|---|---|
| ggraph | 2.0.5 |
| ggrepel | 0.9.1 |
| ggridges | 0.5.3 |
| ggsci | 2.9 |
| ggsignif | 0.6.3 |
| ggstream | 0.1.0 |
| ggtext | 0.1.1 |
| ggthemes | 4.2.4 |
| ggtree | 2.99.0 |
| ggvenn | 0.1.9 |
| gh | 1.3.0 |
| gitcreds | 0.1.1 |
| gld | 2.6.4 |
| GlobalOptions | 0.1.2 |
| globals | 0.14.0 |
| glue | 1.6.1 |
| GO.db | 3.13.0 |
| goftest | 1.2-3 |
| googledrive | 2.0.0 |
| googlesheets4 | 1.0.0 |
| GOSemSim | 2.17.2 |
| gower | 1.0.0 |
| GPfit | 1.0-8 |
| gplots | 3.1.1 |
| graph | 1.70.0 |
| graphics | 4.1.2 |
| graphlayouts | 0.8.0 |
| grDevices | 4.1.2 |
| grid | 4.1.2 |
| gridExtra | 2.3 |

| | |
|---|---|
| gridGraphics | 0.5-1 |
| gridtext | 0.1.4 |
| GSEABase | 1.54.0 |
| GSVA | 1.40.1 |
| gtable | 0.3.0 |
| gtools | 3.9.2 |
| hardhat | 0.2.0 |
| harmony | 1.0 |
| haven | 2.4.3 |
| HDF5Array | 1.20.0 |
| here | 1.0.1 |
| highr | 0.9 |
| hms | 1.1.1 |
| htmltools | 0.5.2 |
| htmlwidgets | 1.5.4 |
| httpuv | 1.6.5 |
| httr | 1.4.2 |
| ica | 1.0-2 |
| ids | 1.0.1 |
| igraph | 1.2.11 |
| infer | 1.0.0 |
| ini | 0.3.1 |
| insight | 0.16.0 |
| interactiveDisplayBase | 1.30.0 |
| ipred | 0.9-12 |
| IRanges | 2.25.11 |
| irlba | 2.3.5 |
| isoband | 0.2.5 |
| iterators | 1.0.14 |
| jpeg | 0.1-9 |

| | |
|---|---|
| jquerylib | 0.1.4 |
| jsonlite | 1.7.3 |
| KEGGREST | 1.31.2 |
| kernlab | 0.9-29 |
| KernSmooth | 2.23-20 |
| knitr | 1.37 |
| ks | 1.13.3 |
| labeling | 0.4.2 |
| lambda.r | 1.2.4 |
| later | 1.3.0 |
| lattice | 0.20-45 |
| lava | 1.6.10 |
| lazyeval | 0.2.2 |
| leiden | 0.3.9 |
| lhs | 1.1.4 |
| lifecycle | 1.0.1 |
| limma | 3.47.16 |
| listenv | 0.8.0 |
| lmds | 0.1.0 |
| lme4 | 1.1-28 |
| lmodel2 | 1.7-3 |
| lmom | 2.8 |
| lmtest | 0.9-39 |
| lobstr | 1.1.1 |
| locfit | 1.5-9.4 |
| LoomExperiment | 1.10.1 |
| lubridate | 1.8.0 |
| magick | 2.7.3 |
| magrittr | 2.0.2 |
| mapproj | 1.2.8 |

| | |
|---|---|
| maps | 3.4.0 |
| maptools | 1.1-2 |
| markdown | 1.1 |
| MASS | 7.3-55 |
| Matrix | 1.4-0 |
| MatrixGenerics | 1.3.1 |
| MatrixModels | 0.5-0 |
| matrixStats | 0.61.0 |
| mclust | 5.4.9 |
| memoise | 2.0.1 |
| methods | 4.1.2 |
| mgcv | 1.8-38 |
| mime | 0.12 |
| miniUI | 0.1.1.1 |
| minqa | 1.2.4 |
| misc3d | 0.9-1 |
| modeldata | 0.1.1 |
| ModelMetrics | 1.2.2.2 |
| modelr | 0.1.8 |
| mogene10sttranscriptcluster.db | 8.8.0 |
| mogene10stv1cdf | 2.18.0 |
| mouse4302.db | 3.13.0 |
| mouse4302cdf | 2.18.0 |
| msigdbr | 7.4.1 |
| multicool | 0.1-12 |
| munsell | 0.5.0 |
| mvtnorm | 1.1-3 |
| mycor | 0.1.1 |
| Nebulosa | 1.1.1 |
| nlme | 3.1-155 |

| | |
|---|---|
| nloptr | 2.0.0 |
| nnet | 7.3-17 |
| numDeriv | 2016.8-1.1 |
| openssl | 1.4.6 |
| openxlsx | 4.2.5 |
| org.Mm.eg.db | 3.13.0 |
| packrat | 0.7.0 |
| pals | 1.7 |
| PANTHER.db | 1.0.11 |
| parallel | 4.1.2 |
| parallelly | 1.30.0 |
| parsnip | 0.1.7 |
| patchwork | 1.1.1 |
| pbapply | 1.5-0 |
| pbkrtest | 0.5.1 |
| pheatmap | 1.0.12 |
| pillar | 1.7.0 |
| pkgbuild | 1.3.1 |
| pkgconfig | 2.0.3 |
| pkgload | 1.2.4 |
| plogr | 0.2.0 |
| plot3D | 1.4 |
| plotly | 4.10.0 |
| plyr | 1.8.6 |
| png | 0.1-7 |
| polyclip | 1.10-0 |
| polynom | 1.4-0 |
| ppcor | 1.1 |
| pracma | 2.3.6 |
| praise | 1.0.0 |

| | |
|---|---|
| preprocessCore | 1.54.0 |
| prettyunits | 1.1.1 |
| princurve | 2.1.6 |
| pROC | 1.18.0 |
| processx | 3.5.2 |
| prodlim | 2019.11.13 |
| progress | 1.2.2 |
| progressr | 0.10.0 |
| promises | 1.2.0.1 |
| proxy | 0.4-26 |
| proxyC | 0.2.4 |
| pryr | 0.1.5 |
| ps | 1.6.0 |
| purrr | 0.3.4 |
| quantreg | 5.88 |
| qvalue | 2.23.0 |
| R.methodsS3 | 1.8.1 |
| R.oo | 1.24.0 |
| R.utils | 2.11.0 |
| R6 | 2.5.1 |
| ranger | 0.13.1 |
| RANN | 2.6.1 |
| rappdirs | 0.3.3 |
| rcmdcheck | 1.4.0 |
| RColorBrewer | 1.1-2 |
| Rcpp | 1.0.8 |
| RcppAnnoy | 0.0.19 |
| RcppArmadillo | 0.10.8.1.0 |
| RcppEigen | 0.3.3.9.1 |
| RcppHNSW | 0.3.0 |

| | |
|---|---|
| RcppParallel | 5.1.5 |
| RcppProgress | 0.4.2 |
| RcppTOML | 0.1.7 |
| RCurl | 1.98-1.6 |
| readr | 2.1.2 |
| readxl | 1.3.1 |
| recipes | 0.2.0 |
| rematch | 1.0.1 |
| rematch2 | 2.1.2 |
| remotes | 2.4.2 |
| reprex | 2.0.1 |
| reshape | 0.8.8 |
| reshape2 | 1.4.4 |
| reticulate | 1.24 |
| rhdf5 | 2.36.0 |
| rhdf5filters | 1.4.0 |
| Rhdf5lib | 1.14.1 |
| rio | 0.5.29 |
| rjson | 0.2.21 |
| rlang | 1.0.1 |
| rmarkdown | 2.11 |
| ROCR | 1.0-11 |
| rootSolve | 1.8.2.3 |
| roxygen2 | 7.1.2 |
| rpart | 4.1.16 |
| rprojroot | 2.0.2 |
| rsample | 0.1.1 |
| rsconnect | 0.8.25 |
| RSpectra | 0.16-0 |
| RSQLite | 2.2.10 |

| | |
|---|---|
| rstatix | 0.7.0 |
| rstudioapi | 0.13 |
| rsvd | 1.0.5 |
| Rtsne | 0.15 |
| rvcheck | 0.1.8 |
| rversions | 2.1.1 |
| rvest | 1.0.2 |
| S4Vectors | 0.29.19 |
| sass | 0.4.0 |
| ScaledMatrix | 0.99.2 |
| scales | 1.1.1 |
| scater | 1.19.13 |
| scattermore | 0.8 |
| scatterpie | 0.1.7 |
| sceasy | 0.0.6 |
| scico | 1.3.0 |
| SCORPIUS | 1.0.8 |
| scrattch.io | 0.1.0 |
| sctransform | 0.3.3 |
| scuttle | 1.1.21 |
| selectr | 0.4-2 |
| sessioninfo | 1.2.2 |
| Seurat | 4.1.0 |
| SeuratObject | 4.0.4 |
| SeuratWrappers | 0.3.0 |
| shadowtext | 0.1.1 |
| shape | 1.4.6 |
| shiny | 1.7.1 |
| SingleCellExperiment | 1.13.14 |
| sitmo | 2.0.2 |

| | |
|---|---|
| sjlabelled | 1.1.8 |
| sjmisc | 2.8.9 |
| slider | 0.2.2 |
| snow | 0.4-4 |
| sourcetools | 0.1.7 |
| sp | 1.4-6 |
| SparseM | 1.81 |
| sparseMatrixStats | 1.3.8 |
| spatial | 7.3-11 |
| spatstat.core | 2.4-0 |
| spatstat.data | 2.1-2 |
| spatstat.geom | 2.3-2 |
| spatstat.random | 2.1-0 |
| spatstat.sparse | 2.1-0 |
| spatstat.utils | 2.3-0 |
| splines | 4.1.2 |
| splus2R | 1.3-3 |
| SQUAREM | 2021.1 |
| stats | 4.1.2 |
| stats4 | 4.1.2 |
| stringi | 1.7.6 |
| stringr | 1.4.0 |
| SummarizedExperiment | 1.21.3 |
| survival | 3.2-13 |
| sys | 3.4 |
| systemfonts | 1.0.4 |
| tcltk | 4.1.2 |
| tensor | 1.5 |
| testthat | 3.1.2 |
| tibble | 3.1.6 |

| | |
|---|---|
| tidygraph | 1.2.0 |
| tidymodels | 0.1.4 |
| tidyr | 1.2.0 |
| tidyselect | 1.1.1 |
| tidytree | 0.3.8 |
| tidyverse | 1.3.1 |
| timeDate | 3043.102 |
| tinytex | 0.37 |
| tools | 4.1.2 |
| treeio | 1.15.7 |
| TSP | 1.1-11 |
| tune | 0.1.6 |
| tweenr | 1.0.2 |
| tzdb | 0.2.0 |
| usethis | 2.1.5 |
| utf8 | 1.2.2 |
| utils | 4.1.2 |
| uuid | 1.0-3 |
| uwot | 0.1.11 |
| vctrs | 0.3.8 |
| vipor | 0.4.5 |
| viridis | 0.6.2 |
| viridisLite | 0.4.0 |
| vroom | 1.5.7 |
| waldo | 0.3.1 |
| warp | 0.2.0 |
| whisker | 0.4 |
| withr | 2.4.3 |
| workflows | 0.2.4 |
| workflowsets | 0.1.0 |

| | |
|---|---|
| xfun | 0.29 |
| XML | 3.99-0.8 |
| xml2 | 1.3.3 |
| xopen | 1.0.0 |
| xtable | 1.8-4 |
| xts | 0.12.1 |
| XVector | 0.31.1 |
| yaml | 2.3.4 |
| yardstick | 0.0.9 |
| yulab.utils | 0.0.4 |
| zip | 2.2.0 |
| zlibbioc | 1.37.0 |
| zoo | 1.8-9 |

## Table 2.1.7 Module scores

| iNKT Cell Activation | Cytokine Production | Glycolysis |
|---|---|---|
| Nr4a1 | Ifng | Pkm |
| Il2ra | Il2 | Pgk1 |
| Il2 | Il4 | Hk1 |
| Cd69 | Il13 | Hk2 |
| | Il17a | Ldha |
| | Csf2 | Gapdh |
| | Tnf | Eno1 |
| | Il10 | Pgam1 |
| | Il21 | Pfkp |
| | | Pfkl |
| | | Slc2a1 |
| | | Slc16a1 |
| | | Pgm1 |
| | | Pgm2 |
| | | Tpi1 |

| Amino Acid Uptake and Metabolism | Polyamine Synthesis | Oxidative Metabolism |
|---|---|---|
| Slc1a5 | Odc1 | Acly |
| Slc7a5 | Srm | Aco1 |
| Slc3a2 | Sms | Aco2 |
| Slc7a1 | Amd1 | Cs |
| Slc38a1 | | Dlat |
| Gls | | Pdha1 |
| Glud1 | | Pdhb |
| Got1 | | Dlst |
| Got2 | | Idh2 |
| | | Idh3a |

| | | |
|---|---|---|
| | | Idh3b |
| | | Idh3g |
| | | Mdh1 |
| | | Mdh2 |
| | | Ogdh |
| | | Sdha |
| | | Sdhb |
| | | Sdhc |
| | | Sdhd |
| | | Sucla2 |
| | | Suclg1 |
| | | Suclg2 |
| | | Cox10 |
| | | Cox11 |
| | | Cox15 |
| | | Cyc1 |
| | | mt-Atp6 |
| | | mt-Atp8 |
| | | mt-Co1 |
| | | mt-Co2 |
| | | mt-Co3 |
| | | mt-Nd1 |
| | | mt-Nd2 |
| | | mt-Nd3 |
| | | mt-Nd4 |
| | | mt-Nd5 |
| | | mt-Nd6 |
| | | Ndufa1 |
| | | Ndufa10 |
| | | Ndufa11 |

| | | |
|---|---|---|
| | | Ndufa2 |
| | | Ndufa3 |
| | | Ndufa4 |
| | | Ndufa5 |
| | | Ndufa6 |
| | | Ndufa7 |
| | | Ndufa8 |
| | | Ndufa9 |
| | | Ndufab1 |
| | | Ndufb10 |
| | | Ndufb2 |
| | | Ndufb3 |
| | | Ndufb4 |
| | | Ndufb5 |
| | | Ndufb6 |
| | | Ndufb7 |
| | | Ndufb8 |
| | | Ndufb9 |
| | | Ndufc1 |
| | | Ndufc2 |
| | | Ndufs1 |
| | | Ndufs2 |
| | | Ndufs3 |
| | | Ndufs4 |
| | | Ndufs5 |
| | | Ndufs6 |
| | | Ndufs7 |
| | | Ndufs8 |
| | | Ndufv1 |
| | | Ndufv2 |

| | | |
|---|---|---|
| | | Ndufv3 |
| | | Ppa1 |
| | | Ppa2 |
| | | Sdha |
| | | Sdhb |
| | | Sdhc |
| | | Sdhd |
| | | Tcirg1 |
| | | Uqcr10 |
| | | Uqcr11 |
| | | Uqcrb |
| | | Uqcrc1 |
| | | Uqcrc2 |
| | | Uqcrfs1 |
| | | Uqcrh |
| | | Uqcrq |

| **Fatty acid β-oxidation** | **Fatty acid biosynthesis** | **$NKT_{FH}$ Gene Score** |
|---|---|---|
| Abcd1 | Abcd1 | Cxcr5 |
| Abcd2 | Abcd2 | Pdcd1 |
| Abcd3 | Abcd3 | Maf |
| Abcd4 | Abhd2 | Tox2 |
| Acaa1a | Acaca | Tox |
| Acaa2 | Acacb | Il21r |
| Acadm | Acly | Btla |
| Acadvl | Acot7 | Cxcr4 |
| Acat1 | Acsbg1 | Cd40lg |
| Acat2 | Acsf3 | Stat3 |
| Acat3 | Acsl3 | Bcl6 |
| Acox1 | Acss1 | Icos |

| | | |
|---|---|---|
| Acox3 | Acss2 | Cd4 |
| Acoxl | Alox8 | Il6ra |
| Auh | Anxa1 | Slamf1 |
| Bdh2 | Asah2 | Il21 |
| Cpt2 | Brca1 | Il4 |
| Crot | Cbr4 | Tnfrsf4 |
| Decr1 | Cd74 | Slamf6 |
| Echdc1 | Decr2 | |
| Echdc2 | Degs1 | |
| Echs1 | Eif6 | |
| Eci1 | Elovl1 | |
| Eci2 | Elovl4 | |
| Ehhadh | Elovl5 | |
| Hadh | Elovl6 | |
| Hadha | Elovl7 | |
| Hadhb | Fabp5 | |
| Hsd17b4 | Fads1 | |
| Hsd17b10 | Fads2 | |
| Pex2 | Fads6 | |
| Pex5 | Fasn | |
| Pex7 | Gstm4 | |
| Scp2 | H2-Ke6 | |
| Sesn2 | Hacd1 | |
| Slc25a17 | Hacd2 | |
| Slc27a2 | Hacd3 | |
| Tuba8 | Hacd4 | |
| Acad11 | Hpgds | |
| Acadl | Il1b | |
| Acads | Lias | |
| Etfa | Lipc | |

| | | |
|---|---|---|
| Etfb | Lipg | |
| Etfdh | Liph | |
| Gcdh | Lpgat1 | |
| Ivd | Lpl | |
| Crat | Ltc4s | |
| Acsl5 | Mapk9 | |
| Akt2 | Mcat | |
| Cpt1a | Mecr | |
| Irs2 | Mgll | |
| Twist1 | Mid1ip1 | |
| Lonp2 | Mlxipl | |
| Mlycd | Mlycd | |
| Mtor | Myo5a | |
| Tysnd1 | Ndufab1 | |
| | Nr1h2 | |
| | Nr1h3 | |
| | Oxsm | |
| | Pecr | |
| | Pla2g3 | |
| | Pla2g4a | |
| | Plp1 | |
| | Prkaa1 | |
| | Prkab1 | |
| | Prkag1 | |
| | Prkag2 | |
| | Ptges | |
| | Ptges2 | |
| | Ptges3 | |
| | Ptgs1 | |
| | Ptgs2 | |

| | | |
|---|---|---|
| | Qk | |
| | Scap | |
| | Scd1 | |
| | Scd2 | |
| | Scd4 | |
| | Srebf1 | |
| | Tbxas1 | |
| | Tecr | |

| **ISG Gene Score** | **Tr1 Gene Score** |
|---|---|
| Ifit1 | Il10 |
| Ifit3 | Il21 |
| Isg15 | Il27ra |
| Irf7 | Stat3 |
| Stat1 | Stat1 |
| Bst2 | Il10ra |
| | Il10rb |
| | Lag3 |
| | Itga2 |
| | Ccr5 |
| | Batf |
| | Irf1 |
| | Pdcd1 |
| | Maf |
| | Ahr |
| | Prdm1 |
| | Tgfb1 |
| | Gzmb |
| | Gzma |
| | Prf1 |

| | |
|---|---|
| | Ctla4 |
| | Cd226 |
| | Cd4 |

## 2.2 Animals

Male C57BL/6J mice were purchased from Jackson Laboratory or Harlan Laboratory. BALB/c mice were purchased from Harlan Laboratory. Male and female BALB/c mice were bred under specific-pathogen-free facilities at Trinity College Dublin. Mice were used in experiments at 6-14 weeks of age. All animal work was approved and conducted in compliance with the Trinity College Dublin University Ethics Committee and the Health Products Regulatory Authority Ireland, and the Institutional Animal Care and Use Committee guidelines of The Dana Farber Cancer Institute and Harvard Medical School.

## 2.3 *In vivo* stimulations

αGalCer was prepared by dissolving in sterile DMSO at a concentration of 1mg/mL. αGalCer was diluted in sterile PBS for injection and the final concentration of DMSO was adjusted to less than 10% vol/vol. Mice were given an interpertioneal (IP) injection with 1μg of αGalCer or PBS vehicle. Mice were sacrificed after either 4 or 72 hours, and tissues were harvested immediately. For analysis of memory-like iNKT cells, mice were given an IP injection with 4μg of αGalCer and sacrificed after 4 weeks, with some animals receiving an additional IP injection of 1μg of αGalCer 4 hours before sacrifice, to assay secondary iNKT cell activation. All injections had a final volume of 100μL.

## 2.4 Tissue processing

Epididymal adipose tissue was excised and minced with a razor or scissors. 1mg/ml Collagenase Type II solution was prepared by diluting Collagenase Type II powder in RPMI. Minced adipose tissue was then digested in Collagenase Type II solution with shaking for 25-30 minutes at 37°C. Digested cells were immediately diluted in ice cold RMPI and then filtered through 70μM

nylon or metal mesh. Filtered cells were centrifuged at 15,000 rpm for 5-7 minutes to pellet the stromovascular fraction. Spleens and thymi were disrupted through a 70μM filter and pelleted. Red blood cells in the spleen and thymus were lysed with ACK Lysing Buffer or RBC Lysis Buffer prior to further analysis.

### 2.5 *Ex vivo* stimulations and mitochondrial staining

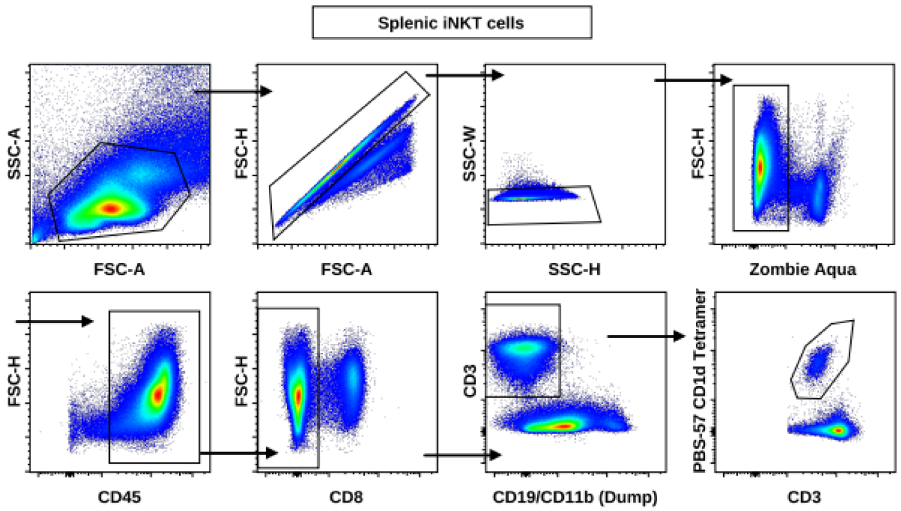
Where indicated, thymocytes were cultured for 4 hours in the presence of 50ng/mL PMA and 1μg/mL Ionomycin (Cell Stimulation Cocktail) and Brefeldin A, in the presence or absence of 40nM oligomycin. Cell cultures were performed in RPMI supplemented with 10% FBS, L-glutamine, penicillin, and streptomycin. Mitochondrial staining was performed by culturing whole splenocytes or thymocytes were in complete RPMI containing 100nM TMRM and/or 100nM Mitotracker Green FM for 30 minutes.

### 2.6 Flow cytometry and cell sorting

Dead cells were excluded with Fixable Viability dyes (UV or eFluor 780), Zombie Aqua, or Zombie Yellow. Live/Dead staining was performed in PBS at a dilution of 1/1000, prior to surface staining. Staining of live cells for flow cytometry was performed in a solution of PBS with 1-2% FBS. Single cell suspensions were incubated in purified anti-mouse CD16/32 antibody during surface staining to prevent non-specific binding of conjugated antibodies to Fc receptors. For intracellular staining, cells were fixed and permeabilized using True-Nuclear Transcription Factor Buffer set, Foxp3/Transcription Factor Fixation/Permeabilization kit, or Cytofix/Cytoperm Fixation/Permeablization Kit, according to the manufacturer's instructions. iNKT cells were identified as live, single lymphocytes binding to anti-TCRβ or anti-CD3 antibodies and αGalCer analog PBS57-loaded CD1d tetramer. A "dump" channel with antibodies against CD19, or CD19 and CD11b or F4/80, or CD19, CD8a and CD11b was

used to eliminate nonspecific staining. For staining of BALB/c thymic iNKT cell subsets, NKT1 cells were gated as CD43-HG$^{-}$ ICOS$^{-}$ CD3$^{low}$ cells, NKT2 cells were gated as CD43-HG$^{-}$ ICOS$^{+}$ CD3$^{high}$ cells, and NKT17 cells were gated as CD43-HG$^{+}$ cells. Live cells were acquired immediately after staining, and fixed cells were acquired within 36 hours of staining. Flow Cytometry analysis and plots were created using FlowJo version 10.0.7r2.

A.




B.

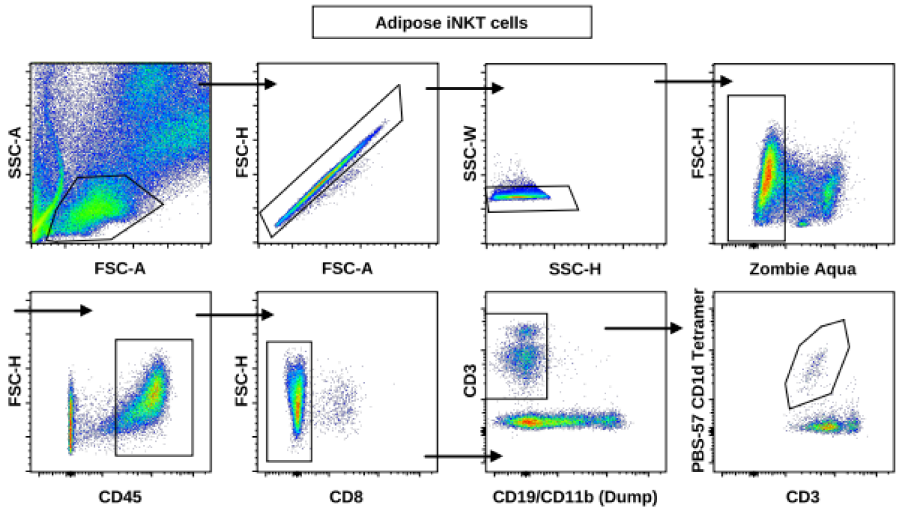
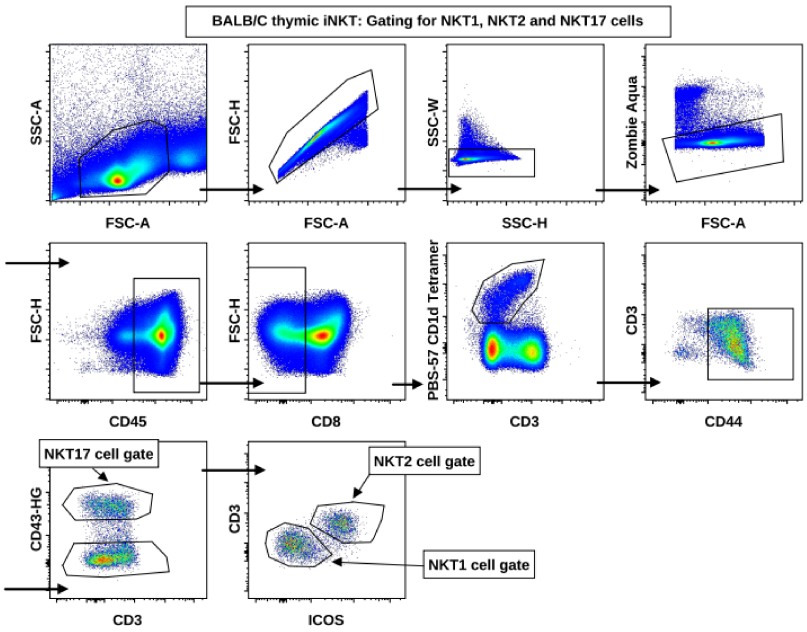



**Figure 2.6.1: Gating strategy for C57BL/6 splenic (A) and adipose (B) iNKT cells.**

A.




B.

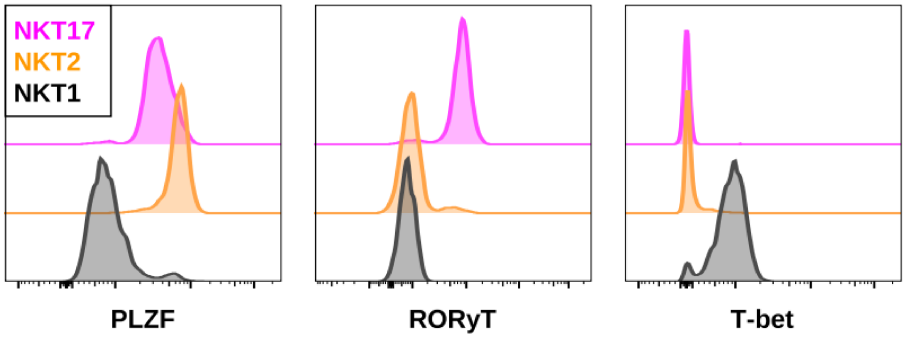



**Figure 2.6.2: (A) Gating strategy for BALB/c CD44$^{+}$ thymic NKT1, NKT2, and NKT17 cells using CD43-HG and ICOS. (B) Validation of flagship transcription factor expression in gated NKT1, NKT2, and NKT17 cells.**

## 2.7 scRNA-Seq sequencing and data pre-processing

scRNA-Seq was performed on single cell suspensions of sorted iNKT cells from the epididymal adipose tissue and spleens of mice using the 10x Genomics platform. A total of thirty-five epididymal adipose tissue deposits or five spleens were pooled for each sample. Nine biological samples were sequenced in three batches (Table 2.1.4, Figure 2.1). For some samples, cells were first tagged using TotalSeq-A anti-mouse antibodies before being pooled for sequencing. Single cell suspensions were loaded onto a 10x Chromium Controller to generate Gel Beads-in-emulsion (GEMS), and GEMs were processed to generate unique molecular identifier (UMI)-based libraries according to the 10X Genomics Chromium Single Cell 3' protocol. Libraries were sequenced using a NextSeq 500 sequencer. Raw BCL files were demultiplexed using Cell Ranger v3.0.2 mkfastq to generate fastq files with default parameter. Fastq files were aligned to the mm10 genome (v1.2.0) and feature reads were quantified simultaneously using Cell Ranger count for feature barcoding. Filtered feature-barcode UMI count matrices containing quantification of gene expression and hashtag antibody binding were used for downstream analysis.

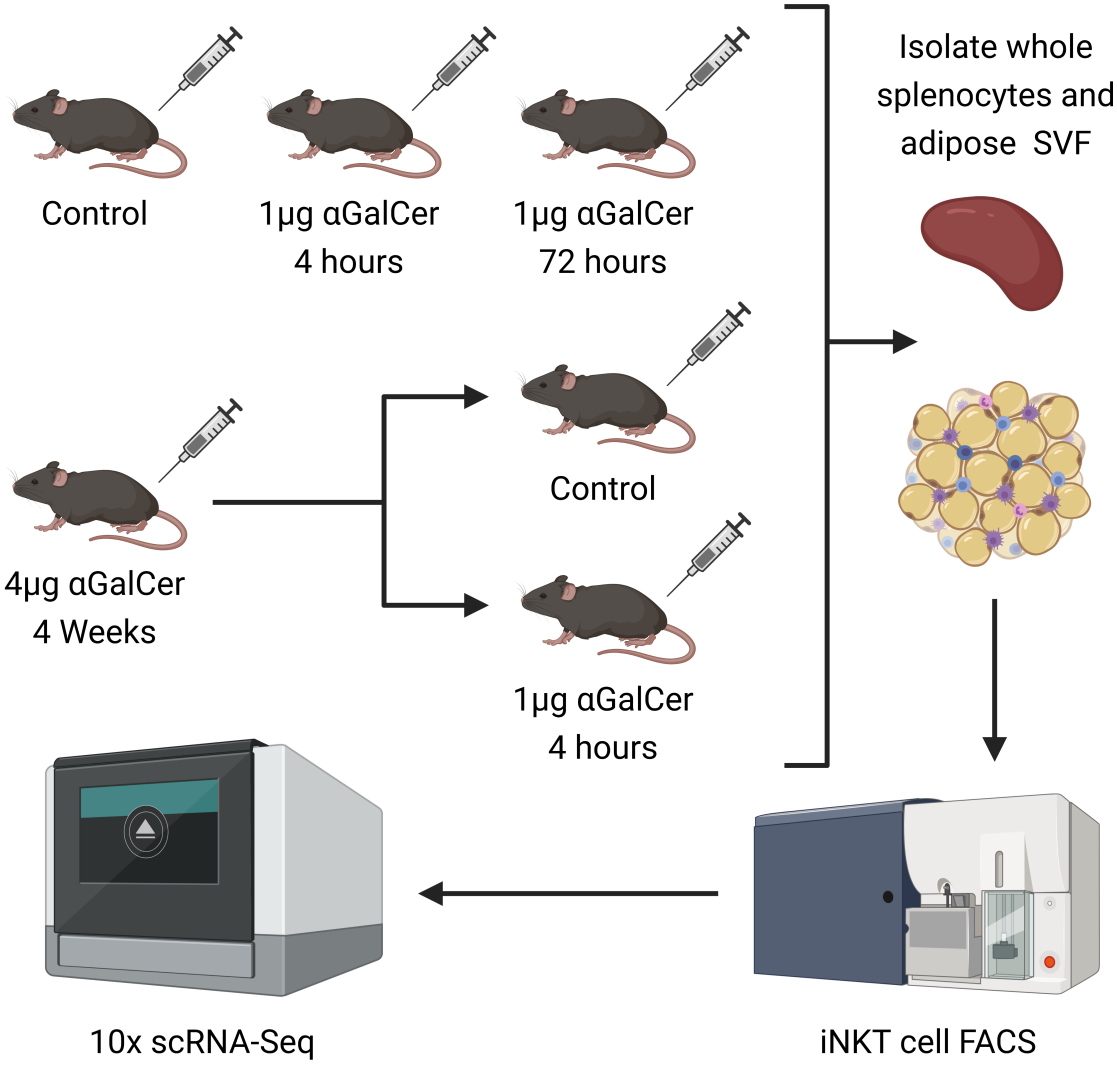



**Figure 2.7: Cartoon illustration of scRNA-Seq experimental design.**

## 2.8 Downstream scRNA-Seq data analysis

48,813 cells murine iNKT cells expressing a median of 1,567 genes per cell and 4,163 UMIs per cell were loaded from feature-barcode UMI count matrices using the Seurat v4.1.0 package[308]. Raw human iNKT cell scRNA-Seq data files were kindly provided by Dr Tom Erkers and Dr Bryan Xie (source data available at PRJNA563899 and PRJNA565590) or was downloaded from GSE128243 and GSE124731[133–135]. Antibody hashtag data was demultiplexed using the Seurat HTODemux function with a positive quantile of 0.99 and centered log ratio transformation normalization. Cells positive for more than one antibody were removed from the analysis. Genes expressed in less than three cells were excluded from all analyses to prevent false positive identification of transcripts. Cells expressing less than 1% or more than 12.5% of mitochondrial genes as a % of total gene counts were considered to represent empty droplets or apoptotic/dead cells and were removed from the analysis. Cells were also filtered based on total UMI counts and total gene counts on a per sample basis to remove empty droplets, poor quality cells and doublets, with a minimum cutoff of at least 500 genes per cell across all samples. UMI counts were normalized using regularized negative binomial regression using sctransform v0.3.3[309]. Where indicated, cycle regression was performed by first normalizing UMI counts using sctransform, then performing cell cycle scoring using the CellCycleScoring() function and cell cycle gene lists provided with the Seurat package, and then re-normalizing raw RNA count data with sctransform and regression of computed cell cycle scores applied.

Dimensionality reduction was performed using principal component analysis (PCA) with n = 100 dimensions and 2000 or 3000 variable features, and an elbow plot was used to determine the number of PCA dimensions used as input for uniform manifold approximation and projection (UMAP)[310]. For collective analysis of cells from different batches, the harmony v1.0 package[311] was used with default settings to remove batch effects, and batch-corrected harmony embeddings were used for UMAP. Outlier cells expressing

genes associated with macrophages (ex. *Adgre1*, *Cd14*), B cells (ex. *Cd19*) or adaptive T cells (ex. *Cd8a*) were also identified and removed prior to the final analysis. UMAP was performed using a minimum distance of 0.3 and a spreading factor of 1. Shared nearest neighbor (SNN) graphs were calculated using k = 20 nearest neighbors. Graph-based clustering was performed using the louvain algorithm. In some cases, overclustering was performed and clusters were manually collapsed, and/or the first two dimensions of the UMAP reduction were used as input for graph-based clustering instead of PCA or harmony embeddings.

Gene expression analysis was performed using the FindMarkers() or FindAllMarkers() Seurat functions and the wilcoxon rank sum test, using log-normalized RNA counts. GSEA[265] was performed using the FGSEA v1.17.0[312] and clusterProfiler v3.99.2[313] packages. KEGG[314] pathway data was retrieved from the Molecular signatures database (MSigDB)[315] using the msigdbr v7.4.1 package. Over-representation analysis was performed using g:Profiler[316]. Heatmaps were generated using the Complex Heatmap v2.7.11 and circlize v0.4.14 packages[317]. Module scores were calculated using the AddModuleScore() Seurat function with n = 10 control features. Density plots were produced using the Nebulosa v1.1.1 package[318]. Gene regulatory network analysis was performed using GENIE3 v1.14.0[319] with n = 10 iterations and link weight values were averaged between replicate analyses. The full library of R packages (including dependencies) used during this study is provided in Table 2.1.6. The critical R packages used to generate specific plots (e.g. violin plots, lollipop plots) are described in section 2.12. The full list of genes used to calculate each of the gene module scores used in this study is provided in Table 2.1.7.

### 2.9 Bulk RNA-Seq and microarray analysis

Raw RNA-Seq count files were downloaded from GEO repository GSE161492[92]. Microarray data was downloaded from GEO repository GSE47959[91]. Raw CEL files were annotated against the Mouse430_2 Array (mouse4302.db) and Robust Multichip Average (RMA) normalized using the affy v1.7.0 R package. Discrete probes corresponded to the same gene were merged and values were averaged. Raw RNA-Seq counts were transformed to log2(counts per million) (logCPM) and normalized using trimmed mean of M-values (TMM) normalization with EdgeR using edgeR v3.33.7[320]. Genes with low read counts were filtered out using the edgeR filterByExpr() function. Testing for differential gene expression was performed with Limma-Voom using limma v3.47.16[321–323] with standard settings. PCA plots were generated using the prcomp function (stats v4.1.2 package) and total logCPM values across the entire array of genes in the dataset. Other plots were generated using the same libraries as used for scRNA-Seq data plotting.

### 2.10 Statistics

Pilot studies were performed to estimate required sample size for adequate power. Significance was determined by Student's two-tailed t test with Holm–Bonferroni correction, or one-way ANOVA with post-hoc Tukey test, where indicated. Significance is presented as *$P < 0.05$, **$P < 0.01$, ***$P < 0.001$, with $P > 0.05$ considered non-significant. All statistical analysis outside of scRNA-Seq, bulk RNA-Seq, or microarray pipelines were performed using the rstatix v0.7.0 package. All computational analysis was performed using R 4.1.2 and RStudio Desktop v1.4.1712 on an Ubuntu 20.04 Linux GNU (64 bit) system, and FlowJo analysis was performed on a Windows 10 (64 bit) system.

## 2.11 Data availability

scRNA-seq data from this study have been deposited in the Gene Expression Omnibus under the accession codes GSE142845 and GSE190201 (see Table 2.1.4).

## 2.12 Explanation of bioinformatic terms, plots, and analyses

1. UMAP – Uniform manifold approximation and projection (UMAP) is a technique used in scRNA-Seq to perform dimensionality reduction, typically after previously performing PCA (principal component analysis). Since there are thousands of different genes (variables) to consider when trying to understand or visualize how different cells or populations of cells relate to each other (i.e. scRNA-Seq data is highly multidimensional), it becomes necessary to reduce these many variables or data dimensions down to something more relatable. PCA does this by reducing many variables down to a series of components describing a proportion of the total variance. This can help to visualize data. UMAP is a different technique or algorithm that does basically the same thing, reducing lots of variables or dimensions down to a series of components (usually just two in the case of scRNA-Seq, which represent the UMAP 1 and UMAP 2 scales on a plot depicting a UMAP reduction). Another analogous technique to UMAP is t-SNE. UMAP is the current favored dimensionality reduction technique in scRNA-Seq. The Seurat R package[309], which I used to compute PCA and UMAP reductions in this thesis, uses PCA embeddings (or coordinates in dimensional space) as an input to perform UMAP.

2. UMAP plot – a plot of a UMAP reduction or projection. It can show gene expression, in which case it is called a feature plot, or it can show clustering of cells. I used the Seurat package to generate these plots.

3. Harmony embeddings – when scRNA-Seq data, like bulk RNA-Seq data, comes from different batches (for example different experiments, or if it was sequenced on a different day) it becomes necessary to employ batch correction techniques (basically an algorithm to remove or mitigate batch effects in the data). In this thesis I used Harmony[311], a recently published batch correction algorithm. Harmony works by taking PCA embeddings as an input, performing batch correction, and generating new batch-corrected embeddings that can be passed to UMAP for generating the final UMAP reduction. These new embeddings generated by harmony are known as harmony embeddings. I used the harmony package to generate harmony embeddings.

4. Seurat functions – a function is just executable code built into an R package. A function takes an input from the user and performs some operation or function. For example, in the Seurat R package there is a function to generate a plot of gene expression overlaid on to a UMAP reduction The user provides a gene name (such as *Ifng* or *Il4*) in a command called “FeaturePlot” and this function will generate an image of *Ifng* or *Il4* expression overlaid on a given UMAP reduction. This function concept applies to all R packages that contain functions.

5. Violin plot – a violin plot is a plot showing the distribution of a given set of data. Consider the example of a box plot which shows normalized expression values for *Ifng* expression in 5000 iNKT cells. Let’s say that we have a bimodal distribution of data, with one half of the iNKT cells expressing about 0.5 units of *Ifng* RNA while the other half of the iNKT cells express 1.5 units of *Ifng*. If we plot these data using a box plot we will get a box plot centered on a value of 1 unit of *Ifng* RNA (the mean value across all of the cells) and the box plot height will range from 0.5 to 1.5 units (the range of the data). However, we lose information by using a box plot. From this box plot it is impossible to tell if we

have a smooth distribution of cells expressing *Ifng* RNA across the 0.5 to 1.5 unit range, a bimodal population at 0.5 and 1.5 units, a trimodal population at 0.5, 1, and 1.5 units etc. - most of the information associated with actual value distribution has been lost. A violin plot does a better job of showing these data because the width of the violin plot correlates with the data distribution, preserving information about data distribution. Using our *Ifng* example, a violin plot of these data will give us all of the information available from a box plot (the range and mean) but we will also see that there is a bimodal data distribution, with a large population of cells at 0.5 units, and a second population at 1.5 units. Therefore, violin plots are typically recommended over box plots, although the combination of both a violin plot and a box plot on the graph can be very effective. I used the Seurat and ggplot2 packages to generate violin plots.

6. Scatter plot – a scatter plot is just a plot of data points (usually dots) on two axes. Some commonly used versions of scatter plots have been assigned their own names, such as volcano plots. Scatter plots can be combined with lines to connect different data points, in which case they may be called line plots.

7. Volcano plot – a volcano plot is generally considered to refer to a scatter plot which shows log fold change values between two conditions or samples along one axis (usually the X axis) and the adjusted P value of the enrichment along the other axis (usually the Y axis). A volcano plot is so named because the typical distribution of log fold change and adjusted P values from an RNA-Seq experiment forms a shape similar to that of a volcano, with most genes grouping together in a “dip” or “rise” (depending on the orientation of the plot) along the center of the log fold change axis and the bottom of the adjusted P value axis (forming the mouth of the volcano), and then as you move outwards from the center of the log fold change axis in either direction you will find

observe a trend of genes moving along the adjusted P value axis (forming the “side” of the volcano).

8. Lollipop plot – a lollipop plot is just a scatter plot where there are lines connecting each scatter point to an axis.

9. Elbow plots – an elbow plot is a specific type of scatter plot used for determining the number of embeddings that should be used to generate a dimensionality reduction, such as a UMAP. Performing PCA generates principal components (PCs), which are basically a small set of artificial computed variables that encompass a relatively large amount of the real variance in a dataset. An elbow plot is generated by plotting the PCs generated by PCA in order from PC1 to PC(N) along one axis (e.g. PC1, PC2, PC3, PC4, etc.) where N = the number of PCs computed. The standard deviation between PCs is plotted on the second axis. This will produce a characteristic “elbow”-shaped plot, as the standard deviation will be highest with PC1, then rapidly decline from PC2 onwards before finally stabilizing at higher PCs.

10. Module score – a module score or gene module score is a computed score representing the average expression of a group or “module” of genes. It can be used as a relative measure of how much a group of genes is expressed between cells from different populations, clusters or conditions. It can be computed using the Seurat package with the function “AddModuleScore”. Please see Tirosh *et al.* (2016)[324] or the Seurat package for further computational details.

11. Louvain algorithm – the Louvain algorithm is an algorithm used to extract the community structure of large networks. It essentially allows many discrete

data points in a network (e.g. cells in a single cell dataset) to be effectively classified into groups or clusters. The Louvain algorithm is the standard clustering algorithm used in the Seurat R package. Please see Blondel *et al.* (2008)[325] for further details about the Louvain algorithm, or the Seurat package for details about its implementation of the Louvain algorithm for analysis of scRNA-Seq data.

12. GSEA – GSEA, or gene set enrichment analysis, is a computational algorithm or tool used to determine the enrichment of gene pathways in a dataset. Typically, the user will first perform differential gene expression analysis and generate ranking values for all genes in the analysis (i.e. all genes in the dataset). These ranking values can be log fold change values, as I used in my thesis, but the most ideal values to use (if it is possible to do so) are t-statistic values generated from pairwise comparisons performed using bulk RNA-Seq or pseudobulk RNA-Seq analysis tools, like DESeq2[326], edgeR[320], and Limma-Voom[321,322]. The GSEA algorithm essentially "walks" down the list of ranked values (which are ordered by rank) and using this list it will output enrichment scores (and P-values) for each individual gene pathway provided to the algorithm. The enrichment of pathways is based on the ranking of constituent genes in any given pathway within the ranked list of values. The output of GSEA will be a ranked list of gene pathways which are enriched (or not enriched) in the pairwise comparison. For example, if I performed a GSEA on a ranked list of values from differential gene expression of activated versus steady state iNKT cells I would get out a list of pathways, some of which would be enriched in activated iNKT cells (e.g. cytokine production), others which would be enriched in steady state iNKT cells (e.g. oxidative phosphorylation), and some pathways which might show not change at all between the conditions (e.g. muscle contraction). Please see the GSEA website (https://www.gsea-msigdb.org/gsea/index.jsp) or the seminal paper from Subramanian *et al.* (2005)[265] describing GSEA. A wide range of different gene

pathways can be provided to GSEA, including custom ones, but researchers most commonly used gene pathways from well-described published gene pathway databases, such as the KEGG[314] or REACTOME[327] databases.

13. KEGG – the Kyoto Encyclopedia of Genes and Genomes (KEGG) database is a well known and widely used curated database of biological gene pathways, genes, molecules, diseases and reactions. The curated KEGG pathways are often used for the purpose of determining pathway enrichment using GSEA or over-representation analysis. For more information please see the publication by Kanehisa *et al.* (2021)[314] or the KEGG website (https://www.genome.jp/kegg/).

14. Limma-Voom – The limma R package is one of the major computational toolkits available for analysis of microarray and RNA-Seq data. Please see the seminal publication by Smyth *et al.* (2005)[321]. Voom, which is a component of the limma package, was a later major extension to the limma toolkit[322]. Limma-Voom is often used in combination with edgeR (please see the edgeR R package)[320,323].

15. Granular analysis – granular or fine analysis is a term which can be used in place of the term subclustering. What it essentially means is to perform further or more detailed analysis of a subset of scRNA-Seq data, often on a subset of one or more cell clusters or populations. For example, say I have a single cell dataset containing different activated T cells. I would first perform an overall analysis of all of the data together. However, I notice that within the Th1 cell population there is some additional heterogeneity that cannot be resolved at the resolution of looking at all of the activated T cells together. Therefore, I take the Th1 cells as a subset and recluster them to analyze these cells at a

higher resolution. This is an example of granular or fine analysis, as well as an example of subclustering.

# Chapter 3: Transcriptional analysis of iNKT cell heterogeneity and early stage iNKT cell activation

## Introduction

Numerous studies over the last 15-20 years have characterized the phenotype of iNKT cells, especially during iNKT development in the thymus, and at steady state, most commonly in mice and in the peripheral blood of human donors[68,328]. This body of work has revealed that the iNKT cell repertoire is heterogeneous and contains different subsets. For example, murine iNKT cells can be separated into functionally and transcriptionally distinct NKT1, NKT2, and NKT17 cell subsets[46,60,61,92,93,107]. A defining characteristic of iNKT cells is that they rapidly respond to antigen and cytokine signals[17,178,188,200,209], and can mount potent effector responses. Despite this, the transcriptional signatures, pathways, and mechanisms underpinning iNKT cell activation have received relatively little attention, especially compared to adaptive $CD4^+$ and $CD8^+$ T cells[153,154,173,329]. Moreover, it was unknown whether NKT1, NKT2, and NKT17 cell subsets utilize different pathways or transcriptional programs to support their diverse effector functions.

To investigate iNKT cell activation, we performed 10x scRNA-Seq of whole murine splenic iNKT cells at steady state and 4 hours after *in vivo* activation with the glycolipid antigen αGalCer, which is a well-established and widely used ligand for studying iNKT cell activation and effector function[10,49,93,208]. This study design enabled us to compare iNKT cells at rest versus during the rapid effector phase following TCR ligation[17] and facilitated differential gene expression and pathway enrichment analysis. Moreover, utilization of scRNA-Seq, rather than bulk RNA-Seq, also permitted us to examine iNKT cell heterogeneity, and analyze iNKT cell subsets for potential differences in gene expression before and after activation. We also performed reanalysis of published human PBMC iNKT cell scRNA-Seq data[133–135], and published bulk microarray data of splenic iNKT cells at steady state and 1 hour post-αGalCer[91], both for the purpose of validating our scRNA-Seq data, and to compare activation-induced transcriptional remodeling in murine versus human iNKT cells.

Tissue localization and residency also have important implications for iNKT cell phenotype and function. Research using parabiotic congenic mouse models by Thomas *et al*. (2011) and Lynch *et al.* (2015) has demonstrated that iNKT cells are mainly tissue resident and re-circulate much less than adaptive $CD4^+$ and $CD8^+$ T cells[49,50]. This suggests that tissue-specific biology may play an important role in regulating iNKT cell homeostasis. In support of this, work by Lynch *et al.* (2015) and others has shown that iNKT cells in adipose tissue display a unique phenotype, distinct to that of iNKT cells in lymphoid organs such as the spleen. Adipose iNKT cells are characterized by enrichment of regulatory NKT10 cells, reduced expression of IFNγ and IL-4 in response to αGalCer stimulation compared to splenic iNKT cells, reduced or absent expression of the lineage defining transcription factor PLZF, and expression of the transcription factor E4BP4[49,91,114]. At the time of starting my PhD, however, it was unclear whether adipose iNKT cells were a single monolithic population, or if they were heterogeneous.

To address this question, and to complement our 10x scRNA-Seq of splenic iNKT cells, we performed 10x scRNA-Seq of adipose iNKT cells at steady state and 4 hours post-αGalCer. This enabled us to characterize adipose iNKT cell heterogeneity, and also permitted us to analyze iNKT cell activation among a second, regulatory population of iNKT cells.

## Hypothesis

We hypothesized that adipose iNKT cells were heterogeneous, and that there would be distinct NKT1, NKT2 and/or NKT17 cell populations present in adipose tissue. We hypothesized that activation would induce transcriptional remodeling in both splenic and adipose iNKT cells, but that there would be differences in the extent or type of transcriptional changes exhibited by adipose and splenic iNKT cells in response to αGalCer. We hypothesized that NKT1, NKT2, and NKT17 cells would exhibit differential transcriptional remodeling, or differential utilization of molecular pathways during activation. We also hypothesized that human iNKT cells would share some similarities with murine iNKT cells with respect to activation-induced transcriptional remodeling and might also display some heterogeneity.

## Aims

We analyzed scRNA-Seq of iNKT cells from spleen and adipose tissue at steady state and 4 hours post-αGalCer, in combination with reanalysis of published transcriptomic iNKT cell data, including human iNKT cell scRNA-Seq data, and focused in particular on the following:

- The composition of the splenic and adipose iNKT cell repertoire at steady state
- The transcriptional signatures of murine and human iNKT cell activation, including iNKT cell subsets, e.g. NKT1, NKT2, and NKT17 cells

### 3.1 Exploring splenic iNKT cell heterogeneity at steady state

We began our analysis of our 10x scRNA-Seq data by analyzing murine splenic iNKT cell heterogeneity under steady state conditions. After quality control measures, we retrieved 5,798 splenic iNKT cells expressing a median of 3,522 UMIs and 1,491 genes per cell. UMAP and clustering analysis revealed five separate clusters (Figure 3.1.A), including two clusters of NKT1 cells expressing *Tbx21* (NKT1-A and NKT1-B), a population of NKT2 cells expressing *Zbtb16*, a population of NKT17 cells co-expressing *Zbtb16* and *Rorc*, and small population of cycling cells expressing the proliferation marker *Mki67* (Figure 3.1.A, Figure 3.1.B). NKT1 cells comprised a majority (>85%) of all iNKT cells present in the spleen, consistent with previous analyses of C57BL/6 splenic iNKT cells[59,67], and only a minority of cells were actively cycling, consistent with previous measurements of splenic iNKT cell proliferation at steady state by Sag *et al.* (2014)[91].

We next performed gene expression and correlation analysis to further investigate the gene signatures and transcriptional relatedness of each cluster. Both clusters of NKT1 cells displayed broad expression of NKT1 cell markers previously reported in the literature, including *Klrb1c*, *Cxcr3, Ccl5*, *Il2rb*, *Xcl1*, the slam family member *Slamf7*, the Id transcription factor *Id2*, and *Nkg7* (Figure 3.1.C)[45,46,61,67,330]. However, NKT1-B cells, but not NKT1-A cells, also showed enrichment of the transcription factor *Klf2*, and the KLF2 regulon genes *S1pr1*, *Emp3*, and *S100a6*, while expression of *S100a4* was specific to NKT17 cells (Figure 3.1.C). KLF2 has been shown to play a key role in egress of developing iNKT cells from the thymus[54,65], and is known to be enriched among recent thymic emigrants (RTEs) that traffic from the thymus to the peripheral tissues[51,67]. This suggests that NKT1-B cells could be RTEs, whereas NKT1-A cells, which lacked expression of *Klf2* and had high expression of *Cxcr3* (Figure 3.1.C), could represent a resident population of splenic NKT1 cells, similar to previously described resident $CXCR3^+$ NKT1 cells in the thymus[54]. NKT1-B cells also displayed enrichment of genes

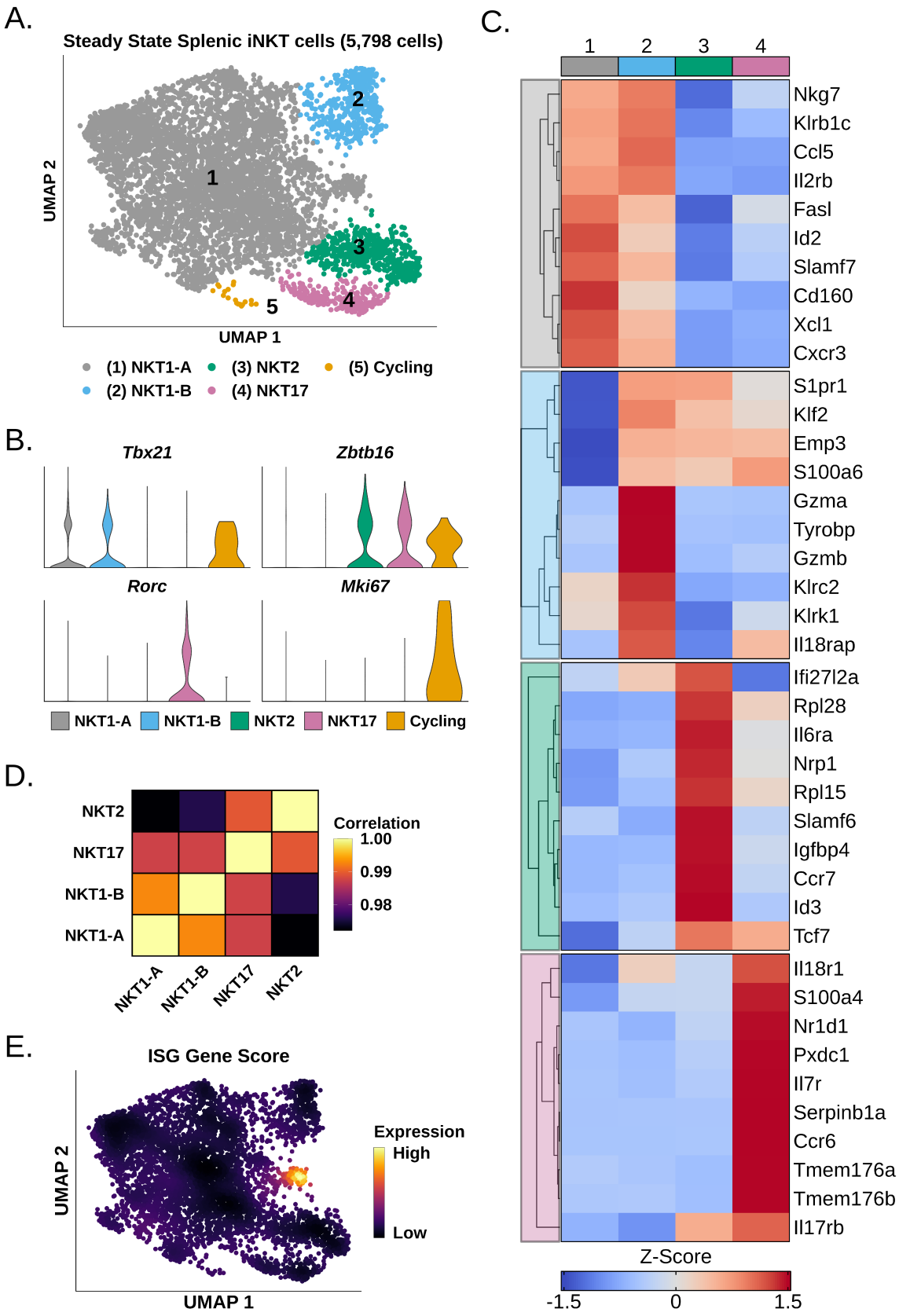
associated with cytotoxicity, including *Gzma*, *Klrk1*, the killer-cell inhibitory receptor (KIR) adapter protein *Tyrobp*, and the IL-18 receptor accessory subunit *Il18rap*.

Profiling of NKT2 cells revealed enrichment of *Il6ra*, *Ccr7*, the RTE marker *Nrp1*, *Slamf6*, *Tcf7*, and *Il17rb*, although expression of *Il17rb* was highest among NKT17 cells (Figure 3.1.C). Interestingly, we detected co-enrichment of many differentially expressed genes (DEGs) between NKT2 and NKT17 cells, including KLF2-regulon genes (Figure 3.1.C), reflecting known enrichment of NKT2 and NKT17 cells among RTEs[51,67]. Notably, we found that both NKT2 and NKT17 cells, but especially NKT2 cells, showed increased expression of ribosomal genes (Figure 3.1.C), such as *Rpl28* and *Rpl15*, and KEGG Ribosome was significantly enriched by GSEA in NKT2 cells (adjusted P value = 1.487113e-24, normalized enrichment score = 2.7574399)[265,312,314]. Other genes enriched among NKT2 cells included the transcription factor *Id3*, which has previously been linked to NKT2 cells[330], the interferon stimulated gene (ISG) *Ifi27l2a*, which has been identified as an Nur77 inhibitor and binding partner[331], and the insulin-like growth factor binding protein *Igfbp4* (Figure 3.1.C). Genes enriched among NKT17 cells included *Serpinb1a*, *Il7r*, *Ccr6*, the Th17 cation receptors *Tmem176a* and *Tmem176b*[332], *Nr1d1*, and the uncharacterized gene *Pxdc1* (Figure 3.1.C). NKT17 cells also displayed enriched of *Il18rap* and the IL-18 receptor *Il18r1*. IL-18 has been shown to inhibit Th17 responses[333,334], suggesting that it might also negatively regulate NKT17 cell function. Correlating with published work[92], whole transcriptome correlation analysis demonstrated that NKT1 and NKT2 cells were the most transcriptomically distant subsets, with NKT17 cells displaying an intermediate phenotype, but clustering more closely with NKT2 than NKT1 cells (Figure 3.1.D).

Among NKT1 cells, in addition to the previously described NKT1-A and NKT1-B cell heterogeneity, we also identified a small population of cells enriched for transcripts associated with ISGs (Figure 3.1.E). A population of iNKT cells

enriched for ISGs has previously been described in the thymus by Baranek *et al.* (2020), also among NKT1 cells[65]. This suggests that these ISG$^{high}$ iNKT cells might represent a conserved population or cell state, although further analysis and data will be required to characterize these cells more fully.

**Figure 3.1: Exploring splenic iNKT cell heterogeneity at steady state (overleaf).** A. UMAP of steady state splenic iNKT cells. B. Violin plots showing gene expression in the clusters from Figure 3.1.A. C. Scaled average heatmap with hierarchical clustering of gene expression in the clusters from Figure 3.1.A. Cycling cells were excluded from the analysis. D. Correlation plot of whole normalized transcriptomes in the clusters from Figure 3.1.A. Cycling cells were excluded from the analysis. E. Density plot of ISG gene module scoring in steady state iNKT cells.


A.
Steady State Splenic iNKT cells (5,798 cells)
UMAP 2
UMAP 1
1
2
3
4
5
(1) NKT1-A
(2) NKT1-B
(3) NKT2
(4) NKT17
(5) Cycling
B.
Tbx21
Zbtb16
Rorc
Mki67
NKT1-A
NKT1-B
NKT2
NKT17
Cycling
C.
1
2
3
4
Nkg7
Klrb1c
Ccl5
Il2rb
Fasl
Id2
Slamf7
Cd160
Xcl1
Cxcr3
S1pr1
Klf2
Emp3
S100a6
Gzma
Tyrobp
Gzmb
Klrc2
Klrk1
Il18rap
Ifi27l2a
Rpl28
Il6ra
Nrp1
Rpl15
Slamf6
Igfbp4
Ccr7
Id3
Tcf7
Il18r1
S100a4
Nr1d1
Pxdc1
Il7r
Serpinb1a
Ccr6
Tmem176a
Tmem176b
Il17rb
Z-Score
-1.5
0
1.5
D.
NKT2
NKT17
NKT1-B
NKT1-A
Correlation
1.00
0.99
0.98
E.
ISG Gene Score
UMAP 2
UMAP 1
Expression
High
Low

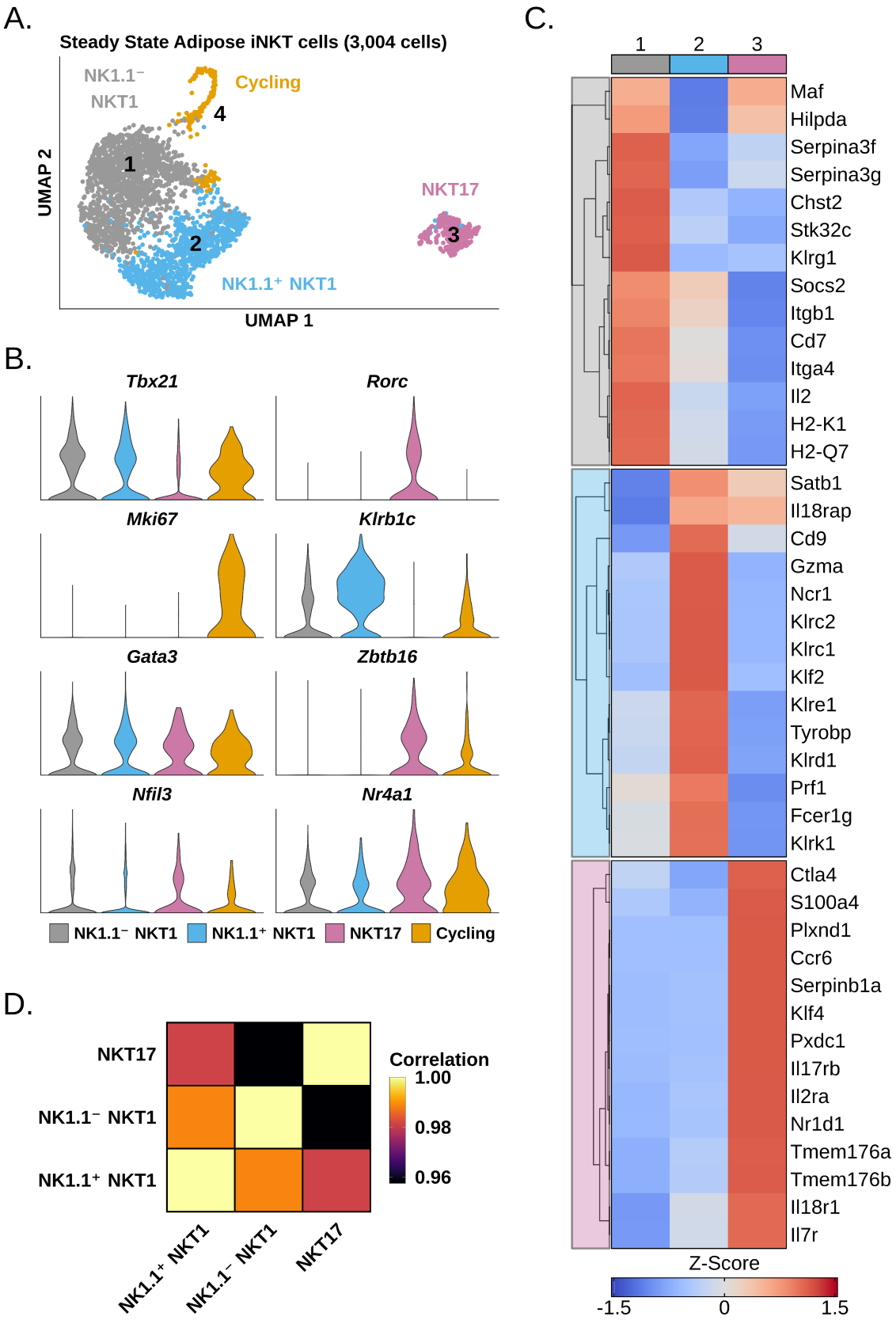
### 3.2 Exploring adipose iNKT cell heterogeneity at steady state

We next analyzed steady state transcriptional heterogeneity among murine adipose iNKT cells. After quality control measures, we retrieved 3,004 adipose iNKT cells expressing a median of 6,319 UMIs and 2,167 genes per cell. UMAP and clustering analysis revealed four separate clusters (Figure 3.2.1.A), including two clusters of NKT1 cells (NK1.1$^{+}$ NKT1 cells and NK1.1$^{-}$ NKT1 cells) expressing *Tbx21*, a population of NKT17 cells co-expressing *Zbtb16* and *Rorc*, and a population of cycling cells expressing the proliferation marker *Mki67* (Figure 3.1.A, Figure 3.1.B). Notably, we did not identify a PLZF$^{high}$ NKT2 cell population (Figure 3.1.A), and *Gata3*, which has been used as a marker for NKT2 cells[63], was expressed by all adipose iNKT cell clusters (Figure 3.2.1.B), consistent with previous analysis by Lynch *et al.* (2015) demonstrating that most adipose iNKT cells express GATA3[49]. The absence of NKT2 cells in adipose tissue was confirmed by LaMarche *et al.* (2020), who found that that PLZF$^{high}$ NKT2 cells are not present in the adipose tissue of adult mice, although they are present in neonates[115]. All adipose iNKT cell clusters showed enrichment of the adipose iNKT cell transcription factor *Nfil3*, and the activation marker *Nr4a1* (Figure 3.2.1.B), matching previous analysis of adipose iNKT cells by Lynch *et al.* (2015)[49]. As with splenic iNKT cells, NKT1 cells comprised a majority (>80%) of adipose iNKT cells. Notably, unlike splenic NKT1 cells, adipose NKT1 cells separated into two distinct clusters based on expression of *Klrb1c*, which encodes the surface receptor NK1.1 (Figure 3.2.1.A, Figure 3.2.1.B). Work by Lynch *et al.* (2015) has previously shown that the frequency of NK1.1$^{+}$ iNKT cells is reduced among adipose versus splenic iNKT cells[49], and our scRNA-Seq analysis demonstrates that a significant proportion of adipose NKT1 cells (~61%) are *Klrb1c*$^{neg}$ or *Klrb1c*$^{low}$.

We next performed gene expression analysis to characterize each adipose iNKT cell subset. NK1.1$^{-}$ NKT1 cells showed enrichment of the transcription factor *Maf* and the lipid accumulation factor *Hilpda*, both of which were also highly expressed by NKT17 cells, the surface receptor *Klrg1*, the antigen

specific T cell and memory-like iNKT cell marker *Itga4*[206,335,336], *Il2*, the serine and/or cysteine protease inhibitors *Serpina3g* and *Serpina3f*, the sulfotransferase *Chst2*, the histocompatibility genes *H2-Q7* and *H2-K1*, and the integrin β subunit *Itgb1* (Figure 3.2.1.C). NK1.1$^{+}$ NKT1 cells displayed increased expression of many different immunoreceptors, and genes associated with cytotoxicity, including *Klrc1*, *Klrc2*, *Ncr1*, *Klrk1*, *Prf1*, *Gzma*, *Klre1* and *Tyrobp* (Figure 3.2.1.C), as well as *Klf2*, *Il18rap*, the transcription factor *Satb1*, which was also expressed by NKT17 cells, and the tetraspanin *Cd9*. Overall, the transcriptional profile of adipose NK1.1$^{+}$ NKT1 cells was similar to that of the NKT1-B cell cluster identified among splenic iNKT cells (Figure 3.1.A, Figure 3.1.C). Similarly, adipose NKT17 cells showed enrichment of many of the same genes as splenic NKT17 cells, including *Nr1d1*, *Tmem176a* and *Tmem176b*, *Serpinb1a*, *Il7rb*, *Il7r*, *Pxdc1*, *Ccr6* and *S100a4* (Figure 3.1.C, Figure 3.2.1.C). Uniquely enriched transcripts among adipose NKT17 cells included the IL-2 receptor α subunit *Il2ra*, the immunoregulatory receptor *Ctla4*, the kruppel-like transcription factor *Klf4*, and the semaphorin receptor *Plxnd1* (Figure 3.2.1.C). Whole transcriptome correlation analysis revealed that NKT17 cells were more similar to NK1.1$^{+}$ NKT1 cells than NK1.1$^{-}$ NKT1 cells, with NK1.1$^{+}$ and NK1.1$^{-}$ NKT1 cells displaying the greatest transcriptional overlap.

**Figure 3.2.1: Exploring adipose iNKT cell heterogeneity at steady state (overleaf).** A. UMAP of steady state adipose iNKT cells. B. Violin plots showing gene expression in the clusters from Figure 3.2.1.A. C. Scaled average heatmap with hierarchical clustering of gene expression in the clusters from Figure 3.2.1.A. Cycling cells were excluded from the analysis. D. Correlation plot of whole normalized transcriptomes in the clusters from Figure 3.2.1.A. Cycling cells were excluded from the analysis.

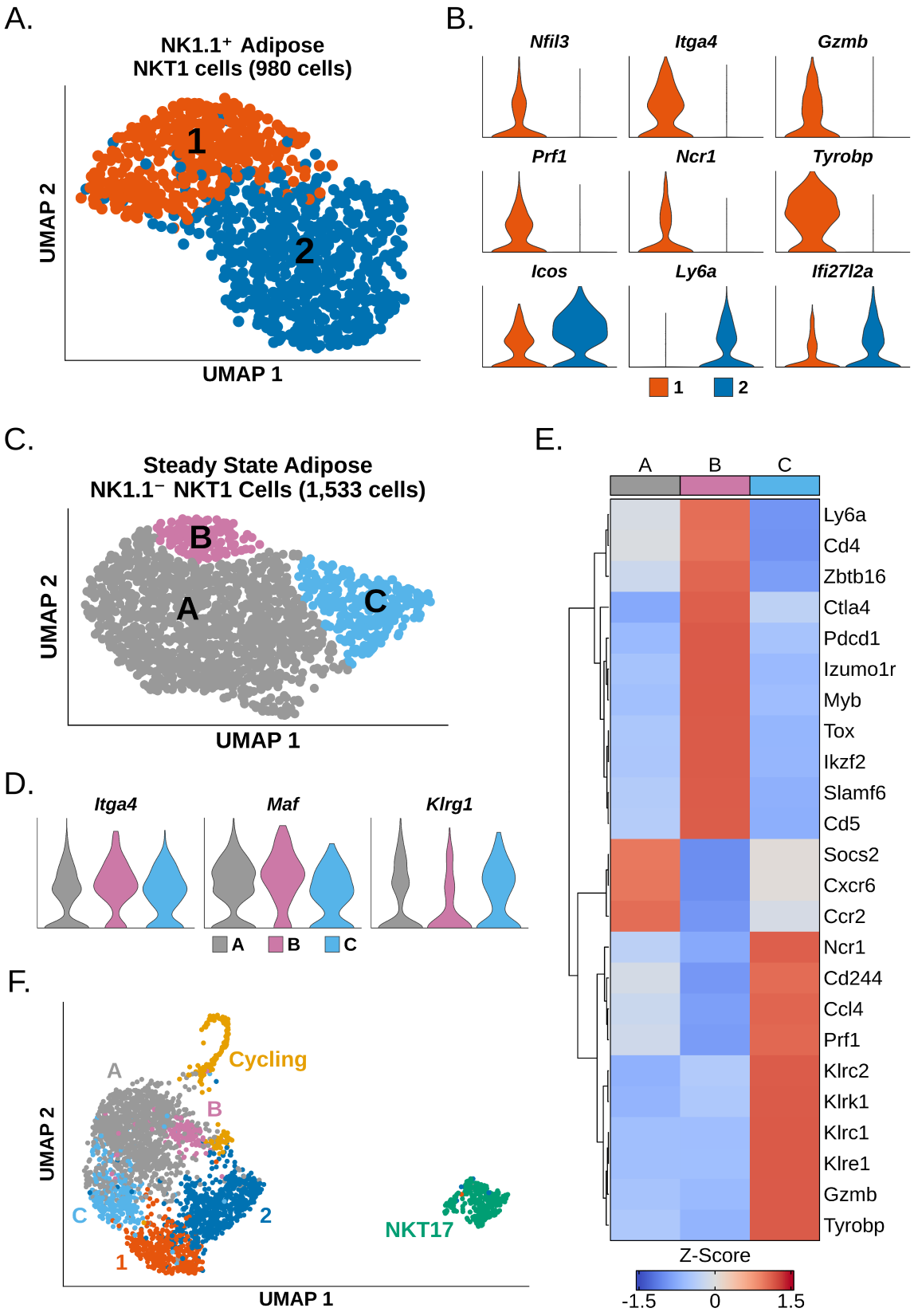

A.
Steady State Adipose iNKT cells (3,004 cells)
NK1.1⁻ NKT1
Cycling
4
1
2
NKT17
3
NK1.1⁺ NKT1
UMAP 2
UMAP 1
B.
Tbx21
Rorc
Mki67
Klrb1c
Gata3
Zbtb16
Nfil3
Nr4a1
NK1.1⁻ NKT1
NK1.1⁺ NKT1
NKT17
Cycling
C.
1
2
3
Maf
Hilpda
Serpina3f
Serpina3g
Chst2
Stk32c
Klrg1
Socs2
Itgb1
Cd7
Itga4
Il2
H2-K1
H2-Q7
Satb1
Il18rap
Cd9
Gzma
Ncr1
Klrc2
Klrc1
Klf2
Klre1
Tyrobp
Klrd1
Prf1
Fcer1g
Klrk1
Ctla4
S100a4
Plxnd1
Ccr6
Serpinb1a
Klf4
Pxdc1
Il17rb
Il2ra
Nr1d1
Tmem176a
Tmem176b
Il18r1
Il7r
Z-Score
-1.5
0
1.5
D.
NKT17
NK1.1⁻ NKT1
NK1.1⁺ NKT1
Correlation
1.00
0.98
0.96
NK1.1⁺ NKT1
NK1.1⁻ NKT1
NKT17

Having broadly profiled adipose iNKT cell heterogeneity, we next decided to perform more granular analysis. Visual examination of the adipose iNKT cell UMAP suggested that there might be additional heterogeneity among NK1.1$^{+}$ and NK1.1$^{-}$ NKT1 cells. Granular analysis of NK1.1$^{+}$ NKT1 cells revealed two distinct subclusters, Cluster 1 and Cluster 2 (Figure 3.2.2.A). Gene expression analysis demonstrated that cells in Cluster 1 were enriched for the adipose iNKT cell marker *Nfil3*, and this correlated with increased expression of the memory-like marker *Itga4*, and genes associated with cytotoxicity, including *Gzmb*, *Prf1*, *Ncr1*, and *Tyrobp* (Figure 3.2.2.B). By contrast, cells in Cluster 2, displaying reduced expression of *Nfil3*, showed enrichment for the co-stimulatory receptor *Icos*, *Ly6a* (encoding Sca-1), and *Ifi27l2a*, which was previously associated with NKT2 cells in the spleen (Figure 3.1.C). Since work by LaMarche *et al.* (2020) has demonstrated that *Nfil3* expression is acquired by adipose iNKT cells in response to lipids after they localize to the adipose tissue[115], reduced *Nfil3* expression in Cluster 2 cells could indicate that this population of iNKT cells only recently localized to the adipose tissue, and had yet to upregulate *Nfil3*, although we did not identify co-enrichment of RTE markers. It is also possible that iNKT cells in Cluster 2 could be resident in a less lipid rich environment within the adipose tissue, such as the vasculature.

We next performed granular analysis of NK1.1$^{-}$ NKT1 cells. UMAP and clustering analysis revealed three different clusters of NK1.1$^{-}$ NKT1 cells, Cluster A, Cluster B, and Cluster C (Figure 3.2.2.C). While all three subclusters expressed the prominent NK1.1$^{-}$ NKT1 cell markers *Itga4*, *Maf*, and *Klrg1* (Figure 3.2.2.D), gene expression analysis identified multiple DEGs specifically enriched in Cluster A, Cluster B, and Cluster C cells (Figure 3.2.2.E). Clusters B cells demonstrated increased expression of the immunoregulatory receptors *Pdcd1* (encoding PD-1), *Lag3*, and *Ctla4*, the Treg marker *Izumo1r* (encoding FR4), the NKT2 cell markers *Slamf6*, *Zbtb16* and Cd4, and the transcription factors *Tox*, *Ikzf2,* and *Myb* (Figure 3.2.2.E). Cluster A cells displayed enrichment of *Socs2*, *Cxcr6* and *Ccr2* (Figure 3.2.2.E), while Cluster C cells

showed increased expression of genes associated with cytotoxicity, including *Gzmb*, *Prf1*, *Ncr1*, *Klrc1*, *Klrc2*, *Klre1*, *Klrk1*, *Cd244* (encoding 2B4), the chemokine *Ccl4*, and *Tyrobp* (Figure 3.2.2.E). We next tested the robustness of our granular analysis by mapping NK1.1$^{+}$ and NK1.1$^{-}$ subclusters back to the original adipose iNKT cell UMAP. We found that NK1.1$^{+}$ and NK1.1$^{-}$ NKT1 cell subclusters separated from each other in dimensional space (Figure 3.2.2.F), analogous to clustering at a higher resolution on the original adipose iNKT cell UMAP. This indicates that these subclusters are transcriptomically robust and constitute a second level of heterogeneity among adipose NKT1 cells at steady state.

**Figure 3.2.2: Granular analysis of NK1.1$^{+}$ and NK1.1$^{-}$ adipose NKT1 cells at steady state (overleaf).** A. UMAP of steady state adipose NK1.1$^{+}$ NKT1 cells. B. Violin plots showing gene expression in the clusters from Figure 3.2.2.A. C. UMAP of adipose NK1.1$^{-}$ NKT1 cells at steady state. D. Violin plots showing gene expression in the clusters from Figure 3.2.2.C. E. Scaled average heatmap with hierarchical clustering of gene expression in the clusters from Figure 3.2.2.C. F. UMAP of steady state adipose iNKT cells with mapping of the subclustering from Figure 3.2.2.A and Figure 3.2.2.C applied.


A.
NK1.1⁺ Adipose
NKT1 cells (980 cells)
UMAP 2
UMAP 1
1
2
B.
Nfil3
Itga4
Gzmb
Prf1
Ncr1
Tyrobp
Icos
Ly6a
Ifi27l2a
1
2
C.
Steady State Adipose
NK1.1⁻ NKT1 Cells (1,533 cells)
UMAP 2
UMAP 1
A
B
C
D.
Itga4
Maf
Klrg1
A
B
C
E.
A
B
C
Ly6a
Cd4
Zbtb16
Ctla4
Pdcd1
Izumo1r
Myb
Tox
Ikzf2
Slamf6
Cd5
Socs2
Cxcr6
Ccr2
Ncr1
Cd244
Ccl4
Prf1
Klrc2
Klrk1
Klrc1
Klre1
Gzmb
Tyrobp
Z-Score
-1.5
0
1.5
F.
UMAP 2
UMAP 1
A
B
C
Cycling
1
2
NKT17

### 3.3 Transcriptional analysis of adipose versus splenic iNKT cells at steady state

After profiling steady state heterogeneity among splenic and adipose iNKT cells, we next sought to compare adipose versus splenic iNKT cells. To do this, we combined our adipose and splenic steady state data into a single normalized file of 8,833 iNKT cells for further analysis. Strikingly, adipose and splenic iNKT cells displayed almost no overlap by UMAP (Figure 3.3.1.A), suggesting that the transcriptomes of adipose and splenic iNKT cells are highly distinct. Gene expression analysis identified 7,566 DEGs between splenic and adipose iNKT cells, of which 3,021 were enriched among splenic iNKT cells, and 4,545 were enriched among adipose iNKT cells. We next performed over-representation analysis against the KEGG pathway database to compare DEGs enriched in adipose versus splenic iNKT cells. Splenic iNKT cells demonstrated enrichment of genes associated with the ribosome, oxidative phosphorylation, and immune function, including *Il7r*, *Il4*, *Ltb*, and *Cxcr6* (Figure 3.3.1.B). Adipose iNKT cells displayed enrichment of genes associated with cell death and cytotoxicity (Apoptosis, Natural killer cell mediated cytotoxicity), the actin cytotskeleton and cellular adhesion (Transendothelial leuckocyte migration, Focal adhesion), IL-17 signaling, DNA replication, and cellular senescence (Figure 3.3.1.B). We noted that our over-representation analysis correlated closely with the composition of the adipose and splenic iNKT cell repertoires, as enrichment of ribosomal transcripts correlated with the presence of NKT2 cells in the spleen but not adipose tissue (Figure 3.1.C, Figure 3.3.1.C), while a three-fold enrichment of NKT17 cells and >ten-fold enrichment of cycling cells correlated with over-representation of IL-17 signaling and DNA replication pathways among adipose iNKT cells.

We next analyzed leading edge genes from our pathway analysis in more detail. Adipose iNKT cells demonstrated enrichment of both pro-apoptotic genes, including *Bcl2l11*, *Casp3*, *Bid*, and *Apaf1*, and anti-apoptotic genes, such as *Bcl2*, *Bcl2a1b*, *Bcl2a1d*, and *Bcl2l1* (Figure 3.3.1.D). This suggested

that adipose iNKT cells might be subject to increased apoptotic pressure or stress, and work by LaMarche *et al.* (2020) showed that adipose iNKT cells undergo apoptosis at an increased rate compared to splenic iNKT cells[115]. Similarly, we identified enrichment of both positive and negative markers of cellular senescence among adipose iNKT cells, including positive markers such as *Klrg1*, *Cdkn1a*, *Map2k3*, *Mapk3*, *Akt1*, *Mapk14*, and *Klrk1*, and the negative markers *Foxo3* and *Sirt1* (Figure 3.3.1.D)[337,338]. Adhesion and actin cytoskeleton genes enriched among adipose iNKT cells included *Itgb1*, *Itga4*, *Itga1*, *Actb*, *Flna* and *Actg1*, while *Gzmb*, *Fasl*, and *Hcst* were among the top cytotoxicity markers (Figure 3.3.1.D). The enrichment of genes associated with oxidative phosphorylation in splenic iNKT cells, such as *mt-Co2*, *mt-Cytb*, *mt-Nd4*, and *Cox7a2l*, is intriguing, as it suggests that adipose and splenic iNKT cells might utilize distinct metabolic programs. Aside from genes detected through over-representation analysis, we also independently identified enrichment of genes associated with ER stress. Work by LaMarche *et al.* (2020) found that adipose iNKT cells undergo lipid-mediated ER stress through the IRE1a-XBP1s arm of the UPR, which induces expression of E4BP4 (*Nfil3*), promoting expression of IL-10[115]. In support of this finding, adipose iNKT cells showed enrichment of ER stress markers and XBP1 target genes, including *Dnaj9b*, *Atf4*, *Atf3*, *P4hb*, *Xbp1* and *Atf6* (Figure 3.3.1.D). As prolonged ER stress can also induce cell death[339], this finding synergizes with the apoptotic phenotype of adipose iNKT cells, implicating the lipid rich microenvironment in adipose tissue as both an inducer of E4BP4 and IL-10 expression among iNKT cells, and as a source of cellular stress leading to increased apoptosis[115].

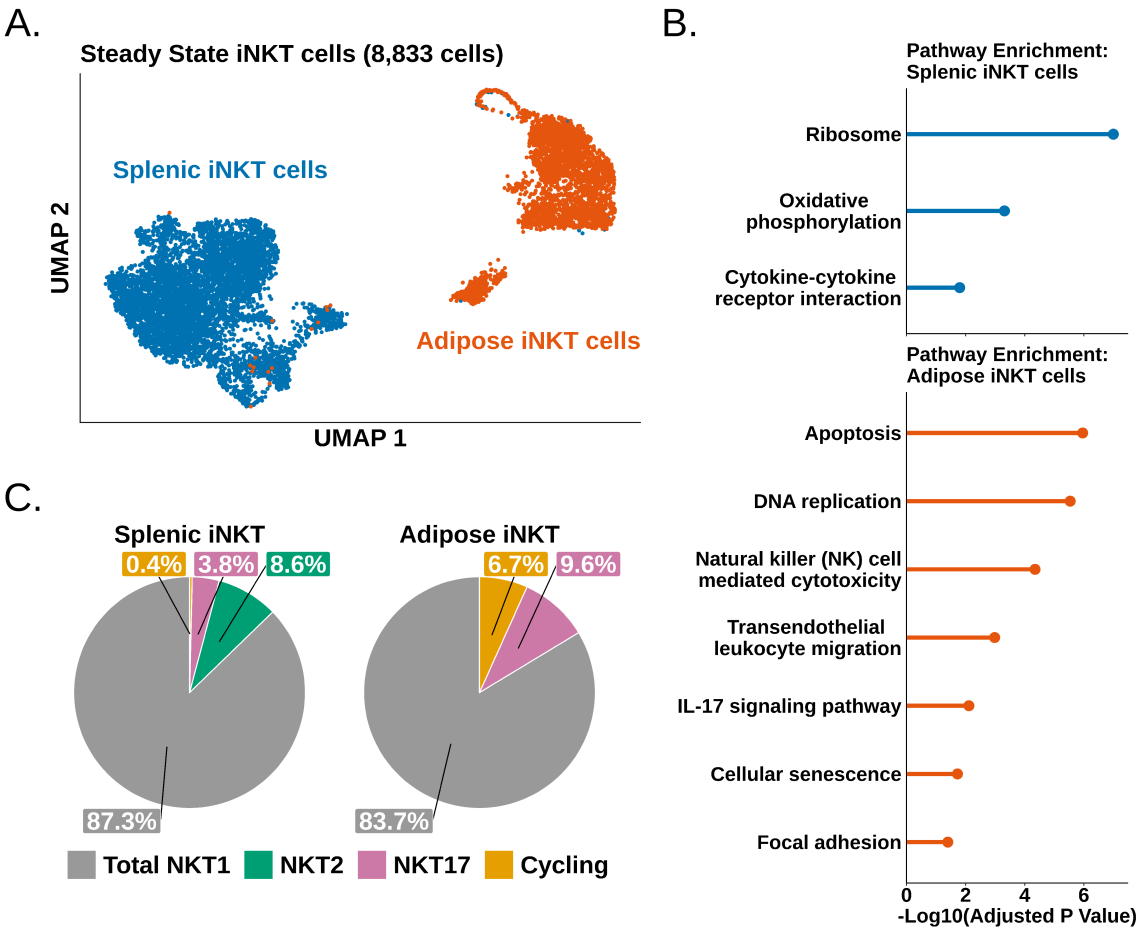

A.
Steady State iNKT cells (8,833 cells)
Splenic iNKT cells
Adipose iNKT cells
UMAP 2
UMAP 1
B.
Pathway Enrichment:
Splenic iNKT cells
Ribosome
Oxidative phosphorylation
Cytokine-cytokine receptor interaction
Pathway Enrichment:
Adipose iNKT cells
Apoptosis
DNA replication
Natural killer (NK) cell mediated cytotoxicity
Transendothelial leukocyte migration
IL-17 signaling pathway
Cellular senescence
Focal adhesion
0
2
4
6
-Log10(Adjusted P Value)
C.
Splenic iNKT
0.4%
3.8%
8.6%
87.3%
Adipose iNKT
6.7%
9.6%
83.7%
Total NKT1
NKT2
NKT17
Cycling
D.
Apoptosis
Apaf1
Bcl2l11
Bcl2
Bcl2a1b
Bcl2a1d
Bcl2l1
Casp3
Bid
Senescence
Mapk14
Klrg1
Cdkn1a
Foxo3
Map2k3
Mapk3
Akt1
Sirt1
NK Cell Cytotoxcity
Klrk1
Fcer1g
Klra1
Fasl
Tyrobp
Gzmb
Cd244
Hcst
Adhesion/Actin Cytoskeleton
Rap1b
Itgb1
Zyx
Itga4
Itga1
Flna
Actb
Actg1
-Log10(Adjusted P Value)
Oxidative Phosphorylation
mt-Co1
mt-Co2
mt-Nd4
mt-Co3
mt-Atp6
mt-Cytb
mt-Nd2
Cox7a2l
ER Stress
Atf6
Dnajb9
Atf4
Atf3
Edem1
P4hb
Xbp1
Dnajb11
300
200
100
0
150
50

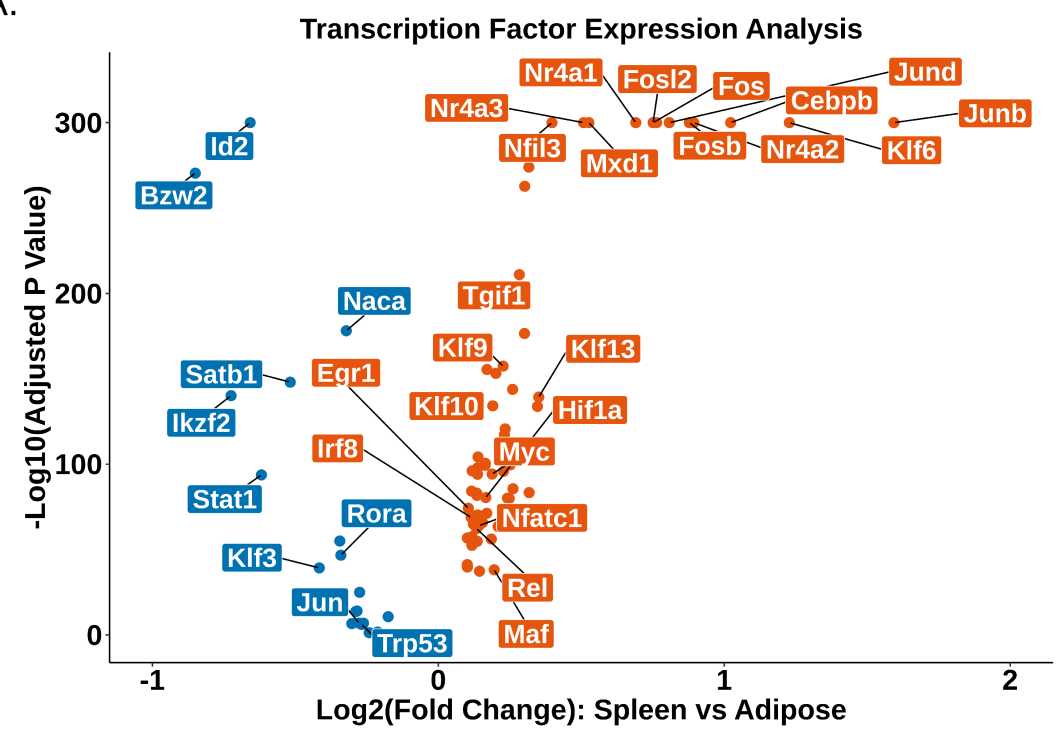
**Figure 3.3.1: Transcriptional comparison of adipose versus splenic iNKT cells at steady state (previous page).** A. UMAP of adipose and splenic cells at steady state. B. Lollipop plots showing KEGG pathway enrichment from over-representation analysis of adipose versus splenic iNKT cells. C. Pie charts comparing the frequency of total NKT1 ($NK1.1^+$ and $NK1.1^-$), NKT2, NKT17, and cycling cells among the splenic and adipose iNKT cells in Figure 3.3.1.A, based on the individual clustering analysis in Figure 3.1.A and Figure 3.2.1.A. D. Radar charts showing over-representation of different biological pathways in adipose (orange radar charts) or splenic (blue radar chart) iNKT cells.

We next sought to characterize transcription factor enrichment among adipose and splenic iNKT cells. Transcription factors enriched among splenic iNKT cells included *Bzw2*, *Id2*, which has previously been associated with regulation of iNKT cell activation and responsiveness to antigen[340], *Satb1*, which has also been implicated during T cell activation and may play a role in preventing premature exhaustion of activated T cells[341], *Naca*, which plays a role in directing protein trafficking, *Ikzf2*, and the AP1 family member *Jun* (Figure 3.3.2.A). Adipose iNKT cells showed increased expression of transcription factors associated with TCR stimulation and T cell activation, including *Nr4a1*, *Nr4a2*, *Nr4a3*, *Irf8*, *Myc*, *Hif1a*, and *Egr1* (Figure 3.3.2.A)[40,152,291,342,343]. Adipose iNKT cells also expressed T cell activation markers such as *Il2* and *Cd69*, and metabolic genes associated with T cell activation, including *Tfrc*, *Ldha*, *Pkm*, *Slc3a2*, and *Slc1a5* (Figure 3.3.2.B)[152,160,161,163]. This suggests that adipose iNKT cells may be more activated than splenic iNKT cells at steady state. Other transcription factors enriched among adipose iNTK cells included *Nfil3*, a suite of different AP1 family members, including *Junb*, *Fos*, *Fosb*, *Fosl2*, *Maf*, and *Jund*, the Kruppel-like factor family members *Klf6*, *Klf9*, *Klf13*, and *Klf10*, the *Myc* binding partner and inhibitor *Mxd1*, *Stat1*, and *Nfatc1* (Figure 3.3.2.A), as well as *Nfatc2*, *Nfatc3*, and *Tox* (Figure 3.3.2.B). Interestingly, co-

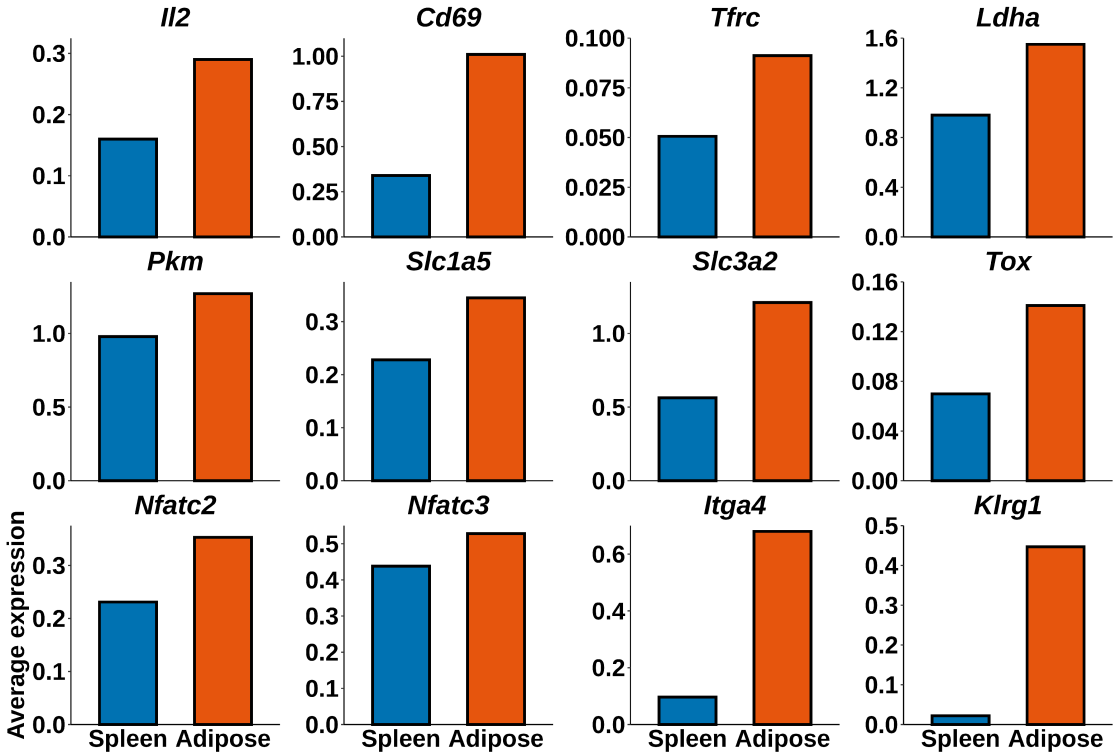
enrichment of *Nr4a* and *Nfat* transcription factors has previously been linked to chronic TCR signaling, chronic activation, and T cell exhaustion[170,172], suggesting that adipose iNKT cells could be exhausted at steady state[170]. Since adipose iNKT cells also demonstrated enrichment of the memory-like and antigen experience markers *Klrg1* and *Itga4* (Figure 3.3.2.B), the transcriptional phenotype of adipose iNKT cells collectively suggests that these cells are exposed to chronic endogenous activation, possibly as a result of the lipid rich microenvironment in adipose tissue, and thus may already be antigen experienced at steady state.

**Figure 3.3.2: Transcriptional comparison of adipose versus splenic iNKT cells at steady state (continued; overleaf).** A. Volcano plot of transcription factors enriched in splenic (blue) versus adipose (orange) iNKT cells at steady state. B. Bar plots showing mean gene expression of genes enriched in adipose versus splenic iNKT cells at steady state.

A.


Transcription Factor Expression Analysis
-Log10(Adjusted P Value)
300
200
100
0
-1
0
1
2
Log2(Fold Change): Spleen vs Adipose
Nr4a1
Fosl2
Fos
Jund
Nr4a3
Cebpb
Junb
Nfil3
Mxd1
Fosb
Nr4a2
Klf6
Id2
Bzw2
Naca
Tgif1
Klf9
Klf13
Satb1
Egr1
Klf10
Hif1a
Ikzf2
Irf8
Myc
Stat1
Rora
Nfatc1
Klf3
Rel
Jun
Maf
Trp53

B.


Il2
Cd69
Tfrc
Ldha
Pkm
Slc1a5
Slc3a2
Tox
Nfatc2
Nfatc3
Itga4
Klrg1
Average expression
Spleen Adipose

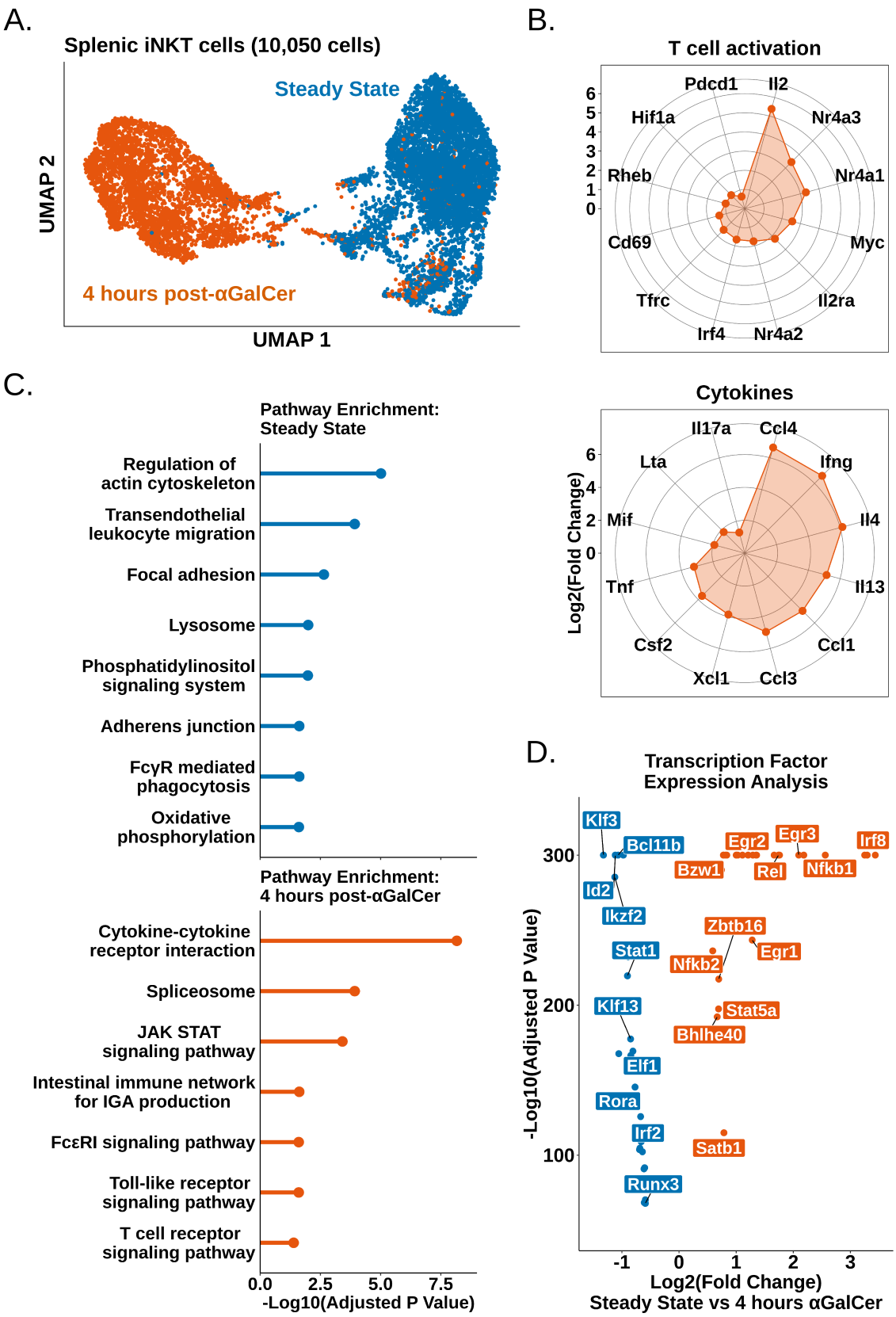
### 3.4 Splenic iNKT cells undergo rapid and dramatic transcriptional remodeling after activation with αGalCer

We next analyzed transcriptional remodeling during splenic iNKT cell activation. Quality control measures returned 4,152 splenic iNKT cells at 4 hours post-αGalCer, expressing a median of 5,950 UMIs and 1,730 genes per cell. We then merged these data with our steady state splenic iNKT cell data to create a combined file of 10,050 splenic iNKT cells. UMAP revealed that iNKT cells at steady state and 4 hours post-αGalCer displayed little overlap (Figure 3.4.1.A), indicating that splenic iNKT cells undergo rapid and extensive transcriptional remodeling after activation with αGalCer. Gene expression analysis of bulk iNKT cells at 4 hours post-αGalCer versus steady state identified enrichment of a suite of different iNKT cell and T cell activation markers, and markers of metabolic activation and remodeling, including *Il2*, *Nr4a* family transcription factors, *Myc*, *Il2ra*, *Tfrc*, which encodes the transferrin receptor, *Irf4*, *Cd69*, *Rheb*, which binds to and activates mTOR[344], *Hif1a*, and *Pdcd1* (Figure 3.4.1.B). iNKT cells at 4 hours post-αGalCer also showed significant enrichment of many cytokines and chemokines, including *Ccl4*, *Ccl3* and *Ccl1*, *Ifng*, *Il4*, *Il13*, *Xcl1*, *Csf2*, *Tnf*, *Lta*, and *Il17a* (Figure 3.4.1.B), indicative of rapid cytokine production after αGalCer stimulation.

We next performed GSEA of iNKT cells at 4 hour post-αGalCer versus steady state. Steady state iNKT cells demonstrated enrichment of genes associated with adhesion, the actin cytoskeleton, and uptake from the extracellular environment (Regulation of actin cytoskeleton, Transendothelial leukocyte migration, Focal adhesion, Adherens junction, FcγR mediated phagocytosis), as well as lysosomal genes, and genes associated with oxidative phosphorylation (Figure 3.4.1.C). By contrast, iNKT cells at 4 hours post-αGalCer were enriched for genes associated with immune activation and signaling, protein splicing, and TCR signaling (Figure 3.4.1.C). We also profiled transcription factor expression. Top transcription factors downregulated following iNKT cell activation included *Klf3*, *Id2*, which is required for normal

iNKT cell activation[340], *Stat1*, *Bcl11b*, and *Ikzf2* (Figure 3.4.1.D). Transcription factors upregulated at 4 hours post-αGalCer included *Bzw1*, *Irf8*, *Egr1* and *Erg2*, the NF-κb family members *Nfkb1*, *Nfkb2* and *Rel*, *Bhlhe40*, and *Zbtb16* (Figure 3.4.1.D). Notably, PLZF upregulation has previously been documented during iNKT cell development[41], and at 72 hours post-αGalCer[74], but here our data demonstrate that *Zbtb16* expression is rapidly increased following iNKT cell activation, correlating with previous reports indicating that PLZF is associated with the “poised” innate phenotype of iNKT cells[43].

**Figure 3.4.1: Transcriptional signatures of splenic iNKT cell activation (overleaf).** A. UMAP of splenic cells at steady state and 4 hours after *in vivo* activation with αGalCer. B. Radar charts showing enrichment of genes encoding T cell activation markers, cytokines, and secreted factors among iNKT cells at 4 hours post-αGalCer. C. Lollipop plots showing KEGG pathway enrichment from GSEA of splenic iNKT cells at 4 hours post-αGalCer versus steady state. D. Volcano plot of transcription factors enriched in splenic iNKT cells at steady state (blue) versus 4 hour post-αGalCer (orange).


A.
Splenic iNKT cells (10,050 cells)
Steady State
4 hours post-αGalCer
UMAP 2
UMAP 1
B.
T cell activation
Pdcd1
Il2
Nr4a3
Nr4a1
Myc
Il2ra
Nr4a2
Irf4
Tfrc
Cd69
Rheb
Hif1a
0
1
2
3
4
5
6
Cytokines
Il17a
Ccl4
Ifng
Il4
Il13
Ccl1
Ccl3
Xcl1
Csf2
Tnf
Mif
Lta
Log2(Fold Change)
C.
Pathway Enrichment:
Steady State
Regulation of actin cytoskeleton
Transendothelial leukocyte migration
Focal adhesion
Lysosome
Phosphatidylinositol signaling system
Adherens junction
FcγR mediated phagocytosis
Oxidative phosphorylation
Pathway Enrichment:
4 hours post-αGalCer
Cytokine-cytokine receptor interaction
Spliceosome
JAK STAT signaling pathway
Intestinal immune network for IGA production
FcεRI signaling pathway
Toll-like receptor signaling pathway
T cell receptor signaling pathway
0.0
2.5
5.0
7.5
-Log10(Adjusted P Value)
D.
Transcription Factor Expression Analysis
Klf3
Bcl11b
Egr2
Egr3
Irf8
Bzw1
Rel
Nfkb1
Id2
Ikzf2
Zbtb16
Stat1
Nfkb2
Egr1
Klf13
Stat5a
Bhlhe40
Elf1
Rora
Irf2
Satb1
Runx3
300
200
100
-Log10(Adjusted P Value)
-1
0
1
2
3
Log2(Fold Change)
Steady State vs 4 hours αGalCer

Having identified enrichment of key metabolic markers of T cell activation in iNKT cells at 4 hours post-αGalCer, including *Myc*, *Hif1a*, and *Tfrc*, we next decided to profile metabolic gene remodeling during iNKT cell activation. To do this, we compiled a series of metabolic module scores using the KEGG pathway[314] and Gene Ontology Consortium[345] databases (see Table 2.1.7) and scored our iNKT cell data. Module scoring revealed that splenic iNKT cells upregulated expression of genes associated with glycolysis, amino acid uptake and metabolism, polyamine synthesis, and fatty acid synthesis (Figure 3.4.2.A), metabolic pathways which have previously been linked to T cell activation, growth, proliferation, and effector function[152,156,160–162,346]. iNKT cells have also recently been shown to require glucose for effector cytokine production[94,304]. By contrast, activated splenic iNKT cells displayed reduced enrichment of genes associated with oxidative metabolism and β-oxidation of lipids (Figure 3.4.2.A), indicating that iNKT cells may reduce their reliance on oxidative metabolism after activation, and instead utilize aerobic glycolysis to support biosynthetic pathways[156,160].

A.

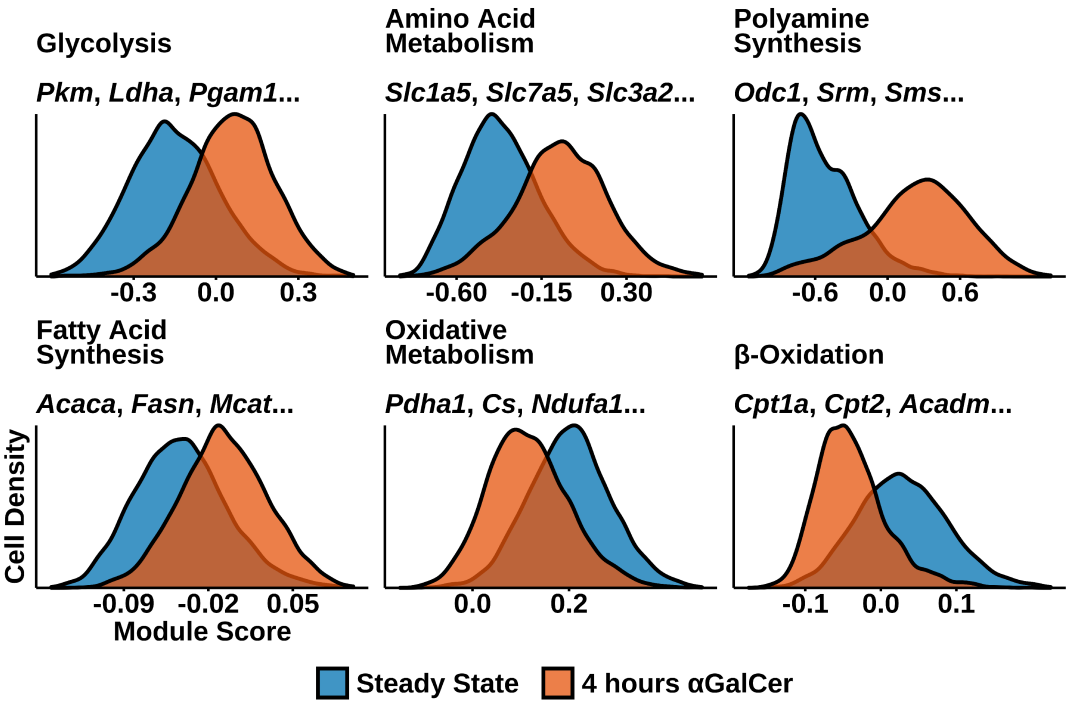
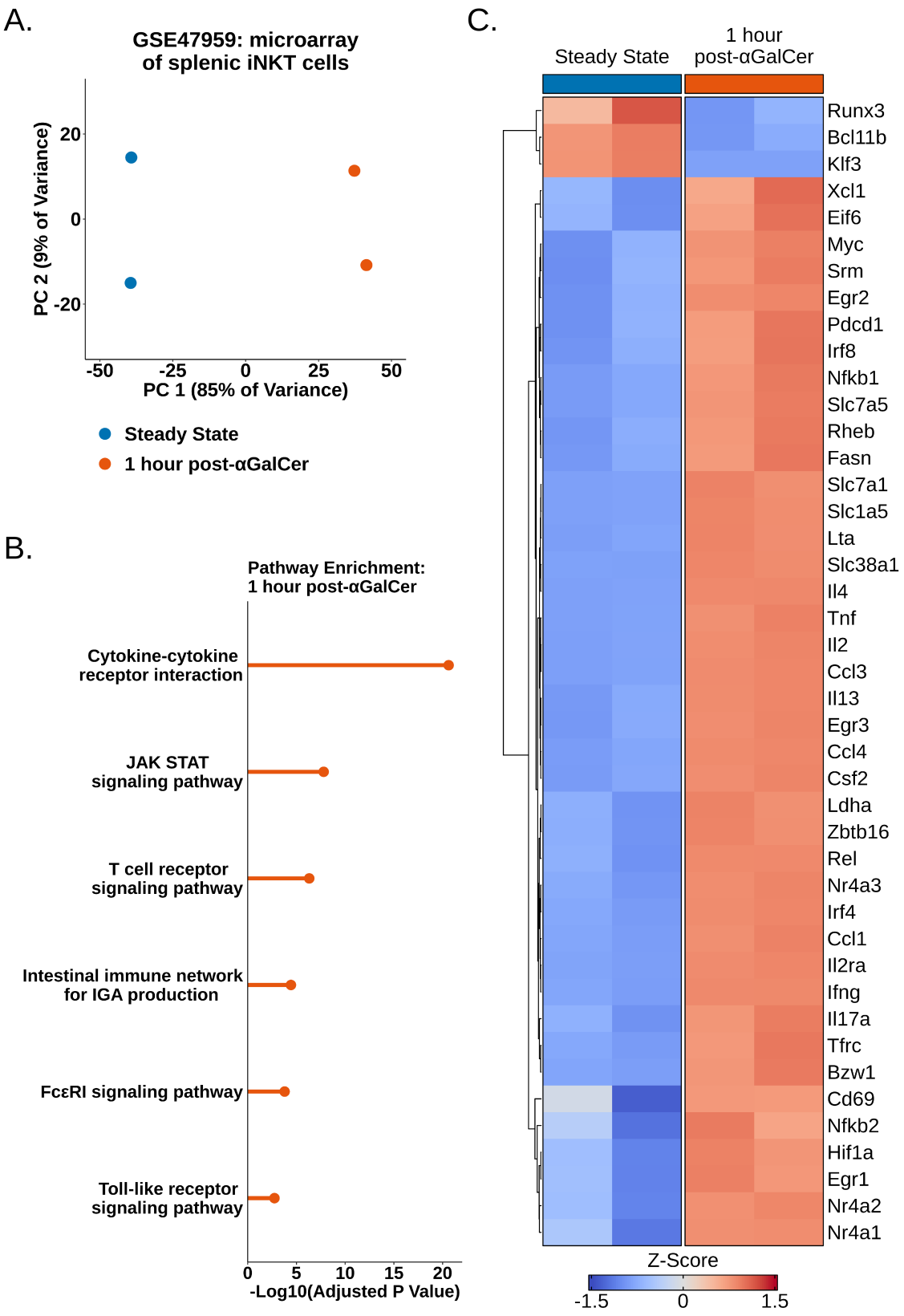



**Figure 3.4.2: Remodeling of metabolic gene expression following splenic iNKT cell activation.** A. Histograms showing expression of metabolic gene module scores in splenic iNKT cells at steady state or 4 hours post-αGalCer. Examples of the genes used for module scoring are displayed above the respective module score histograms.

Having profiled splenic iNKT cell activation using our scRNA-Seq data, we next sought to validate our findings using published microarray data. Sag *et al.* (2014) previously published a dataset containing bulk sequencing of splenic iNKT cells at steady state and 1 hour post-αGalCer (GSE47959)[91], and we reanalyzed these data. PCA showed that steady state and 1 hour post-αGalCer samples were transcriptomically distinct (Figure 3.4.3.A), indicative of rapid transcriptomic remodeling following αGalCer stimulation, similar to our scRNA-Seq data. Likewise, iNKT cell samples at 1 hour post-αGalCer displayed enrichment of multiple KEGG pathways previously associated with iNKT cell activation, including Cytokine-cytokine receptor interaction, JAK STAT signaling, and TCR signaling (Figure 3.4.3.B), indicating close correlation with our scRNA-Seq data. Moreover, gene expression analysis comparing steady state and 1 hour post-αGalCer iNKT cells identified enrichment of most of the same activation markers, cytokines, chemokines, transcription factors, and metabolic genes enriched in our scRNA-Seq data (Figure 3.4.3.C), validating our scRNA-Seq analysis.

**Figure 3.4.3: Bulk microarray analysis of splenic iNKT cell activation (overleaf).** A. PCA of splenic iNKT cells at steady state or 1 hour post-αGalCer (reanalyzed from GSE47959). B. Lollipop plot showing KEGG pathway enrichment from GSEA of splenic iNKT cells at 1 hour post-αGalCer (orange) versus steady state. C. Scaled average heatmap with hierarchical clustering of gene expression in the samples from Figure 3.4.3.A.


A.
GSE47959: microarray
of splenic iNKT cells
PC 2 (9% of Variance)
20
0
-20
-50
-25
0
25
50
PC 1 (85% of Variance)
Steady State
1 hour post-αGalCer
B.
Pathway Enrichment:
1 hour post-αGalCer
Cytokine-cytokine
receptor interaction
JAK STAT
signaling pathway
T cell receptor
signaling pathway
Intestinal immune network
for IGA production
FcεRI signaling pathway
Toll-like receptor
signaling pathway
0
5
10
15
20
-Log10(Adjusted P Value)
C.
Steady State
1 hour
post-αGalCer
Runx3
Bcl11b
Klf3
Xcl1
Eif6
Myc
Srm
Egr2
Pdcd1
Irf8
Nfkb1
Slc7a5
Rheb
Fasn
Slc7a1
Slc1a5
Lta
Slc38a1
Il4
Tnf
Il2
Ccl3
Il13
Egr3
Ccl4
Csf2
Ldha
Zbtb16
Rel
Nr4a3
Irf4
Ccl1
Il2ra
Ifng
Il17a
Tfrc
Bzw1
Cd69
Nfkb2
Hif1a
Egr1
Nr4a2
Nr4a1
Z-Score
-1.5
0
1.5

### 3.5 Granular analysis of splenic iNKT cell at 4 hours post-αGalCer

Having profiled bulk signatures of splenic iNKT cell activation, we next decided to perform granular analysis of splenic iNKT cells at 4 hours post-αGalCer. UMAP and clustering analysis revealed discrete NKT1, NKT2 and NKT17 cell clusters (Figure 3.5.A), which we validated by analyzing cytokine gene expression. As expected, NKT1 cells displayed enrichment of *Ifng*, both NKT1 and NKT2 cells expressed *Il4* and *Il13*, and NKT17 cells were specifically enriched for *Il17a* and *Il17f* (Figure 3.5.B). *Tnf* and *Il2* were broadly expressed by all three subsets, whereas the chemokines *Ccl4*, *Ccl1* and *Ccl3* were mainly expressed by NKT1 cells. This analysis demonstrates that NKT1, NKT2, and NKT17 cells are all activated by *in vivo* stimulation with αGalCer. However, when we performed module scoring of iNKT cell subsets using the activation markers *Il2*, *Il2ra*, *Nr4a1* and *Cd69*, we observed that activation was reduced in NKT2 cells versus NKT1 and NKT17 cells (Figure 3.5.C), and a significant proportion of NKT2 cells displayed little to no expression of *Il4*, *Il13*, and *Il2* (Figure 3.5.B). Delayed activation of NKT2 cells after *in vivo* stimulation with αGalCer has previously been reported by Lee *et al*. (2015)[59]. Therefore, to normalize activation and enable accurate comparison of gene signatures among NKT1, NKT2 and NKT17 cells, we decided to perform activation-based reclustering of iNKT cell subsets. Total NKT1, NKT2 and NKT17 cells from both steady state (Figure 3.1.A) and 4 hours post-αGalCer (Figure 3.5.A) were combined on a per subset basis and reclassified using low level reclustering. This produced discrete steady state and activated clusters for NKT1, NKT2 and NKT17 cells (Figure 3.5.D), and we confirmed that only iNKT cells in the activated clusters displayed enrichment of activation markers (Figure 3.5.E), providing normalized data for comparison of activated NKT1, NKT2, and NKT17 cells.

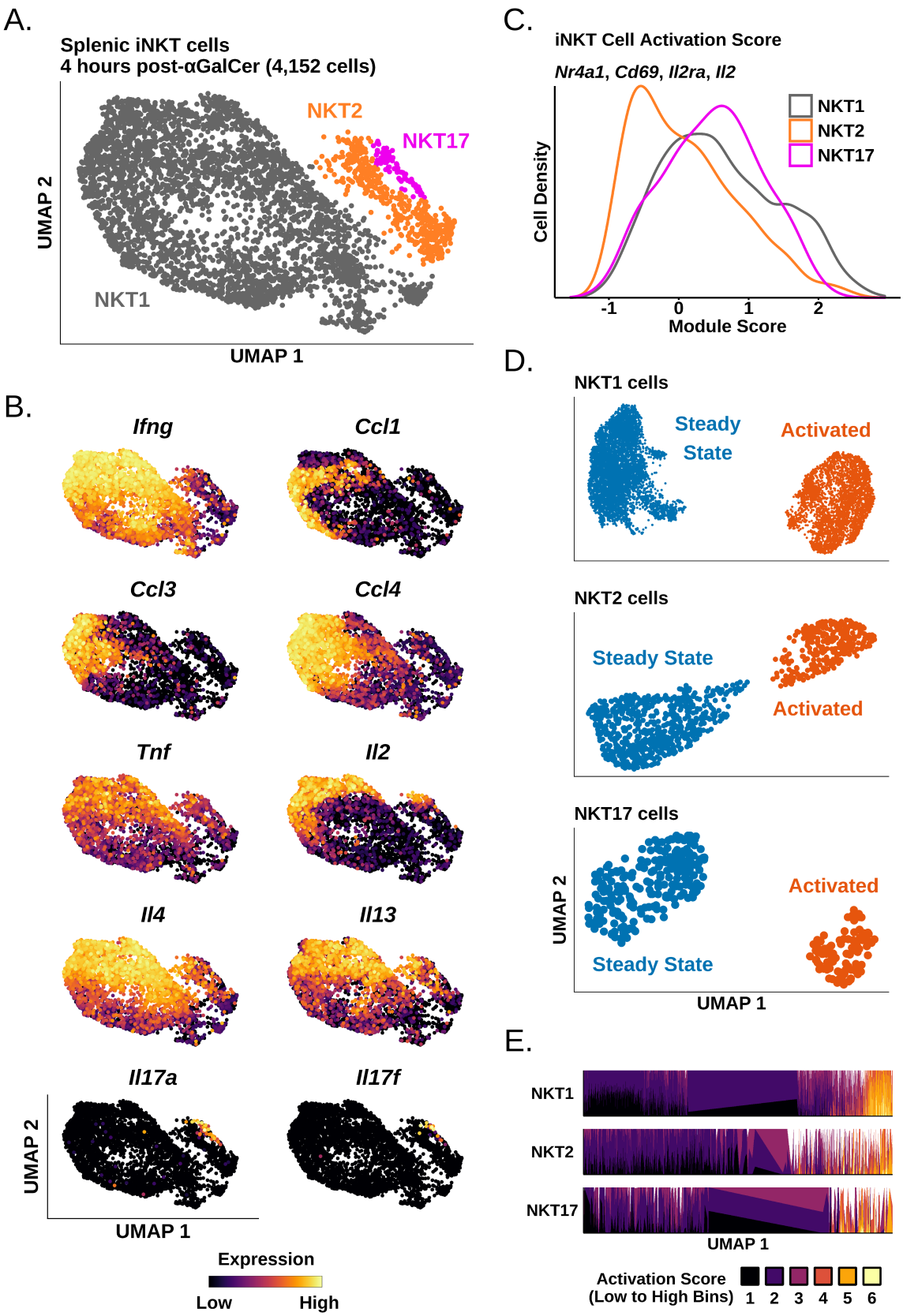

A.
Splenic iNKT cells
4 hours post-αGalCer (4,152 cells)
NKT2
NKT17
NKT1
UMAP 2
UMAP 1
B.
Ifng
Ccl1
Ccl3
Ccl4
Tnf
Il2
Il4
Il13
Il17a
Il17f
UMAP 2
UMAP 1
Expression
Low
High
C.
iNKT Cell Activation Score
Nr4a1, Cd69, Il2ra, Il2
NKT1
NKT2
NKT17
Cell Density
-1
0
1
2
Module Score
D.
NKT1 cells
Steady State
Activated
NKT2 cells
Steady State
Activated
NKT17 cells
Activated
Steady State
UMAP 2
UMAP 1
E.
NKT1
NKT2
NKT17
UMAP 1
Activation Score
(Low to High Bins)
1 2 3 4 5 6

**Figure 3.5: Granular analysis of splenic iNKT cells at 4 hours post-αGalCer (previous page).** A. UMAP of splenic iNKT cells at 4 hours post-αGalCer. B. Feature plots of cytokine and secreted factor gene expression in splenic iNKT cells at 4 hours post-αGalCer. C. Histogram showing expression of a gene module score for iNKT cell activation in the NKT1, NKT2 and NKT17 cell clusters from Figure 3.5.A. D. UMAP plots of reclustered NKT1, NKT2 and NKT17 cells derived from steady state (see Figure 3.1.A) and 4 hours post-αGalCer (See Figure 3.5.A) data. For reclustering purposes, steady state NKT1-A and NKT1-B clusters from Figure 3.1.A were pooled, and cycling cells were excluded. E. Horizon plots showing binned expression of a gene module score for iNKT cell activation (as used in Figure 3.5.C) along the UMAP 1 coordinate from the NKT1, NKT2, and NKT17 cell UMAP plots in Figure 3.5.D.

### 3.6 NKT1, NKT2, and NKT17 cells share transcriptional signatures of activation, but NKT2 and NKT17 cells are distinguished by oxidative metabolic enrichment

To compare transcriptional signatures of activation between iNKT cell subsets, we merged the individual NKT1, NKT2 and NKT17 cell analysis files that we had previously generated (Figure 3.5.D) and combined them into a single normalized analysis file of 9,929 cells. UMAP demonstrated that steady state and activated NKT1, NKT2 and NKT17 cells predominantly clustered based on activation status (Figure 3.6.1.A). We next performed gene expression analysis to profile transcriptional signatures of activation among iNKT cell subsets. Gene signatures enriched among bulk splenic iNKT cells were well conserved among iNKT cell subsets, including activation markers such as *Cd69*, *Pdcd1*, *Il2* and *Il2ra*, and the metabolic markers *Myc*, *Hif1a*, *Rheb*, and *Tfrc*, suggesting that all iNKT cell subsets undergo metabolic remodeling after activation, while expression of *Il7r* was globally reduced (Figure 3.6.1.B). NKT1, NKT2, and NKT17 cells also demonstrated a similar transcription factor enrichment after activation, displaying increased expression of *Irf4*, *Irf8*, *Bzw1*, *Bhlhe40*, and NR4A, EGR, and NF-αB family members. All activated iNKT cell subsets displayed enrichment of *Zbtb16* and *Tbx21*, suggesting that these factors might play subset-independent roles during splenic iNKT cell activation, while *Rorc* was only expressed by NKT17 cells (Figure 3.6.1.B). We next performed metabolic module scoring. Activated NKT1, NKT2, and NKT17 cells all demonstrated enrichment of gene signatures associated with glycolysis, amino acid metabolism, polyamine synthesis, and fatty acid synthesis (Figure 3.6.1.C), while expression of oxidative metabolism and β-oxidation signatures was reduced, indicative of conserved metabolic remodeling across functionally diverse iNKT cell populations. Overall, this analysis suggests that transcriptional signatures of iNKT cell activation are highly conserved among NKT1, NKT2, and NKT17 cell subsets.

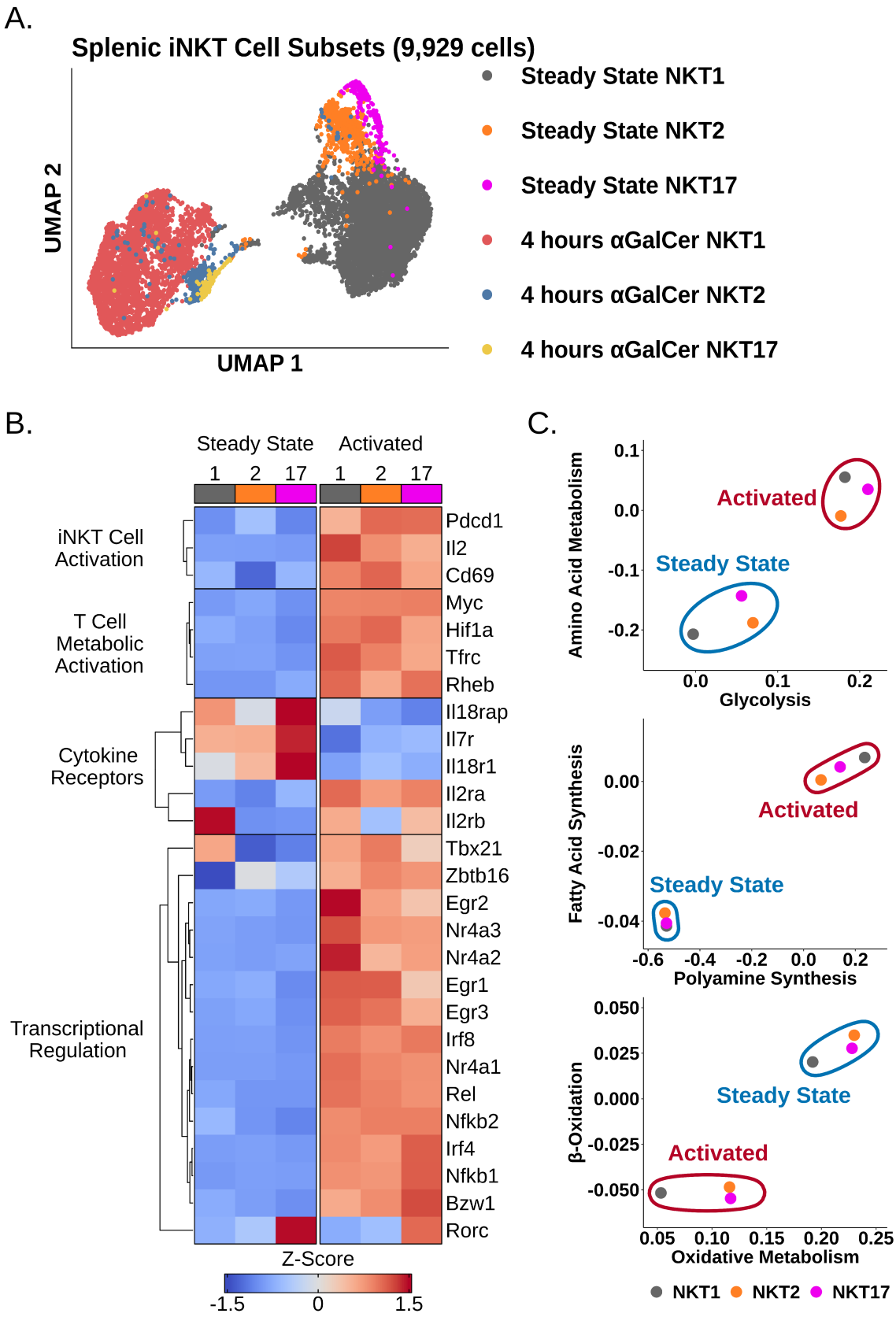

A.
Splenic iNKT Cell Subsets (9,929 cells)
UMAP 2
UMAP 1
Steady State NKT1
Steady State NKT2
Steady State NKT17
4 hours αGalCer NKT1
4 hours αGalCer NKT2
4 hours αGalCer NKT17
B.
Steady State
Activated
1 2 17 1 2 17
iNKT Cell Activation
T Cell Metabolic Activation
Cytokine Receptors
Transcriptional Regulation
Pdcd1
Il2
Cd69
Myc
Hif1a
Tfrc
Rheb
Il18rap
Il7r
Il18r1
Il2ra
Il2rb
Tbx21
Zbtb16
Egr2
Nr4a3
Nr4a2
Egr1
Egr3
Irf8
Nr4a1
Rel
Nfkb2
Irf4
Nfkb1
Bzw1
Rorc
Z-Score
-1.5 0 1.5
C.
Amino Acid Metabolism
Glycolysis
Activated
Steady State
Fatty Acid Synthesis
Polyamine Synthesis
Activated
Steady State
β-Oxidation
Oxidative Metabolism
Steady State
Activated
NKT1 NKT2 NKT17

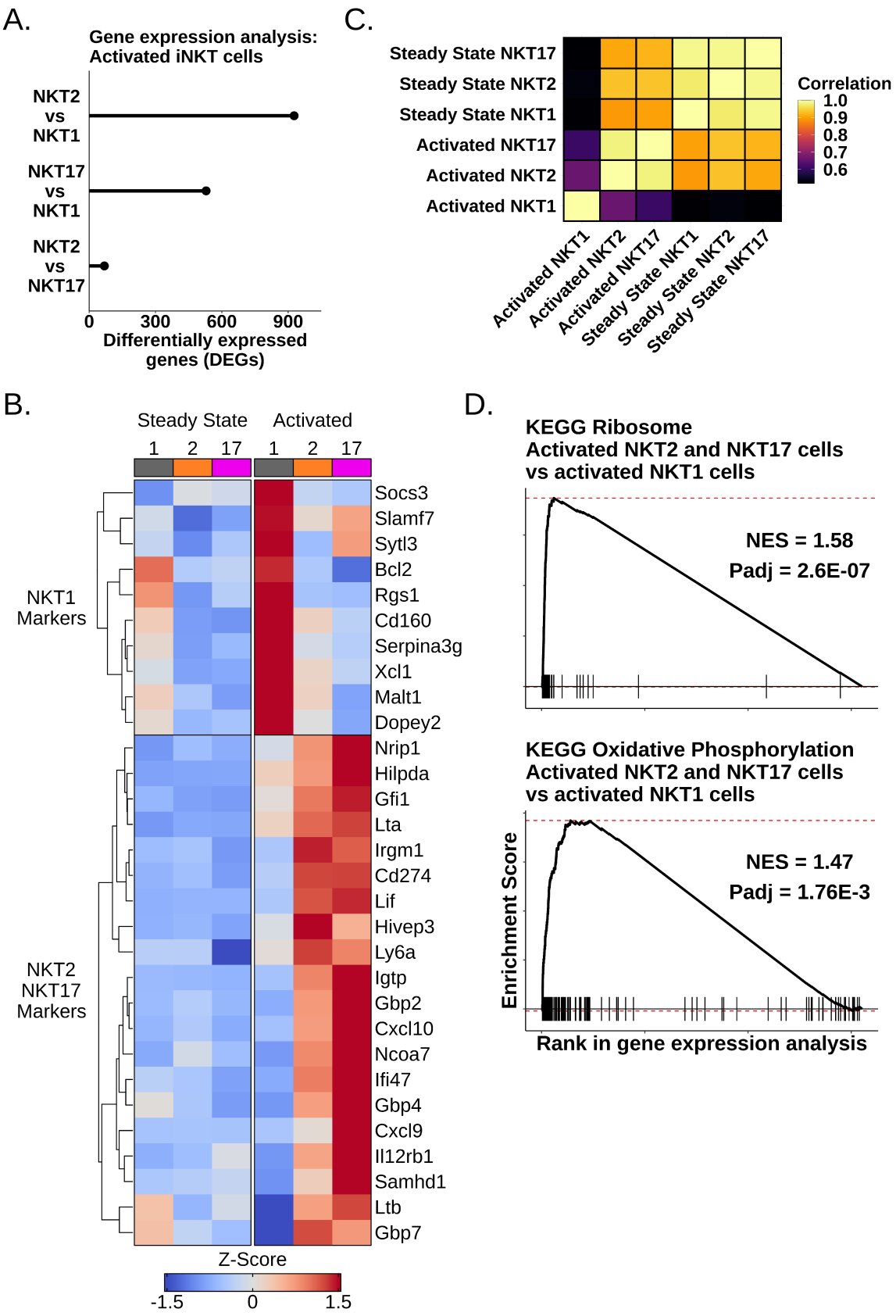
**Figure 3.6.1: Common features of transcriptional remodeling in activated NKT1, NKT2, and NKT17 cells (previous page).** A. Combined UMAP of reclustered steady state and activated NKT1, NKT2, and NKT17 cells from the clusters generated in Figure 3.5.D. B. Scaled average heatmap with hierarchical clustering of gene expression in the clusters from Figure 3.6.1.A. C. Scatter plots showing median expression of metabolic gene module scores in the clusters from Figure 3.6.1.A. Ellipses represent 95% confidence intervals for the distribution of either steady state (blue ellipse) or activated iNKT cells (red ellipse).

We next sought to investigate expression of subset specific transcriptional signatures after activation. Cross-comparison of activated NKT1, NKT2, and NKT17 cells using pairwise gene expression analysis revealed that NKT2 and NKT17 cells were closely transcriptionally interrelated compared to NKT1 cells (Figure 3.6.2.A), which we confirmed by performing whole transcriptome correlation analysis (Figure 3.6.2.B). This was also apparent from granular analysis of DEGs in activated NKT1, NKT2, and NKT17 cells, as NKT2 and NKT17 cells, but not NKT1 cells, shared enrichment of many of the same top DEGs (Figure 3.6.2.C). Genes enriched in activated NKT2 and NKT17 cells included *Lta*, *Ltb*, *Cd274* (encoding PD-L1), the G proteins *Irgm1* and *Gbp7*, the IL-6 family cytokine *Lif*, the transcription factor *Gfi1*, *Igtp*, and *Ly6a* (Figure 3.6.2.C). NKT2 cells displayed particular enrichment of the transcription factor *Hivep3*, which has been shown to play a role in iNKT cell development[64] and can inhibit NF-kB through competition for DNA binding[347], while NKT17 cells demonstrated increased expression of the chemokines *Cxcl9* and *Cxcl10*, the G proteins *Gbp4* and *Gbp7*, the transcriptional regulators *Nrip1* and *Ncoa7*, *Hilpda*, *Il12rb1*, and the restriction enzyme *Samhd1* (Figure 3.6.2.C). DEGs enriched in NKT1 cells included *Slamf7*, *Bcl2*, the immunoreceptor *Cd160*, the membrane trafficking regulator *Dopey2*, the G protein regulator *Rgs1*,

*Serpina3g*, *Sytl3*, and *Socs3* (Figure 3.6.2.C), as well the chemokines *Xcl1*, *Ccl4*, *Ccl3*, and *Ccl1* (Figure 3.5.B, Figure 3.6.2.C).

Having found that activated NKT2 and NKT17 cells were closely transcriptionally interrelated, and also transcriptionally distinct to activated NKT1 cells (Figure 3.6.2.A, Figure 3.6.2.B), we next performed GSEA of activated NKT2 and NKT17 cells to relate these transcriptional differences were related to molecular pathways. We found that NKT2 and NKT17 cells displayed significant enrichment of KEGG Ribosome and KEGG Oxidative Phosphorylation (Figure 3.6.2.D). Although all iNKT cell subsets displayed reduced expression of genes associated with oxidative metabolism after activation (Figure 3.6.1.C), we noted that NKT2 and NKT17 cells consistently demonstrated enrichment of genes associated with oxidative metabolism compared to NKT1 cells, both at steady state and 4 hours post-αGalCer. Combined with our GSEA analysis, this suggested that oxidative metabolism might phenotypically or functionally distinguish NKT2 and NKT17 cells from NKT1 cells. In support of this hypothesis, recent work by Zhao *et al*. (2021) has shown that NKT2 cells are more oxidative than NKT1 cells at steady state[303], while a study by Raynor *et al.* (2020) has suggested that downregulation of oxidative metabolism is required for NKT1 cell differentiation, but not NKT2 and NKT17 cell differentiation[302].

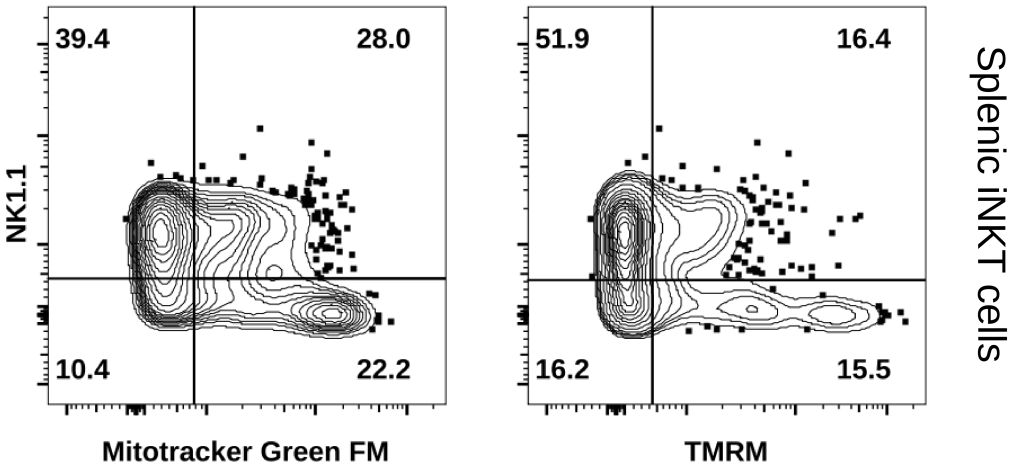
**Figure 3.6.2: Differential gene expression among activated NKT1, NKT2, and NKT17 cells (overleaf).** A. Lollipop plot comparing the total number of differentially expressed genes (DEGs) identified after pairwise comparison of activated NKT1, NKT2 and NKT17 cells. B. Scaled average heatmap with hierarchical clustering of gene expression in the NKT1, NKT2 and NKT17 cell clusters from Figure 3.6.1.A. C. Correlation plot of whole normalized transcriptomes in the NKT1, NKT2 and NKT17 cell clusters from Figure 3.6.1.A. D. GSEA plots showing enrichment of KEGG Ribosome and KEGG Oxidative Phosphorylation in activated NKT2 and NKT17 cells versus activated NKT1 cells. "NES" denotes Normalized Enrichment Score and "Padj" denotes the adjusted P value for the enrichment.


A.
Gene expression analysis:
Activated iNKT cells
NKT2 vs NKT1
NKT17 vs NKT1
NKT2 vs NKT17
0
300
600
900
Differentially expressed genes (DEGs)
C.
Steady State NKT17
Steady State NKT2
Steady State NKT1
Activated NKT17
Activated NKT2
Activated NKT1
Correlation
1.0
0.9
0.8
0.7
0.6
Activated NKT1
Activated NKT2
Activated NKT17
Steady State NKT1
Steady State NKT2
Steady State NKT17
B.
Steady State
Activated
1 2 17 1 2 17
NKT1 Markers
NKT2 NKT17 Markers
Socs3
Slamf7
Sytl3
Bcl2
Rgs1
Cd160
Serpina3g
Xcl1
Malt1
Dopey2
Nrip1
Hilpda
Gfi1
Lta
Irgm1
Cd274
Lif
Hivep3
Ly6a
Igtp
Gbp2
Cxcl10
Ncoa7
Ifi47
Gbp4
Cxcl9
Il12rb1
Samhd1
Ltb
Gbp7
Z-Score
-1.5
0
1.5
D.
KEGG Ribosome
Activated NKT2 and NKT17 cells
vs activated NKT1 cells
NES = 1.58
Padj = 2.6E-07
KEGG Oxidative Phosphorylation
Activated NKT2 and NKT17 cells
vs activated NKT1 cells
NES = 1.47
Padj = 1.76E-3
Enrichment Score
Rank in gene expression analysis

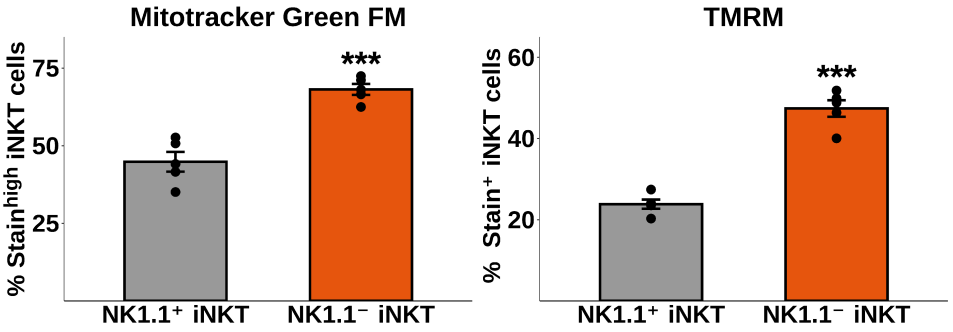
To validate our GSEA and gene expression analysis, we performed staining of steady state C57BL/6 splenic iNKT cells with the mitochondrial dyes Mitotracker Green FM, to measure mitochondrial mass, and TMRM, to measure mitochondrial membrane potential, with increased mitochondrial mass and membrane potential suggesting a more oxidative metabolic profile[109]. We found that NK1.1$^{-}$ iNKT cells, which are enriched for NKT2 and NKT17 cells[45,46,60], showed significantly increased mitochondrial mass and membrane potential compared to NK1.1$^{+}$ iNKT cells, which are enriched for NKT1 cells (Figure 3.6.3.A, Figure 3.6.3.B). We next repeated this staining in CD44$^{+}$ BALB/c thymic iNKT cells, which can be separated into NKT1, NKT2, and NKT17 cell subsets using CD43-HG and ICOS[93]. We found that NKT2 and NKT17 cells displayed significantly increased mitochondrial mass and membrane potential compared to NKT1 cells (Figure 3.6.3.C, Figure 3.6.3.D), demonstrating that NKT2 and NKT17 cells display an enhanced mitochondrial phenotype compared to NKT1 cells.

**Figure 3.6.3: NKT2 and NKT17 cells display a distinct mitochondrial phenotype to NKT1 cells (overleaf).** A. Representative contour plots of Mitotracker Green FM and TMRM staining versus NK1.1 expression in splenic iNKT cells. iNKT cells were defined as live, single $CD19^{-}$ $CD3^{low}$ CD1d $Tetramer^{+}$ cells. B. Bar plots showing Mitotracker Green FM and TMRM median fluorescence intensity (MFI) of N = 5 biological replicates from one experiment. Experiment repeated at least three times. Student's two-tailed t-test. Asterisks denote significance, * padj < 0.05; ** padj <0.01; *** padj < 0.001. C. Representative histograms showing staining of Mitotracker Green FM and TMRM in $CD44^{+}$ NKT1, NKT2 and NKT17 cells from BALB/c mouse thymus. Histograms were normalized to the mode. iNKT cells were defined as live, single $CD8^{-}$ $CD3^{low}$ CD1d $Tetramer^{+}$ cells. D. Scatter plot showing Mitotracker Green FM and TMRM MFI of N = 4 biological replicates from one experiment. Experiment performed at least twice. Ellipses denote 95% confidence intervals of the replicate distributions for each iNKT cell subset.

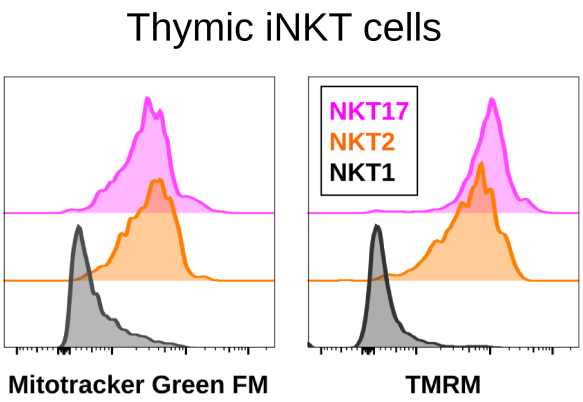
A.


39.4
28.0
10.4
22.2
NK1.1
Mitotracker Green FM
51.9
16.4
16.2
15.5
TMRM
Splenic iNKT cells

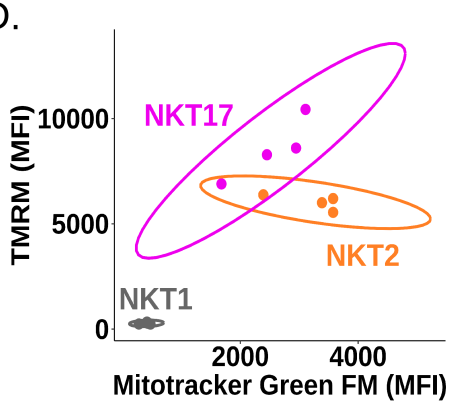
B.


Mitotracker Green FM
% Stain^high iNKT cells
75
50
25
***
NK1.1⁺ iNKT
NK1.1⁻ iNKT
TMRM
% Stain⁺ iNKT cells
60
40
20
***
NK1.1⁺ iNKT
NK1.1⁻ iNKT

C.


Thymic iNKT cells
NKT17
NKT2
NKT1
Mitotracker Green FM
TMRM

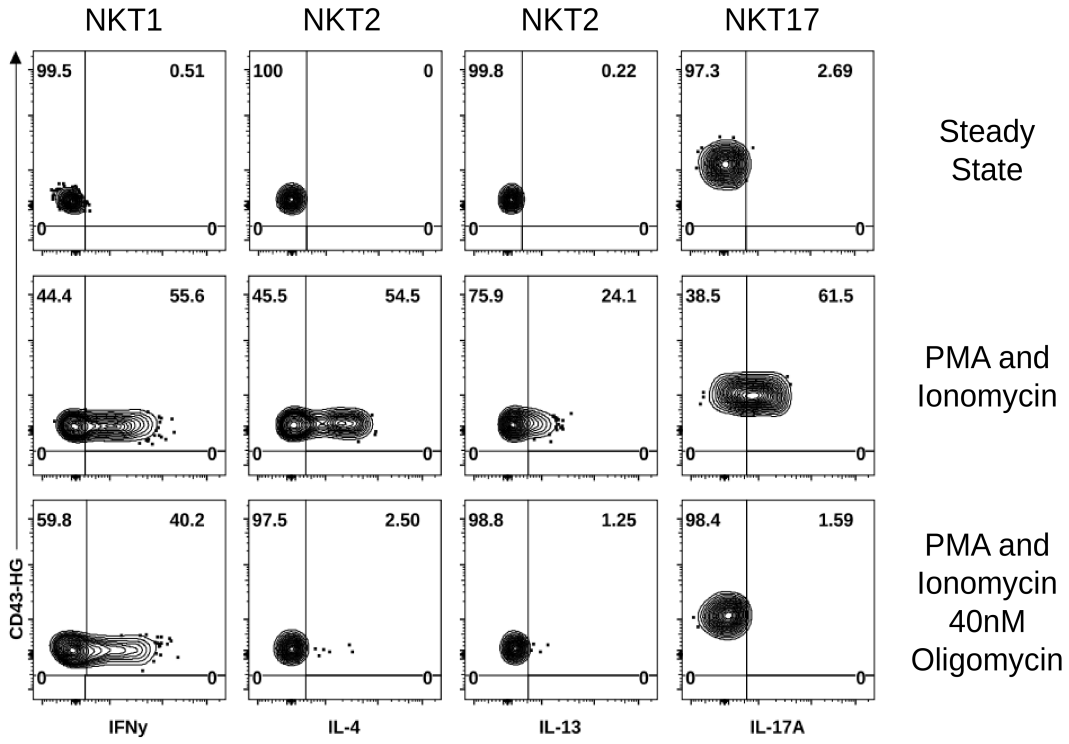
D.


TMRM (MFI)
10000
5000
0
NKT17
NKT2
NKT1
2000
4000
Mitotracker Green FM (MFI)

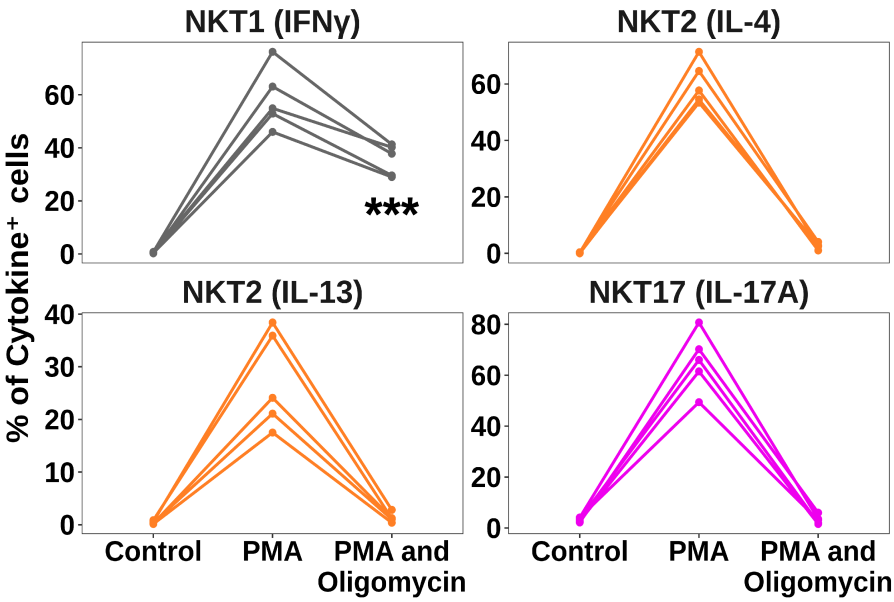
We next performed functional analysis of NKT1, NKT2, and NKT17 cells by stimulating $CD44^+$ BALB/c thymic iNKT cells with PMA and Ionomycin *ex vivo* for 4 hours in the presence or absence of oligomycin, which inhibits the electron transport chain and switches off oxidative phosphorylation[109,286]. Treatment with oligomycin almost completely ablated production of IL-4, IL-13, and IL-17A by NKT2 and NKT17 cells, while production of IFNγ by NKT1 cells was significantly less affected (Figure 3.6.4.A, Figure 3.6.4.B). This result demonstrates that NKT2 and NKT17 cells are more reliant on oxidative phosphorylation than NKT1 cells for their effector function. Overall, our data provide evidence that oxidative metabolism functionally and phenotypically distinguishes NKT2 and NKT17 cells from NKT1 cells.

**Figure 3.6.4: Oxidative metabolism differentially regulates cytokine production in NKT2 and NKT17 cells versus NKT1 cells (overleaf).** A. Representative contour plots of flagship cytokine production by $CD44^+$ BALB/c mouse thymic iNKT cells: NKT1 (IFNγ), NKT2 (IL-4 and IL-13), and NKT17 cells (IL-17A) without stimulation, after 50ng PMA and 1µg Ionomycin, and after 50ng PMA and 1µg Ionomycin in the presence of 40nM Oligomycin (all 4 hours *ex vivo*). B. Line plots of flagship cytokine production by NKT1, NKT2 and NKT17 cells after PMA and Ionomycin stimulation in the presence or absence of oligomycin. N = 5 biological replicates from one experiment. Experiment performed at least twice. One way ANOVA and Tukey's post hoc test. Asterisks denote significance, * padj < 0.05; ** padj <0.01; *** padj < 0.001.

A.


NKT1
NKT2
NKT2
NKT17
99.5
0.51
100
0
99.8
0.22
97.3
2.69
44.4
55.6
45.5
54.5
75.9
24.1
38.5
61.5
59.8
40.2
97.5
2.50
98.8
1.25
98.4
1.59
CD43-HG
IFNy
IL-4
IL-13
IL-17A
Steady State
PMA and Ionomycin
PMA and Ionomycin 40nM Oligomycin

B.

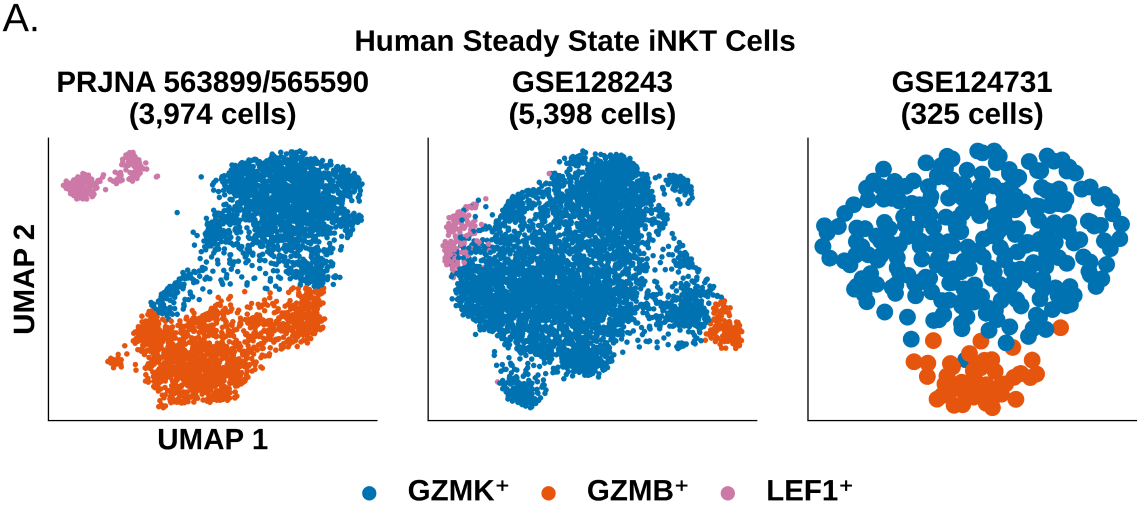

NKT1 (IFNy)
NKT2 (IL-4)
NKT2 (IL-13)
NKT17 (IL-17A)
% of Cytokine+ cells
***
Control
PMA
PMA and Oligomycin

### 3.7 Exploring human iNKT cell heterogeneity at steady state

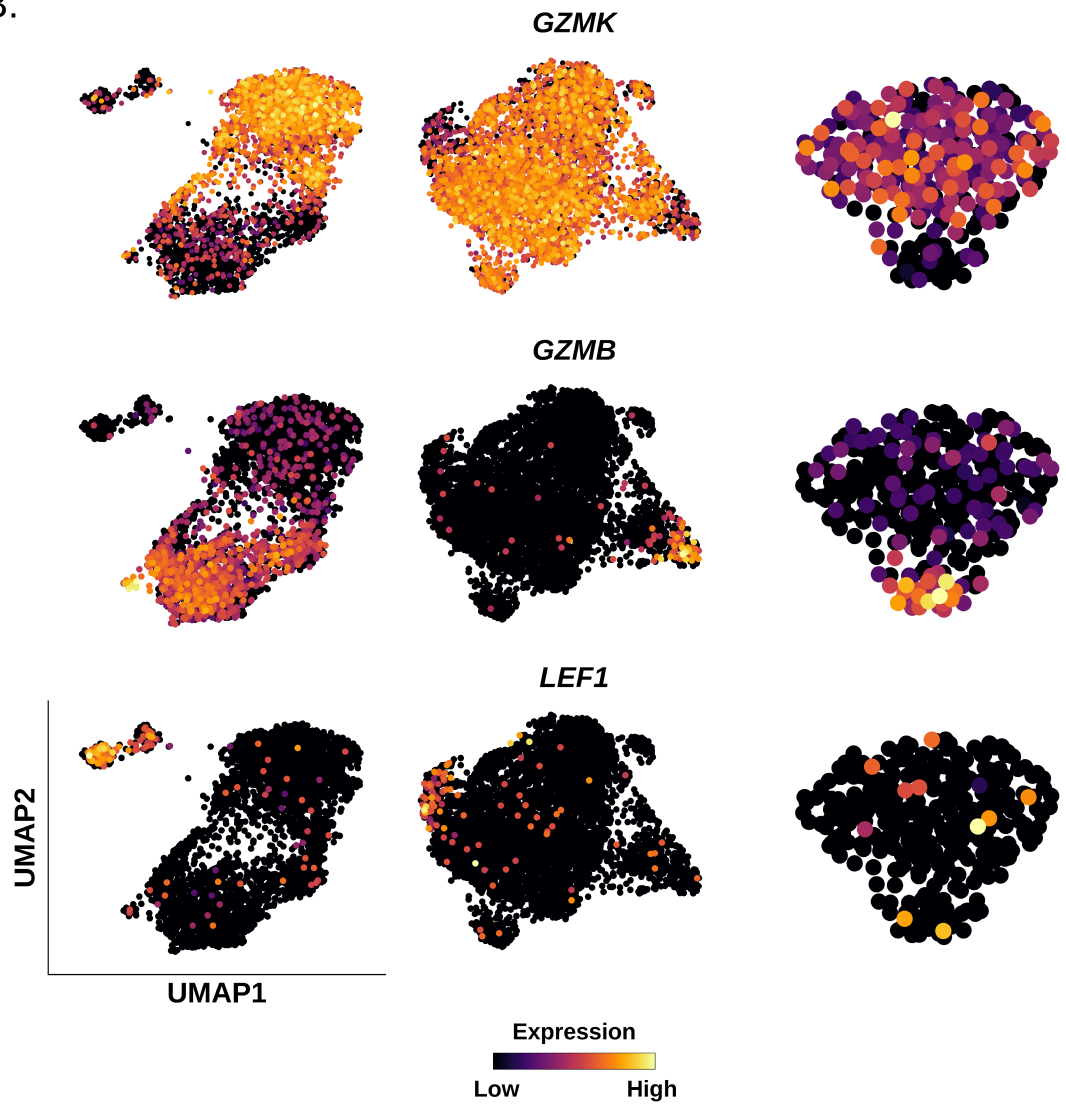
Having previously analyzed murine iNKT cell heterogeneity at steady state, we next performed reanalysis of three published human iNKT cell scRNA-Seq datasets to profile human iNKT cell heterogeneity at steady state. Following quality control measures, we obtained a total of 3,974 cells from PRJNA563899 and PRJNA565590, reanalyzed from Erkers *et al.* (2020)[134], 5,398 cells from GSE128243, reanalyzed from Zhou *et al.* (2020)[135], and 325 cells from GSE124731, reanalyzed from Gutierrez-Arcelus *et al.* (2019)[133]. UMAP and clustering analysis identified conserved separation of human iNKT cells based on expression of *GZMK*, *GZMB*, and the transcription factor *LEF1* (Figure 3.7.1.A, Figure 3.7.1.B). GZMK$^+$ iNKT cells expressed *GZMK*, but lacked expression of either *GZMB* or *LEF1*, GMZB$^+$ iNKT cells expressed *GZMB*, but lacked expression of *GMZK* and *LEF1*, and LEF1$^+$ iNKT cells expressed LEF1, but lacked expression of either *GZMK* or *GMZB* (Figure 3.7.1.B). We identified GZMK$^+$ and GMZB$^+$ iNKT cells across all three datasets, but only found LEF1$^+$ iNKT cells in the larger datasets from Erkers *et al.* (2020) and Zhou *et al.* (2020), possibly due to the limited number of iNKT cells in the data from Gutierrez-Arcelus *et al.* (2019). While expression of CD4 and CD8 has previously been used to stratify iNKT cells in applications such as flow cytometry[125–127,129], we did not identify robust expression of *CD4* or *CD8* by scRNA-Seq. We also did not identify differential expression of *TBX21*, *ZTBT16*, or *RORC*, suggesting that human iNKT cells do not segregate into NKT1, NKT2, or NKT17-like populations.

**Figure 3.7.1: Exploring human iNKT cell heterogeneity at steady state (overleaf).** A. UMAP plots of human steady state PBMC iNKT cells reanalyzed from PRJNA563899 /PRJNA565590, GSE128243, and GSE124731. B. Feature plots of *GZMK*, *GZMB*, and *LEF1* expression in the data from Figure 3.7.1.A.

A.


Human Steady State iNKT Cells
PRJNA 563899/565590
(3,974 cells)
GSE128243
(5,398 cells)
GSE124731
(325 cells)
UMAP 2
UMAP 1
GZMK+
GZMB+
LEF1+

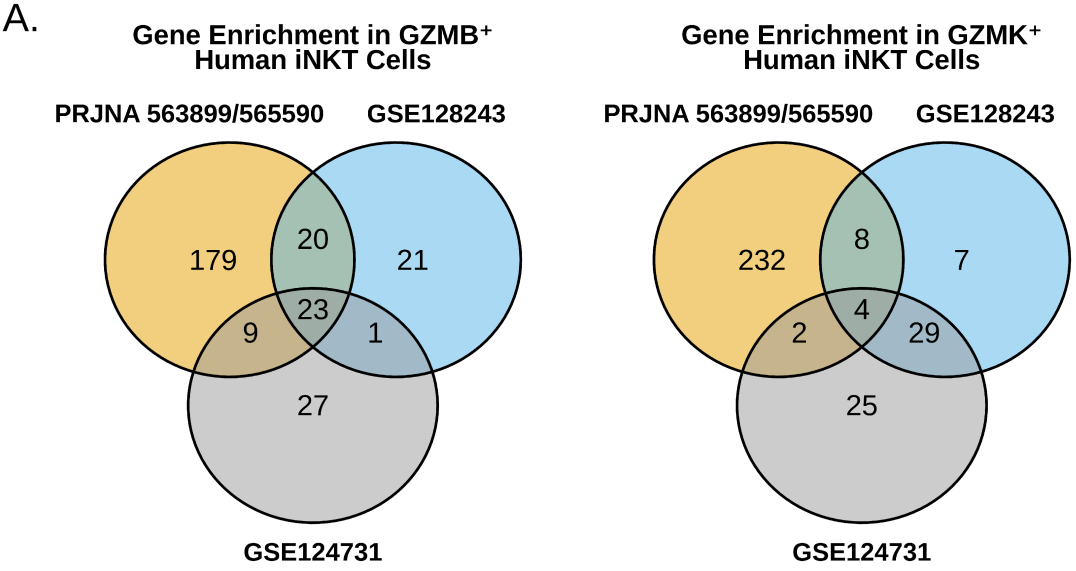
B.


GZMK
GZMB
LEF1
UMAP2
UMAP1
Expression
Low
High

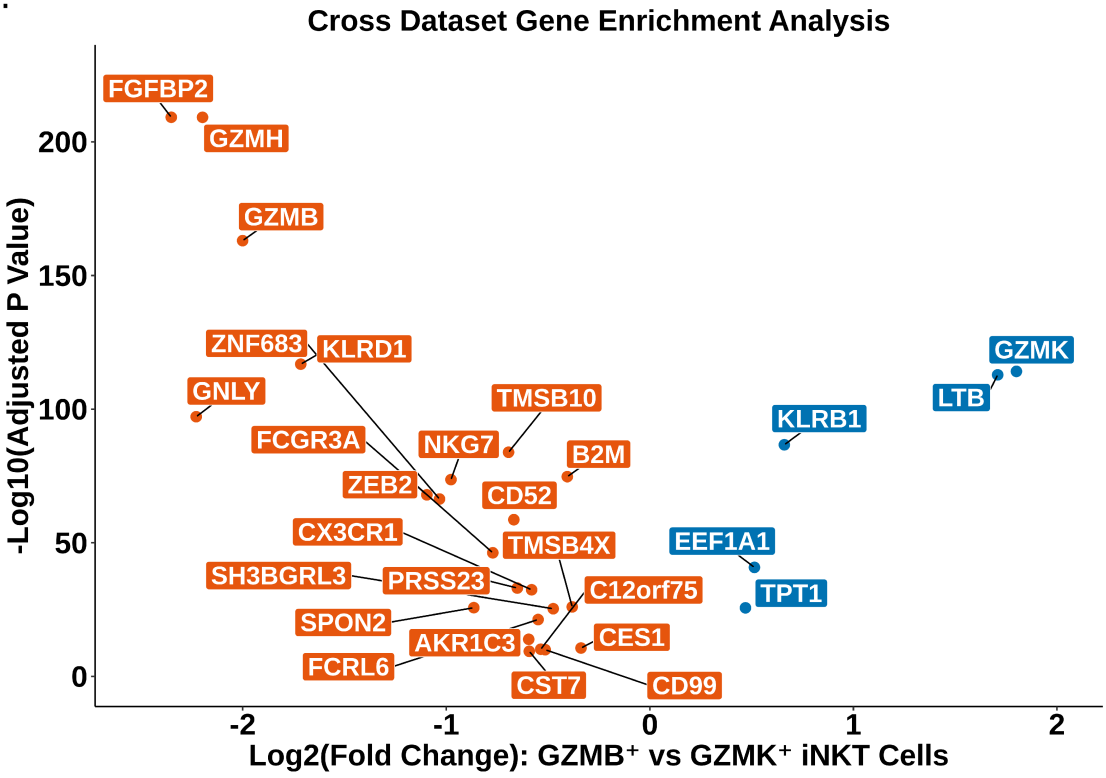
We next performed pairwise cross-dataset gene expression analysis to characterize gene enrichment among GZMK$^+$, GMZB$^+$, and LEF1$^+$ iNKT cells. We identified 4 genes always enriched in GZMK$^+$ versus GMZB$^+$ iNKT cells, and 23 genes always enriched in GZMB$^+$ versus GMZK$^+$ iNKT cells (Figure 3.7.2.A). GZMK$^+$ iNKT cells showed conserved enrichment of *LTB*, a ligand for the LtβR[348], and *KLRB1*, encoding CD161. GMZB$^+$ iNKT cells showed enrichment for several genes associated with cytotoxic lymphocytes, including *GZMH*, *GNLY*, the cytotoxic lymphocyte secretory factor *FGFBP2*, and the transcription factor *ZEB2*, which is associated with terminally differentiated cytotoxic CD8$^+$ T cells[349] (Figure 3.7.2.B). Over-representation analysis of significantly enriched genes also identified general enrichment of cytotoxic genes in GZMB$^+$ versus GMZK$^+$ iNKT cells (Figure 3.7.2.C). The relatively low number of conserved DEGs identified in this analysis suggests that GZMK$^+$ and GZMB$^+$ iNKT cells are, overall, transcriptomically similar, but GZMB$^+$ iNKT cells may represent a more cytotoxic population of human iNKT cells.

**Figure 3.7.2: Cross-dataset analysis of transcriptional signatures enriched in GZMB$^+$ versus GZMK$^+$ human iNKT cells (overleaf)**. A. Venn diagram of DEGs enriched in GZMB$^+$ versus GZMK$^+$ human iNKT cells across all three of the datasets shown in Figure 3.7.1.A. B. Volcano plot of of DEGs enriched in GZMB$^+$ versus GZMK$^+$ human iNKT cells. C. Bar plot showing results from over-representation analysis of genes enriched in GZMB$^+$ human iNKT cells against the KEGG pathway database.

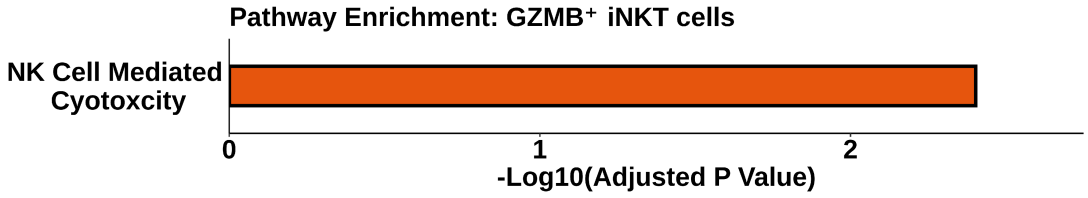
A.


Gene Enrichment in GZMB+
Human iNKT Cells
PRJNA 563899/565590
GSE128243
179
20
21
23
9
1
27
GSE124731
Gene Enrichment in GZMK+
Human iNKT Cells
PRJNA 563899/565590
GSE128243
232
8
7
4
2
29
25
GSE124731

B.


Cross Dataset Gene Enrichment Analysis
FGFBP2
GZMH
GZMB
ZNF683
KLRD1
GNLY
TMSB10
FCGR3A
NKG7
B2M
ZEB2
CD52
CX3CR1
TMSB4X
SH3BGRL3
PRSS23
C12orf75
SPON2
AKR1C3
CES1
FCRL6
CST7
CD99
GZMK
LTB
KLRB1
EEF1A1
TPT1
200
150
100
50
0
-Log10(Adjusted P Value)
-2
-1
0
1
2
Log2(Fold Change): GZMB+ vs GZMK+ iNKT Cells

C.


Pathway Enrichment: GZMB+ iNKT cells
NK Cell Mediated
Cytoxcity
0
1
2
-Log10(Adjusted P Value)

We next performed analysis of LEF1$^{+}$ iNKT cells versus pooled GZMK$^{+}$ and GZMB$^{+}$ iNKT cells. LEF1$^{+}$ iNKT cells displayed enrichment for *CCR7*, *CD79A*, which encodes an immunoglobulin-associated protein typically expressed in B cells, the immune adapter protein *MAL*, and *SELL* (Figure 3.7.3.A), which encodes CD62L, a marker of naive and central memory T cells that mediates trafficking to and from peripheral lymph nodes[350]. Notably, co-enrichment of LEF1 and CCR7 in murine iNKT cells is associated with immature iNKT cells[66], suggesting that LEF1$^{+}$ iNKT cells may represent an analogous immature or progenitor-like population among human iNKT cells. By contrast, LEF1$^{-}$ iNKT cells displayed enrichment of cytotoxic gene signatures and markers associated with terminally differentiated Stage 3 or NKT1 cells in mice, such as *NKG7* and *CTSW*[45,46] (Figure 3.7.3.A, Figure 3.7.3.B). Overall, these data suggest that steady state human iNKT cells are less heterogeneous than steady state murine iNKT cells.

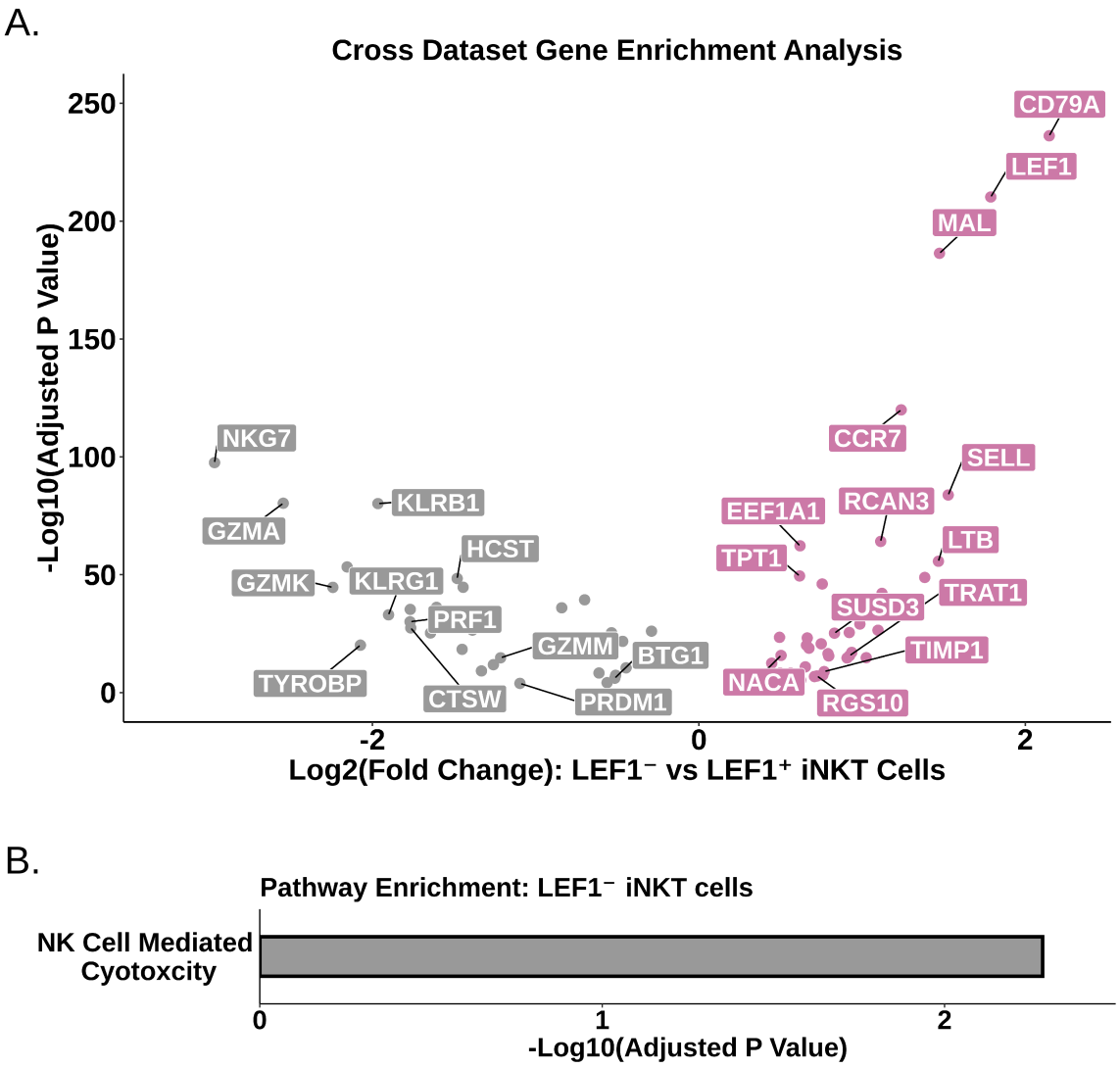


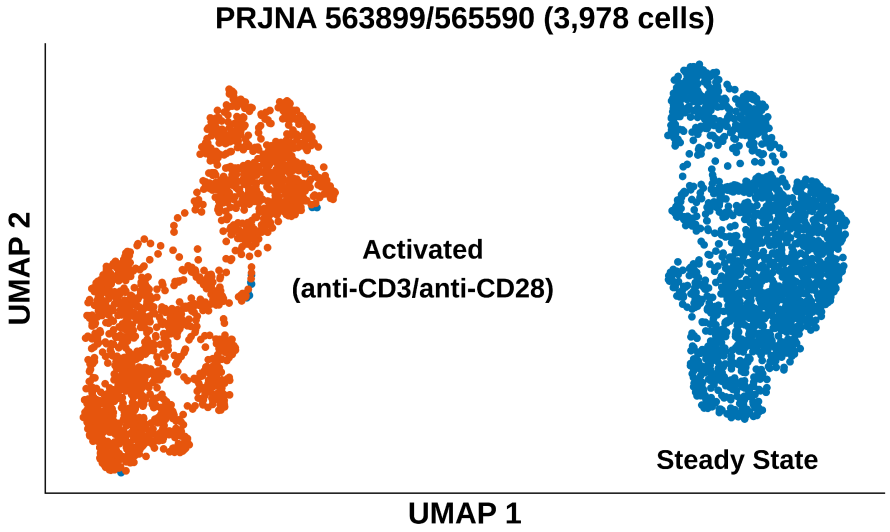

**Figure 3.7.3: Cross-dataset analysis of transcriptional signatures enriched in LEF1$^{-}$ versus LEF1$^{+}$ human iNKT cells.** A. Volcano plot of DEGs enriched in LEF1$^{-}$ versus LEF1$^{+}$ human iNKT cells across all three of the datasets shown in Figure 3.7.1.A. B. Bar plot showing results from over-representation analysis of genes enriched in LEF1$^{-}$ human iNKT cells against the KEGG pathway database.

### 3.8 Activated human iNKT cells undergo rapid and dramatic transcriptional remodeling

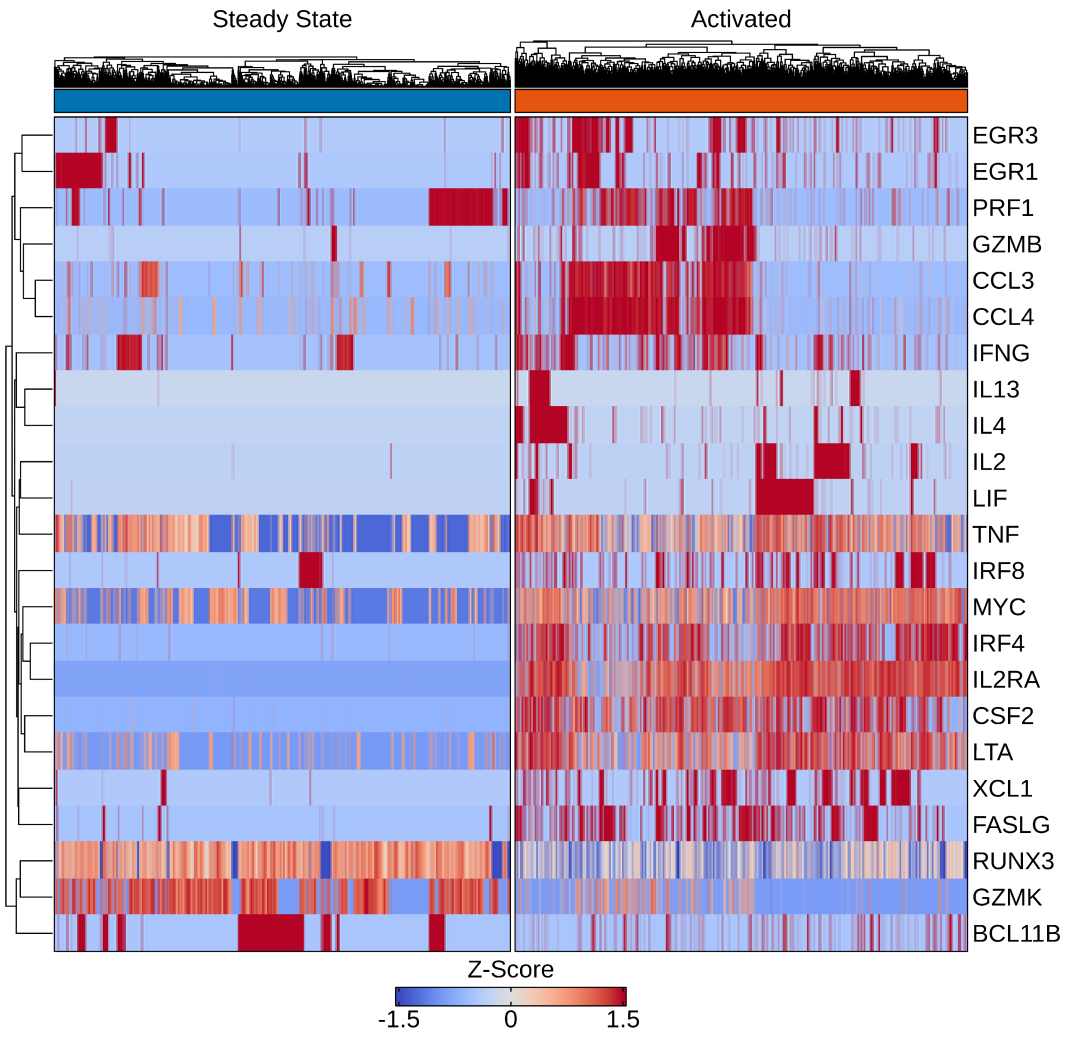
Having profiled transcriptional heterogeneity among steady state human iNKT cells, we next characterized human iNKT cell activation by reanalyzing scRNA-Seq data published by Erkers *et al.* (2020) (PRJNA563899 and PRJNA565590)[134], and Zhou *et al.* (2020) (GSE128243)[135]. We first analyzed the data published by Erkers *et al.* (2020), who performed *ex vivo* stimulation of 4000 human iNKT cells with anti-CD3 and anti-CD28 overnight and sequenced a targeted panel of 312 T cell genes[134]. Comparison of the 3,978 cells that passed quality control measures revealed that steady state and activated human iNKT cells showed little overlap by UMAP (Figure 3.8.1.A), similar to murine iNKT cells after αGalCer (Figure 3.4.1.A), indicating that human iNKT cells undergo extensive transcriptional remodeling after activation. Gene expression analysis demonstrated that activated human iNKT cells expressed many of the same activation markers and cytokines that were expressed by activated murine iNKT cells, including *IL2RA*, *IL2*, *IRF4*, *IRF8*, *MYC*, *EGR1* and *EGR3*, *CCL4*, *IFNG*, *IL4*, and *IL13* (Figure 3.8.1.B, Figure 3.4.1.B), indicating that activated human and murine iNKT cells are transcriptionally similar. Notably, while GZMK expression was downregulated after activation, expression of *GZMB*, and other cytotoxic genes such as *PRF1*, was upregulated after activation (Figure 3.8.1.B). This suggests that *GZMB* expression is more associated with activation, whereas *GZMK* expression is more associated with a steady state or resting phenotype.

**Figure 3.8.1: Analysis of transcriptional remodeling among activated human iNKT cells (overleaf).** A. UMAP of human PBMC iNKT cells at steady state (blue) and after *ex vivo* activation with anti-CD3/anti-CD28 dynabeads overnight (orange). Reanalyzed from PRJNA563899 /PRJNA565590. B. Scaled heatmap with hierarchical clustering of gene expression in the clusters from Figure 3.8.1.A.

A.


PRJNA 563899/565590 (3,978 cells)
UMAP 2
Activated
(anti-CD3/anti-CD28)
Steady State
UMAP 1

B.

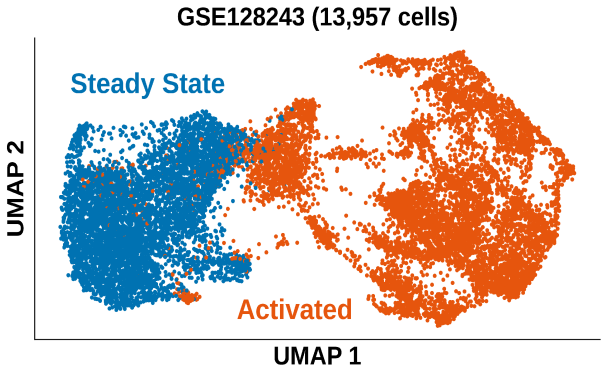

Steady State
Activated
EGR3
EGR1
PRF1
GZMB
CCL3
CCL4
IFNG
IL13
IL4
IL2
LIF
TNF
IRF8
MYC
IRF4
IL2RA
CSF2
LTA
XCL1
FASLG
RUNX3
GZMK
BCL11B
Z-Score
-1.5
0
1.5

We next analyzed the data published by Zhou *et al.* (2020), who performed *ex vivo* stimulation of human iNKT cells with PMA and Ionomycin for 2 hours[135]. As with the previous dataset (Figure 3.8.1.A), we found that steady state and activated iNKT cells were transcriptionally distinct and displayed little overlap by UMAP (Figure 3.8.2.A). Gene expression analysis revealed enrichment of activation markers, cytokines, and metabolic genes among activated human iNKT cells, similar to activated murine iNKT cells (Figure 3.8.2.B). Notably, *IL17A* was not expressed, and we could not find evidence of a Th17 population among activated human iNKT cells, although there was expression of IL23A, which a known ligand for Th17-like cells[61]. We did identify co-enrichment of Th1 and Th2 cytokines, in line with previous studies of activated human iNKT cells[122], and found robust expression of the chemokines *CCL4*, *CCL3*, and *XCL1*, suggesting that most human iNKT cells are functionally similar to murine NKT1 cells. GSEA of activated versus steady state human iNKT cells revealed enrichment of pathways associated with immune activation and signaling, TCR signaling, and effector cytokine production, whereas genes associated with oxidative phosphorylation were downregulated (Figure 3.8.2.C), similar to murine iNKT cells (Figure 3.4.1.C). Moreover, transcription factor analysis demonstrated that activated human iNKT cells displayed a very similar regulatory profile to activated murine iNKT cells, including enrichment of *ZBTB16*, *REL*, *NFKB1*, *NFKB2*, *EGR1*, *ERG2*, *EGR3*, *IRF4*, *IRF8*, *BHLHE40*, and *BZW1* (Figure 3.8.2.D, Figure 3.4.1.D).

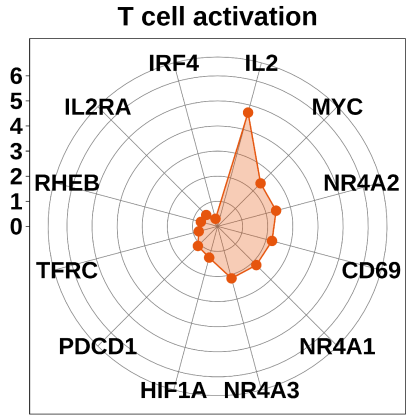
We also performed module scoring of steady state and activated human iNKT cells. We found that activated human iNKT cells recapitulated the metabolic remodeling shown by activated murine iNKT cells, demonstrating enrichment of genes associated with glycolysis, amino acid metabolism, and polyamine synthesis, while expression of genes associated with oxidative metabolism was reduced (Figure 3.8.3.A, Figure 3.4.2.A). Overall, these data demonstrate that a conserved transcriptional framework underpins the activation of both human and murine iNKT cells.

**Figure 3.8.2: Analysis of transcriptional remodeling among activated human iNKT cells (continued; overleaf).** A. UMAP of human cells at steady state and after activation with PMA and Ionomycin. B. Radar charts showing enrichment of genes encoding T cell activation markers, cytokines, and secreted factors in activated human iNKT cells. C. Lollipop plots showing KEGG pathway enrichment from GSEA of activated versus steady state iNKT cells. D. Scaled heatmap with hierarchical clustering of transcription factor expression in the clusters from Figure 3.8.2.A.

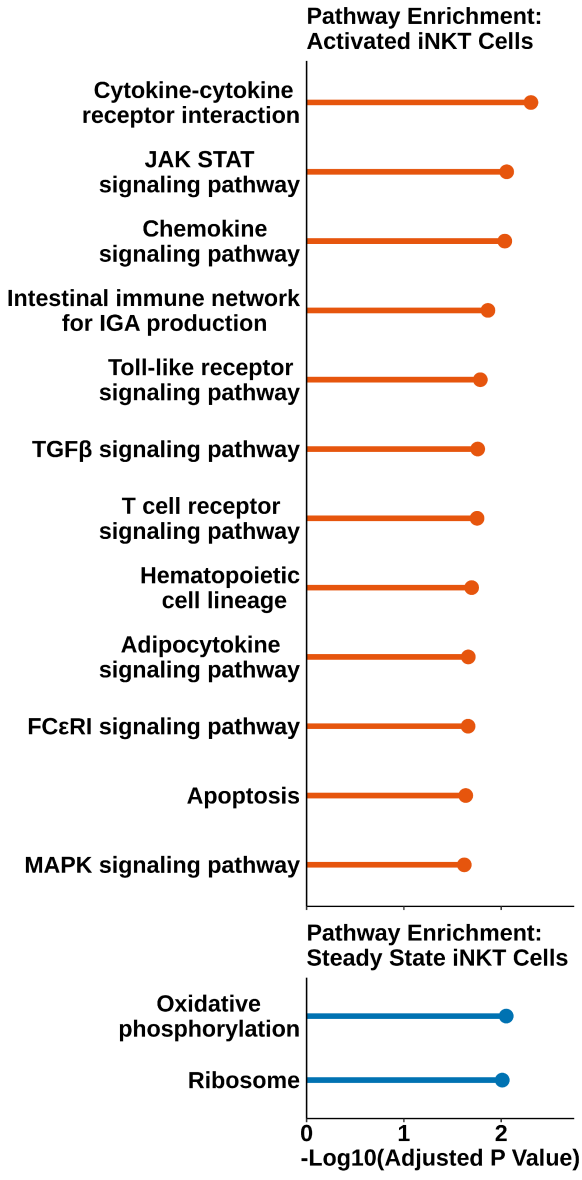
A.

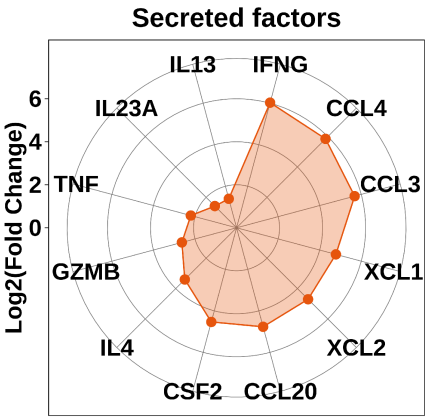

GSE128243 (13,957 cells)
Steady State
Activated
UMAP 2
UMAP 1

B.

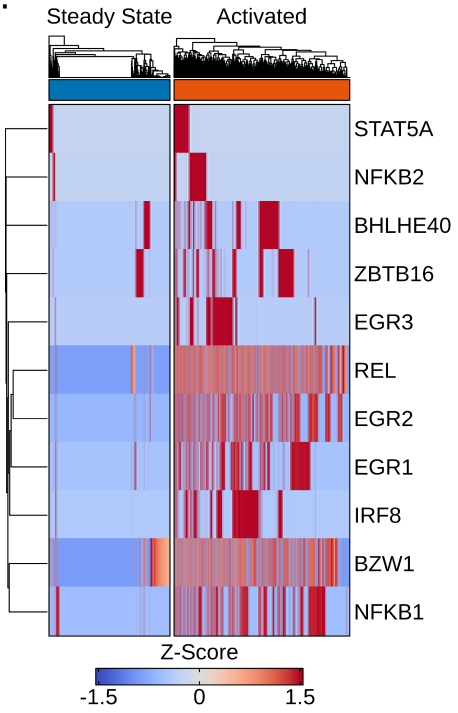

T cell activation
IRF4
IL2
IL2RA
MYC
RHEB
NR4A2
TFRC
CD69
PDCD1
NR4A1
HIF1A
NR4A3
0
1
2
3
4
5
6

C.


Pathway Enrichment:
Activated iNKT Cells
Cytokine-cytokine receptor interaction
JAK STAT signaling pathway
Chemokine signaling pathway
Intestinal immune network for IGA production
Toll-like receptor signaling pathway
TGFβ signaling pathway
T cell receptor signaling pathway
Hematopoietic cell lineage
Adipocytokine signaling pathway
FCεRI signaling pathway
Apoptosis
MAPK signaling pathway
Pathway Enrichment:
Steady State iNKT Cells
Oxidative phosphorylation
Ribosome
0
1
2
-Log10(Adjusted P Value)


Secreted factors
Log2(Fold Change)
IL13
IFNG
IL23A
CCL4
TNF
CCL3
GZMB
XCL1
IL4
XCL2
CSF2
CCL20
0
2
4
6

D.


Steady State
Activated
STAT5A
NFKB2
BHLHE40
ZBTB16
EGR3
REL
EGR2
EGR1
IRF8
BZW1
NFKB1
Z-Score
-1.5
0
1.5

A.

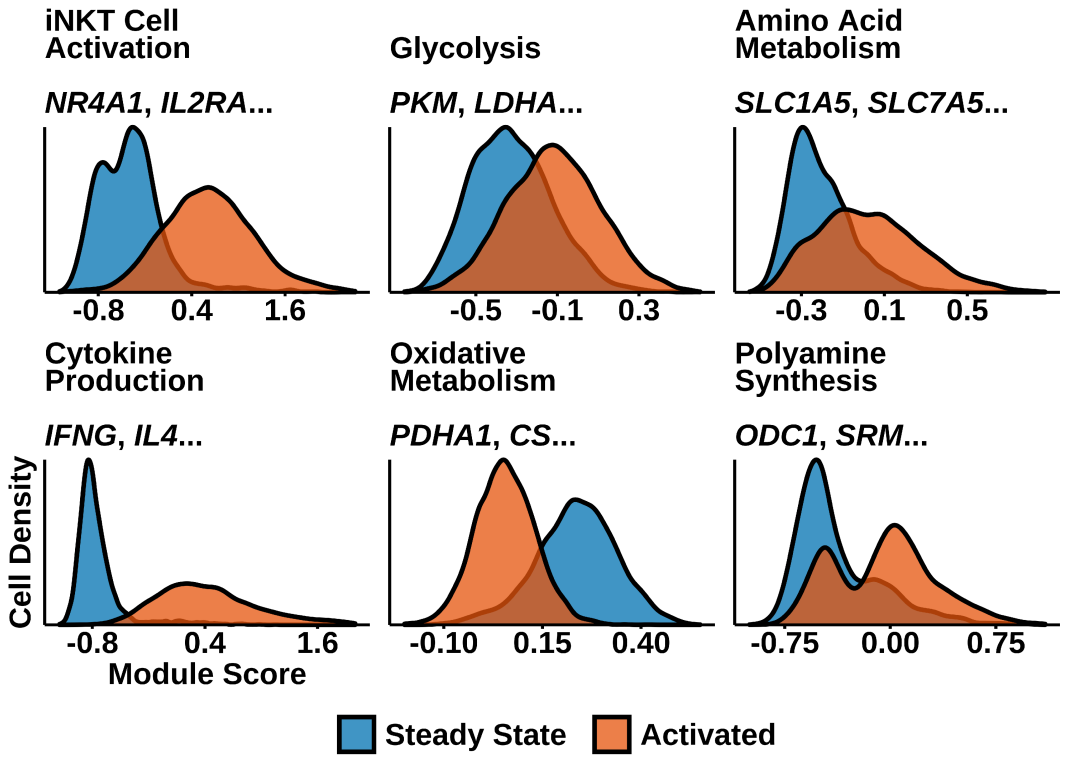



**Figure 3.8.3: Remodeling of metabolic gene expression following human iNKT cell activation.** A. Histograms showing expression of metabolic gene module scores in human iNKT cells at steady state or after activation with PMA and Ionomycin.

### 3.9 Granular analysis of activated human iNKT cells

Having analyzed transcriptional signatures of bulk human iNKT cell activation, we next performed granular analysis of activated human iNKT cells. We first analyzed the data from Erkers *et al.* (2020) and identified two clusters of activated iNKT cells. Cells from Cluster 3 demonstrated enrichment of cytotoxic genes, including *GZMB*, *GNLY*, and *PRF1*, and the chemokines *CCL4* and *CCL3* (Figure 3.9.1.A, Figure 3.9.1.B). Cells from the other activated cluster, Cluster 2, displayed increased expression of cytokines and immunomodulatory factors such as *IL2*, *IL13*, *IL4*, *LIF*, *TNF*, and *LTA*, while both clusters expressed *IFNG* (Figure 3.9.1.B). Overall, this pattern of clustering and gene expression closely mirrored previous analysis by Erkers *et al*. (2020)[134]. However, interestingly, we were able to detect expression of *CD4* and *CD8*, enabling mapping of *CD4* and *CD8* expression to cytokine and effector gene signatures. We found that expression of *CD8* was associated with co-expression of cytotoxic genes in Cluster 3 whereas Cluster 2 cells displayed increased expression of *CD4* (Figure 3.9.1.B, Figure 3.9.1.C). This suggests that $CD4^+$ and $CD8^+$ iNKT cells are functionally and transcriptionally distinct and may parallel $CD8^+$ and $CD4^+$ adaptive T cells. Steady state iNKT cells also showed differences in expression of *CD8* and *CD4*, with Cluster 0 iNKT cells demonstrating enrichment of *CD4*, and Cluster 1 cells demonstrating enrichment of *CD8* (Figure 3.9.1.A, Figure 3.9.1.B, Figure 3.9.1.C), suggesting that $CD8^+$ and $CD4^+$ iNKT cells remain transcriptionally distinct at steady state. Expression of *GZMK* was almost ubiquitous among steady state iNKT cells in this dataset (Figure 3.9.1.B, Figure 3.9.1.C), and it was not possible to directly compare these data to our previous $GZMK^+$ versus $GZMB^+$ iNKT cell analysis, although these data do suggest that cytotoxic gene expression (including *GZMB*) generally correlates more with expression of *CD8* than *CD4* in human iNKT cells, particularly after activation.

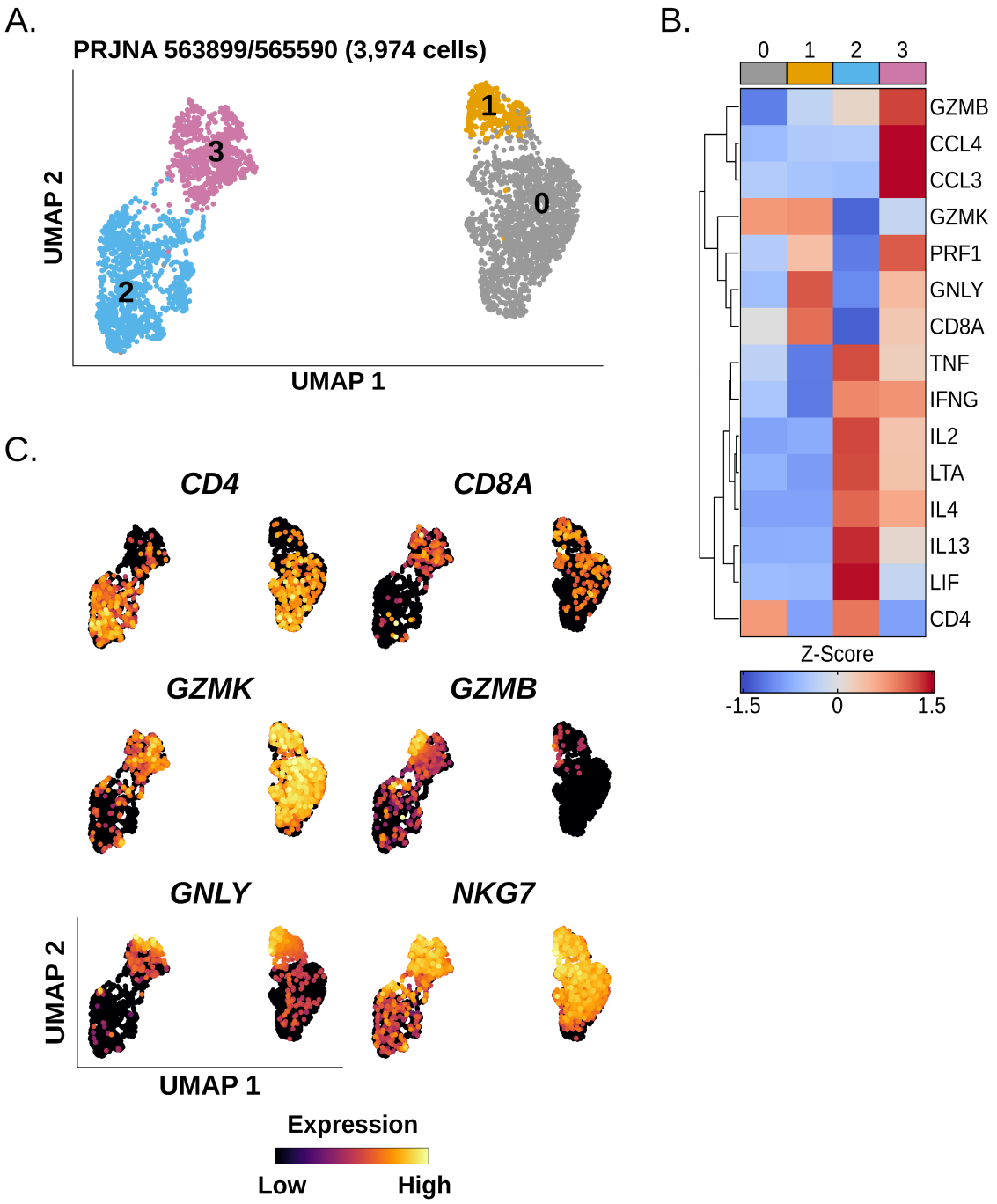

A.
PRJNA 563899/565590 (3,974 cells)
UMAP 2
UMAP 1
0
1
2
3
B.
0 1 2 3
GZMB
CCL4
CCL3
GZMK
PRF1
GNLY
CD8A
TNF
IFNG
IL2
LTA
IL4
IL13
LIF
CD4
Z-Score
-1.5 0 1.5
C.
CD4
CD8A
GZMK
GZMB
GNLY
NKG7
UMAP 2
UMAP 1
Expression
Low
High

**Figure 3.9.1: Granular analysis of activated human iNKT cells (previous page).** A. UMAP of human PBMC iNKT cells at steady state and after *ex vivo* activation with anti-CD3/anti-CD28 dynabeads overnight, with clustering applied. Reanalyzed from PRJNA563899 /PRJNA565590. B. Scaled average heatmap with hierarchical clustering of gene expression in the clusters from Figure 3.9.1.A. C. Feature plots of gene expression in the data from Figure 3.9.1.A.

We next performed granular analysis of the activated iNKT cell data from Zhou *et al.* (2020). Unlike the Erkers *et al.* (2020) dataset (Figure 3.9.1), we did not detect robust expression of *CD8* or *CD4.* Expression of *IFNG* was almost ubiquitous among activated iNKT cells (Figure 3.9.2.A), as was expression of the NKT1 cell-associated genes *CCL5*, *CCL4* and *CCL3*, suggesting that most human iNKT cells are functionally NKT1 or Th1-like. However, as previously reported by Zhou *et al.* (2020), we identified a distinct population of iNKT cells co-expressing the Th2 cytokines *IL4* and *IL13*, the majority of which also expressed the chemokines *XCL1* and *XCL2* (Figure 3.9.2.A). We also identified subpopulations of iNKT cells that specifically expressed *IL2*, *IL10*, or *GZMB* and *GNLY* (Figure 3.9.2.A), suggesting that there is functional heterogeneity among human iNKT cells. However, we could not identify any obvious patterns of differential gene expression among these functional subpopulations (data not shown), as had been possible for murine iNKT cells (Figure 3.6). Therefore, deeper elucidation of functional heterogeneity among human iNKT cells will likely require further research beyond the scope of this thesis.

A.

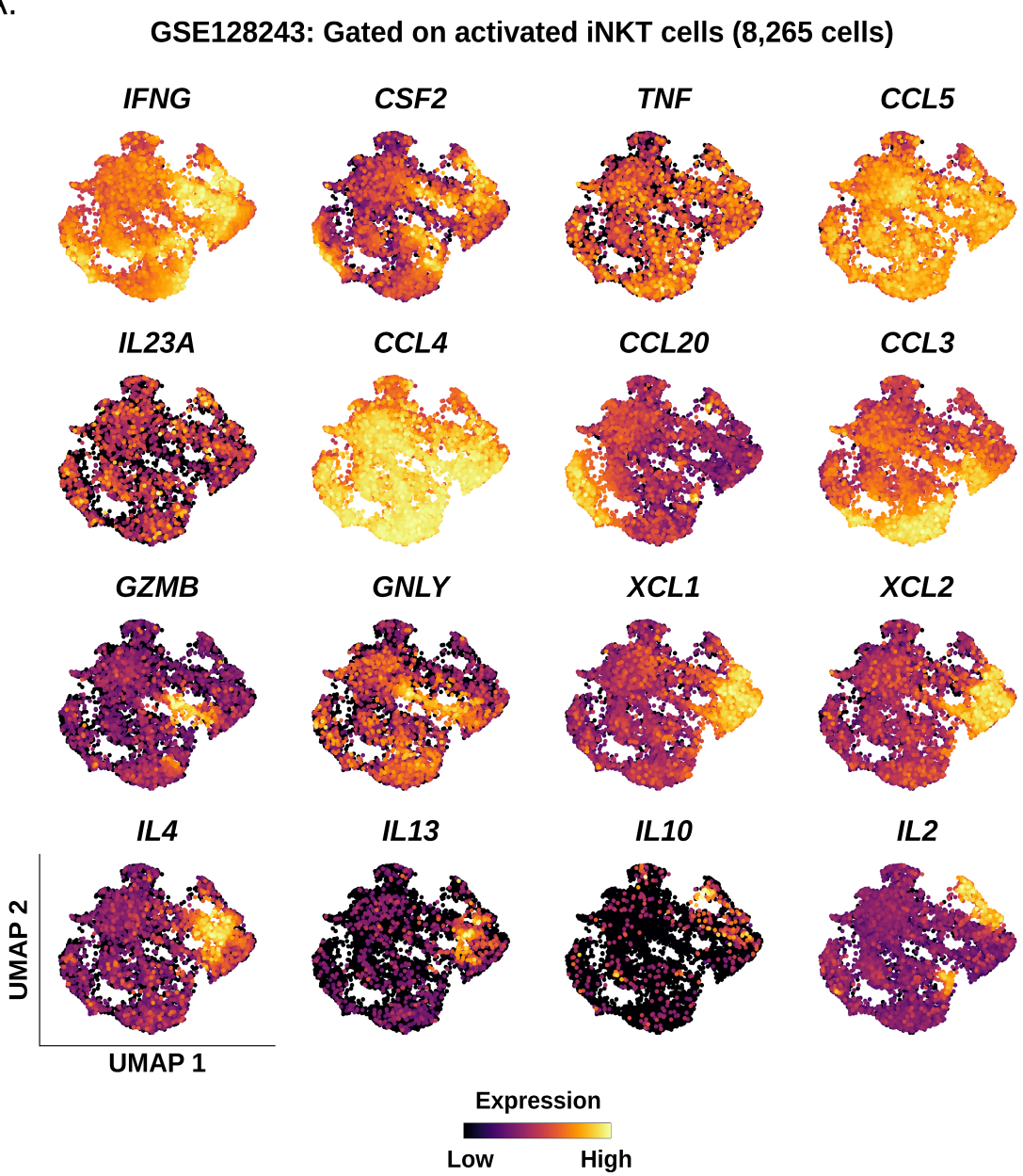



**Figure 3.9.2: Granular analysis of activated human iNKT cells (continued).** A. Feature plots of cytokine and secreted factor gene expression in human iNKT cells after activation with PMA and Ionomycin. Reanalyzed from GSE128243.

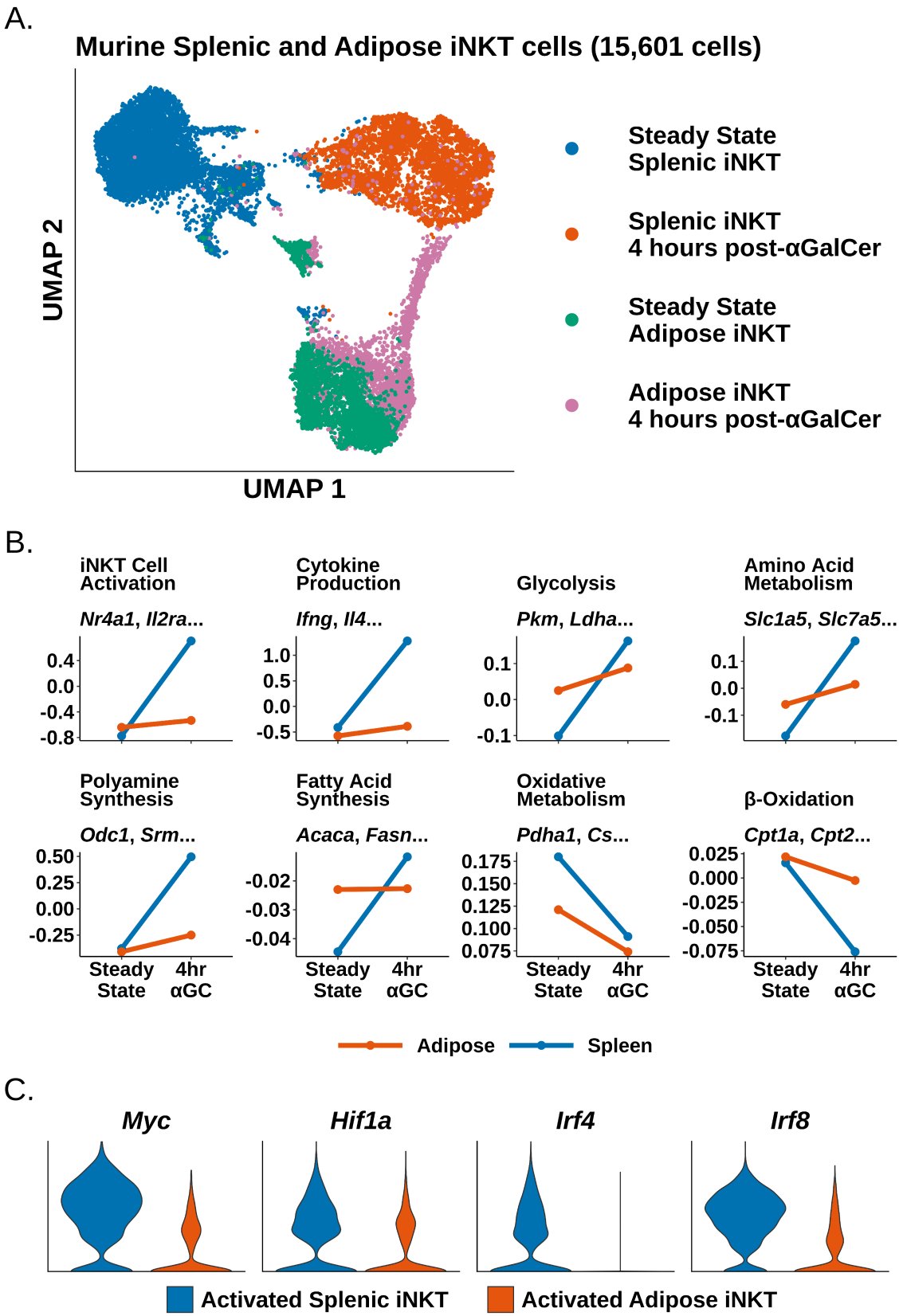
### 3.10 Adipose iNKT cells display a blunted transcriptional response to stimulation with αGalCer

Having identified a conserved transcriptional framework underpinning the activation of both human PBMC iNKT cells and murine splenic iNKT cells, we next decided to characterize transcriptional signatures of activation among the unique regulatory population of iNKT cells resident in adipose tissue[49]. Quality control measures returned 2,950 murine adipose iNKT cells at 4 hour post-αGalCer, expressing a median of 4,964 UMIs and 1,797 genes per cell. After removing cycling cells from the data (100 cells total), we combined these data with our steady state adipose iNKT cell data (Figure 3.2.1.A; cycling cells were removed), and our splenic iNKT cell data at steady state and 4 hours post-αGalCer (Figure 3.6.1.A), generating a combined file of 15,580 splenic and adipose iNKT cells. Adipose and splenic iNKT cells showed little overlap by UMAP at 4 hours post-αGalCer (Figure 3.10.A), as they had at steady state (Figure 3.3.1.A), indicating that adipose and splenic iNKT cells remained transcriptionally distinct after αGalCer stimulation. Notably, unlike splenic iNKT cells, which demonstrated rapid and dramatic transcriptional remodeling after αGalCer stimulation, and separated in dimensional space, most of the 4 hour post-αGalCer adipose iNKT cells clustered with steady state adipose iNKT cells (Figure 3.10.1.A), suggestive of reduced activation and transcriptional remodeling among adipose iNKT cells.

We next performed module scoring to compare the expression of activation, cytokine, and metabolic gene signatures between adipose and splenic iNKT cells. We found that adipose iNKT cells showed greatly reduced enrichment of activation and cytokine gene signatures compared to splenic iNKT cells at 4 hours post-αGalCer (Figure 3.10.B), which was accompanied by blunted metabolic remodeling in adipose iNKT cells. Adipose iNKT cells also displayed reduced expression of key markers of metabolic activation compared, such as *Myc* and *Hif1a*, and showed reduced expression of other transcription factors associated with activation, including *Irf4* and *Irf8* (Figure 3.10.1.B). Although

we observed the same trends in expression among activated adipose and splenic iNKT cells, including increased expression of genes associated with glycolysis, amino acid metabolism, and polyamine metabolism, and reduced expression of genes associated with oxidative metabolism, the overall magnitude of transcriptional remodeling was much lower among adipose iNKT cells (Figure 3.10.1.B). Interestingly, adipose iNKT cells displayed increased expression of some activation and metabolic markers at baseline, aligning with our previous analysis of adipose versus splenic iNKT cells at steady state (Figure 3.3.2). This suggests that adipose iNKT cells may already be activated at steady state, and that their capacity to undergo further activation may be limited. Moreover, we previously found that adipose iNKT cells displayed enrichment of transcriptional signatures associated with T cell exhaustion and chronic activation, which might also have blunted the response of adipose iNKT cells to αGalCer stimulation (Figure 3.3). Overall, these data indicate that adipose iNKT cells respond to αGalCer, as has previously been demonstrated using functional assays[49,91], but activation and transcriptional remodeling is blunted in adipose iNKT cells compared to splenic iNKT cells, at least over the course of ~4 hours when iNKT cells typically produce a burst of cytokines in response to antigen challenge[17,146].

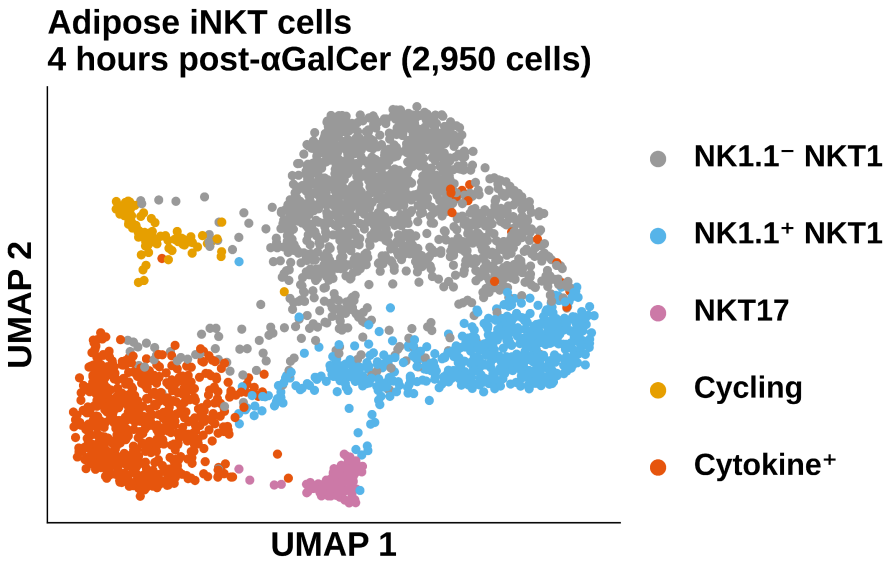
**Figure 3.10.1: Comparison of the iNKT cell response to activation with αGalCer in adipose tissue versus spleen (overleaf).** A. UMAP of murine adipose and splenic iNKT cells at steady state and 4 hours post-αGalCer. Cycling cells were excluded from the analysis. B. Line plots showing median expression of iNKT cell activation, cytokine production, and metabolic gene module scores in adipose and splenic iNKT cells at steady state and 4 hours post-αGalCer. C. Violin plots showing expression of *Myc*, *Hif1a*, *Irf4*, and *Irf8* in splenic versus adipose iNKT cells 4 hours post-αGalCer.


A.
Murine Splenic and Adipose iNKT cells (15,601 cells)
UMAP 2
UMAP 1
Steady State Splenic iNKT
Splenic iNKT 4 hours post-αGalCer
Steady State Adipose iNKT
Adipose iNKT 4 hours post-αGalCer
B.
iNKT Cell Activation
Nr4a1, Il2ra...
Cytokine Production
Ifng, Il4...
Glycolysis
Pkm, Ldha...
Amino Acid Metabolism
Slc1a5, Slc7a5...
Polyamine Synthesis
Odc1, Srm...
Fatty Acid Synthesis
Acaca, Fasn...
Oxidative Metabolism
Pdha1, Cs...
β-Oxidation
Cpt1a, Cpt2...
Steady State
4hr αGC
Adipose
Spleen
C.
Myc
Hif1a
Irf4
Irf8
Activated Splenic iNKT
Activated Adipose iNKT

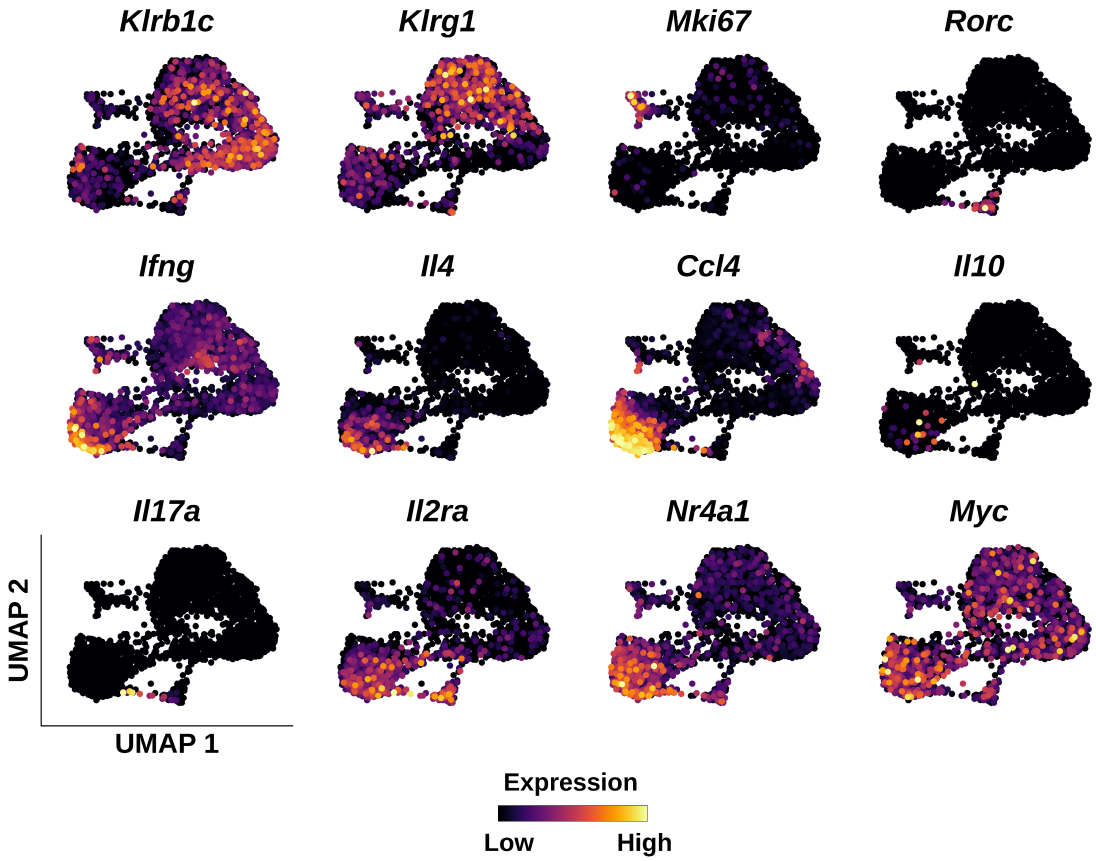
To gain further insight into the blunted activation phenotype of adipose iNKT cells, we next performed granular analysis of whole adipose iNKT cells at 4 hours post-αGalCer (2,950 cells). We identified a total of 5 clusters, including clusters corresponding to NK1.1$^{+}$ and NK1.1$^{-}$ NKT1 cells, a cluster of NKT17 cells, a cluster of cycling cells, and cluster of iNKT cells that showed enrichment of cytokine transcripts (Cytokine$^{+}$) (Figure 3.10.2.A, Figure 3.10.2.B). Unlike in the spleen, where most iNKT cells demonstrated expression of chemokine and cytokine transcripts at 4 hour post-αGalCer (Figure 3.5.B), only some NKT17 cells and Cytokine$^{+}$ iNKT cells displayed enrichment of cytokine and chemokine genes (Figure 3.10.2.B), which was paired with expression of activation markers such as *Il2ra* and *Nr4a1*, and metabolic activation markers such as *Myc*. By contrast, the NK1.1$^{+}$ and NK1.1$^{-}$ NKT1 cell clusters, which comprised a majority (~70%) of adipose iNKT cells at 4 hours post-αGalCer, displayed little to no expression of activation and cytokine markers (Figure 3.10.2.B). This indicates that the blunted activation phenotype in adipose iNKT cells is granular, as some adipose adipose iNKT cells displayed increased activation and expression of cytokine genes in responses to αGalCer stimulation, while a majority of adipose iNKT cells did not.

**Figure 3.10.2: Granular analysis of adipose iNKT cells at 4 hours post-αGalCer (overleaf).** A. UMAP of total adipose iNKT cells 4 hours post-αGalCer. B. Feature plots of selected gene expression in total adipose iNKT cells 4 hours post-αGalCer.

A.


Adipose iNKT cells
4 hours post-αGalCer (2,950 cells)
UMAP 2
UMAP 1
NK1.1⁻ NKT1
NK1.1⁺ NKT1
NKT17
Cycling
Cytokine⁺

B.


Klrb1c
Klrg1
Mki67
Rorc
Ifng
Il4
Ccl4
Il10
Il17a
Il2ra
Nr4a1
Myc
UMAP 2
UMAP 1
Expression
Low
High

### 3.11 Transcriptional analysis of adipose iNKT cell subset activation

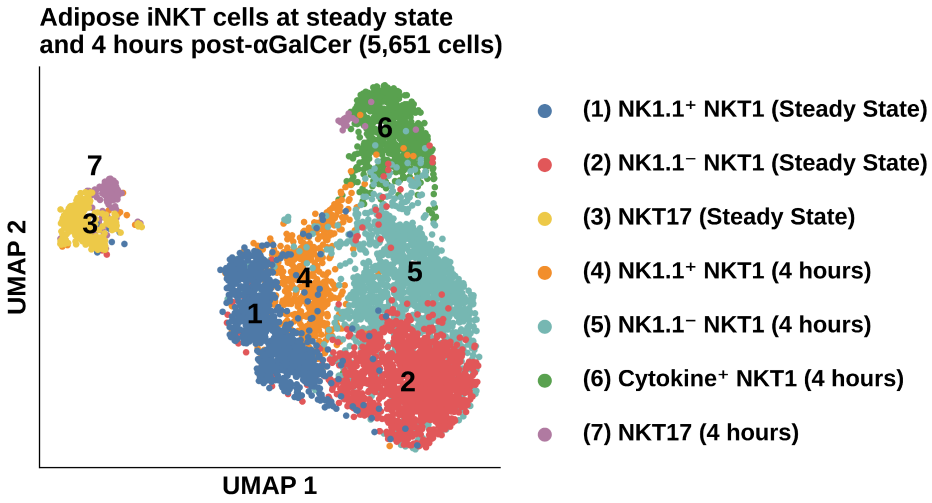
Having profiled the bulk transcriptional phenotype of adipose iNKT cells at 4 hours post-αGalCer, we next decided to analyze adipose iNKT cell subset activation. We also sought to compare the activation of adipose and splenic iNKT cell subsets. To do this, we first generated a combined analysis file of adipose iNKT cells at steady state and 4 hours post-αGalCer, excluding cycling cells, and performed fine reclustering of adipose iNKT cells at 4 hours post-αGalCer. This generated a final analysis file of 5,651 adipose iNKT cells that split into 7 clusters based on their activation status: steady state NK1.1$^{+}$ and NK1.1$^{-}$ NKT1 cells (Cluster 1 and Cluster 2), steady state NKT17 cells (Cluster 3), NK1.1$^{+}$ and NK1.1$^{-}$ NKT1 cells at 4 hours post-αGalCer (Cluster 4 and Cluster 5), Cytokine$^{+}$ NKT1 cells (4 hours post-αGalCer; Cluster 6), and NKT17 cells at 4 hours post-αGalCer (Cluster 7; Figure 3.11.1.A). Interestingly, previous UMAP of splenic iNKT cells at steady state and 4 hours post-αGalCer had shown that splenic iNKT cells separated primarily (i.e. along UMAP 1) by activation status (Figure 3.6.1.A). By contrast, UMAP of adipose iNKT cells at steady state and 4 hours post-αGalCer demonstrated that adipose iNKT cells separated first by subset (i.e. NKT17 cells versus NKT1 cells), and only second (i.e. along UMAP 2) by activation status (Figure 3.11.1.A). This indicates that transcriptional differences between adipose iNKT cell subsets predominate over transcriptional differences induced by activation at 4 hours post-αGalCer.

We next performed gene expression analysis. Expression of genes associated with activation, cytokine production, and metabolic remodeling were enriched among Cytokine$^{+}$ NKT1 cells (Cluster 6) and NKT17 cells at 4 hours post-αGalCer (Cluster 7), indicating that adipose NKT17 cells and some adipose NKT1 cells undergo a similar process of activation and transcriptional remodeling to splenic NKT1, NKT2, and NKT17 cells after αGalCer stimulation (Figure 3.11.1.B). Key transcriptional regulators previously identified among activated splenic iNKT cells were also upregulated by activated adipose NKT1

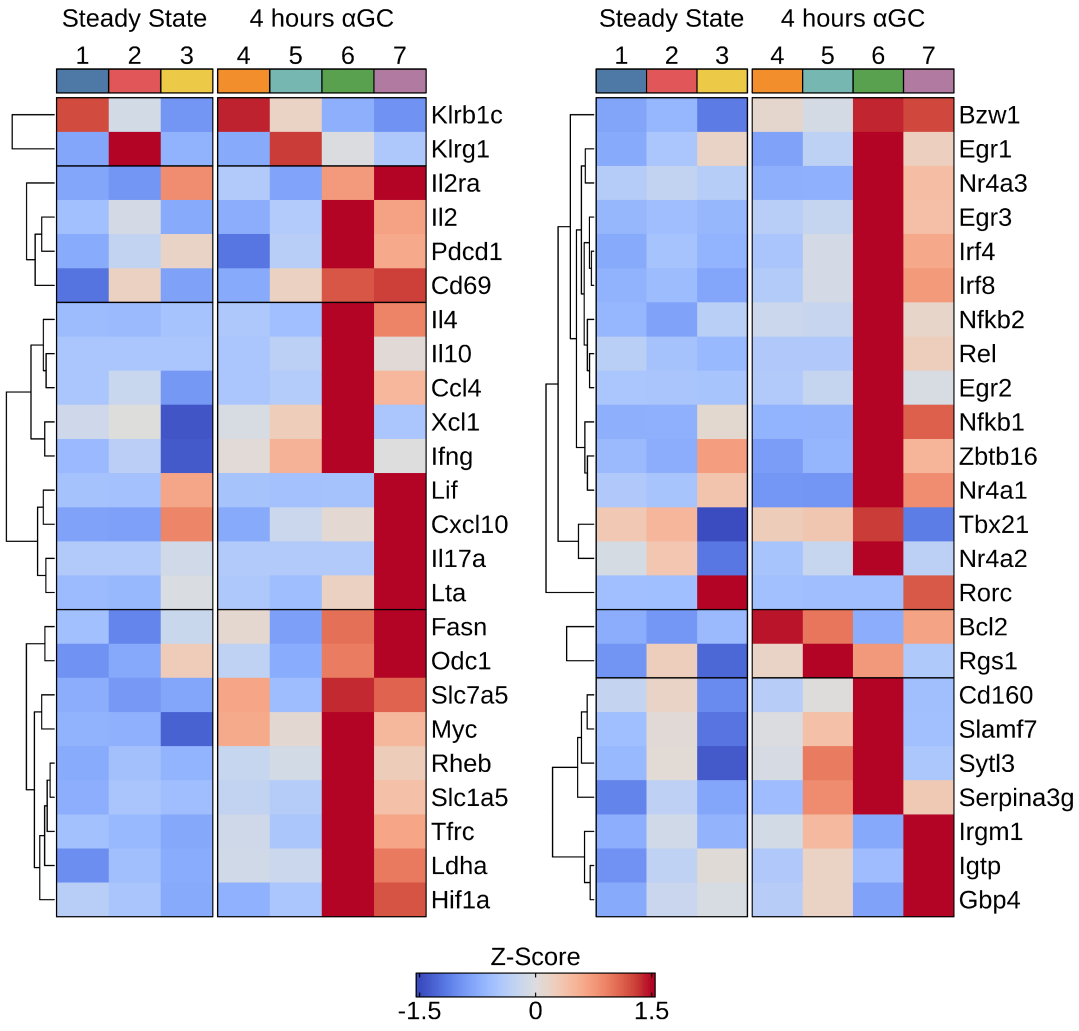
and NKT17 cells, including *Zbtb16*, *Bzw1*, *Irf4*, *Ir8*, *Bhlhe40*, and NR4A, NF-κB, and EGR family members (Figure 3.11.1.B). Although PLZF expression is typically low or absent in adipose iNKT cells at steady state[49], our data here suggest that, as in splenic and human iNKT cells, *Zbtb16* expression is rapidly upregulated in activated adipose iNKT cells. By contrast, adipose NK1.1$^{+}$ and NK1.1$^{-}$ NKT1 cells at 4 hours post-αGalCer (Cluster 4 and Cluster 5) generally lacked expression of activation and cytokine markers, although interestingly we found that these cells displayed subtly increased expression of *Myc* and *Ifng*, and transiently upregulated *Rgs1* and *Bcl2* (Figure 3.11.1.B). This suggests that adipose NK1.1$^{+}$ and NK1.1$^{-}$ NKT1 cells at 4 hours post-αGalCer (Cluster 4 and Cluster 5) might represent an early activation state, raising the possibility that activation of iNKT cells in adipose tissue is delayed compared to the spleen. We also profiled DEG expression among adipose NKT1 and NKT17 cells. Adipose NKT1 and NKT17 cells demonstrated enrichment of similar DEGs to their splenic counterparts, including *Ifng*, *Ccl4*, *Xcl1*, *Cd160* and *Slamf7* among NKT1 cells, and *Il17a*, *Lif*, *Cxcl10*, *Lta*, and *Irgm1* among NKT17 cells. Notably, *Il10* was only expressed by NKT1 cells (Figure 3.11.1.B), suggesting that adipose NKT10 cells are NKT1-like, or might represent a subset of NKT1 cells.

**Figure 3.11.1: Transcriptional signatures of adipose iNKT cell subset activation (overleaf).** A. UMAP of adipose iNKT cells at steady state and 4 hours post-αGalCer. Cycling cells were excluded from the analysis. B. Scaled average heatmaps with hierarchical clustering of gene expression in the clusters from Figure 3.11.1.A. αGC = αGalCer.

A.


Adipose iNKT cells at steady state
and 4 hours post-αGalCer (5,651 cells)
UMAP 2
UMAP 1
1
2
3
4
5
6
7
(1) NK1.1+ NKT1 (Steady State)
(2) NK1.1− NKT1 (Steady State)
(3) NKT17 (Steady State)
(4) NK1.1+ NKT1 (4 hours)
(5) NK1.1− NKT1 (4 hours)
(6) Cytokine+ NKT1 (4 hours)
(7) NKT17 (4 hours)

B.


Steady State
4 hours αGC
1 2 3 4 5 6 7
Klrb1c
Klrg1
Il2ra
Il2
Pdcd1
Cd69
Il4
Il10
Ccl4
Xcl1
Ifng
Lif
Cxcl10
Il17a
Lta
Fasn
Odc1
Slc7a5
Myc
Rheb
Slc1a5
Tfrc
Ldha
Hif1a
Bzw1
Egr1
Nr4a3
Egr3
Irf4
Irf8
Nfkb2
Rel
Egr2
Nfkb1
Zbtb16
Nr4a1
Tbx21
Nr4a2
Rorc
Bcl2
Rgs1
Cd160
Slamf7
Sytl3
Serpina3g
Irgm1
Igtp
Gbp4
Z-Score
-1.5
0
1.5

We next compared adipose and splenic iNKT cell subsets by performing module scoring of matched steady state and activated NKT1, NKT2, and NKT17 cells from spleen and adipose tissue, using a single normalized file containing data from Figure 3.6.1.A and Figure 3.11.1.A. We excluded adipose NK1.1$^{+}$ and NK1.1$^{-}$ NKT1 cell clusters at 4 hours post-αGalCer (Cluster 4 and Cluster 5, Figure 3.11.1.A) due to their low expression of activation makers and cytokine genes, since this might skew our comparison between activated, cytokine producing adipose and splenic iNKT cell subsets. Since it was not possible to stratify Cytokine$^{+}$ adipose NKT1 cells (Figure 3.11.1.A, Cluster 6) using expression of *Klrb1c* (encoding NK1.1) due to *Klrb1c* downregulation after activation (Figure 3.11.1.B), we used Cytokine$^{+}$ adipose NKT1 cells as the end point for both adipose NK1.1$^{+}$ and NK1.1$^{-}$ NKT1 cell activation.

Even after matching steady state and activated iNKT cell subsets, we still found that adipose iNKT cell subsets displayed reduced activation and cytokine gene expression, and metabolic remodeling compared to splenic iNKT cell subsets (Figure 3.11.2.A), although the difference was not as striking as it had been when we compared bulk adipose and splenic iNKT cells (Figure 3.10.1.B, Figure 3.11.2.A). Interestingly, adipose NKT17 cells displayed enrichment of oxidative metabolic gene signatures compared to adipose NKT1 cells (Figure 3.11.2.A), similar to our previous finding in splenic iNKT cells, suggesting that increased oxidative metabolic enrichment in NKT2 and NKT17 cells versus NKT1 cells is highly conserved. Furthermore, we identified increased glycolytic and amino acid metabolism gene expression among adipose iNKT cell subsets at steady state (Figure 3.11.2.A), and found enrichment of chronic activation and exhaustion markers among all adipose iNKT cell subsets (Figure 3.11.2.B). This suggests that both adipose NKT1 and NKT17 cells are exposed to chronic endogenous activation signals, although we detected the greatest overall enrichment of these genes among adipose NK1.1$^{-}$ NKT1 cells (Figure 3.11.2.B).

We next decided to profile conserved transcription factor enrichment in adipose versus splenic iNKT cell subsets. To do this, we leveraged the fact that NKT1 and NKT17 cells are present in both spleen and adipose tissue and performed matched gene expression analysis of NKT1 and NKT17 cells in adipose tissue versus spleen, both at steady state and after activation, utilizing the same data previously used for matched module scoring (Figure 3.11.2.A). We then identified transcription factors which were always enriched among NKT1 and NKT17 cells in either adipose tissue or spleen. We identified a total of 7 transcription factors enriched among splenic iNKT cells, and 29 transcription factors enriched among adipose iNKT cells. Splenic iNKT cells showed constitutive enrichment of the NF-κB components *Nfkb1* and *Nfkb2*, *Naca*, and *Bzw2* (Figure 3.11.2.C). Notably, *Nfkb1*, encoding p105/p50, has previously been shown to regulate the production of several cytokines in iNKT cells, including IFNγ, IL-2, IL-13 and GM-CSF[351], and constitutively increased expression of this transcription factor among splenic iNKT cells may be reflective of the increased cytokine production and more inflammatory phenotype of splenic iNKT cells after activation, relative to adipose iNKT cells. Transcription factors enriched among adipose iNKT cells included *Nfil3*, the Kruppel-like factors *Klf13*, *Kfl9*, *Klf2*, *Klf4*, and *Klf6*, *Maf* and *Maff*, *Nfact2*, *Nr4a2*, *Cebpb*, *Mxd1*, *Stat4*, and the AP1 transcription factors *Junb*, *Fos*, *Fosb*, *Jund*, and *Fosl2* (Figure 3.11.2.C). Interestingly, many of these transcription factors have previously been associated with transcriptional profiling of memory or chronically activated/exhausted virus specific $CD4^+$ and/or $CD8^+$ T cells[102]. This provides further evidence that adipose iNKT cells may experience chronic endogenous activation and suggests that adipose iNKT cells may be transcriptionally “poised” to produce a muted response to strong antigen challenge.

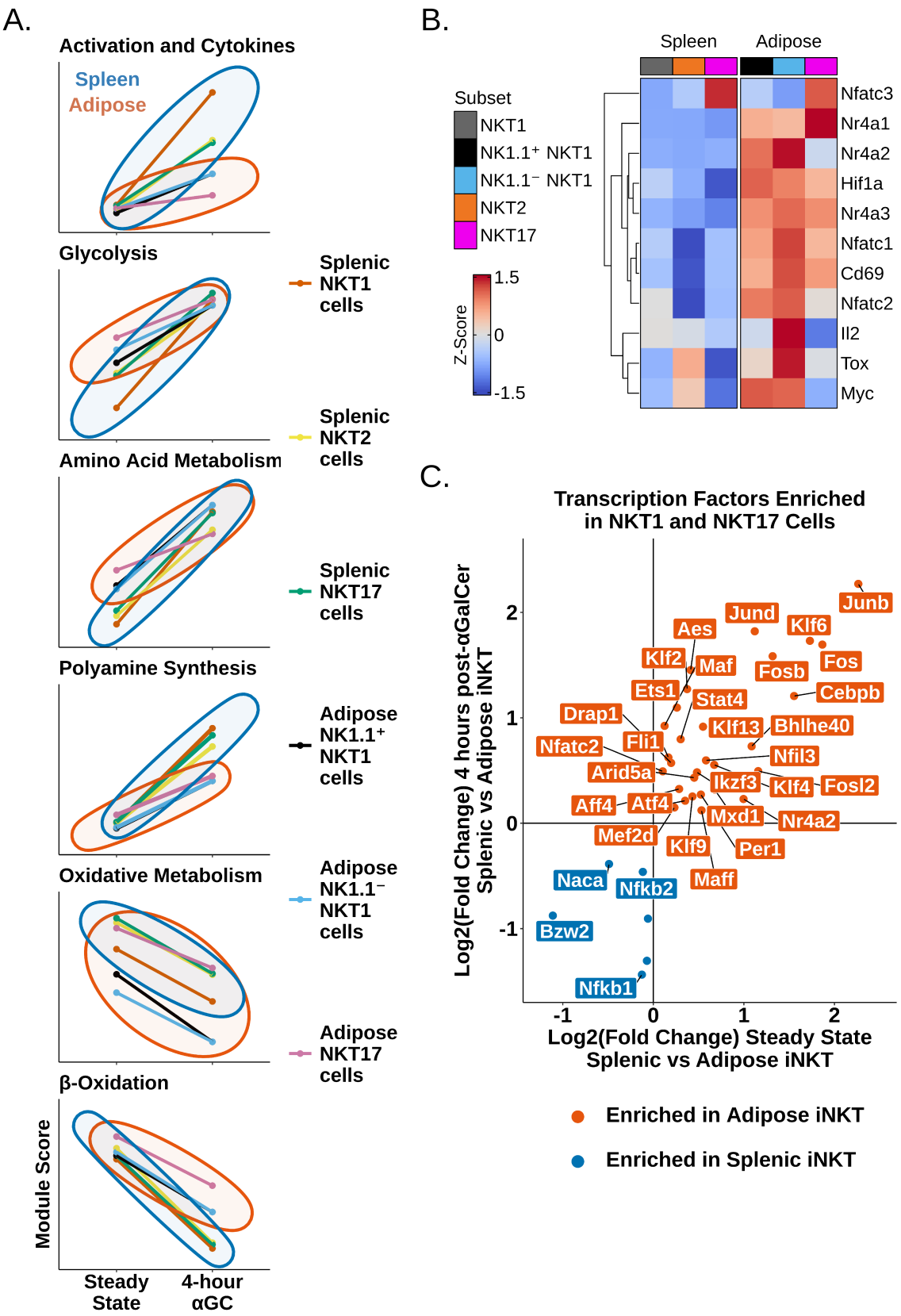

A.
Activation and Cytokines
Spleen
Adipose
Glycolysis
Amino Acid Metabolism
Polyamine Synthesis
Oxidative Metabolism
β-Oxidation
Module Score
Steady State
4-hour αGC
Splenic NKT1 cells
Splenic NKT2 cells
Splenic NKT17 cells
Adipose NK1.1+ NKT1 cells
Adipose NK1.1− NKT1 cells
Adipose NKT17 cells
B.
Spleen
Adipose
Subset
NKT1
NK1.1+ NKT1
NK1.1− NKT1
NKT2
NKT17
Z-Score
1.5
0
-1.5
Nfatc3
Nr4a1
Nr4a2
Hif1a
Nr4a3
Nfatc1
Cd69
Nfatc2
Il2
Tox
Myc
C.
Transcription Factors Enriched in NKT1 and NKT17 Cells
Log2(Fold Change) 4 hours post-αGalCer Splenic vs Adipose iNKT
Log2(Fold Change) Steady State Splenic vs Adipose iNKT
Junb
Jund
Klf6
Aes
Klf2
Maf
Fosb
Fos
Ets1
Stat4
Cebpb
Drap1
Klf13
Bhlhe40
Nfatc2
Fli1
Nfil3
Arid5a
Ikzf3
Klf4
Fosl2
Aff4
Atf4
Mxd1
Nr4a2
Mef2d
Klf9
Per1
Naca
Nfkb2
Maff
Bzw2
Nfkb1
Enriched in Adipose iNKT
Enriched in Splenic iNKT

**Figure 3.11.2: Transcriptional features of adipose iNKT cells subsets at steady state and 4 hours post-αGalCer (previous page).** A. Line plots showing median expression of iNKT cell activation/cytokine and metabolic gene module scores in adipose and splenic iNKT cell NKT1, NKT2 and NKT17 cells at steady state and 4 hours post-αGalCer. Splenic NKT1, NKT2, and NKT17 cell clusters were taken from Figure 3.6.1.A, while adipose NKT1 and NKT17 cell clusters were taken from Figure 3.11.1.A (Cluster 1, Cluster 2, Cluster 3, Cluster 6 and Cluster 7; Clusters 4 and 5 were excluded). All data were normalized from raw counts in the same analysis file. Cluster 6 from 3.11.1.A was treated as the end activation point for both $NK1.1^{+}$ and $NK1.1^{-}$ adipose iNKT cells since it was not possible to stratify cytokine producing NKT1 cells (Cluster 6 cells) using expression of NK1.1 (*Klrb1c*). Ellipses represent 95% confidence intervals for all splenic (blue) or adipose (orange) subset values. B. Scaled average heatmap with hierarchical clustering of gene expression in adipose and splenic NKT1, NKT2 and NKT17 cells. C. Scatter plot of transcription factors enriched in both NKT1 and NKT17 cells in adipose tissue versus splenic iNKT cells at steady state and/or 4 hours post-αGalCer. Transcription factors constitutively enriched in splenic iNKT cells, regardless of activation status, are shown in blue, while genes that are constitutively enriched in adipose iNKT cells, regardless of activation status, are shown in orange.

## Discussion

Modern high throughput sequencing technologies, including microarray, bulk RNA-Seq, ATAC-Seq, and scRNA-Seq, have had a transformative impact on the field of iNKT cell biology, and provided new insights into iNKT cell development, differentiation and heterogeneity[45,46,49,61,64,65,67,91,92,115]. In this study, we sought to utilize scRNA-Seq to gain new insights into the transcriptional signatures underlying iNKT cell activation and effector function, a topic which has generally received less attention compared to iNKT cell development, or the composition of the iNKT cell repertoire at steady state. We also sought to untangle adipose iNKT cell heterogeneity, and to characterize the transcriptional profile of this unusual regulatory population of iNKT cells[49,90,91,115], again using scRNA-Seq.

Analysis of murine adipose iNKT cells at steady state revealed three major subsets, comprised of two populations of NKT1 cells, and a population of NKT17 cells, demonstrating that adipose iNKT cells are not a monolithic population. Notably, unlike the spleen, we did not identify a population of NKT2 cells in adipose tissue, and work by LaMarche *et al.* (2020) has demonstrated that NKT2-like PLZF$^{high}$ iNKT cells are not present in the adipose tissue of adult mice[115]. We also found that adipose NKT1 cells segregated based on expression of NK1.1[109], which has historically been an important marker for analysis of iNKT cell development and heterogeneity[40,99,100]. Furthermore, granular analysis of NK1.1$^{+}$ and NK1.1$^{-}$ NKT1 cells revealed additional heterogeneity, demonstrating that adipose NKT1 cells are transcriptionally diverse. While cycling iNKT cells were substantially more enriched in adipose tissue compared to spleen, indicating that adipose iNKT cells are more proliferative, we also found that adipose iNKT cells displayed enrichment of genes associated with apoptosis and cell death. Moreover, work by LaMarche *et al.* (2020) found that adipose iNKT undergo apoptosis at an increased rate compared to splenic iNKT cells. Therefore, although adipose iNKT cells are more proliferative, they also undergo apoptosis at an increased rate.

Interestingly, this proliferative/apoptotic phenotype could be linked to cell stress. We identified enrichment of gene signatures associated with ER stress among adipose iNKT cells, and work by LaMarche *et al.* (2020) has shown that adipose iNKT cells undergo lipid-mediated ER stress through the IRE1a-XBP1s arm of the UPR, which induces expression of the transcription factor E4BP4[115]. Prolonged ER stress is a known inducer of apoptosis[339], and so it is possible that the same ER stress pathway that induces expression of E4BP4 may also contribute to increased adipose iNKT cell apoptosis.

After analyzing steady state iNKT cell heterogeneity, we turned our attention to iNKT cell activation. Analysis of splenic iNKT cells at steady state versus 4 hours post-αGalCer revealed that rapid iNKT cell activation and cytokine production in response to antigen challenge is accompanied by equally rapid and extensive transcriptional remodeling, including changes in metabolic gene signatures, and rewiring of the regulatory transcription factor landscape. Like activated adaptive T cells[152,155,160–162], activated iNKT cells demonstrate increased expression of genes associated with glycolysis, amino acid uptake and metabolism, and polyamine synthesis, while gene signatures associated with oxidative metabolism were decreased compared to steady state iNKT cells. Although scRNA-Seq cannot analyze metabolic flux, these changes in metabolic pathway gene signatures are suggestive of iNKT cells adopting a more aerobic glycolytic profile after activation, a metabolic program which is used by T cells to support growth, proliferation, and effector function[152,156,160]. Our data also correlate with recent reports demonstrating that glucose is an important fuel for iNKT cell effector function[94,304]. Notably, while these changes typically occur over a period of days in naive adaptive T cells, as they undergo activation and differentiation[149,152–154,156], in iNKT cells we found evidence of this transcriptional remodeling on a timescale of hours. This indicates that transcriptional remodeling among activated iNKT cells is more akin to memory T cells[168] and correlates with past work demonstrating that iNKT cells are developmentally poised for rapid activation and effector function[42,43,45,133,352].

Interestingly, we also found enrichment of *Zbtb16*, encoding PLZF, among activated iNKT cells. PLZF has been identified as a master regulator of the innate-like activation scheme of iNKT cells, and is essential for establishment of the hybrid, poised iNKT cell phenotype[41–43,45,352]. Our identification of increased *Zbtb16* expression during early iNKT cell activation, combined with previous work showing that PLZF is enriched during downstream iNKT cell activation[74], suggests that PLZF may play a role in iNKT activation in response to antigen challenge.

We also profiled activation among iNKT cell subsets as part of our study. Overall, we found that NKT1, NKT2, and NKT17 cells shared expression of the same activation-associated transcriptional framework that we identified among bulk splenic iNKT cells, including enrichment of genes encoding T cell activation markers and cytokines, changes in the iNKT cell regulatory landscape, increased expression of *Zbtb16*, and remodeling of metabolic gene modules. This indicates that a common transcriptional network underpins the activation and effector program of functionally diverse iNKT cell subsets. However, we also found that activated NKT1, NKT2, and NKT17 cells displayed differential gene expression. Activated NKT2 and NKT17 cells were transcriptomically distinct to activated NKT1 cells, and shared enrichment of genes associated with oxidative phosphorylation. Analysis of the mitochondrial phenotype of NKT1, NKT2, and NKT17 cells, and functional analysis of iNKT cell cytokine production in the presence or absence of oligomycin, a potent inhibitor of the electron transport chain[109], revealed that NKT2 and NKT17 cells displayed and enhanced mitochondrial phenotype compared to NKT1 cells, and NKT2 and NKT17 cells were specifically dependent on flux through the electron transport chain for effector cytokine production. This indicates that while NKT1, NKT2, and NKT17 cells share many transcriptional signatures during activation, they are also metabolically distinct. Notably, our work correlates with recent reports by Zhao *et al*. (2021) and Raynor *et al.* (2020), which have shown oxidative metabolism and mitochondrial phenotype

distinguishes NKT2 and NKT17 cells from NKT1 cells during iNKT cell development and in thymus[302,303], and work by Lopes *et al.* (2021) has shown that γδ17 cells, which are transcriptionally similar to NKT17 cells[61], display enrichment of oxidative metabolism compared to γδ1 cells[109], which are transcriptionally similar to NKT1 cells. This suggests that utilization of oxidative metabolism may represent a conserved phenotypic difference between Th1-like and Th2 or Th17-like innate T cells.

Having profiled transcriptional signatures of activation among murine iNKT cells, we also sought to profile human iNKT cell activation by reanalyzing previously published human iNKT cell sequencing data[133–135]. Notably, we found that activated human iNKT cells displayed enrichment of the same conserved transcriptional framework as murine iNKT cells, demonstrating that the transcriptional signatures underpinning iNKT cell activation are well conserved across species. However, human iNKT cells did not display the same degree of heterogeneity that murine iNKT cells did, and we did not identify discrete human iNKT cell subsets corresponding to murine NKT1, NKT2, and NKT17 cells. Instead, we found that human iNKT cells segregated on the basis of *GZMK*, *GZMB*, and *LEF1* expression at steady state, while most activated human iNKT cells appeared to be Th1 or NKT1-like and expressed *IFNG*. We did identify functional heterogeneity on the basis of *CD4* and *CD8* expression in one of the datasets that we reanalyzed[134], correlating with previous reports in the literature demonstrating that expression of CD4 and CD8 can demarcate functional human iNKT cell heterogeneity[125–127,245,284]. However, the lack of consistent *CD4* and *CD8* expression across different datasets hampered our ability to correlate iNKT cell function against *CD4* and *CD8* expression, and to draw conclusions about functional diversity among human iNKT cells. Therefore, detailed transcriptional profiling of human iNKT cell heterogeneity, including correlation against *CD4* and *CD8* expression, will require further work, possibly leveraging antibody labeling or other multiomic

techniques to effectively capture the spectrum of human iNKT cell heterogeneity[353].

Finally, we profiled the phenotype of activated murine adipose iNKT cells and compared adipose iNKT cell activation to splenic iNKT cell activation. While most splenic iNKT cells displayed significant enrichment of genes associated with activation, cytokine production, and metabolic remodeling at 4 hours post-αGalCer, adipose iNKT cells displayed a blunted response to αGalCer stimulation and demonstrated greatly reduced transcriptomic remodeling. Granular analysis of adipose iNKT cells at 4 hours post-αGalCer revealed that only a minority of adipose iNKT cells showed enrichment of gene signatures associated with activated splenic and human iNKT cells, and we identified some evidence that adipose iNKT cell activation could be delayed relative to splenic iNKT cell activation. Interestingly, we noted that steady state adipose iNKT cells were enriched for markers of activation, such as *Il2*, and genes associated with memory-like iNKT cells and antigen-specific memory T cells, such as *Itga4* and *Klrg1*[206,336]. This correlates with previous work by Lynch *et al.* (2015) and Sag *et al.* (2014)[49,91], and suggests that adipose iNKT cells might experience endogenous activation in adipose tissue, and thus may already be antigen experienced at steady state. In support of this hypothesis, we detected enrichment of genes associated with chronic TCR stimulation among adipose iNKT cells, including *Nr4a1*, *Nr4a2*, *Nr4a3*, *Nfact1*, *Nfatc2*, and *Tox*[170,172,280]. Furthermore, work by Lynch *et al.* (2015) and LaMarche *et al.* (2020) has shown that adipose iNKT cells can mount potent cytokine responses after stimulation with PMA and Ionomycin[49,115], and reduced activation compared to splenic iNKT cells is only observed in response to αGalCer stimulation. Notably, this is similar to the phenotype of αGCPT iNKT cells in other organs, such as the spleen, which remain capable of mounting potent cytokine responses upon bypass of proximal TCR signaling but are anergic in response to TCR restimulation[208]. Therefore, we propose that blunted or delayed activation of adipose iNKT cells in response to αGalCer

may be due to chronic TCR stimulation and activation of these cells in the lipid rich environment of adipose tissue, leading to a TCR “block” and a refractory response to subsequent strong TCR stimulation.

# Chapter 4: Transcriptional analysis of downstream iNKT cell activation and memory-like iNKT cells

## Introduction

iNKT cells, and other innate T cells such as γδ T cells and MAIT cells, are typically characterized by their ability to rapidly respond to antigen and cytokine stimulus, and by their ability to mount rapid and potent effector responses[1,2]. However, although iNKT cell activation is rapid, occurring over a timescale of minutes to hours, the iNKT cell effector response is not limited to this initial phase of acute activation. While iNKT cells produce a rapid cytokine burst within hours of activation[17], production of cytokines can continue for several days after activation[15,142,146,180]. Moreover, numerous studies have demonstrated that activated iNKT cells undergo a proliferative burst over a period of ~2-3 days, analogous to clonal expansion of adaptive T cells[354]. For example, the number of murine splenic iNKT cells increases by ~10-15 fold after *in vivo* stimulation with αGalCer[198,200]. Notably, these proliferated iNKT cells retain their ability to rapidly mount cytokine responses[93] and can therefore be considered analogous to a population of clonally expanded effector T cells. This expansion phase of iNKT cell activation is also significant because it represents the earliest point at which memory-like or “trained” iNKT cells can be detected[107,201,203,266,267]. However, transcriptional characterization of this activation state has been limited to date.

To characterize downstream iNKT cell activation, and the expanded pool of iNKT cells generated several days after iNKT cell activation, we performed 10x scRNA-Seq of whole splenic and adipose iNKT cells at 72 hours post-αGalCer, facilitating granular analysis of iNKT cells from both tissues at 72 hours post-αGalCer, and comparative analysis against our previous scRNA-Seq data of adipose and splenic iNKT cells at steady state and 4 hours post-αGalCer.

Following this proliferative burst at ~1-3 days post-activation, most expanded iNKT cells subsequently undergo apoptosis, and the iNKT cell population contracts to baseline levels within 1-2 weeks[198,200]. However, during this period, novel memory-like iNKT cells appear, including KLRG1$^{+}$ iNKT cells, NKT$_{FH}$

cells, and a regulatory population of iNKT10 cells[16,91,92,131,201,202,206]. While the frequency of some of these memory-like populations, such as KLRG1$^+$ iNKT cells and NKT$_{FH}$ cells, peaks around ~5-7 days post-activation before subsequently declining[92,206], there is also evidence that memory-like iNKT cells can demonstrate long term persistence. For example, Shimizu *et al.* (2014) found that pulmonary KLRG1$^+$ iNKT cells were most numerous at 7 days post-αGalCer but could still be detected 8-9 months later[206]. This indicates that activation can induce long term remodeling of the iNKT cell repertoire. Activation of iNKT cells has also been shown to induce long term changes in iNKT cell functionality. For example, antigen experienced iNKT cells have been shown to display an anergic, refractory response to secondary antigen challenge[91,195,208]. This anergic phenotype is also accompanied by changes in the cytokine production profile of iNKT cells, whereby production of inflammatory cytokines, such as IFNγ, is reduced, and production of IL-10 is increased[16,91]. similar to adipose iNKT cells[49,91,115]. However, at the time of starting my PhD, it was unknown whether similar transcriptional signatures or iNKT cell populations underpinned the anergic and regulatory phenotype shared by adipose iNKT cells and antigen experienced iNKT cells. Moreover, the transcriptional relationship between iNKT10 cells, adipose iNKT cells, and memory-like KLRG1$^+$ and NKT$_{FH}$ cells remained unclear.

To address these questions, and to complement our previous scRNA-Seq of splenic and adipose iNKT cells, we performed 10x scRNA-Seq of splenic and adipose iNKT cells 4 weeks after *in vivo* activation with αGalCer. We also performed 10x scRNA-Seq of splenic iNKT cells after secondary *in vivo* activation with αGalCer, to analyze the functional profile of antigen experienced iNKT cells. We also performed reanalysis of bulk microarray data of αGCPT iNKT cells at 4 weeks post-αGalCer, previously published by Sag *et al.* (2014)[91], and bulk RNA-Seq data of memory-like NKT$_{FH}$ and non-NKT$_{FH}$ cells at 6 days post-αGalCer, previously published by Murray *et al.* (2021)[92], to validate our findings, and complement our scRNA-Seq data.

## Hypothesis

We hypothesized that iNKT cells at 72 hours post-αGalCer would be transcriptionally distinct to iNKT cells at steady state and 4 hours post-αGalCer, in both adipose tissue and spleen, and that iNKT cells would be heterogeneous at 72 hours post-αGalCer. We hypothesized that we would identify transcriptional remodeling between steady state and antigen experienced iNKT cell repertoires at 4 weeks post-αGalCer, and that we might identify novel iNKT cell populations. We hypothesized that we would identify conserved transcriptional signatures and/or populations underpinning the regulatory and anergic phenotype of adipose and antigen experienced splenic iNKT cells. We also hypothesized that we would identify enrichment of conserved gene signatures among adipose NKT10 cells and iNKT10 cells in the spleen, providing new insight into the biology of NKT10 cells.

## Aims

We analyzed scRNA-Seq of iNKT cells from spleen and adipose tissue at 4 weeks post-αGalCer, in combination with reanalysis of published transcriptomic iNKT cell data, and focused in particular on the following:

- The composition of the splenic and adipose iNKT cell repertoire after antigen exposure at 4 weeks post-αGalCer
- The transcriptional signatures of expanded iNKT cells at 72 hours post-αGalCer, and reactivated iNKT cells after secondary αGalCer stimulation
- The phenotype of memory-like iNKT cell populations, including KLRG1$^{+}$ iNKT cells, $NKT_{FH}$ cells, and NKT10 cells

### 4.1 Activation with αGalCer induces extensive, rapid, and sustained transcriptional remodeling of splenic iNKT cells

We began our analysis of our 72 hour post-αGalCer and memory-like iNKT cell data by performing comparative analysis of whole splenic iNKT cells at steady state, 4 hours post-αGalCer, and 72 hours post-αGalCer. Quality control measures returned 6,651 splenic iNKT cells at 72 hours post-αGalCer, expressing a median of 13,700 UMIs and 3,310 genes per cell. We then combined these data with our steady state and 4 hour post-αGalCer splenic iNKT cell data, for a final analysis of 16,071 cells. After performing UMAP we observed minimal overlap between iNKT cells from different activation states (Figure 4.1.1.A), indicating that activated splenic iNKT cells continue to undergo extensive transcriptional remodeling after an initial burst of transcriptional reprogramming at 4 hours post-αGalCer. We quantified this observation by performing comparative gene expression analysis, which identified over 10,000 DEGs between splenic iNKT cells at 4 hours post-αGalCer versus 72 hours post-αGalCer (Figure 4.1.1.B). Interestingly, a majority (>7000) of these DEGs were upregulated among iNKT cells at 72 hours post-αGalCer, suggesting that downstream transcriptional remodeling is characterized by the acquisition of new gene expression programs.

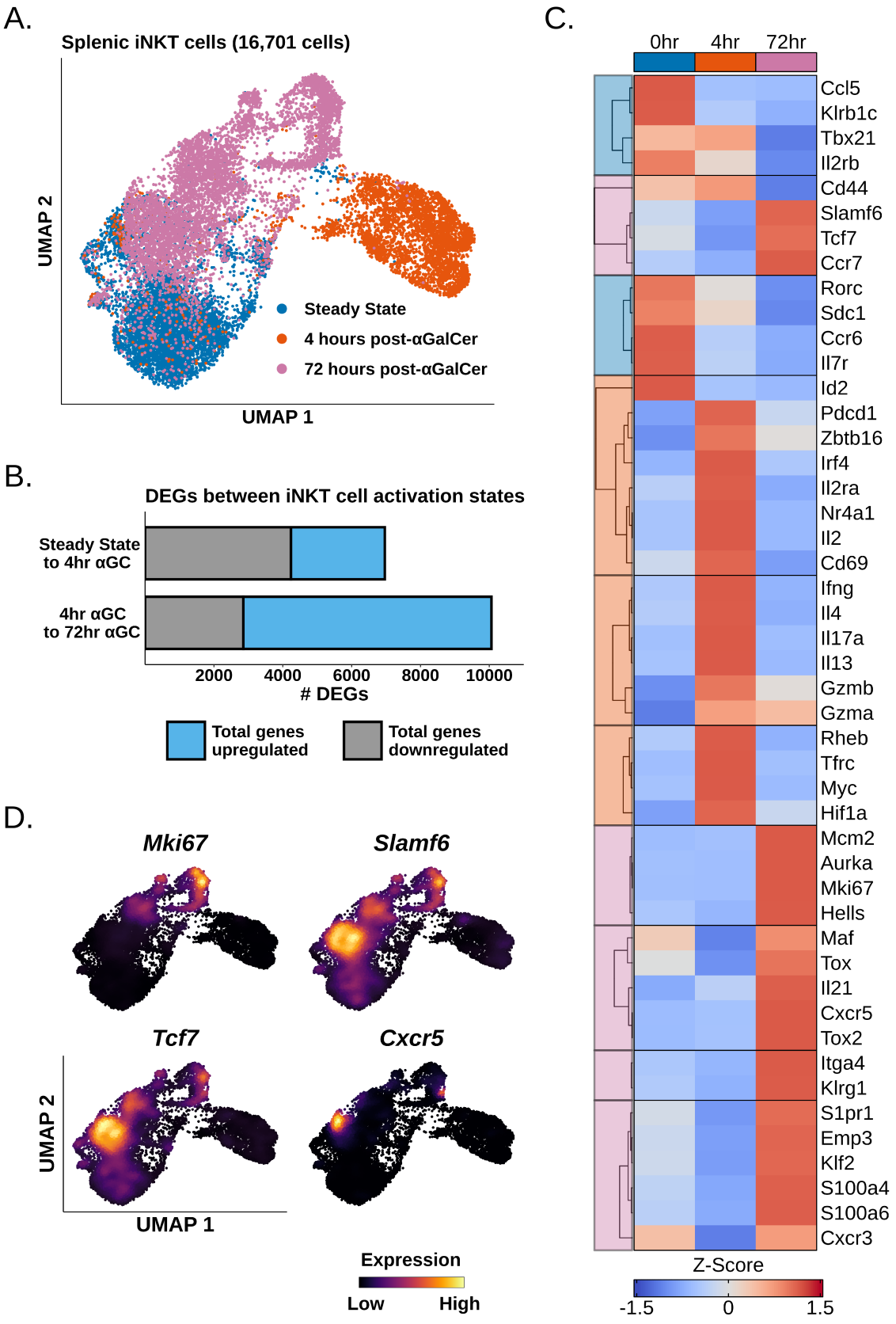
We next performed temporal analysis of gene expression among activated splenic iNKT cells. iNKT cells at 72 hours post-αGalCer demonstrated enrichment of motifs associated with NKT2 cells and immature thymic NKTp cells, including reduced expression of *Cd44*, and increased expression of *Slamf6*, *Tcf7*, and *Ccr7* (Figure 4.1.1.C)[46,61,66], while genes associated with NKT1 and NKT17 cells were most enriched among iNKT cells at steady state and 4 hours post-αGalCer. However, previous functional analysis of iNKT cells at 72 hours post-αGalCer by Cameron *et al.* (2018) has shown that expanded iNKT cells retain the capacity to produce copious amounts of IFNγ after restimulation[93], suggesting that the phenotype of expanded iNKT cells is distinct to that of NKTp cells. Notably, enrichment of *Tcf7* and *Slamf6*

(encoding Ly108) has also been linked with stem-like memory T cells[100], suggesting that 72 hour iNKT cells could be similar to stem-like memory T cells. Expression of *Zbtb16* was increased at 72 hours post-αGalCer compared to steady state, as previously demonstrated by Oleinika *et al.* (2018)[74] but reduced compared to 4 hours post-αGalCer. In agreement with previous functional analysis[15], we found that iNKT cells at 72 hours post-αGalCer lacked enrichment of genes associated with cytokine production and acute activation, and also did not display robust expression of acute metabolic activation markers, such as *Tfrc*, *Myc*, *Hif1a*, and *Rheb* (Figure 4.1.1.C).

We found that iNKT cells at 72 hours post-αGalCer displayed increased expression of many genes associated with proliferation and the cell cycle, including *Mki67*, *Aurka*, *Hells*, and *Mcm2* (Figure 4.1.1.C), demonstrating that iNKT cells continue to actively proliferate at this time. Interestingly, only a subset of 72 hour iNKT cells actually expressed proliferation and cell cycle markers (Figure 4.1.1.D), while other 72 hour iNKT cells showed enrichment of the stem-like markers *Slamf6* and *Tcf7*, as well as genes associated with memory-like iNKT cell subsets, such as *Cxcr5*. Therefore, our data demonstrate that iNKT cells at 72 hours post-αGalCer are transcriptionally heterogeneous. As exemplified by expression of *Cxcr5*, iNKT cells at 72 hours post-αGalCer displayed enrichment of genes associated with $T_{FH}$ cells, $NKT_{FH}$ cells, and KLRG1$^{+}$ iNKT cells, such as *Tox2*, *Il21*, *Klrg1*, and *Itga4*, which is in line with previous studies documenting the appearance of memory-like iNKT cells at ~3 days post-activation[201,203]. Gene expression analysis also revealed the enrichment of numerous genes associated with the KLF2 regulon among 72 hour iNKT cells, including *Klf2*, *S1pr1*, *S100a4*, and *S100a6* (Figure 4.1.1.C). While most iNKT cells are tissue resident at steady state[49,50], the enrichment of promigratory factors such as *Klf2* and *S1pr1* at 72 hours post-αGalCer potentially suggests that activated iNKT cells might become mobilized and traffic to other sites, although past analysis of iNKT cell migration by Geissmann *et al*. (2005), Velázquez *et al*. (2008), Lee *et al*.

(2010), and Liew *et al*. (2017) has demonstrated that activation of iNKT cells present in liver sinusoids induces arrest, rather than migration[142,355–357].

**Figure 4.1.1: Transcriptional signatures of splenic iNKT cell activation over 72 hours (overleaf).** A. UMAP of total splenic iNKT cells at steady state, 4 hours post-αGalCer, and 72 hours post-αGalCer. Cell cycle regression was performed during dimensionality reduction. B. Bar plots showing the total number of DEGs identified after gene expression analysis of splenic iNKT cells at 4 hours post-αGalCer versus steady state (top bar), and 72 hours post-αGalCer versus 4 hours post-αGalCer (bottom bar). The breakdown of DEGs found to be upregulated (blue) versus downregulated (gray) in each comparison is also shown. C. Scaled average heatmap with hierarchical clustering of gene expression in the cell activation states from Figure 4.1.1.A. D. Density plots of *Mki67*, *Slamf6*, *Tcf7*, and *Cxcr5* expression in splenic iNKT cells.


A.
Splenic iNKT cells (16,701 cells)
UMAP 2
UMAP 1
Steady State
4 hours post-αGalCer
72 hours post-αGalCer
B.
DEGs between iNKT cell activation states
Steady State to 4hr αGC
4hr αGC to 72hr αGC
2000
4000
6000
8000
10000
# DEGs
Total genes upregulated
Total genes downregulated
C.
0hr
4hr
72hr
Ccl5
Klrb1c
Tbx21
Il2rb
Cd44
Slamf6
Tcf7
Ccr7
Rorc
Sdc1
Ccr6
Il7r
Id2
Pdcd1
Zbtb16
Irf4
Il2ra
Nr4a1
Il2
Cd69
Ifng
Il4
Il17a
Il13
Gzmb
Gzma
Rheb
Tfrc
Myc
Hif1a
Mcm2
Aurka
Mki67
Hells
Maf
Tox
Il21
Cxcr5
Tox2
Itga4
Klrg1
S1pr1
Emp3
Klf2
S100a4
S100a6
Cxcr3
Z-Score
-1.5
0
1.5
D.
Mki67
Slamf6
Tcf7
Cxcr5
UMAP 2
UMAP 1
Expression
Low
High

Since we had identified differential expression of metabolic markers among iNKT cells at 72 hours post-αGalCer versus 4 hours post-αGalCer, we next decided to perform module scoring of our data and assess the metabolic profile of iNKT cells at 72 hours post-αGalCer. We found that iNKT cells at 72 hours post-αGalCer were highly enriched for glycolytic genes, similar to iNKT cells at 4 hours post αGalCer, but notably this was not accompanied by co-enrichment of genes associated with amino acid metabolism or polyamine metabolism, as we had found at 4 hours post-αGalCer (Figure 4.1.2.A). iNKT cells at 72 hours post-αGalCer also demonstrated enhanced expression of genes associated with oxidative metabolism and β-oxidation of lipids, even compared to iNKT cells at steady state (Figure 4.1.2.A). This demonstrates that the metabolic phenotype of iNKT cells at 72 hours post-αGalCer is distinct to that of iNKT cells at both steady state and 4 hours post-αGalCer and illustrates that activated iNKT cells undergo multiple rounds of metabolic gene reprogramming, potentially in order to satisfy the changing metabolic requirements.

A.

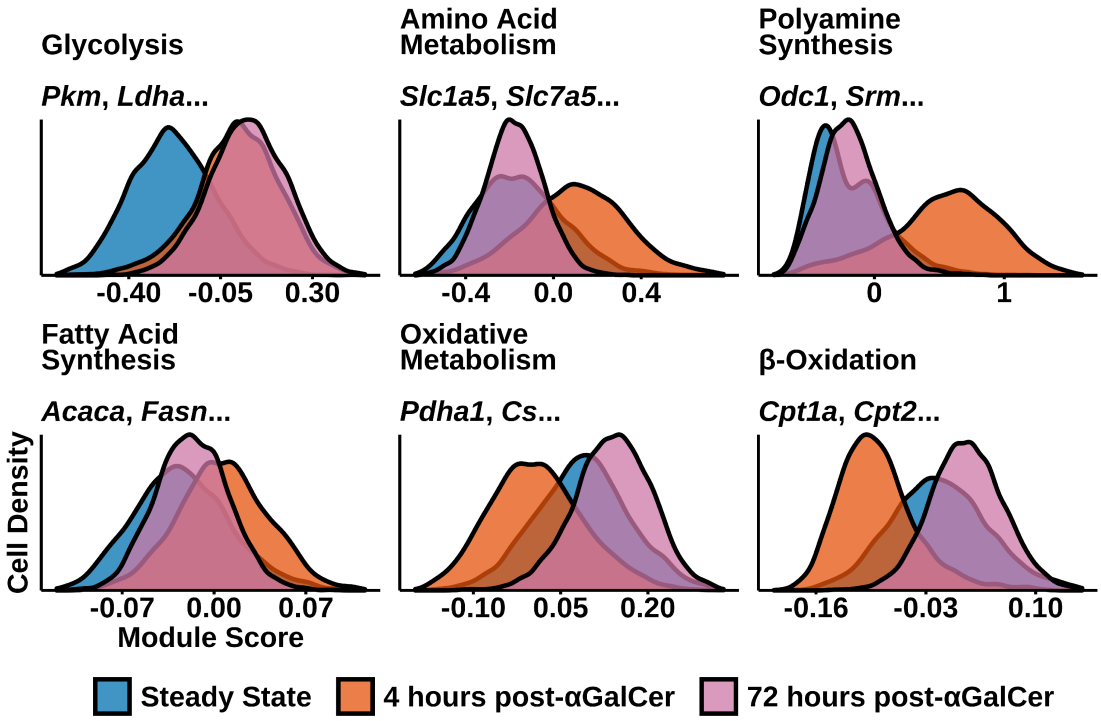


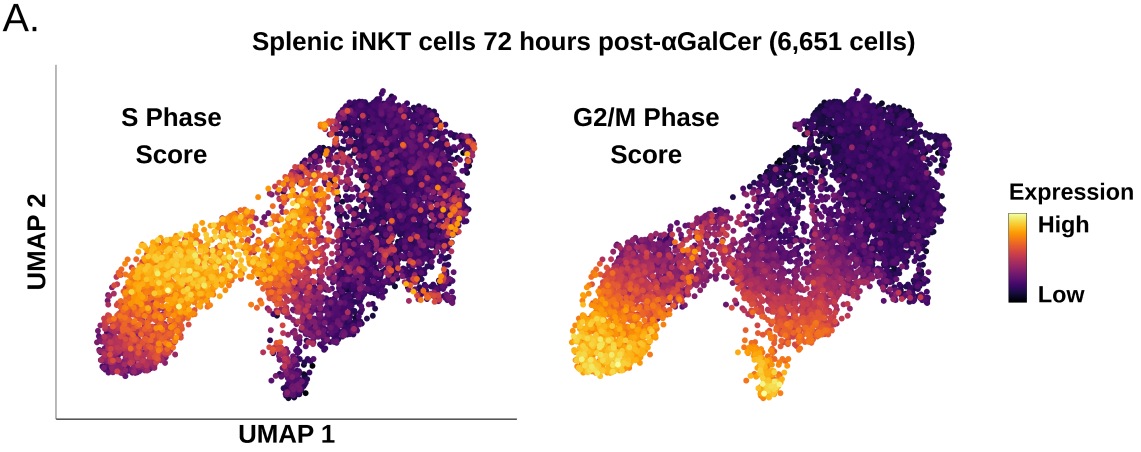

**Figure 4.1.2: Remodeling of metabolic gene expression following splenic iNKT cell activation.** A. Histograms showing expression of metabolic gene module scores in splenic iNKT cells at steady state, 4 hours post-αGalCer, and 72 hours post-αGalCer.

### 4.2 Granular analysis of splenic iNKT cells at 72 hours post-αGalCer

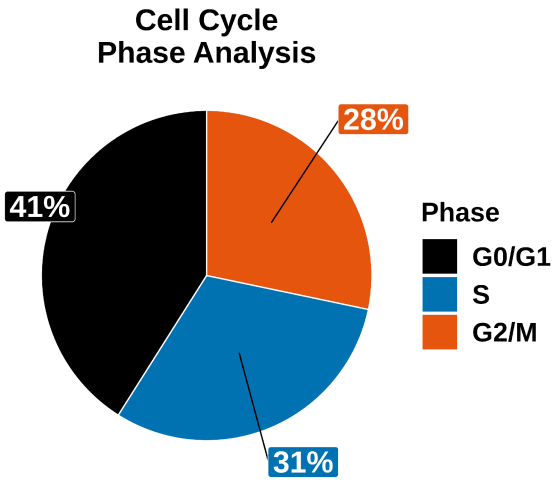
Having identified evidence of heterogeneity among splenic iNKT cells at 72 hours post-αGalCer, we next performed granular analysis of these data. Using cell cycle analysis, we found that ~50% of splenic iNKT cells expressed a transcriptional profile consistent with active proliferation at 72 hours post-αGalCer (Figure 4.2.1.A, Figure 4.2.1.B). We also identified a distinct population of G0/G1 phase iNKT cells that lacked expression of proliferation or cell cycle markers and using clustering analysis we found that G0/G1 iNKT cells were transcriptionally distinct to cycling cells (Figure 4.2.1.C). When we performed gene expression analysis, we found that G0/G1 cells displayed enrichment of genes associated with $T_{FH}$ cells, $NKT_{FH}$ cells and KLRG1$^{+}$ iNKT cells, including *Cxcr5*, *Tox2*, *Tox*, *Maf*, *Gzma*, *Gzmb*, and *Klrk1*, as well as markers of stem-like memory T cells and NKT2 cells, such as *Ifil27l2a*, *Slamf6*, *Tcf7*, and *Zbtb16* (Figure 4.2.1.D). Other genes enriched among G0/G1 cells included *Il7r*, *Ccl5*, *Cd27*, the MYC antagonist *Mxd4*, the anti-proliferative factor *Btg1*, the glycosyltransferase *Ogt*, and the growth arrest factor *Ypel3* (Figure 4.2.1.D).

**Figure 4.2.1: Granular analysis of splenic iNKT cells at 72 hours post-αGalCer (overleaf).** A. Feature plots of S phase or G2/M phase gene module scoring in splenic iNKT cells at 72 hours post-αGalCer. B. Pie chart showing the percentage of the iNKT cells in Figure 4.2.1.A in G0/G1 phase, S phase, or G2/M phase of the cell cycle. C. UMAP of splenic iNKT cells at 72 hours post-αGalCer. D. Scaled average heatmap with hierarchical clustering of gene expression in the cell clusters from Figure 4.2.1.C.

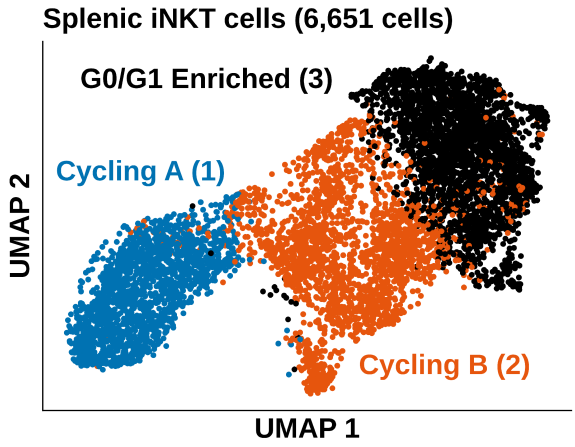
A.


Splenic iNKT cells 72 hours post-αGalCer (6,651 cells)
S Phase Score
G2/M Phase Score
Expression
High
Low
UMAP 2
UMAP 1

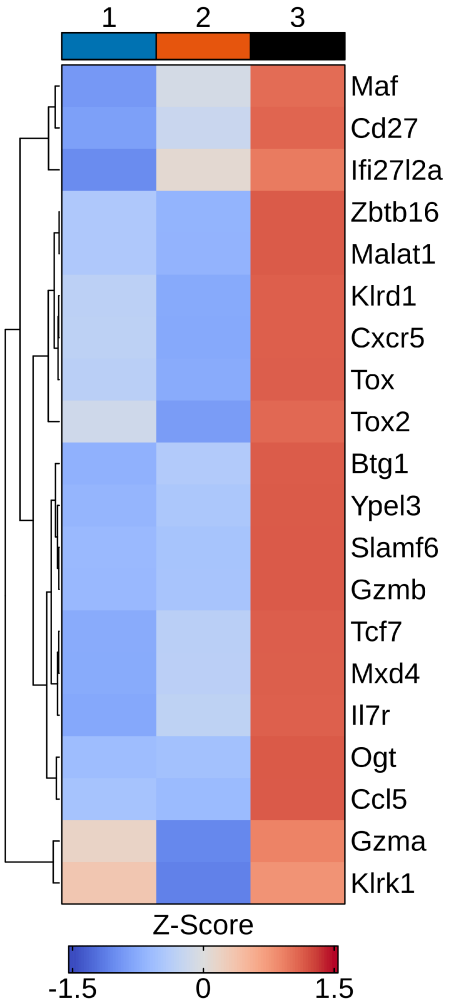
B.


Cell Cycle Phase Analysis
28%
41%
31%
Phase
G0/G1
S
G2/M

C.


Splenic iNKT cells (6,651 cells)
G0/G1 Enriched (3)
Cycling A (1)
Cycling B (2)
UMAP 2
UMAP 1

D.


1
2
3
Maf
Cd27
Ifi27l2a
Zbtb16
Malat1
Klrd1
Cxcr5
Tox
Tox2
Btg1
Ypel3
Slamf6
Gzmb
Tcf7
Mxd4
Il7r
Ogt
Ccl5
Gzma
Klrk1
Z-Score
-1.5
0
1.5

We next analyzed granular gene expression among splenic iNKT cells at 72 hours post-αGalCer using density plot mapping. Interestingly, we found that expression of *Zbtb16* delineated two populations of G0/G1 iNKT cells, *Zbtb16*$^{high}$ cells and *Zbtb16*$^{low}$ cells (Figure 4.2.1.A, Figure 4.2.2.A). We found that some *Zbtb16*$^{high}$ cells showed enrichment of *Slamf6*, *Tcf7*, *Ccr7*, and *Tox*, suggestive of an NKT2-like or stem-like memory T cell phenotype, while a second group of *Zbtb16*$^{high}$ cells showed increased expression of *Cxcr5*, *Pdcd1*, *Tox2*, and *Tox*, indicative of an $NKT_{FH}$ cell phenotype (Figure 4.2.2.A). We also identified heterogeneity among *Zbtb16*$^{low}$ iNKT cells. Some *Zbtb16*$^{low}$ cells demonstrated increased expression of *Cd160*, *Ccl5*, *Slamf7*, and *Fasl*, suggestive of an NKT1 cell phenotype (Figure 4.2.2.A), while a second group of *Zbtb16*$^{low}$ cells displayed enrichment of *Klrg1*, *Gzma*, *Gzmb*, and *Klrk1*, indicative of $KLRG1^{+}$ iNKT cells. Overall, our analysis demonstrates that splenic iNKT cells at 72 hours post-αGalCer are transcriptionally heterogeneous, and there is evidence of distinct iNKT cell phenotypes, including memory-like or “trained” $KLRG1^{+}$ iNKT cells and $NKT_{FH}$ cells.

A.

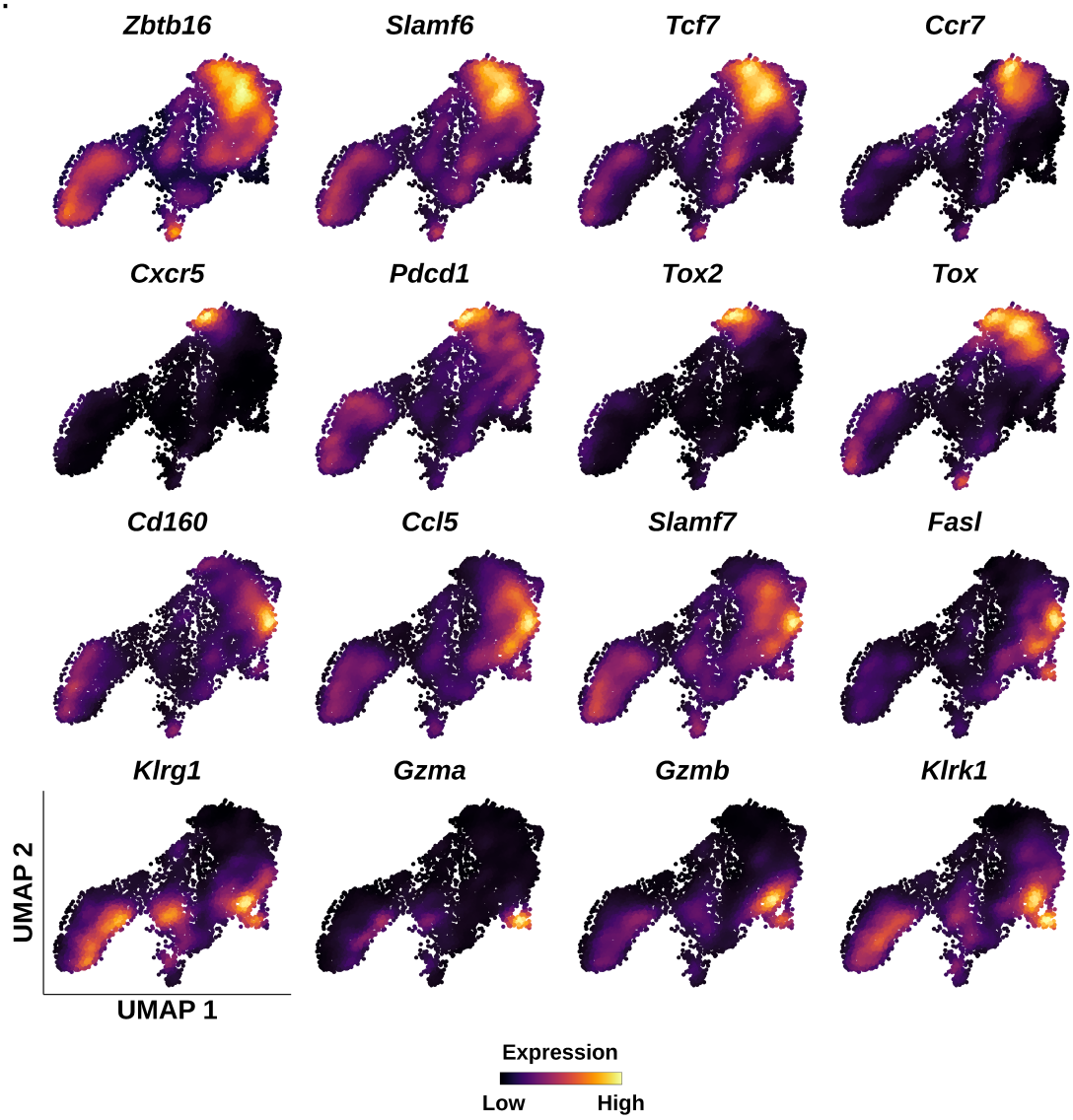


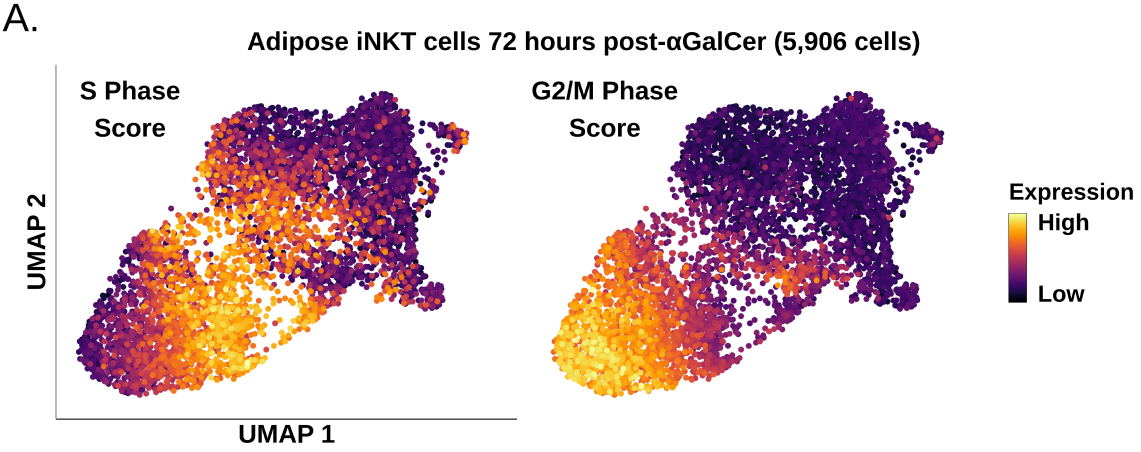

**Figure 4.2.2: Gene expression in splenic iNKT cells at 72 hours post-αGalCer.** A. Density plots of selected gene expression in splenic iNKT cells at 72 hours post-αGalCer.

### 4.3 Granular analysis of adipose iNKT cells at 72 hours post-αGalCer

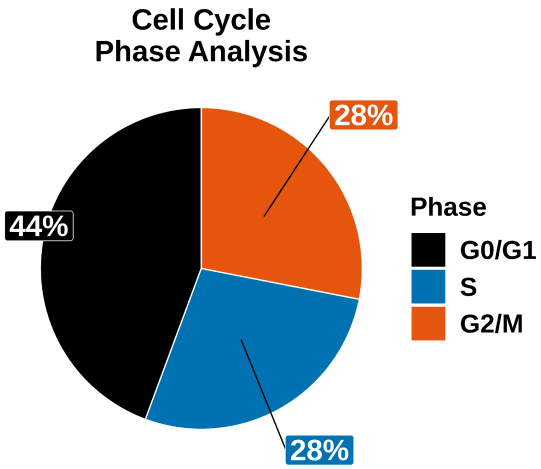
Having analyzed the phenotype of splenic iNKT cells at 72 hours post-αGalCer, we next performed analysis of adipose iNKT cells at 72 hours post-αGalCer. Quality control measures returned 5,096 cells, expressing a median of 16,204 UMIs and 3,677 genes per cell. Similar to splenic iNKT cells, we found that ~56% of 72 hour adipose iNKT cells expressed a transcriptional profile consistent with active proliferation (Figure 4.3.1.A, Figure 4.3.1.B). We also identified a distinct population of G0/G1 phase adipose iNKT cells that lacked expression of proliferation or cell cycle gene signatures and were transcriptionally distinct to cycling adipose iNKT cells (Figure 4.3.1.C), and adipose G0/G1 iNKT cells displayed enrichment of many of the same genes as splenic G0/G1 cells, including *Il7r*, *Ccl5*, *Cd27*, *Mxd4*, *Btg1*, *Ogt*, *Gzma*, *Maf*, and *Ypel3*, *Ifi27l2a*, *Zbtb16*, *Slamf6* and *Tcf7* (Figure 4.3.1.D). However, interestingly, we did not identify the same degree of $NKT_{FH}$ cell gene enrichment among adipose iNKT G0/G1 cells (Figure 4.2.1.D), and we instead identified increased expression of *Il4* and *Klrb1c* (Figure 4.3.1.D).

**Figure 4.3.1: Granular analysis of adipose iNKT cells at 72 hours post-αGalCer (overleaf).** A. Feature plots of S phase or G2/M phase gene module scoring in adipose iNKT cells at 72 hours post-αGalCer. B. Pie chart showing the percentage of the iNKT cells in Figure 4.3.1.A in G0/G1 phase, S phase, or G2/M phase of the cell cycle. C. UMAP of adipose iNKT cells at 72 hours post-αGalCer. D. Scaled average heatmap with hierarchical clustering of gene expression in the cell clusters from Figure 4.3.1.C.

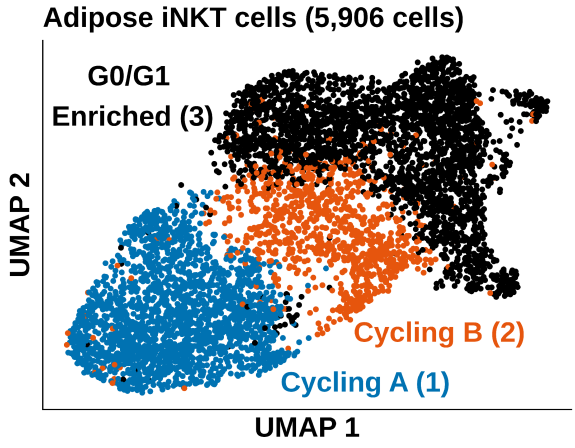
A.


Adipose iNKT cells 72 hours post-αGalCer (5,906 cells)
S Phase Score
G2/M Phase Score
Expression
High
Low
UMAP 2
UMAP 1

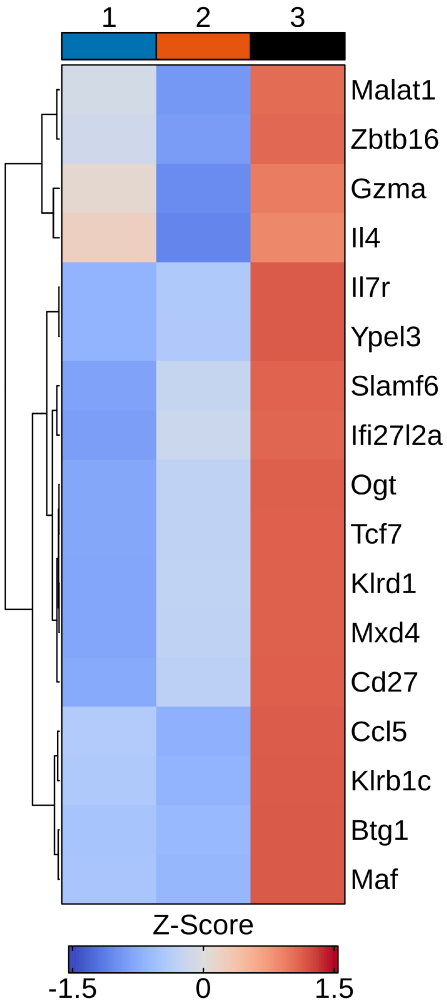
B.


Cell Cycle Phase Analysis
28%
44%
28%
Phase
G0/G1
S
G2/M

C.


Adipose iNKT cells (5,906 cells)
G0/G1 Enriched (3)
Cycling B (2)
Cycling A (1)
UMAP 2
UMAP 1

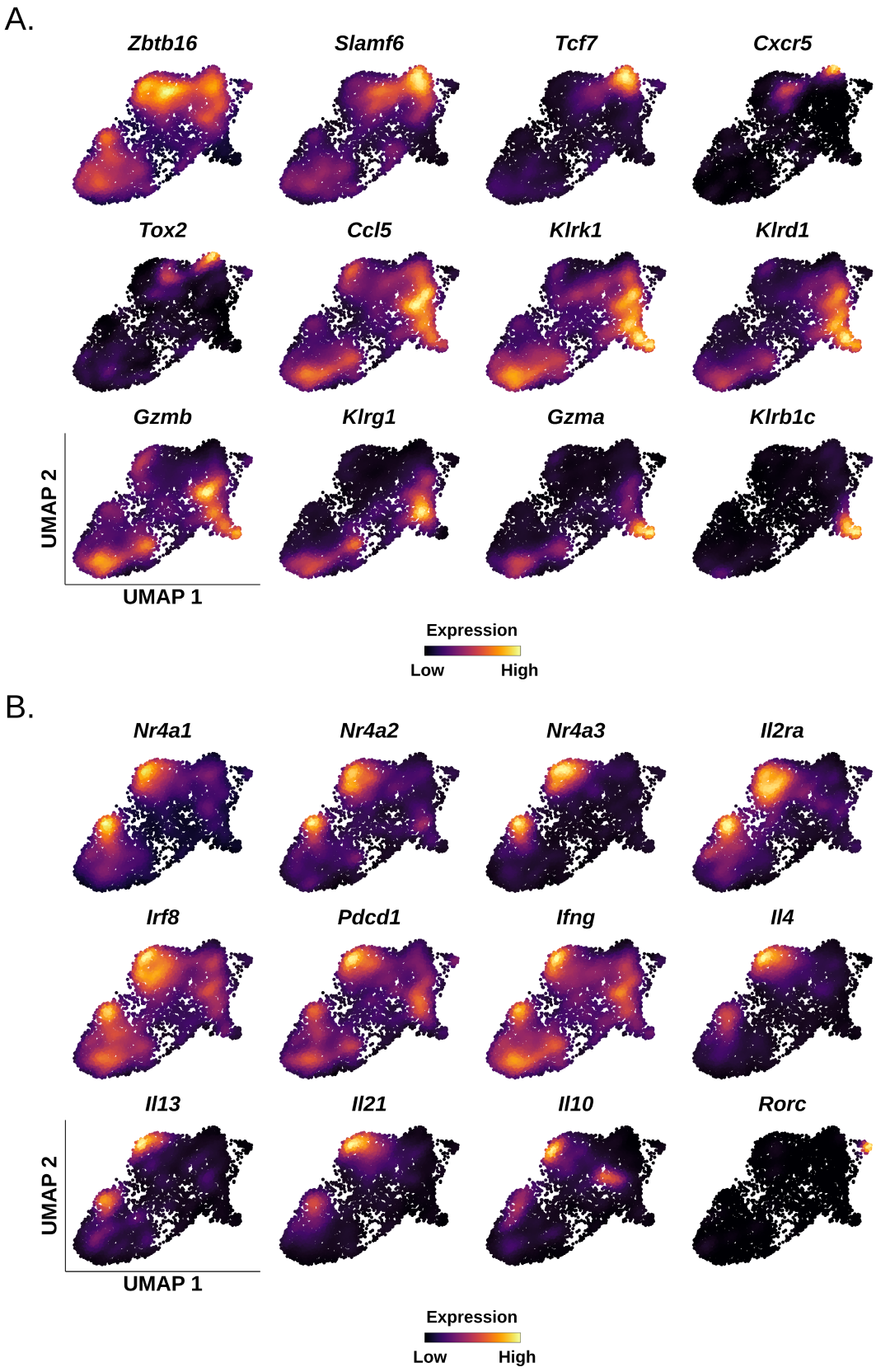
D.


1
2
3
Malat1
Zbtb16
Gzma
Il4
Il7r
Ypel3
Slamf6
Ifi27l2a
Ogt
Tcf7
Klrd1
Mxd4
Cd27
Ccl5
Klrb1c
Btg1
Maf
Z-Score
-1.5
0
1.5

We next performed density plot mapping to profile adipose iNKT cell heterogeneity at 72 hours post-αGalCer in greater detail. As with splenic iNKT cells, we found that adipose G0/G1 iNKT cells displayed enrichment of *Zbtb16* compared to cycling cells (Figure 4.3.2.A), and we identified a subpopulation of cells co-expressing *Slamf6* and *Tcf7*, suggestive of an NKT2-like or stem-like memory T cell phenotype. We also detected a minor subpopulation of $NKT_{FH}$ cells expressing *Cxcr5* and *Tox2* (Figure 4.3.2.A). Unlike splenic iNKT cells, however, some adipose iNKT cells co-expressed *Klrb1c*, *Gzma*, *Gzmb*, *Ccl5*, *Klrk1*, and *Klrd1*, while a separate subpopulation of cells co-expressed *Klrg1*, *Gzmb*, *Ccl5*, *Klrk1*, and *Klrd1* (Figure 4.3.2.A), reminiscent of the phenotype of adipose $NK1.1^+$ and $NK1.1^-$ iNKT cells at steady state (Figure 3.2). We also detected a subset of NKT17 cells expressing *Rorc*, although the frequency of adipose NKT17 cells was greatly reduced at 72 hours post-αGalCer compared to steady state or 4 hours post-αGalCer (Figure 4.3.2.A).

Intriguingly, we found that adipose iNKT cells, in complete contrast to their splenic counterparts, demonstrated evidence of activation and cytokine production at 72 hours post-αGalCer (Figure 4.3.2.B). We identified a subset of iNKT cells that displayed robust enrichment of acute activation markers such as *Nr4a1*, *Nr4a2*, *Nr4a3*, *Il2ra*, *Pdcd1*, and *Irf8*, and the cytokines *Ifng*, *Il4*, *Il13*, *Il21*, and *Il10* (Figure 4.3.2.B). Since this activation occurred in the absence of any additional exogenous stimulation with αGalCer, this finding could be interpreted as further evidence for our hypothesis of chronic endogenous activation among adipose iNKT cells. Alternatively, increased adipose iNKT cell activation at 72 hours post-αGalCer could be representative of a delayed activation phenotype among adipose iNKT cells. In either case, these data illustrate that the phenotype of adipose iNKT cells at 72 hours post-αGalCer is similar in many respects to the phenotype of splenic iNKT cells, but there are distinct differences, most notably that a subset of 72 hour adipose iNKT cells are activated, and display evidence of effector cytokine production.

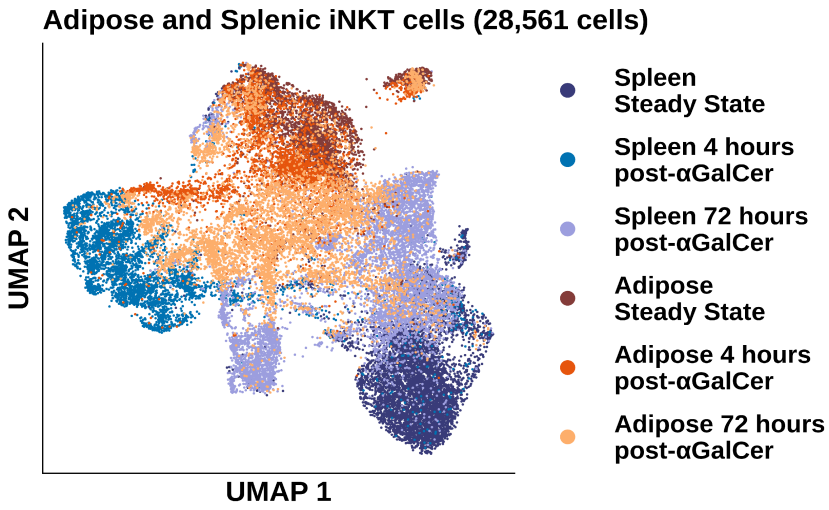
**Figure 4.3.2: Gene expression in adipose iNKT cells at 72 hours post-αGalCer (overleaf).** A and B. Density plots of selected gene expression in adipose iNKT cells at 72 hours post-αGalCer.


A.
Zbtb16
Slamf6
Tcf7
Cxcr5
Tox2
Ccl5
Klrk1
Klrd1
Gzmb
Klrg1
Gzma
Klrb1c
UMAP 2
UMAP 1
Expression
Low
High
B.
Nr4a1
Nr4a2
Nr4a3
Il2ra
Irf8
Pdcd1
Ifng
Il4
Il13
Il21
Il10
Rorc
UMAP 2
UMAP 1
Expression
Low
High

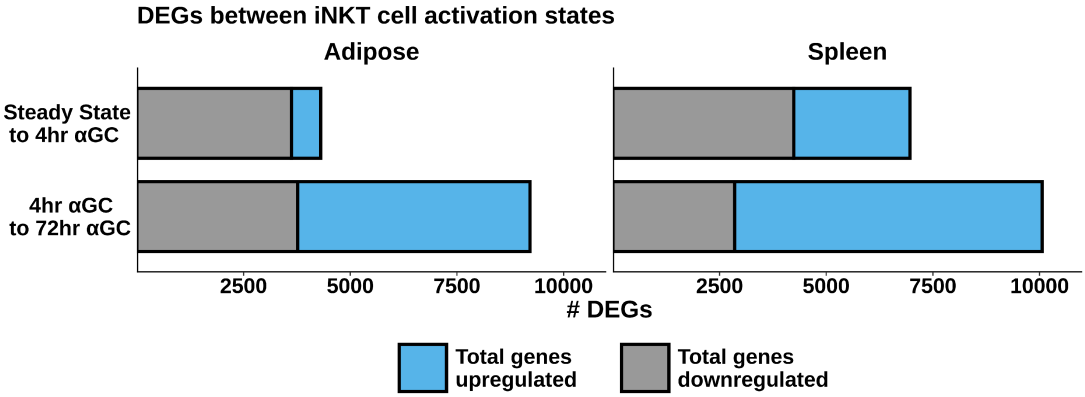
### 4.4 Comparative analysis of transcriptional remodeling among adipose and splenic iNKT cells at steady state, 4 hours post-αGalCer, 72 hours post-αGalCer

We next sought to compare overall transcriptional remodeling and activation among adipose and splenic iNKT cells. To do this, we performed comparative analysis of 28,561 adipose and splenic iNKT cells at steady state, 4 hours post-αGalCer, and 72 hours post-αGalCer. UMAP revealed minimal overlap between adipose and splenic iNKT cells (Figure 4.4.1.A), indicating that adipose and splenic iNKT cells remained transcriptionally distinct across diverse activation states. We also noted that different adipose iNKT cell activation states clustered together more closely than different splenic iNKT activation states (Figure 4.4.1.A), suggesting that activated adipose iNKT cells undergo less transcriptional remodeling than activated splenic iNKT cells, and that different adipose iNKT cell activation states are potentially more transcriptionally interrelated. To quantify these observations, we performed gene expression analysis to determine the total number of DEGs between different adipose and splenic activation states and used these DEGs as a readout of transcriptional remodeling. We found that adipose iNKT cells constitutively displayed reduced transcriptional remodeling compared to splenic iNKT cells (Figure 4.4.1.B), although the difference between adipose and splenic iNKT cells was much more pronounced during the initial burst of transcriptional remodeling from 0-4 hours post-αGalCer versus downstream iNKT cell activation from 4-72 hours post-αGalCer.

A.


Adipose and Splenic iNKT cells (28,561 cells)
UMAP 2
UMAP 1
Spleen Steady State
Spleen 4 hours post-αGalCer
Spleen 72 hours post-αGalCer
Adipose Steady State
Adipose 4 hours post-αGalCer
Adipose 72 hours post-αGalCer

B.


DEGs between iNKT cell activation states
Adipose
Spleen
Steady State to 4hr αGC
4hr αGC to 72hr αGC
2500
5000
7500
10000
# DEGs
Total genes upregulated
Total genes downregulated

C.

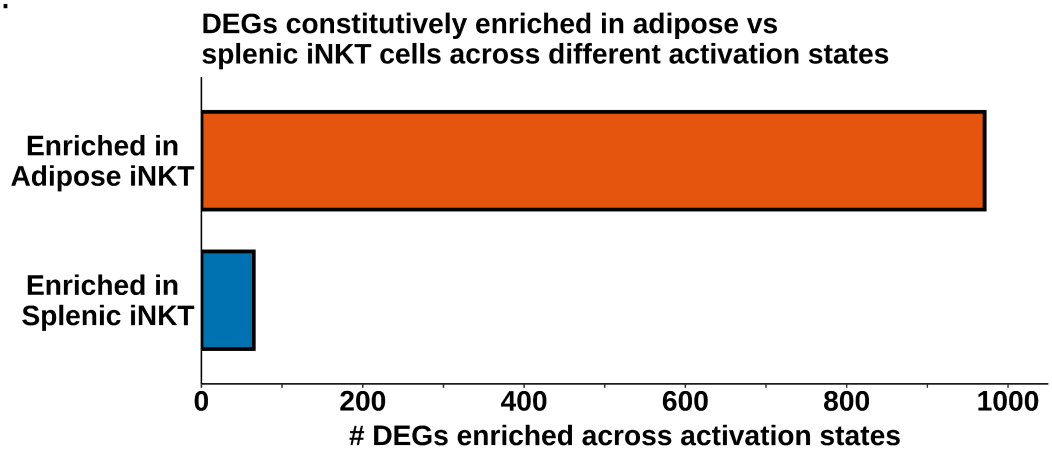

DEGs constitutively enriched in adipose vs splenic iNKT cells across different activation states
Enriched in Adipose iNKT
Enriched in Splenic iNKT
0
200
400
600
800
1000
# DEGs enriched across activation states

**Figure 4.4.1: Transcriptional remodeling among adipose and splenic iNKT cells activation states (previous page).** A. UMAP of adipose and splenic iNKT cells at steady state, 4 hours post-αGalCer, and 72 hours post-αGalCer. B. Bar plots showing the total number of DEGs identified after gene expression analysis of adipose and splenic iNKT cells at 4 hours post-αGalCer versus steady state (top bar), and 72 hours post-αGalCer versus 4 hours post-αGalCer (bottom bar). The breakdown of DEGs in each comparison is also shown. C. Bar plot showing the number of genes constitutively enriched in adipose (orange) or splenic (blue) iNKT cells at steady state, 4 hours post-αGalCer, and 72 hours post-αGalCer.

Since our UMAP had demonstrated that adipose and splenic iNKT cells remained transcriptionally distinct across different activation states, we next sought to identify enrichment of conserved genes that might differentiate adipose versus splenic iNKT cells, regardless of activation status. To do this, we individually compared adipose and splenic iNKT cells at steady state, 4 hours post-αGalCer, and 72 hours post-αGalCer, and then performed overlap analysis of DEGs identified during these comparisons. We identified 971 conserved genes among adipose iNKT cells, versus only 65 conserved genes among splenic iNKT cells (Figure 4.4.1.C). This suggests that transcriptional remodeling is reduced among activated adipose iNKT cells versus activated splenic iNKT cells, as adipose but not splenic iNKT cells retain expression of many conserved genes during activation. We next performed over-representation analysis of these conserved genes against the KEGG pathway database. We identified KEGG Ribosome as the sole enriched pathway among splenic iNKT cells, whereas adipose iNKT cells displayed enrichment of genes relating to uptake of material from the extracellular environment (Endocytosis, Regulation of actin cytoskeleton, FcγR-mediated phagocytosis), adhesion (Focal adhesion, Leukocyte transendothelial migration), cytotoxicity and cell death (NK cell mediated cytotoxicity, Apoptosis), cellular senescence, chemokine signaling, and TCR signaling (Figure 4.4.2.A).

A.

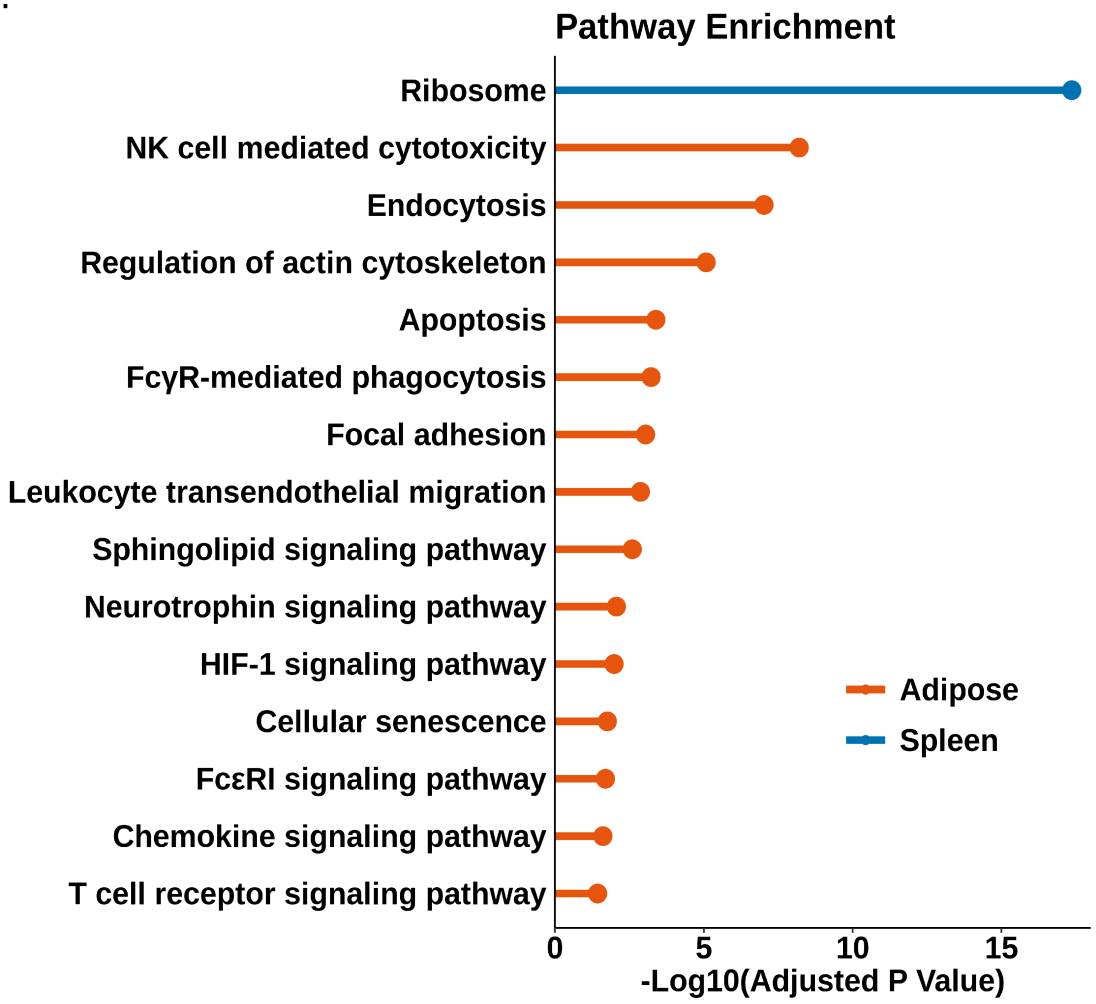



**Figure 4.4.2: Over-representation analysis of genes constitutively enriched in adipose or splenic iNKT cells.** A. Lollipop plot showing results from over-representation analysis against the KEGG pathway database of genes constitutively enriched in adipose or splenic iNKT cells.

We next compared gene expression between individual adipose and splenic iNKT cell activation states. The most prominent transcriptional difference between adipose and splenic iNKT cells at 4 hours post-αGalCer was the reduced expression of activation marker genes and cytokine transcripts among adipose iNKT cells (Figure 4.4.3.A), while adipose iNKT cells showed enrichment of activation and cytokine genes at 72 hours post-αGalCer (Figure 4.3.2.B, Figure 4.4.3.B). However, we noted that the magnitude of activation marker and cytokine gene enrichment among adipose iNKT cells at 72 hours post-αGalCer was much lower than at 4 hours post-αGalCer in the spleen (Figure 4.4.3.A). We found that adipose iNKT cells displayed reduced expression of genes associated with NKT2 and stem-like T cells, including *Tcf7*, *Slamf6*, and *Ccr7* (Figure 4.4.3.A). Adipose iNKT cells also demonstrated reduced expression of markers associated with $NKT_{FH}$ and $T_{FH}$ cells, such as *Cxcr5* and *Tox2*, and were less enriched for some promigratory genes in the KLF2 regulon, including *Klf2* and *S1pr1*, although interestingly we found that adipose iNKT cells constitutively expressed several other KLF2-associated transcripts, such as *S100a6* and *S100a4* (Figure 4.4.3.A).

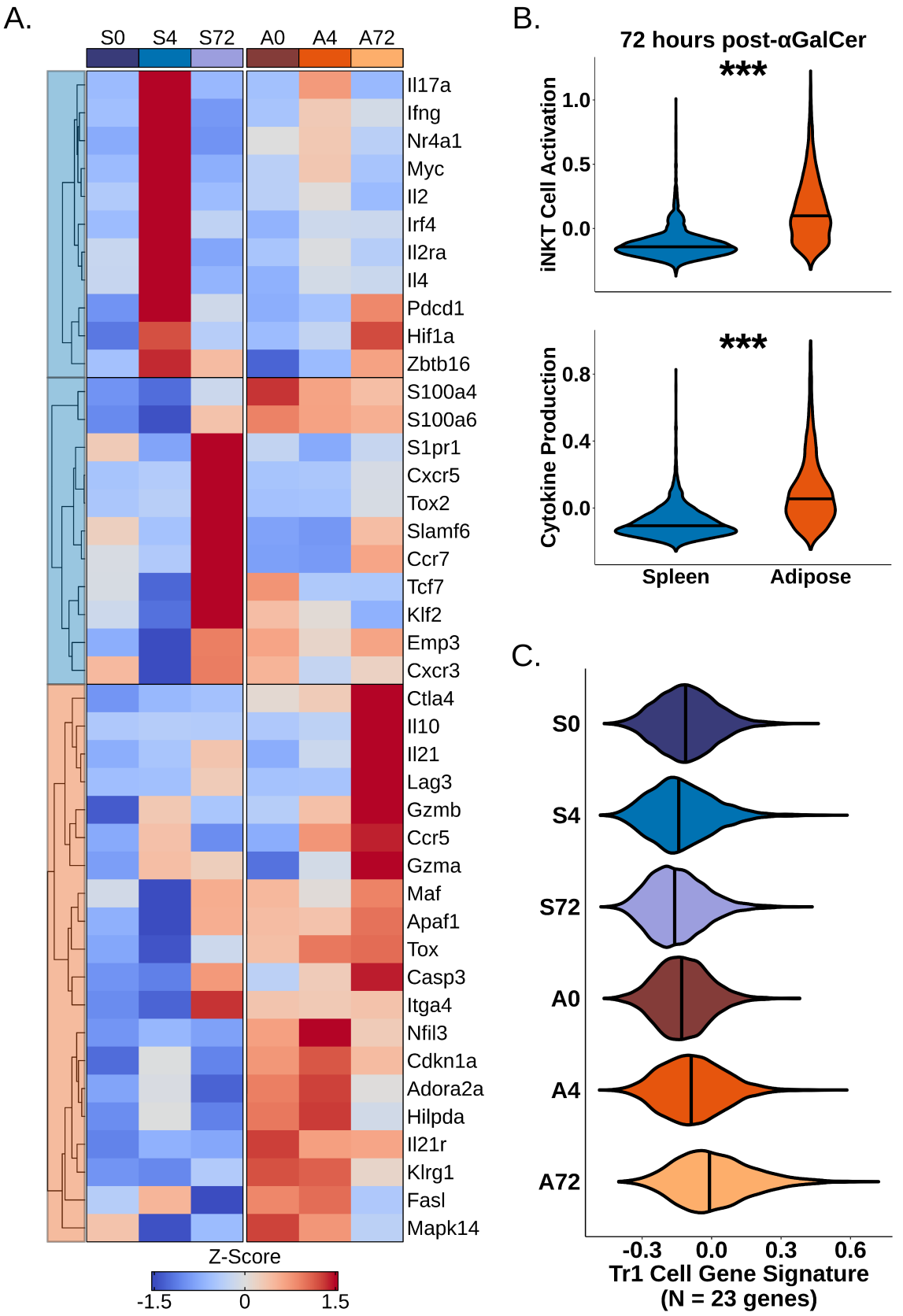
Notably, our analysis revealed that activated adipose iNKT cells displayed enrichment of immunoregulatory markers such as *Il10*, *Ctla4*, *Pdcd1*, and *Lag3* (Figure 4.4.3.A), consistent with multiple previous studies identifying adipose iNKT cells as a regulatory population[49,90,91,115]. Interestingly, we found that *Il10* expression was higher among adipose cells at 72 hours post-αGalCer than at 4 hours post-αGalCer, indicating that the peak of the regulatory response among adipose iNKT cells is delayed compared to the rapid cytokine burst produced by splenic iNKT cells (Figure 4.4.3.A). Other genes enriched among adipose cells at 72 hours post-αGalCer included *Il21*, *Hif1a*, *Ccr5*, *Maf*, *Gzmb*, and *Gzma* (Figure 4.4.3.A). Notably, all of these genes have previously been linked to T regulatory type 1 (Tr1) cells, which are a heterogeneous subset of cytotoxic adaptive T cells that lack expression of FOXP3 but function like Tregs[358–365]. As adipose iNKT cells are known to express E4BP4, and not

FOXP3[49], our data suggest that regulatory adipose iNKT cells could be similar to Tr1 cells. Moreover, when we performed module scoring of splenic and adipose iNKT cells with a larger complement of n = 23 Tr1 cell marker genes, we found that adipose iNKT cells at 72 hours post-αGalCer demonstrated significant enrichment of Tr1 cell genes (Figure 4.4.3.C), suggestive of a Tr1 cell-like phenotype among activated adipose iNKT cells. Other notable genes enriched among adipose iNKT cells included *Il21r*, *Itga4*, *Tox*, *Casp3*, *Apaf1*, the adenosine receptor *Adora2a*, and *Cdkn1a* (Figure 4.4.3.A).

We next performed module scoring of adipose and splenic iNKT cells. While adipose iNKT cells displayed blunted activation, cytokine production, and metabolic remodeling compared to splenic iNKT cells at 4 hours post-αGalCer, we did not identify any significant differences in expression of proliferation and cell cycle gene signatures at 72 hours post-αGalCer (Figure 4.4.4.A). This suggests that the reduced effector response of adipose iNKT cells during early activation does not translate to significant differences in downstream proliferation and expansion. Metabolically, we found that adipose iNKT cells displayed enrichment of genes associated with glycolysis, amino acid metabolism, and polyamine synthesis compared to splenic iNKT cells at 72 hours post-αGalCer (Figure 4.4.4.A), correlating with the enhanced expression of effector gene signatures by adipose iNKT cells at 72 hours post-αGalCer. Like splenic iNKT cells, adipose iNKT cells upregulated expression of gene signatures associated with oxidative metabolism and β-oxidation of lipids at 72 hours post-αGalCer (Figure 4.4.4.A), suggesting that oxidative metabolism is correlated with iNKT cell proliferation. Adipose iNKT cells showed increased expression of genes associated with lipid metabolism across different activation states (Figure 4.4.4.A), which may be reflective of the lipid rich environment that they inhabit. Overall, our module scoring indicates that splenic and adipose iNKT cells generally follow a similar pattern of metabolic gene remodeling during activation but reprogramming of metabolic gene

expression is more limited among adipose iNKT cells compared to splenic iNKT cells.

**Figure 4.4.3: Comparison of gene expression profiles in adipose and splenic iNKT cells at steady state, 4 hours post-αGalCer, and 72 hours post-αGalCer (overleaf).** A. Scaled average heatmap with hierarchical clustering of gene expression in splenic and adipose iNKT cells at steady state (S0 and A0 respectively), 4 hours post-αGalCer (S4 and A4 respectively), and 72 hours post-αGalCer (S72 and A72 respectively), drawn from the data in Figure 4.4.1.A. B. Violin plots showing expression of iNKT cell activation and cytokine production gene module scores in splenic and adipose iNKT cells at 72 hours post-αGalCer. Module scores were calculated using the data shown in Figure 4.4.1.A. C. Violin plots showing expression of a module score for Tr1 cell genes in adipose and splenic iNKT cell activation states. Module scores were calculated using the data shown in Figure 4.4.1.A.


A.
S0
S4
S72
A0
A4
A72
Il17a
Ifng
Nr4a1
Myc
Il2
Irf4
Il2ra
Il4
Pdcd1
Hif1a
Zbtb16
S100a4
S100a6
S1pr1
Cxcr5
Tox2
Slamf6
Ccr7
Tcf7
Klf2
Emp3
Cxcr3
Ctla4
Il10
Il21
Lag3
Gzmb
Ccr5
Gzma
Maf
Apaf1
Tox
Casp3
Itga4
Nfil3
Cdkn1a
Adora2a
Hilpda
Il21r
Klrg1
Fasl
Mapk14
Z-Score
-1.5
0
1.5
B.
72 hours post-αGalCer
***
iNKT Cell Activation
1.0
0.5
0.0
***
Cytokine Production
0.8
0.4
0.0
Spleen
Adipose
C.
S0
S4
S72
A0
A4
A72
-0.3
0.0
0.3
0.6
Tr1 Cell Gene Signature
(N = 23 genes)

A.

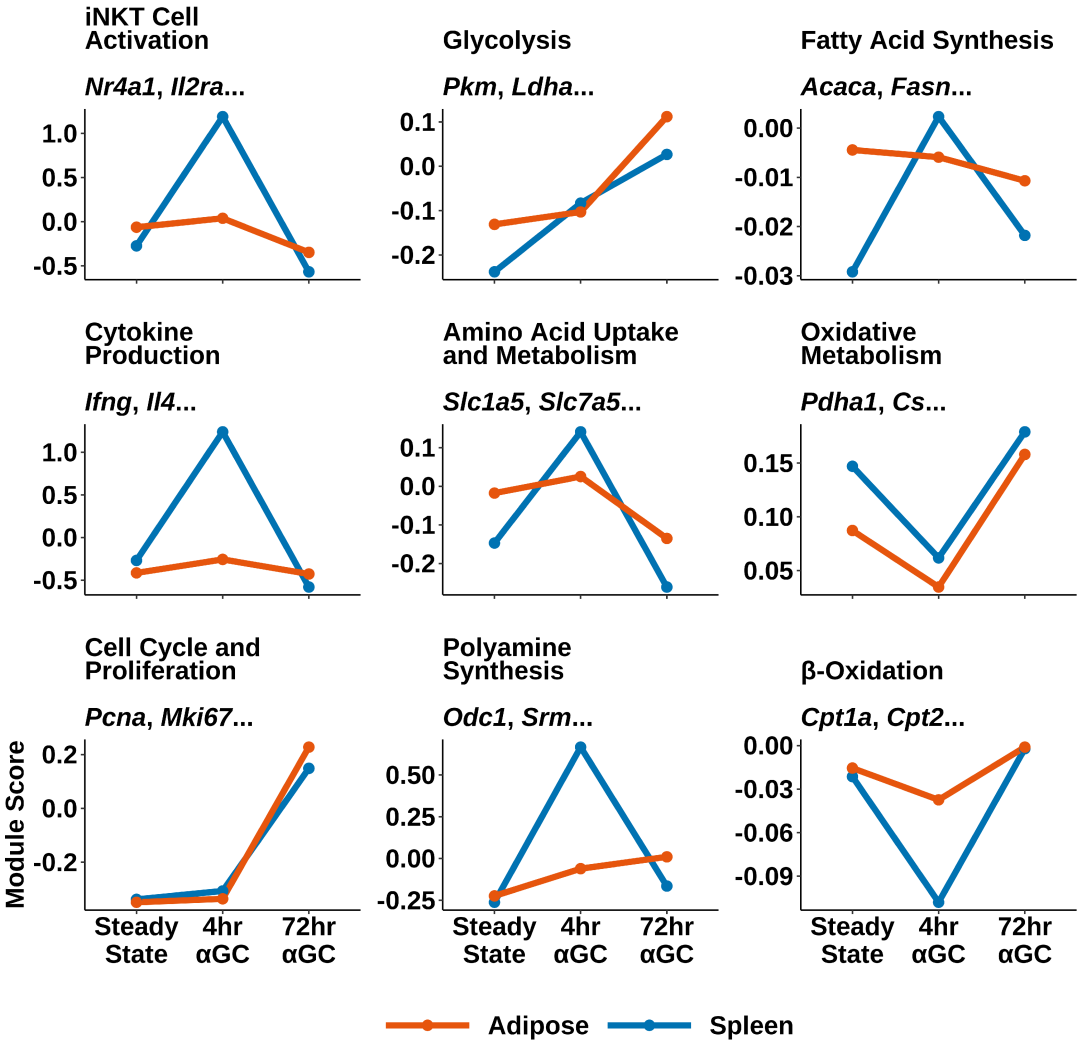



**Figure 4.4.4: Phenotypic and metabolic module scoring of adipose and splenic iNKT cell activation states.** Line plots showing median expression of phenotypic and metabolic gene module scores in adipose (orange) and splenic (blue) iNKT cells at steady state, 4 hours post-αGalCer (4hr αGC), and 72 hours post-αGalCer (72hr αGC). Module scores were calculated using the data shown in Figure 4.4.1.A.

### 4.5 Bulk transcriptional analysis of memory-like iNKT cells at 6 days post-αGalCer

Having profiled the emergence of memory-like $NKT_{FH}$ cells and $KLRG1^+$ iNKT cells at 72 hours post-αGalCer, we next sought to analyze the phenotype of memory-like iNKT cells in more detail. To do this, we reanalyzed bulk RNA-Seq data comparing memory-like $NKT_{FH}$ and non-$NKT_{FH}$ cells at 6 days post-αGalCer versus total steady state iNKT cells, which was previously published by Murray *et al.* (2021; GSE157225)[92]. PCA showed distinct separation of steady state, $NKT_{FH}$, and non-$NKT_{FH}$ cell samples (Figure 4.5.A), with $NKT_{FH}$ and non-$NKT_{FH}$ cells displaying transcriptional divergence along PC 1, and memory-like or “trained” iNKT cell populations clustering versus steady state iNKT cells along PC 2. We next performed gene expression analysis to compare total memory-like iNKT cells ($NKT_{FH}$ and non-$NKT_{FH}$ cells) versus steady state iNKT cells. GSEA revealed enrichment of genes associated with proliferation and the cell cycle, including *Bub1*, *Cdk1*, *Mcm7*, and *Ccnb1*, and adhesion, such as *Cd86*, *Ctla4*, *Itga4*, and *Pdcd1* (Figure 4.5.B). By contrast, steady state iNKT cells displayed enrichment of ribosomal genes, including *Rpl7a*, *Rps15a*, and *Rplp1*, and genes associated with circadian rhythm, such as *Bhlhe40*, *Arntl*, *Cry1*, and *Nr1d1* (Figure 4.5.B). Notably, the enrichment of proliferation and cell cycle genes among day 6 iNKT cells suggests that many of these iNKT cells are still proliferating, similar to iNKT cells at 72 hours post-αGalCer (Figures 4.1 – 4.4). On the other hand, work by Wu *et al.* (2019) has linked reduced expression of circadian clock genes with increased T cell anergy and exhaustion[366], as well as increased expression of immunoregulatory receptors such as PD-1 and CTLA-4, which correlates with the anergic phenotype that has previously been reported for antigen experienced iNKT cells[16,91,195,208].

We next performed individual analysis of gene expression among steady state, $NKT_{FH}$, and non-$NKT_{FH}$ cells. We found that steady state iNKT cells showed enrichment of genes associated with NKT1 and NKT17 cells, including *Cxcr3*,

*Klrb1c*, *Il2rb, Il7r*, *Il1r1*, and *Nr1d1* (Figure 4.5.C), similar to our previous analysis of iNKT cells at steady state versus 72 hours post-αGalCer (Figure 4.1). Notably, Murray *et al.* (2021) also reported that NKT1, NKT2, and NKT17 cells were undetectable at 6 days post-αGalCer[92], suggesting that memory-like populations predominate the iNKT cell repertoire during downstream activation. Other genes expressed by steady state iNKT cells included the chemokine receptor *Ccr9*, while $NKT_{FH}$ and non-$NKT_{FH}$ cells expressed *Itga4* and *Itgb1* (Figure 4.5.C), suggesting that these integrin subunit genes are markers of memory-like iNKT cells. $NKT_{FH}$ cells lacked expression of *Klrb1c* and demonstrated enrichment of known $T_{FH}$ cell markers such as *Cxcr5*, *Pdcd1*, *Il21*, *Maf*, *Tox*, *Tox2*, *Cd4*, and *Bcl6*[268,367,368], as well as *Ly6a*, the Treg marker *Folr4* (also known as *Izumo1r*), the NKT2 cell marker *Id3*, *Hif1a*, *Lag3*, and the stem-like markers *Slamf6* and *Tcf7* (Figure 4.5.C). Collectively, this analysis suggests that $NKT_{FH}$ cells are transcriptionally similar to NKT2 cells, which was also shown by Murray *et al.* (2021)[92]. Interestingly, we also noted that the gene expression profile of $NKT_{FH}$ cells was similar to adipose $NK1.1^-$ NKT1 cells at steady state (Figure 3.2.1, 3.2.2).

By contrast, non-$NKT_{FH}$ cells showed increased expression of many genes previously associated with $KLRG1^+$ iNKT cells, including *Klrg1*, *Klrk1*, *Il2rb*, *Klrb1c*, and *Gzma*[206], and the $NKT_{eff}$ markers identified by Murray *et al.* (2021), *Cx3cr1* and *Spry2*[92] (Figure 4.5.C). Other enriched genes included the transcription factor *Zeb2*, and the surface receptor *S1pr5*, which are typically associated with terminally differentiated $T_{EM}$ and $T_{CM}$ $CD8^+$ T cells[349,369], *Gmzb*, *Klrd1*, *Klre1*, *Ncr1*, *Cd244*, and the KLF2 regulon members *Klf2*, *S100a6*, and *Emp3* (Figure 4.5.C). Notably, we observed that the gene expression profile of non-$NKT_{FH}$ cells was similar to that of adipose $NK1.1^+$ NKT1 cells at steady state (Figure 3.2.1, Figure 4.5.C). Overall, our reanalysis of these data demonstrate that the non-$NKT_{FH}$ or $NKT_{eff}$ cell population identified by Murray *et al*. (2021) is highly enriched for markers of memory-like $KLRG1^+$ iNKT cells[92,206].

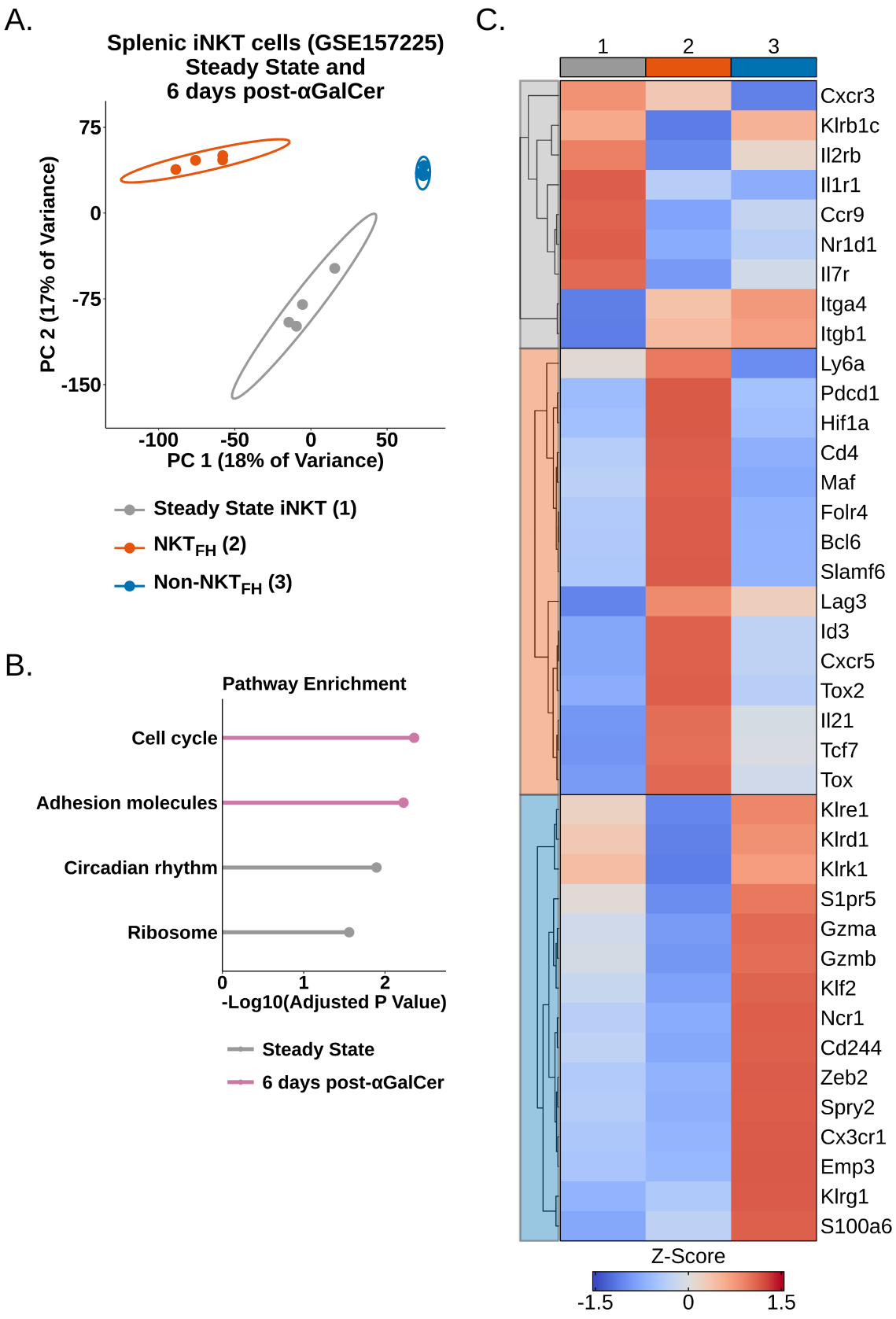

A.
Splenic iNKT cells (GSE157225)
Steady State and
6 days post-αGalCer
PC 2 (17% of Variance)
75
0
-75
-150
-100
-50
0
50
PC 1 (18% of Variance)
Steady State iNKT (1)
NKTFH (2)
Non-NKTFH (3)
B.
Pathway Enrichment
Cell cycle
Adhesion molecules
Circadian rhythm
Ribosome
0
1
2
-Log10(Adjusted P Value)
Steady State
6 days post-αGalCer
C.
1
2
3
Cxcr3
Klrb1c
Il2rb
Il1r1
Ccr9
Nr1d1
Il7r
Itga4
Itgb1
Ly6a
Pdcd1
Hif1a
Cd4
Maf
Folr4
Bcl6
Slamf6
Lag3
Id3
Cxcr5
Tox2
Il21
Tcf7
Tox
Klre1
Klrd1
Klrk1
S1pr5
Gzma
Gzmb
Klf2
Ncr1
Cd244
Zeb2
Spry2
Cx3cr1
Emp3
Klrg1
S100a6
Z-Score
-1.5
0
1.5

**Figure 4.5: Bulk transcriptional analysis of memory-like iNKT cells at 6 days post-αGalCer (previous page).** A. PCA plot of total steady state splenic iNKT cells (no αGalCer), and splenic $NKT_{FH}$ and non-$NKT_{FH}$ iNKT cells at 6 days post-αGalCer (reanalyzed from GSE157225). B. Lollipop plot showing results from GSEA of 6 day post-αGalCer versus steady state splenic iNKT cells, performed against the KEGG pathway database. Pathways enriched in 6 day post-αGalCer iNKT cells are shown in purple, and pathways enriched in steady state iNKT cells are shown in gray. C. Scaled average heatmap with hierarchical clustering of gene expression in the data from Figure 4.5.A.

## 4.6 Prior activation with αGalCer induces long term transcriptional remodeling and an adipose-like activation scheme among splenic iNKT cells

Having profiled the phenotype of memory-like iNKT cells at 6 days post-αGalCer, we next analyzed the phenotype of memory-like iNKT cells at 4 weeks post-αGalCer, when the effector response to αGalCer has subsided[91,198,200,208]. This time point is also significant because it has been reported that splenic iNKT cells display an anergic or hyporesponsive phenotype at ~4 weeks post-αGalCer[91,208], and secondary activation of splenic αGalCer-pretreated (αGCPT) iNKT cells is characterized by significantly increased production of IL-10 compared to primary splenic iNKT cell activation[91,195,208]. Therefore, the analysis of antigen experienced splenic iNKT cells at 4 weeks post-αGalCer presented an opportunity to characterize long term transcriptional remodeling among splenic iNKT cells, and to gain insight into the phenotype of anergic and/or regulatory iNKT cells.

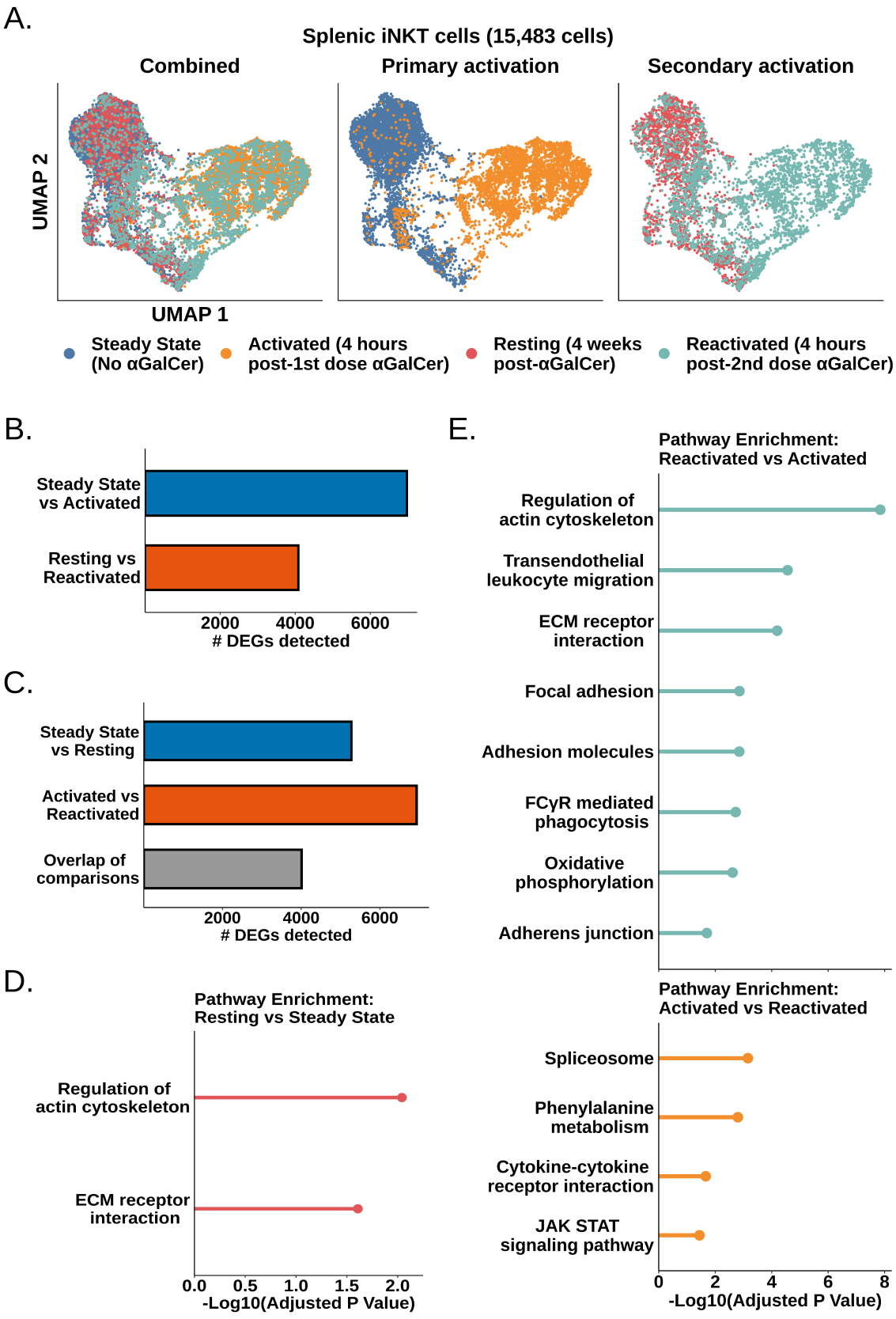
We began our analysis of αGCPT iNKT cells by comparing steady state splenic iNKT cells (no αGalCer) and activated splenic iNKT cells at 4 hours post-αGalCer (1 dose of αGalCer) against resting splenic iNKT cells at 4 weeks post-αGalCer (1 dose of αGalCer) and reactivated splenic iNKT cells at

4 hours post-αGalCer (2 doses of αGalCer; Figure 4.6.1.A). Quality control measures returned 2,117 resting iNKT cells, expressing a median of 5,385 UMIs and 2,016 genes per cell, and 3,316 reactivated iNKT cells expressing a median of 7,248 UMIs and 2,134 genes per cell. UMAP revealed that steady state iNKT cells largely overlapped with resting iNKT cells and activated iNKT cells largely overlapped with reactivated iNKT cells (Figure 4.6.1.A), suggesting that the transcriptional profile of steady state and activated splenic iNKT cells is similar to that of resting and reactivated splenic iNKT cells. However, more detailed inspection of our UMAP revealed greater overlap between resting and reactivated iNKT cells compared to steady state and activated iNKT cells (Figure 4.6.1.A), suggesting that the magnitude of transcriptional remodeling might be reduced during secondary iNKT cell activation. To quantify this, we performed comparative gene expression analysis of primary versus secondary iNKT cell activation. As suggested by our UMAP, we identified fewer DEGs during our comparison of resting versus reactivated iNKT cells than when we compared steady state versus activated iNKT cells (Figure 4.6.1.B), indicating that secondary activation of “trained” iNKT cells with αGalCer induces a more muted transcriptional response than primary activation of steady state iNKT cells with αGalCer.

We next performed individual comparisons of steady state versus resting cells and activated versus reactivated cells. We identified >4000 DEGs in both comparisons (Figure 4.6.1.C), indicating that resting and reactivated cells are transcriptionally distinct to steady state and activated cells. Notably, we found that a majority of the DEGs identified across both comparisons overlapped (Figure 4.6.1.C), identifying a core group of conserved genes constitutively differentially expressed between αGCPT iNKT cells and steady state and primary activated iNKT cells. To further characterize the transcriptional differences between steady and activated versus resting and reactivated iNKT cells, we performed GSEA. We identified enrichment of gene signatures associated with the actin cytoskeleton and interaction with the extracellular

matrix among resting versus steady state iNKT cells, including leading edge genes such as *Itga4*, *Itgb1*, *Itga1*, *Pfn1*, and *Actb* (Figure 4.6.1.D). Comparison of reactivated versus activated iNKT cells yielded similar enrichment of genes associated with adhesion and the cytoskeleton, and genes associated with oxidative phosphorylation (Figure 4.6.1.E). Notably, we found reactivated iNKT cells showed reduced expression of genes associated with immune cell activation, amino acid metabolism, and cytokine production, suggesting that reactivated iNKT cells might display a blunted response to secondary stimulation with αGalCer. We also noted that resting and reactivated iNKT cells displayed increased expression of the integrins *Itga4* and *Itgb1*, which were significantly enriched among memory-like $NKT_{FH}$ and non-$NKT_{FH}$ cells (Figure 4.5). This suggested that resting and reactivated iNKT cells might be enriched for memory-like iNKT cell populations.

**Figure 4.6.1: Prior activation with αGalCer induces long term transcriptional remodeling and an adipose-like activation scheme among splenic iNKT cells (overleaf).** A. UMAP of splenic iNKT cells. B. Bar plot showing the total number of DEGs detected after gene expression analysis comparing steady state versus activated and resting versus reactivated iNKT cells. C. Bar plot showing the total number of DEGs detected after gene expression analysis comparing steady state versus resting (blue) and activated versus reactivated (orange) iNKT cells. A third bar (gray) denotes the total number of DEGs which shared between the two previous comparisons (i.e. DEGs which are always enriched in steady state and activated versus resting and reactivated iNKT cells). D. Lollipop plot showing results from GSEA of resting versus steady state iNKT cells, performed against the KEGG pathway database. E. Lollipop plots showing results from GSEA of reactivated versus activated iNKT cells, performed against the KEGG pathway database.


A.
Splenic iNKT cells (15,483 cells)
Combined
Primary activation
Secondary activation
UMAP 2
UMAP 1
Steady State (No αGalCer)
Activated (4 hours post-1st dose αGalCer)
Resting (4 weeks post-αGalCer)
Reactivated (4 hours post-2nd dose αGalCer)
B.
Steady State vs Activated
Resting vs Reactivated
2000
4000
6000
# DEGs detected
C.
Steady State vs Resting
Activated vs Reactivated
Overlap of comparisons
2000
4000
6000
# DEGs detected
D.
Pathway Enrichment: Resting vs Steady State
Regulation of actin cytoskeleton
ECM receptor interaction
0.0
0.5
1.0
1.5
2.0
-Log10(Adjusted P Value)
E.
Pathway Enrichment: Reactivated vs Activated
Regulation of actin cytoskeleton
Transendothelial leukocyte migration
ECM receptor interaction
Focal adhesion
Adhesion molecules
FCγR mediated phagocytosis
Oxidative phosphorylation
Adherens junction
Pathway Enrichment: Activated vs Reactivated
Spliceosome
Phenylalanine metabolism
Cytokine-cytokine receptor interaction
JAK STAT signaling pathway
0
2
4
6
8
-Log10(Adjusted P Value)

Having identified transcriptional differences between antigen experienced versus steady state and acutely activated iNKT cells, we next decided to characterize these differences in more detail. We first performed module scoring to provide an overview of primary versus secondary iNKT cell activation. Resting iNKT cells displayed a blunted response to restimulation with αGalCer (Figure 4.6.2.A), including reduced expression of activation markers and cytokines, and reduced metabolic remodeling, similar to adipose iNKT cells (Figure 3.10). On a granular level, reactivated iNKT cells showed reduced expression of the metabolic activation markers *Rheb* and *Tfrc*, and cytokines such as *Ifng*, *Il4*, and *Ccl4*, but displayed enrichment of *Il10*, *Il21*, *Gzmb*, and *Gzma* (Figure 4.6.2.B). Resting and reactivated iNKT cells also demonstrated enrichment of the Tr1 cell markers *Ccr5*, *Lag3*, and *Ctla4*, the memory-like markers *Itga4* and *Itgb1*, the KLRG1$^{+}$ and NKT$_{eff}$ cell markers *Klrg1*, *Cd244*, *Spry2*, *Cx3cr1*, *Ncr1*, *Emp3*, *S100a6*, *S1pr1*, and *S1pr5*, and the NKT$_{FH}$ cell markers *Izumo1r*, *Ly6a*, and *Slamf6* (Figure 4.6.2.B), while steady state iNKT cells expressed *Klrb1c*, *Il2rb*, *Il7r*, and *Ccr9* (Figure 4.5). Analysis of transcription factor enrichment in resting and reactivated iNKT cells revealed increased expression of *Klf2* and *Zeb2*, suggestive of KLRG1$^{+}$ cell enrichment, as well as *Maf*, *Ets1*, *Nfatc3*, *Id3*, and *Jund* (Figure 4.6.2.C), whereas expression of *Bzw2*, *Naca*, *Jun*, and *Junb* was associated with steady state iNKT cells. Surprisingly, we did not identify increased expression of key T$_{FH}$ and NKT$_{FH}$ cell transcription factors such as *Bcl6* or *Tox2* among resting or reactivated iNKT cells. We also did not identify enrichment of chronic activation markers such as *Nr4a1* and *Nr4a2*, suggesting that αGCPT splenic iNKT cells do not experience the same chronic endogenous activation as adipose iNKT cells. Overall, our data suggest that αGCPT splenic iNKT cells show a blunted response to secondary αGalCer stimulation, analogous to primary activation of adipose iNKT cells, and display enrichment of markers associated with memory-like iNKT cells.

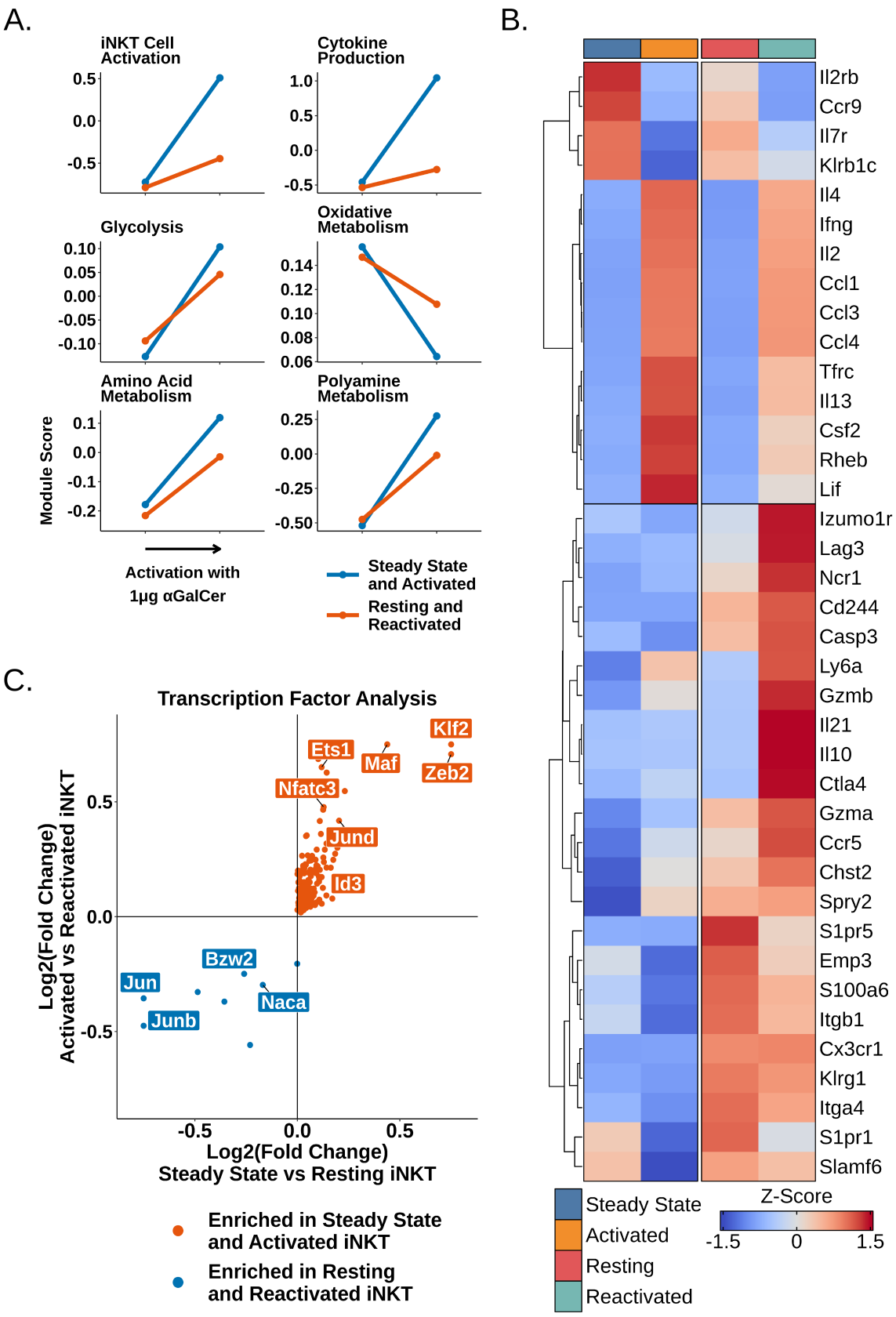
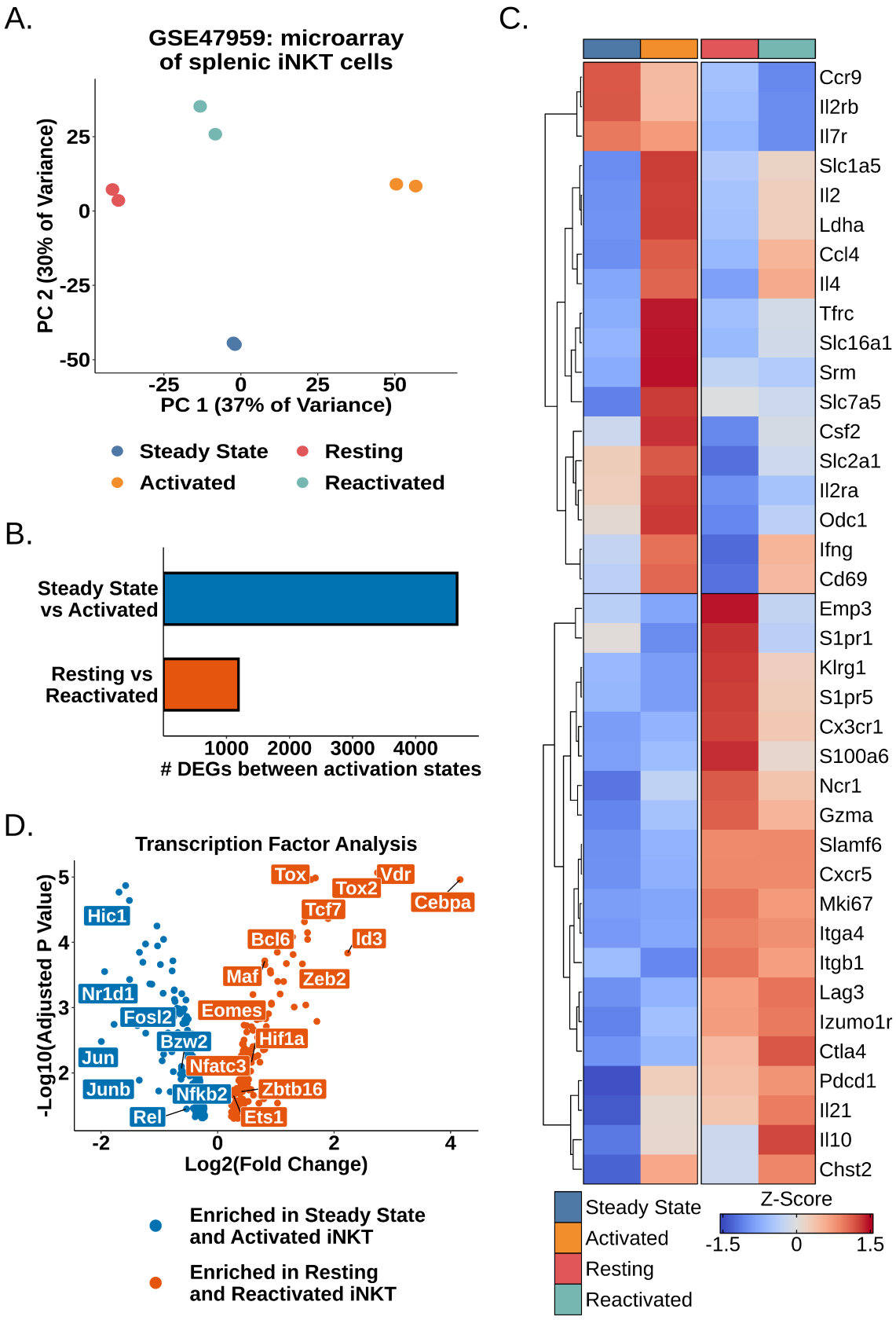

A.
iNKT Cell Activation
Cytokine Production
Glycolysis
Oxidative Metabolism
Amino Acid Metabolism
Polyamine Metabolism
Module Score
Activation with 1µg αGalCer
Steady State and Activated
Resting and Reactivated
B.
Il2rb
Ccr9
Il7r
Klrb1c
Il4
Ifng
Il2
Ccl1
Ccl3
Ccl4
Tfrc
Il13
Csf2
Rheb
Lif
Izumo1r
Lag3
Ncr1
Cd244
Casp3
Ly6a
Gzmb
Il21
Il10
Ctla4
Gzma
Ccr5
Chst2
Spry2
S1pr5
Emp3
S100a6
Itgb1
Cx3cr1
Klrg1
Itga4
S1pr1
Slamf6
Steady State
Activated
Resting
Reactivated
Z-Score
C.
Transcription Factor Analysis
Log2(Fold Change) Activated vs Reactivated iNKT
Log2(Fold Change) Steady State vs Resting iNKT
Klf2
Ets1
Maf
Zeb2
Nfatc3
Jund
Id3
Bzw2
Jun
Naca
Junb
Enriched in Steady State and Activated iNKT
Enriched in Resting and Reactivated iNKT

**Figure 4.6.2: Prior activation with αGalCer induces long term transcriptional remodeling and an adipose-like activation scheme among splenic iNKT cells (continued; previous page).** A. Line plots showing median expression of phenotypic and metabolic gene module scores in steady state and activated (blue) and resting and reactivated (orange) splenic iNKT cells. Module scores were calculated using the data shown in Figure 4.6.1.A. B. Scaled average heatmap with hierarchical clustering of gene expression in the data from Figure 4.6.1.A. C. Scatter plot of transcription factors enriched in steady state versus resting and activated versus reactivated splenic iNKT cells. Transcription factors constitutively enriched in steady state and activated iNKT cells, regardless of activation status, are shown in blue, while genes that are constitutively enriched in resting and reactivated iNKT cells, regardless of activation status, are shown in orange. Genes in gray are conditionally enriched in either steady state and activated or resting and reactivated iNKT cells based on activation status.

Having analyzed the phenotype of αGCPT iNKT cells using scRNA-Seq, we next validated our findings by reanalyzing bulk microarray of αGCPT splenic iNKT cells (GSE47959), originally published by Sag *et al.* (2014)[91]. We divided samples in this dataset into four groups that matched our scRNA-Seq data, including steady state iNKT cells which did not receive αGalCer (Steady State), activated iNKT cells which were stimulated with αGalCer for 1 hour *in vivo* (Activated), resting iNKT cells at 4 weeks post-αGalCer (Resting), and iNKT cells at 4 weeks post-αGalCer which were restimulated with αGalCer for 1 hour *in vivo* (Reactivated; Figure 4.6.3.A). As with our scRNA-Seq, we found that secondary activation of iNKT cells with αGalCer produced a muted transcriptional response (Figure 4.6.3.B). Granular analysis of individual gene expression also recapitulated our scRNA-Seq analysis, as resting and reactivated iNKT cells were enriched for memory-like and regulatory gene signatures (Figure 4.6.3.C), while expression of activation, cytokine, and

metabolic genes was significantly reduced among reactivated versus activated iNKT cells. Transcription factor expression analysis of resting and reactivated versus steady state and activated iNKT cells also mostly matched our scRNA-Seq analysis, with αGCPT iNKT cells showing increased expression of *Zeb2*, *Maf*, *Ets1*, *Nfatc3*, and *Id3* (Figure 4.6.3.D), while steady state and activated iNKT cells demonstrated increased expression of *Jun*, *Junb*, and *Bzw2*. Once again, we did not identify enrichment of chronic markers such as *Nr4a1* and *Nr4a2* among αGCPT iNKT cells, suggesting that splenic αGCPT iNKT cells do not experience chronic endogenous activation like adipose iNKT cells. Other transcription factors enriched among αGCPT iNKT cells included the $NKF_{TH}$ cell markers *Bcl6* and *Tox2*, *Hif1a*, *Tox*, *Eomes*, and *Tcf7* (Figure 4.6.3.D). Overall, reanalysis of this bulk microarray data from Sag *et al.* (2014) validated most of our scRNA-Seq findings.

**Figure 4.6.3: Bulk comparison of splenic iNKT cells previously activated with αGalCer reveals long term transcriptional remodeling and induction of adipose-like activation scheme following reactivation (overleaf).** A. PCA plot of steady state, activated, resting, and reactivated splenic iNKT cells. Reanalyzed from GSE47959. B. Bar plot showing the number of DEGs detected after gene expression analysis comparing steady state versus activated iNKT cells and resting versus reactivated iNKT cells, based on the data shown in Figure 4.6.3.A. C. Scaled average heatmap with hierarchical clustering of gene expression in the data from Figure 4.6.3.A. C. Volcano plot showing transcription factors enriched among steady state and activated (blue) versus resting and reactivated (orange) iNKT cells.


A.
GSE47959: microarray
of splenic iNKT cells
PC 2 (30% of Variance)
PC 1 (37% of Variance)
Steady State
Resting
Activated
Reactivated
B.
Steady State
vs Activated
Resting vs
Reactivated
# DEGs between activation states
C.
Ccr9
Il2rb
Il7r
Slc1a5
Il2
Ldha
Ccl4
Il4
Tfrc
Slc16a1
Srm
Slc7a5
Csf2
Slc2a1
Il2ra
Odc1
Ifng
Cd69
Emp3
S1pr1
Klrg1
S1pr5
Cx3cr1
S100a6
Ncr1
Gzma
Slamf6
Cxcr5
Mki67
Itga4
Itgb1
Lag3
Izumo1r
Ctla4
Pdcd1
Il21
Il10
Chst2
Steady State
Activated
Resting
Reactivated
Z-Score
D.
Transcription Factor Analysis
-Log10(Adjusted P Value)
Log2(Fold Change)
Tox
Vdr
Tox2
Cebpa
Tcf7
Hic1
Bcl6
Id3
Maf
Zeb2
Nr1d1
Eomes
Fosl2
Hif1a
Bzw2
Jun
Nfatc3
Junb
Nfkb2
Zbtb16
Rel
Ets1
Enriched in Steady State
and Activated iNKT
Enriched in Resting
and Reactivated iNKT

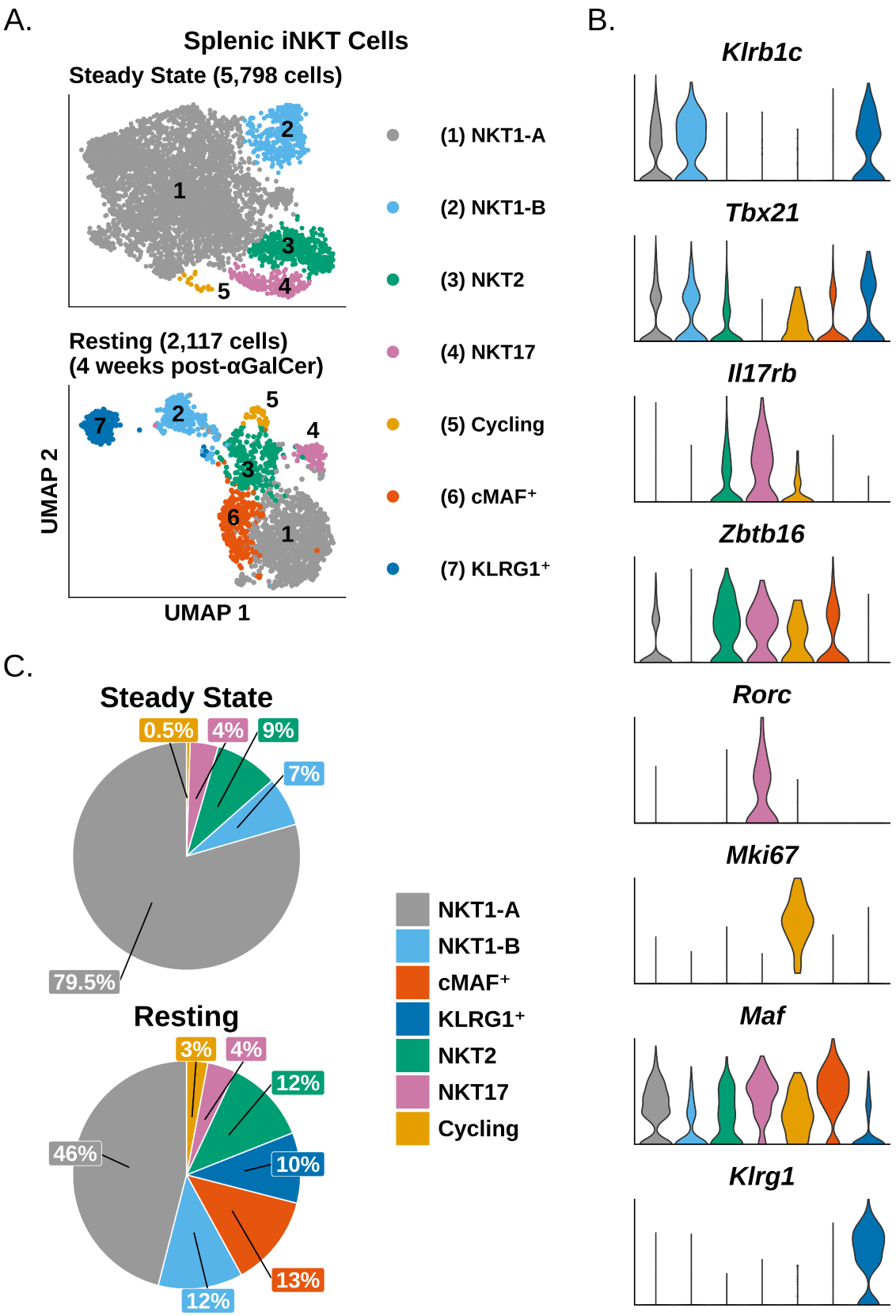
### 4.7 Granular analysis of resting splenic iNKT cells at 4 weeks post-αGalCer

Having profiled the phenotype of bulk splenic iNKT cells at 4 weeks post-αGalCer, we next performed granular analysis of these data. We first analyzed resting iNKT cells and compared these data to steady state splenic iNKT cells (Figure 3.1). We previously identified five clusters among steady state iNKT cells, including two clusters of NKT1 cells (NKT1-A and NKT1-B cells), a cluster of NKT2 cells, a cluster of NKT17 cells, and a cluster of cycling cells (Figure 4.7.1.A, top panel). Strikingly, we also identified these same clusters at 4 weeks post-αGalCer (Figure 4.7.1.A, bottom panel; 4.7.1.B), demonstrating that NKT1, NKT2, and NKT17 cell subsets are still present after prior activation of iNKT cells with αGalCer. Since it has been reported that NKT1, NKT2 and NKT17 cell subsets are not detectable in the spleen at 6 days post-αGalCer[92], this result suggests that NKT1, NKT2, and NKT17 cells reappear later, possibly only after the iNKT cell response subsides. Intriguingly, we also detected two new clusters which were only present among resting iNKT cells at 4 weeks post-αGalCer (Figure 4.7.1.A). Using gene expression analysis, we found that one of these clusters expressed the transcription factor *Maf*, while the other cluster expressed *Klrg1* (Figure 4.7.1.B); therefore, we labeled these two populations as cMAF$^+$ and KLRG1$^+$ iNKT cells respectively (Figure 4.7.1.A). KLRG1$^+$ iNKT cells were NKT1-like, and co-expressed *Tbx21* and *Klrb1c*, while cMAF$^+$ iNKT cells lacked expression of *Klrb1c*, were *Tbx21*$^{low}$, and displayed intermediate *Zbtb16* expression (Figure 4.7.1.B).

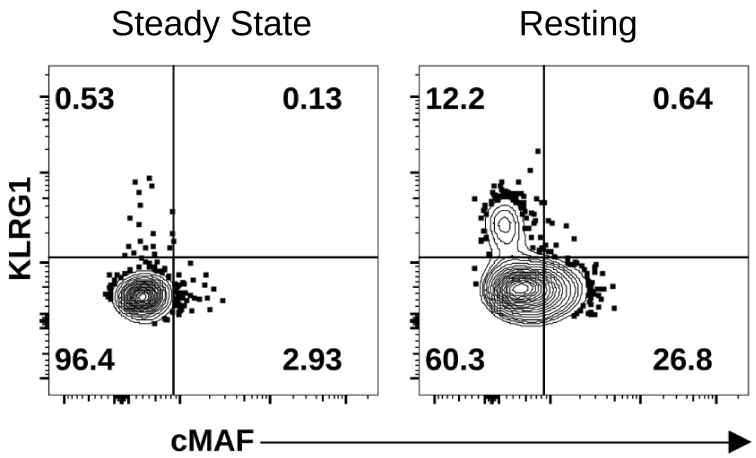
Globally, we found that the appearance of cMAF$^+$ and KLRG1$^+$ iNKT cells at 4 week post-αGalCer was accompanied by a substantial reduction in the frequency of NKT1-A cells (Figure 4.7.1.C), although NKT1-A cells still constituted a majority of iNKT cells in the spleen at 4 weeks post-αGalCer. Other differences between steady state and resting iNKT cells included increases in the frequency of NKT2 and NKT1-B cells at 4 weeks post-αGalCer (Figure 4.7.1.C), and a dramatic increase in the frequency of cycling

cells at 4 weeks post-αGalCer, matching a previous report by Sag *et al.* (2014) which demonstrated that αGCPT iNKT cells proliferate more than iNKT cells at steady state, similar to adipose iNKT cells. We next sought to validate our identification of cMAF$^{+}$ and KLRG1$^{+}$ iNKT cells at 4 weeks post-αGalCer. To do this, we analyzed splenic iNKT cells at steady state and at 4 weeks post-αGalCer using flow cytometry. We detected significantly more cMAF$^{+}$ and KLRG1$^{+}$ iNKT cells among resting versus steady state splenic iNKT cells (Figure 4.7.2.A, Figure 4.7.2.B), proving that splenic cMAF$^{+}$ and KLRG1$^{+}$ iNKT cells are induced following antigen challenge. We also confirmed that this expansion of cMAF$^{+}$ iNKT cells was not due to an expansion of NKT17 cells, which are known to express cMAF[76], as we gated out RORγT$^{+}$ iNKT cells prior to gating on cMAF and KLRG1.

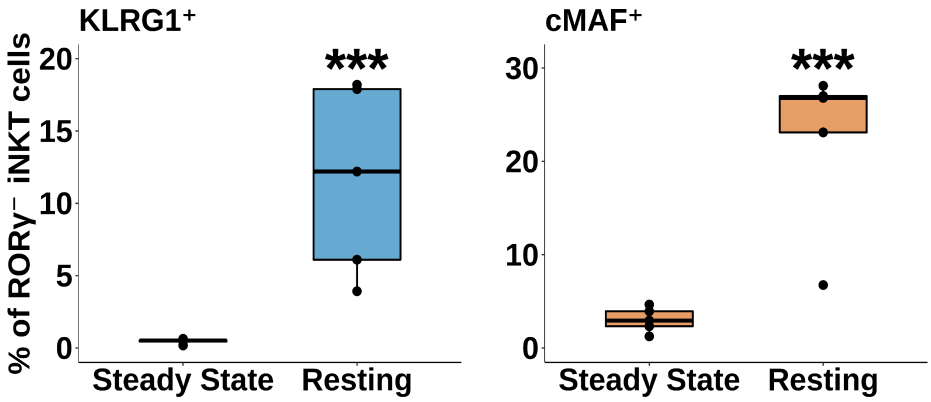
**Figure 4.7.1: Granular analysis of resting splenic iNKT cells (overleaf).** A. UMAP of steady state (top panel) and resting (bottom panel) splenic iNKT cells. B. Violin plots showing gene expression among resting iNKT cells clusters, as shown in the bottom panel of Figure 4.7.1.A. C. Pie charts showing the frequency of matched clusters in steady state and resting splenic iNKT cells. The data correspond to the cells and clusters from the UMAP plots shown in Figure 4.7.1.A.


A.
Splenic iNKT Cells
Steady State (5,798 cells)
Resting (2,117 cells)
(4 weeks post-αGalCer)
UMAP 2
UMAP 1
(1) NKT1-A
(2) NKT1-B
(3) NKT2
(4) NKT17
(5) Cycling
(6) cMAF+
(7) KLRG1+
B.
Klrb1c
Tbx21
Il17rb
Zbtb16
Rorc
Mki67
Maf
Klrg1
C.
Steady State
0.5%
4%
9%
7%
79.5%
Resting
3%
4%
12%
10%
13%
12%
46%
NKT1-A
NKT1-B
cMAF+
KLRG1+
NKT2
NKT17
Cycling

A.


Steady State
Resting
0.53
0.13
96.4
2.93
12.2
0.64
60.3
26.8
KLRG1
cMAF

B.


KLRG1+
cMAF+
% of RORγ− iNKT cells
***
***
0
5
10
15
20
30
Steady State
Resting
Steady State
Resting

C.

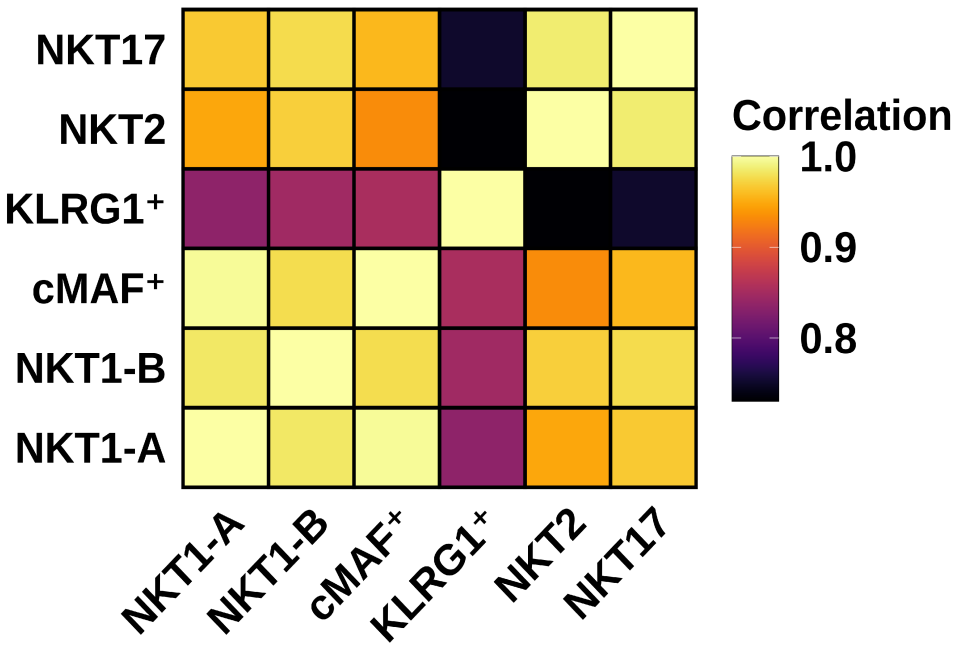

NKT17
NKT2
KLRG1+
cMAF+
NKT1-B
NKT1-A
NKT1-A
NKT1-B
cMAF+
KLRG1+
NKT2
NKT17
Correlation
1.0
0.9
0.8

**Figure 4.7.2: Granular analysis of resting splenic iNKT cells (continued; previous page):** A. Representative contour plots showing expression of cMAF and KLRG1 in RORγT$^{-}$ steady state (left panel) and resting (right panel) splenic iNKT cells. B. Box plots quantifying the data shown in Figure 4.7.2.B. N = 5 biological replicates from one experiment. Experiment performed at least twice for cMAF$^{+}$ iNKT cell enrichment, and N = 1 times for KLRG1$^{+}$ iNKT cell enrichment. Student's two-tailed t-test. Asterisks denote significance, * padj < 0.05; ** padj <0.01; *** padj < 0.001. Horizontal lines represent median values. C. Correlation plot of whole normalized transcriptomes in the resting splenic iNKT cell clusters from Figure 4.7.1.A (bottom panel). Cycling cells were excluded from the analysis.

Having identified enrichment of cMAF$^{+}$ and KLRG1$^{+}$ iNKT cells at 4 weeks post-αGalCer, we next sought to characterize the gene signatures associated with these new populations. We first performed whole transcriptome correlation analysis among the different resting iNKT cell clusters. We found that KLRG1$^{+}$ and cMAF$^{+}$ iNKT cells were more transcriptionally similar to NKT1 cells than to NKT2 or NKT17 cells (Figure 4.7.2.C), suggesting that KLRG1$^{+}$ and cMAF$^{+}$ iNKT cells might differentiate from NKT1 cells. Notably, previous work by Murray *et al.* (2021) has demonstrated that a majority of memory-like NKT$_{eff}$ and NKT$_{FH}$ cells are derived from T-bet$^{+}$ iNKT cells[92], suggesting that most memory-like iNKT cells originate from an NKT1 cell lineage. KLRG1$^{+}$ iNKT cells were highly transcriptionally distinct to other iNKT cell subsets, whereas cMAF$^{+}$ iNKT cells were transcriptionally similar to NKT1-A cells (Figure 4.7.2.C). We next performed granular analysis of cluster gene expression. As suggested by our whole transcriptome correlation analysis, cMAF$^{+}$ and KLRG1$^{+}$ iNKT cells displayed broad expression of NKT1 cell markers (Figure 4.7.3.A), which clearly distinguished these populations from NKT2 and NKT17 cells. cMAF$^{+}$ iNKT cells expressed the stem-like markers *Slamf6* and *Tcf7*, and the NKT17 cell marker *Maf*, but otherwise lacked

expression of most other NKT2 or NKT17 cell markers (Figure 4.7.3.A). KLRG1$^{+}$ iNKT cells displayed enrichment of many genes previously associated with KLRG1$^{+}$ iNKT cells and NKT$_{eff}$ cells[92,131,206], including *Cx3cr1*, *Spry2*, *Klrk1*, *Gzma*, *Gzmb*, the transcription factor *Zeb2*, and the KLF2 regulon genes such as *Klf2*, *S1pr5*, *Emp3*, and *S100a6*. KLRG1$^{+}$ iNKT cells also lacked expression of *Cxcr3* and expressed the memory-associated markers *Itga4* and *Itgb1* (Figure 4.7.3.A, Figure 4.7.3.B). Overall, our data suggest that the KLRG1$^{+}$ iNKT cells identified here by scRNA-Seq are highly similar to the memory-like KLRG1$^{+}$ and NKT$_{eff}$ cell populations previously identified by Shimizu *et al.* (2014) and Murray *et al.* (2021). Transcriptionally, our data also suggest that KLRG1$^{+}$ cells are phenotypically similar to T$_{CM}$ and T$_{EM}$ cells, and could be regulated by the transcription factor ZEB2[349,369].

By contrast, we found that cMAF$^{+}$ iNKT cells displayed increased expression of the serine/cysteine peptidase inhibitors *Serpina3g* and *Serpina3f*, *Chst2*, *Cd4*, *Izumo1r*, the immunoregulatory receptors *Ctla4*, *Pdcd1*, and *Lag3*, *Tox*, *Hif1a*, *Itga4*, *Itgb1*, and *Ly6a* (Figure 4.7.3.A). Overall, we found that the gene signature of cMAF$^{+}$ iNKT cells was most similar to adipose NK1.1$^{-}$ NKT1 cells (Figure 3.2), which are highly enriched for regulatory NKT10 cells[115], and memory-like NKT$_{FH}$ cells (Figure 4.5). Moreover, while we did not detect enrichment of the *bona fide* NKT$_{FH}$ and T$_{FH}$ cell markers *Cxcr5*, *Bcl6*, and *Tox2* among cMAF$^{+}$ iNKT cells, cMAF$^{+}$ iNKT cells displayed the highest overall expression of NKT$_{FH}$ cell-associated genes among all resting iNKT cell clusters (Figure 4.7.3.B). Therefore, out data indicate that cMAF$^{+}$ iNKT cells are a memory-like iNKT cell population similar to NKT$_{FH}$ cells and might also constitute a putative regulatory or NKT10-like population.

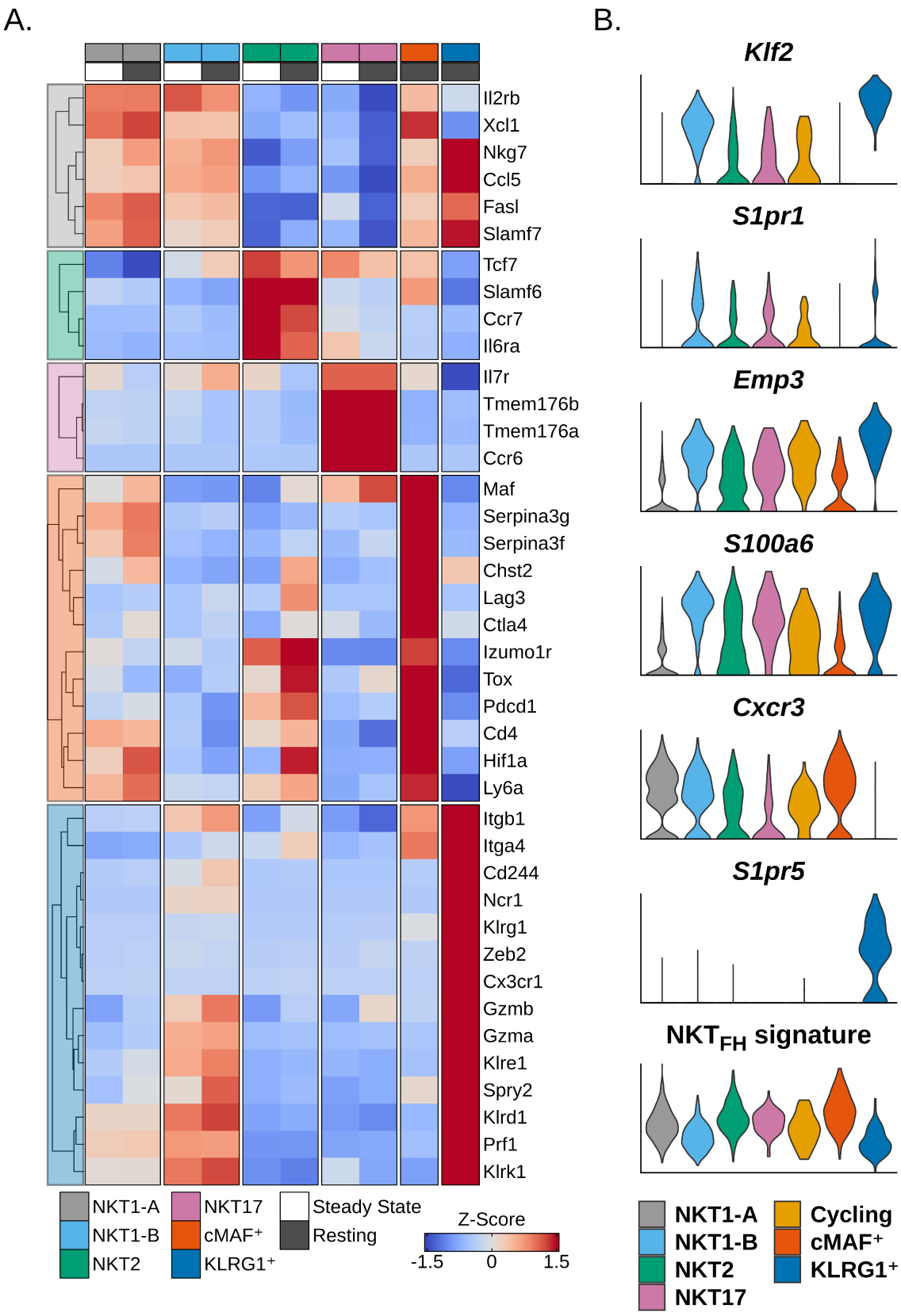

A.
B.
Il2rb
Xcl1
Nkg7
Ccl5
Fasl
Slamf7
Tcf7
Slamf6
Ccr7
Il6ra
Il7r
Tmem176b
Tmem176a
Ccr6
Maf
Serpina3g
Serpina3f
Chst2
Lag3
Ctla4
Izumo1r
Tox
Pdcd1
Cd4
Hif1a
Ly6a
Itgb1
Itga4
Cd244
Ncr1
Klrg1
Zeb2
Cx3cr1
Gzmb
Gzma
Klre1
Spry2
Klrd1
Prf1
Klrk1
NKT1-A
NKT1-B
NKT2
NKT17
cMAF+
KLRG1+
Steady State
Resting
Z-Score
-1.5
0
1.5
Klf2
S1pr1
Emp3
S100a6
Cxcr3
S1pr5
NKTFH signature
NKT1-A
NKT1-B
NKT2
NKT17
Cycling
cMAF+
KLRG1+

**Figure 4.7.3: Transcriptional signatures of memory-like KLRG1$^{+}$ and cMAF$^{+}$ iNKT cells (previous page).** A. Scaled average heatmap with hierarchical clustering of gene expression in the steady state and resting splenic iNKT cell clusters from Figure 4.7.1.A. Cycling cells were excluded from the analysis. B. Violin plots showing gene expression and expression of a module score for $T_{FH}$ and $NKT_{FH}$ cell genes among resting iNKT cells clusters, as shown in the bottom panel of Figure 4.7.1.A.

## 4.8 Granular analysis of reactivated splenic iNKT cells at 4 weeks post-αGalCer

Having performed granular characterization of resting splenic iNKT cells at 4 weeks post-αGalCer, we next performed a similar analysis of reactivated splenic iNKT cells at 4 weeks post-αGalCer. Unlike splenic iNKT cells activated with a single dose of αGalCer (Figure 3.4), were most iNKT cells displayed enrichment of activation and cytokine transcripts, and heterogeneity was mainly driven by NKT1, NKT2 and NKT17 cell subsets, only ~50% of reactivated splenic iNKT cells displayed enrichment of activation and cytokine transcripts (Figure 4.8.1.A, Figure 4.8.1.B). Clustering analysis identified two clusters, Cluster A and Cluster B, which separated based on expression of activation, cytokine, and metabolic genes (Figure 4.8.1.A, Figure 4.8.1.B), and module scoring revealed that only Cluster B cells displayed evidence of activation, effector function, and metabolic remodeling at 4 hours post-αGalCer (Figure 4.8.1.C). This indicates that splenic iNKT cells display a blunted secondary response to strong TCR stimulation, similar to the primary response of adipose iNKT cells to αGalCer.

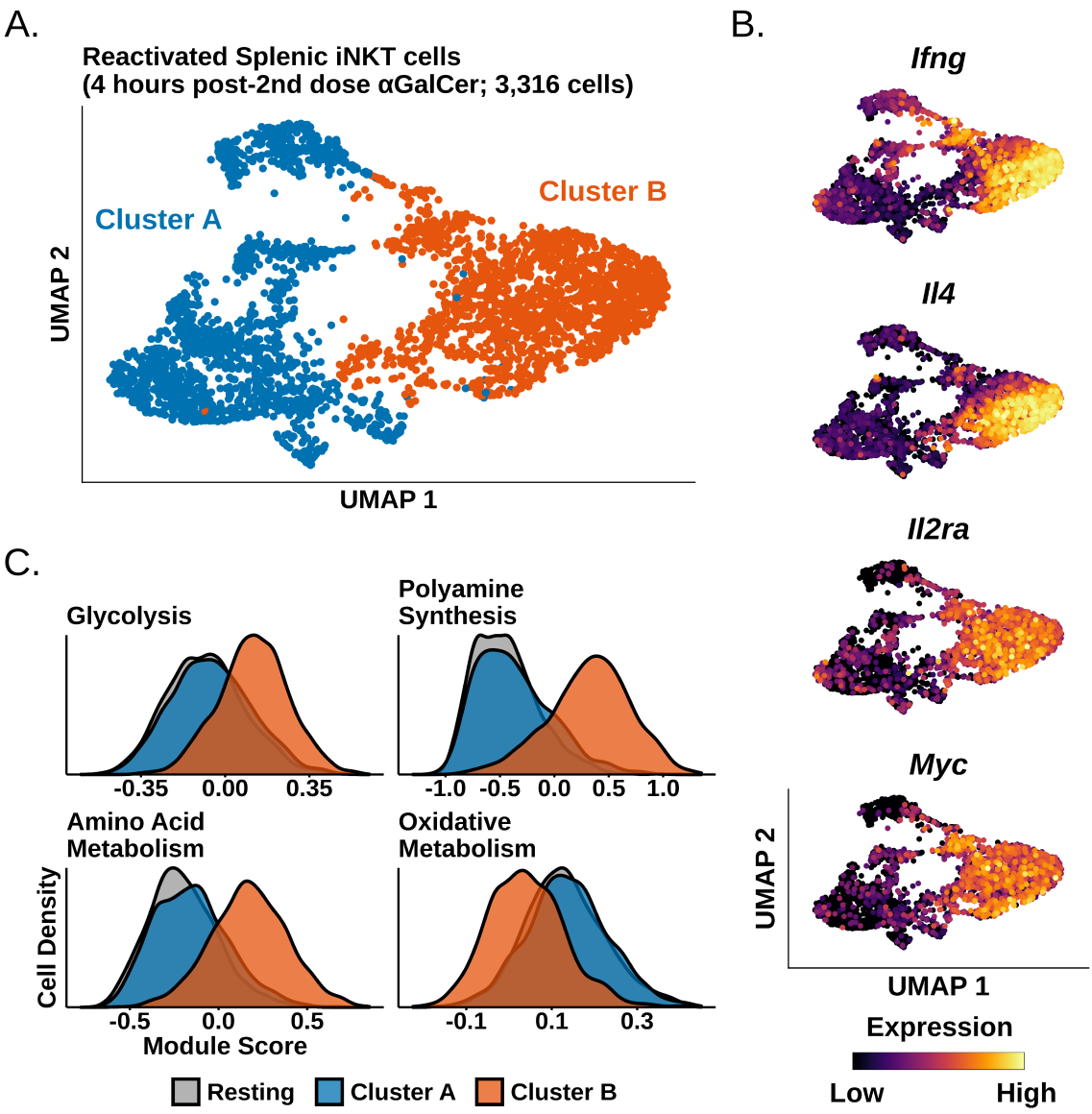
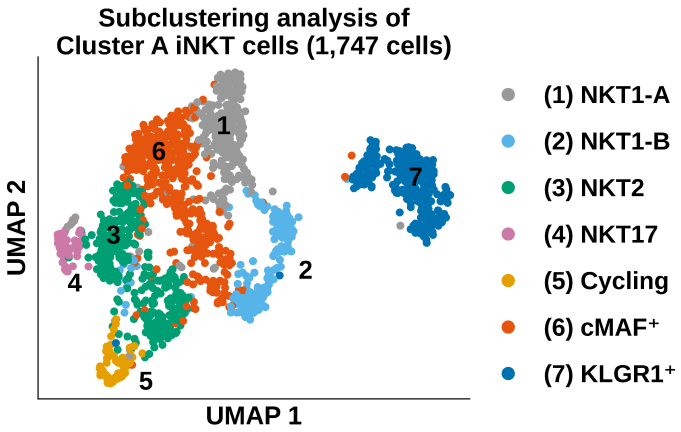



**Figure 4.8.1: Granular analysis of reactivated splenic iNKT cells.** A. UMAP of reactivated splenic iNKT cells. B. Feature plots of gene expression in reactivated splenic iNKT cells. C. Density plots showing expression of metabolic gene module scores in resting, reactivated Cluster A, and reactivated Cluster B splenic iNKT cells. Module scores were calculated using the data shown in Figure 4.8.1.A.

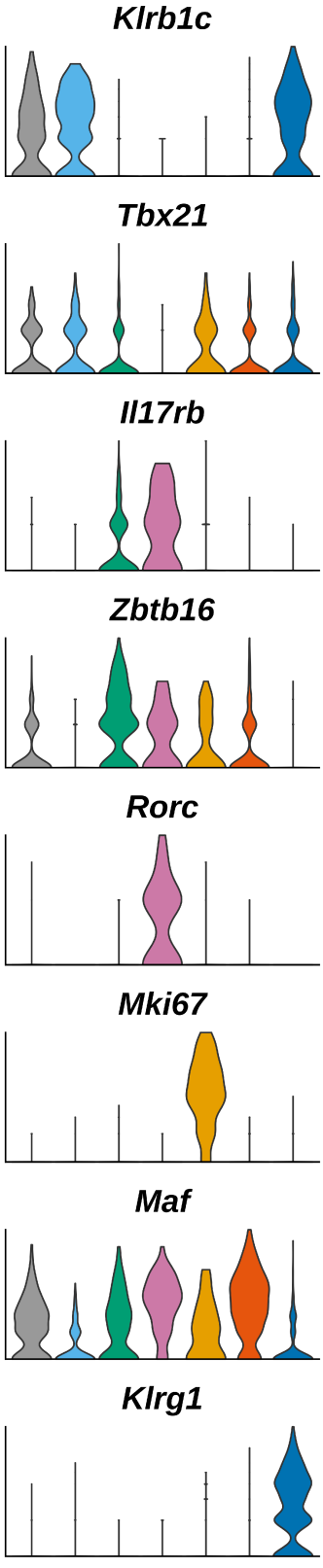
We next performed granular subclustering analysis of Cluster A and Cluster B cells, focusing first on Cluster A cells. Interestingly, we identified the same set of clusters that we previously identified among resting iNKT cells, including NKT1-A and NKT1-B cells, NKT2 cells, NKT17 cells, a population of cycling cells, and memory-like cMAF$^+$ and KLRG1$^+$ cells (Figure 4.8.2.A, Figure 4.8.2.B). However, we identified increased enrichment of cMAF$^+$, KLRG1$^+$, and NKT2 cells compared to resting iNKT cells (Figure 4.8.2.C), while the frequency of NKT1-A cells was reduced. This suggests that cMAF$^+$ and KLRG1$^+$ cells are associated with a blunted iNKT cell response to αGalCer stimulation, as progressive enrichment of these memory-like cMAF$^+$ and KLRG1$^+$ cells correlated with progressively reduced splenic iNKT cell responsiveness to αGalCer (Figure 4.8.2.C). To validate our clustering analysis, we also profiled gene expression among Cluster A cells. We found that the gene expression profiles of our Cluster A iNKT cell populations matched the expression profiles of resting and steady state clusters (Figure 4.8.3.A), and unsupervised hierarchical clustering of Cluster A, resting, and steady state populations showed that matched clusters from different data grouped together (Figure 4.8.3.A), validating our subcluster analysis.

**Figure 4.8.2: Analysis of reactivated splenic Cluster A iNKT cells (overleaf).** A. UMAP of reactivated Cluster A splenic iNKT cells, referencing Cluster A from Figure 4.8.1.A. B. Violin plots showing gene expression among reactivated Cluster A subclusters, as shown in Figure 4.8.2.A. C. Pie charts showing the frequency of matched clusters in steady state, resting, and reactivated Cluster A splenic iNKT cells. The data correspond to the cells and clusters from the UMAP plots shown in Figure 4.8.1.A (steady state and resting iNKT cells) and Figure 4.8.2.A (reactivated Cluster A iNKT cells).

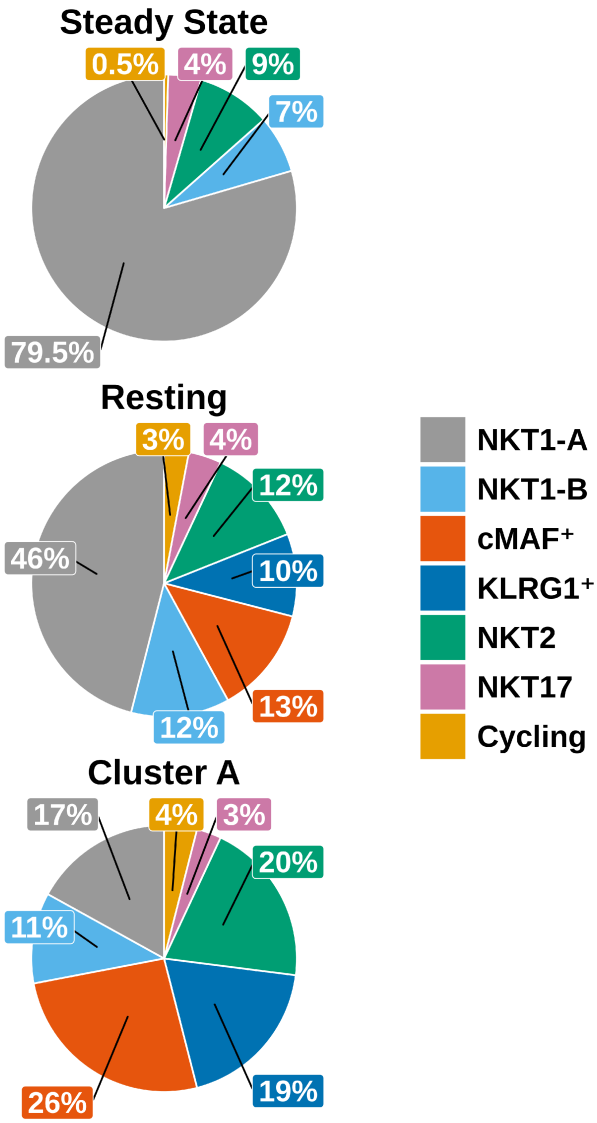
A.


Subclustering analysis of
Cluster A iNKT cells (1,747 cells)
UMAP 2
UMAP 1
1
2
3
4
5
6
7
(1) NKT1-A
(2) NKT1-B
(3) NKT2
(4) NKT17
(5) Cycling
(6) cMAF+
(7) KLGR1+

B.


Klrb1c
Tbx21
Il17rb
Zbtb16
Rorc
Mki67
Maf
Klrg1

C.


Steady State
0.5%
4%
9%
7%
79.5%
Resting
3%
4%
12%
10%
46%
13%
12%
Cluster A
17%
4%
3%
20%
11%
26%
19%
NKT1-A
NKT1-B
cMAF+
KLRG1+
NKT2
NKT17
Cycling

A.

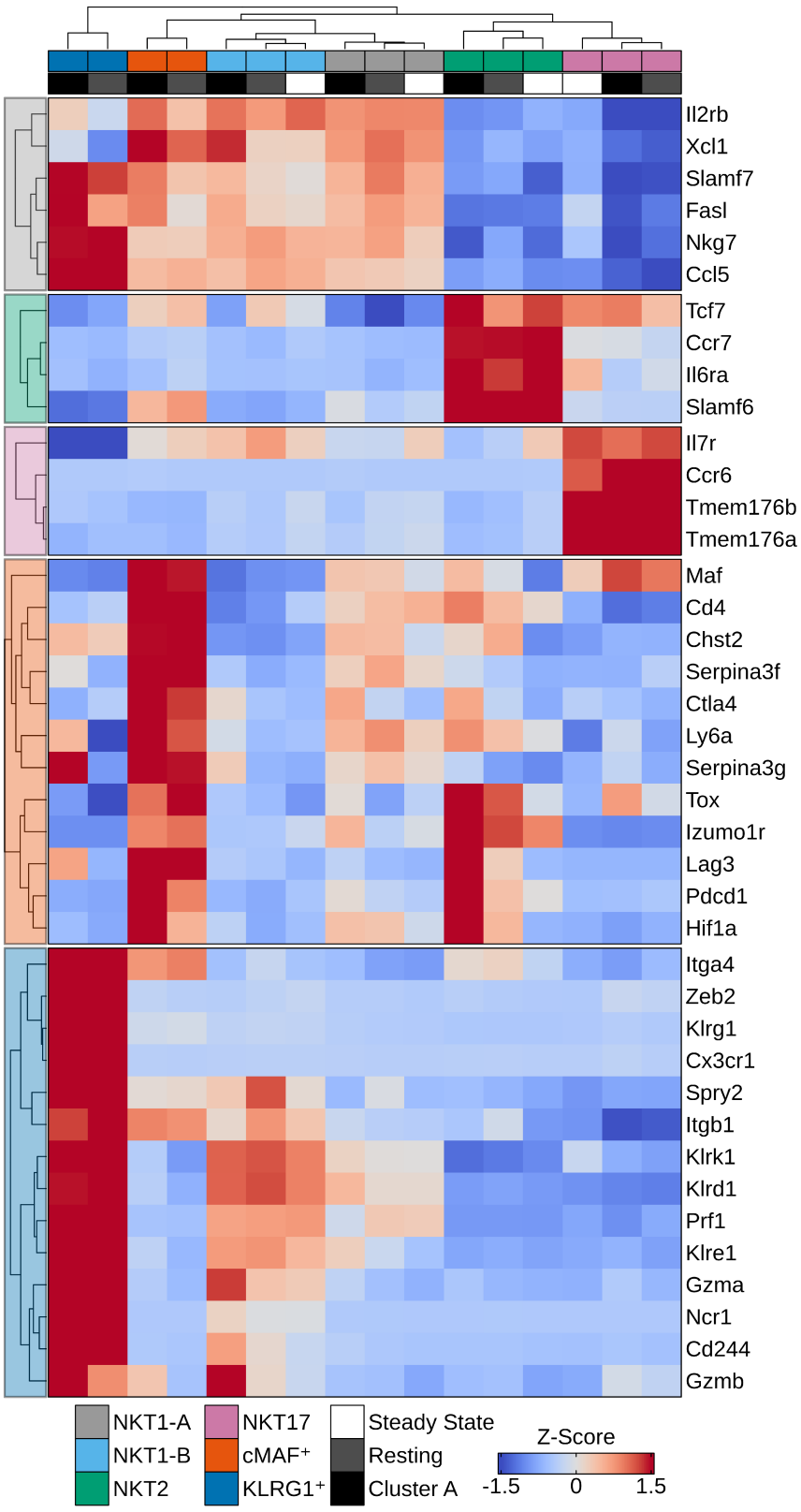

Il2rb
Xcl1
Slamf7
Fasl
Nkg7
Ccl5
Tcf7
Ccr7
Il6ra
Slamf6
Il7r
Ccr6
Tmem176b
Tmem176a
Maf
Cd4
Chst2
Serpina3f
Ctla4
Ly6a
Serpina3g
Tox
Izumo1r
Lag3
Pdcd1
Hif1a
Itga4
Zeb2
Klrg1
Cx3cr1
Spry2
Itgb1
Klrk1
Klrd1
Prf1
Klre1
Gzma
Ncr1
Cd244
Gzmb
NKT1-A
NKT1-B
NKT2
NKT17
cMAF+
KLRG1+
Steady State
Resting
Cluster A
Z-Score
-1.5
0
1.5

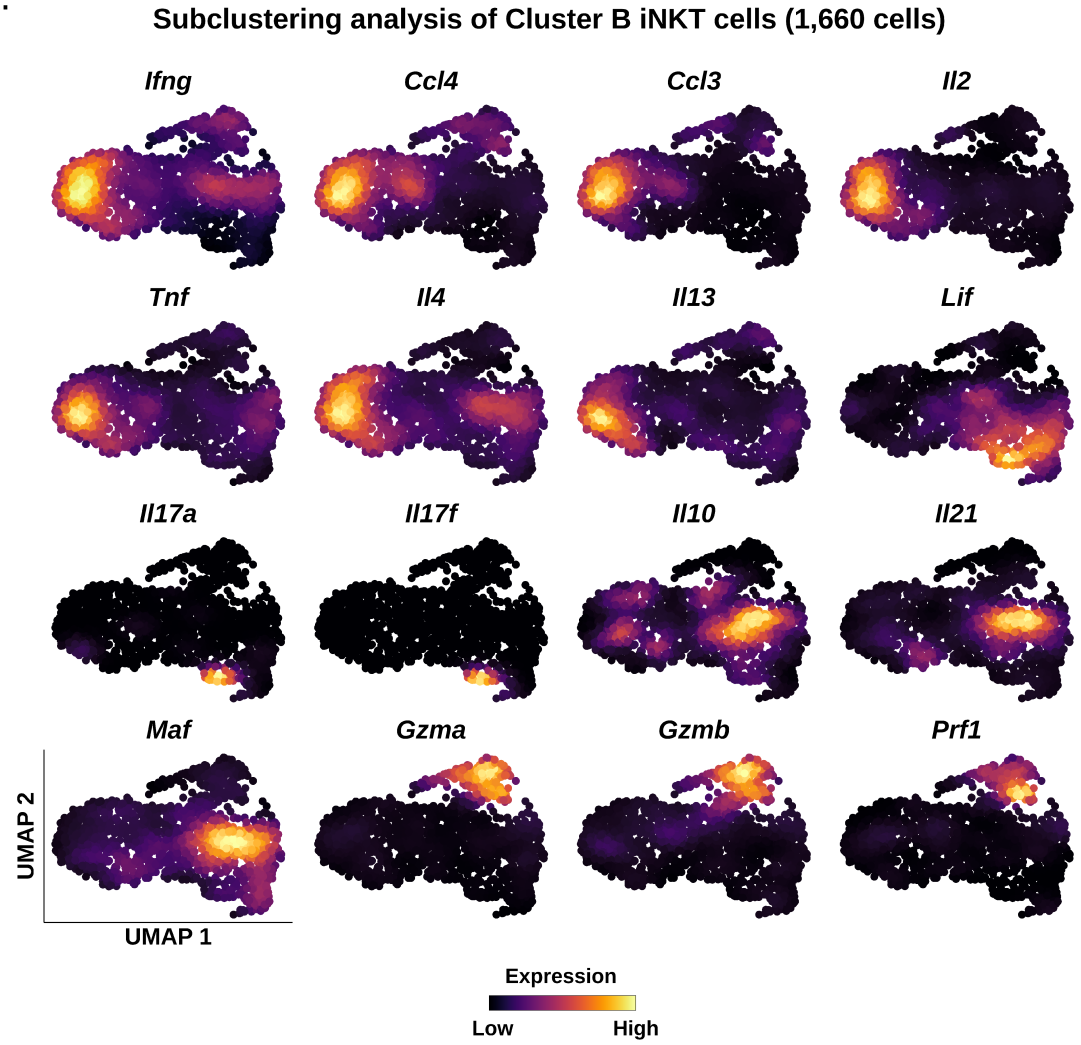
**Figure 4.8.3: Analysis of reactivated splenic Cluster A iNKT cells (previous page).** A. Scaled average heatmap with hierarchical clustering of gene expression in the cell clusters from steady state and resting splenic iNKT cells, and the subclusters from reactivated Cluster A cells. The heatmap corresponds to the data shown in Figure 4.8.1.A (steady state and resting iNKT cells) and Figure 4.8.2.A (reactivated Cluster A iNKT cells).

We next performed granular analysis of the cells from Cluster B. Density mapping of gene expression revealed four major populations (Figure 4.8.4.A). We identified a population of NKT1 cells that co-expressed *Ifng*, *Ccl4*, *Ccl3*, *Il2*, *Tnf*, *Il4*, and *Il13*, a population of NKT17 cells that produced *Lif*, *Il17a*, and *Il17f* (Figure 4.8.4.A), a population of NKT10 cells that co-expressed *Il10*, *Il21*, and *Maf*, and a cytotoxic population expressing *Gzma*, *Gzmb*, and *Prf1* (Figure 4.8.4.A). Based on our previous analysis of resting and Cluster A iNKT cells (Figures 4.7-4.8), we hypothesized that the NKT10 population co-expressing *Il21* and *Maf* might represent an activated state of cMAF$^{+}$ iNKT cells, while *Gzma*$^{high}$ *Gzmb*$^{high}$ cells might be enriched for activated KLRG1$^{+}$ iNKT cells. We tested our hypothesis by performing gene correlation analysis against expression of *Gzma* and *Il10*, which are *bona fide* markers of KLRG1$^{+}$ and NKT10 cells respectively[91,206]. We found that the cMAF$^{+}$ markers *Maf*, *Ctla4*, and *Serpina3g* were among the top 40 genes that correlated with expression of *Il10*, suggesting that cMAF$^{+}$ iNKT cells might represent a population of NKT10 cells, or be enriched for NKT10 cells (Figure 4.8.4.B). Moreover, we previously found that cMAF$^{+}$ iNKT cells were similar to NKT$_{FH}$ cells (Figure 4.7.3) and we noted that *Il10* expression was highly correlated with expression of *Il21*, a flagship NKT$_{FH}$ cytokine[202]. Genes highly correlated against *Gzma* included *Gzmb*, *Klre1*, *Klrk1*, *Cd244*, *Cx3cr1*, KLF2 regulon genes, and *Klrg1* (Figure 4.8.4.B), all markers of KLRG1$^{+}$ iNKT cells (Figure 4.7.3). This suggests that *Gzma*$^{high}$ *Gzmb*$^{high}$ cells may represent an activated state of KLRG1$^{+}$ iNKT cells, or that this population might be enriched for activated

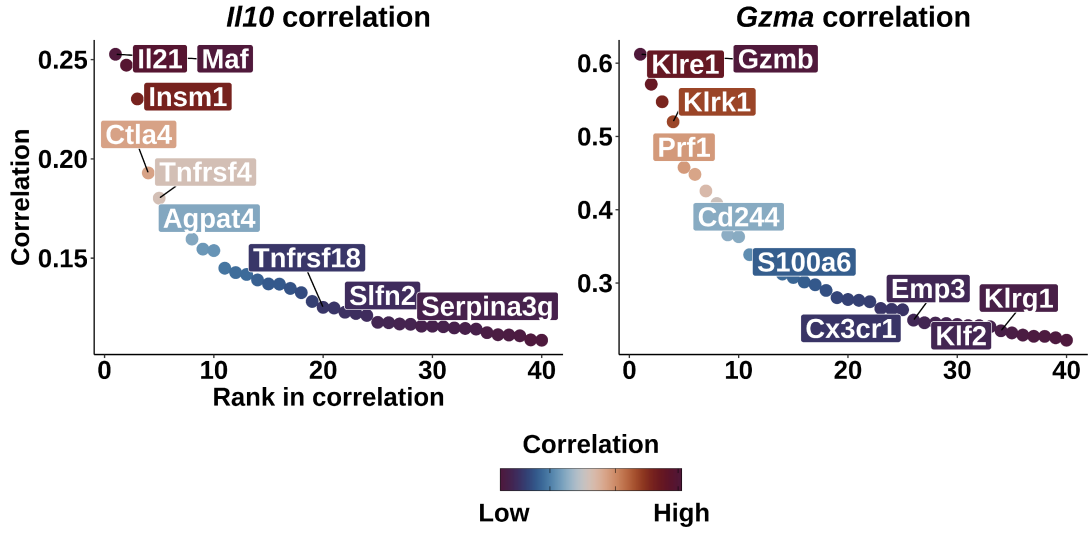
KLRG1$^{+}$ iNKT cells. Therefore, although our analysis of resting and Cluster A cells indicated that KLRG1$^{+}$ and cMAF$^{+}$ iNKT cells are correlated with a blunted response to αGalCer stimulation, our analysis of reactivated Cluster B cells suggests that KLRG1$^{+}$ and cMAF$^{+}$ iNKT cells can respond to αGalCer, similar to other iNKT cells.

**Figure 4.8.4: Analysis of reactivated splenic Cluster B iNKT cells (overleaf).** A. Density plots of gene expression in reactivated Cluster B iNKT cells, referencing Cluster B from Figure 4.8.1.A. B. Dot plots showing ranked correlation values for the top 40 genes most correlated with expression of *Il10* (left) or *Gzmb* (right) among reactivated Cluster B iNKT cells.

A.


Subclustering analysis of Cluster B iNKT cells (1,660 cells)
Ifng
Ccl4
Ccl3
Il2
Tnf
Il4
Il13
Lif
Il17a
Il17f
Il10
Il21
Maf
Gzma
Gzmb
Prf1
UMAP 2
UMAP 1
Expression
Low
High

B.


Il10 correlation
Gzma correlation
Correlation
Rank in correlation
Il21
Maf
Insm1
Ctla4
Tnfrsf4
Agpat4
Tnfrsf18
Slfn2
Serpina3g
Klre1
Gzmb
Klrk1
Prf1
Cd244
S100a6
Emp3
Klrg1
Cx3cr1
Klf2
Correlation
Low
High

### 4.9 Transcriptional analysis and comparison of adipose and splenic iNKT cells at steady state and 4 weeks post-αGalCer

Since we had found that splenic iNKT cells display an adipose-like response to αGalCer challenge at 4 weeks post-αGalCer, we next decided to perform comparative analysis of adipose and splenic iNKT cells at steady state and 4 weeks post-αGalCer. Quality control measures returned 3,014 adipose iNKT cells at 4 weeks post-αGaCer, expressing a median of 4,531 UMIs and 1,806 genes per cell.

We first wondered whether steady state adipose iNKT cells and splenic iNKT cells at 4 weeks post-αGalCer would overlap transcriptionally if analyzed collectively, and we also wondered how these populations would compare to steady state splenic iNKT cells and adipose iNKT cells at 4 weeks post-αGalCer. Combined UMAP of adipose and splenic iNKT cells at steady state and 4 weeks post-αGalCer revealed that adipose and splenic iNKT cells did not overlap at either steady state or 4 weeks post-αGalCer (Figure 4.9.1.A), indicative of conserved transcriptional differences between adipose and splenic iNKT cells before and after antigen challenge. However, quantification of transcriptional differences between adipose and splenic iNKT cells revealed a reduced number of DEGs between adipose and splenic iNKT cells at 4 weeks post-αGalCer compared to steady state (Figure 4.9.1.B), illustrating that the transcriptomes of adipose and splenic iNKT cells are more similar following antigen challenge. We also profiled the relative magnitude of transcriptional remodeling among adipose and splenic iNKT cells in response to antigen challenge. We found that splenic iNKT cells underwent a greater degree of transcriptional remodeling after prior αGalCer challenge, indicating that antigen challenge had a greater long-term impact on the transcriptional phenotype of splenic iNKT cells than adipose iNKT cells, possibly because adipose iNKT cells may already be antigen experienced at steady state. We also noted that transcriptional remodeling among splenic iNKT cells was

primarily associated with the acquisition of gene expression (Figure 4.9.1.B), whereas the opposite was true for adipose iNKT cells.

We next performed gene expression analysis to gain further insight into the biology of adipose versus splenic iNKT cells. We first compared adipose versus splenic iNKT cells at steady state, and then performed a similar comparison of adipose versus splenic iNKT cells at 4 weeks post-αGalCer. We then overlapped the DEGs from these two comparisons against genes previously identified when we compared adipose versus splenic iNKT cells at steady state, 4 hours post-αGalCer, and 72 hours post-αGalCer (Figure 4.4.2.A). This allowed us to leverage the full spectrum of our adipose and splenic iNKT cell scRNA-Seq data. We identified 460 highly conserved genes among adipose iNKT cells (Figure 4.9.1.C) and 59 genes among splenic iNKT cells (data not shown). Notable genes enriched among adipose iNKT cells included *Cpt1a*, *Ctla4*, *Fasl*, *Gzmb*, *Hilpda*, *Maf*, *Klrg1*, *Klrk1*, *Nfil3*, *Pdgfb*, and *Tox*, while *Cd160*, *Ccr7*, *Dtx1*, *Il7r*, *Il17rb*, *Il6ra*, and *Naca*, were enriched among splenic iNKT cells. We next performed over-representation analysis of these conserved genes against the KEGG pathway database. Splenic iNKT cells demonstrated increased expression of genes associated with ribosomes (Figure 4.9.1.D), whereas adipose iNKT cells displayed conserved enrichment of genes associated with cell death and cytotoxicity, adhesion and the cytoskeleton, uptake of material from the extracellular environment, lipids, and multiple signaling pathways, including JAK STAT signaling, TCR signaling, and PI3K signaling (Figure 4.9.1.D).

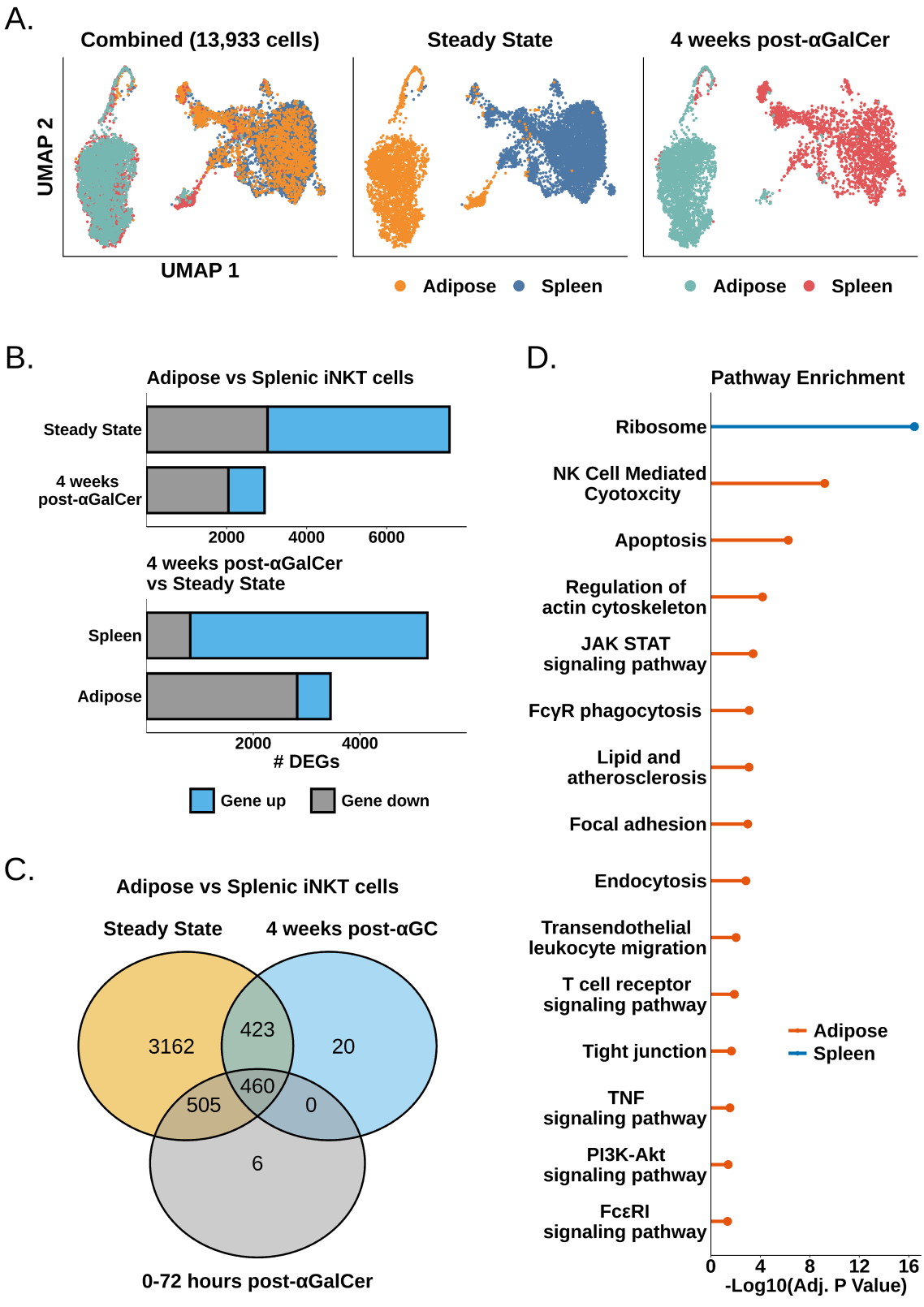

A.
Combined (13,933 cells)
Steady State
4 weeks post-αGalCer
UMAP 2
UMAP 1
Adipose
Spleen
Adipose
Spleen
B.
Adipose vs Splenic iNKT cells
Steady State
4 weeks post-αGalCer
2000
4000
6000
4 weeks post-αGalCer vs Steady State
Spleen
Adipose
2000
4000
# DEGs
Gene up
Gene down
C.
Adipose vs Splenic iNKT cells
Steady State
4 weeks post-αGC
3162
423
20
460
505
0
6
0-72 hours post-αGalCer
D.
Pathway Enrichment
Ribosome
NK Cell Mediated Cyotoxcity
Apoptosis
Regulation of actin cytoskeleton
JAK STAT signaling pathway
FcγR phagocytosis
Lipid and atherosclerosis
Focal adhesion
Endocytosis
Transendothelial leukocyte migration
T cell receptor signaling pathway
Tight junction
TNF signaling pathway
PI3K-Akt signaling pathway
FcεRI signaling pathway
Adipose
Spleen
0
4
8
12
16
-Log10(Adj. P Value)

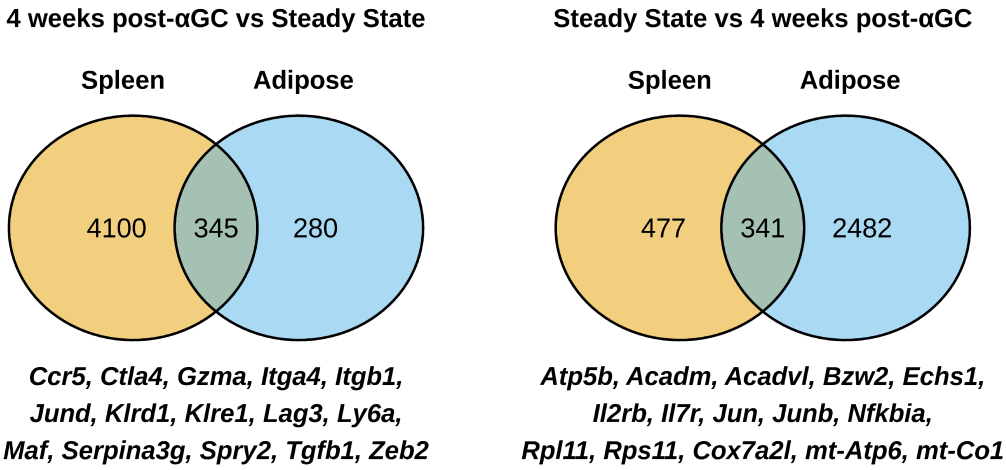
**Figure 4.9.1: Transcriptional analysis of splenic and adipose iNKT cells at steady state and 4 weeks post-αGalCer (previous page).** A. UMAP plots of splenic and adipose iNKT cells at steady state and 4 weeks post-αGalCer. B. Bar plot showing the total number of DEGs identified after gene expression analysis of adipose versus splenic iNKT cells at either steady state (top bar) or 4 weeks post-αGalCer (bottom bar). The breakdown of DEGs found to be upregulated (blue) versus downregulated (gray) in each comparison is also shown. C. Venn diagram showing the breakdown of all DEGs identified after gene expression analysis of adipose versus splenic iNKT cells at 4 weeks post-αGalCer, steady state, or collectively at 72 hours post-αGalCer, 4 hours post-αGalCer and steady state. D. Over-representation analysis of the conserved 460 genes enriched in adipose versus splenic iNKT cells from Figure 4.9.1.C. Orange bars represent pathways derived from genes enriched in adipose iNKT cells, whereas blue bars represent pathways derived from genes enriched in splenic iNKT cells.

We next sought to characterize conserved gene signatures associated with iNKT cells at 4 weeks post-αGalCer or steady state. To do this, we performed gene expression analysis comparing iNKT cells at 4 week post-αGalCer versus steady state in the spleen and adipose tissue, and then performed overlap analysis to identify genes enriched across both comparisons. We detected 345 genes always associated with antigen experienced iNKT cells, regardless of tissue localization, including the Tr1 cell markers *Ccr5* and *Maf*, the immunoregulatory receptors *Ctla4* and *Lag3*, the cMAF$^{+}$ iNKT cell markers *Serpina3g* and *Ly6a*, the KLRG1$^{+}$ iNKT cell markers *Zeb2*, *Spry2*, *Klrd1*, and *Klre1*, and the “trained” iNKT cell markers *Itga4* and *Itgb1* (Figure 4.9.2.A, left). Over-representation of these 345 genes against the KEGG pathway database revealed enrichment of motifs associated with cytotoxicity, and changes in gene expression associated with T cell receptor signaling (Figure 4.9.2.B. left). Leading edge genes contributing to TCR signaling motif enrichment included

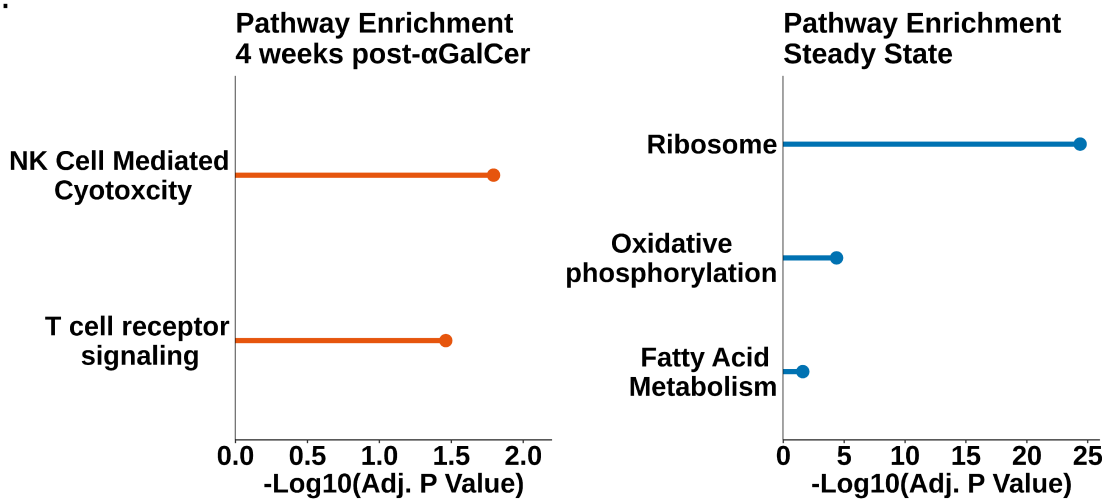
*Akt2*, *Ctla4*, the caspase-like protease *Malt1*, *Nfatc2*, the calcineurin subunit *Ppp3r1*, *Ptpn6* (SHP-1), and *Zap70*. Steady state iNKT cells demonstrated enrichment of 341 genes, including genes associated with oxidative metabolism, such as *Cox7a2l*, *Atp5b*, *mt-Atp6* and *mt-Co1*, lipid metabolism, such as *Acadm*, *Acadvl*, and *Echs1*, *Il7r*, *Nfkbia*, *Il2rb*, the transcription factors *Bzw2*, *Jun*, and *Junb*, and ribosomal genes, including *Rpl11* and *Rps11* (Figure 4.9.2.A, right). Over-representation of these genes revealed increased expression of genes associated with oxidative phosphorylation, fatty acid metabolism, and the ribosome (Figure 4.9.2.B, right), suggesting that long term transcriptional remodeling associated with antigen experience could involve changes in the metabolic profile of iNKT cells.

**Figure 4.9.2: Transcriptional analysis of splenic and adipose iNKT cells at steady state and 4 weeks post-αGalCer (continued; overleaf).** A. Venn diagrams showing cross-analysis of genes upregulated (left) or downregulated (right) in splenic and adipose iNKT cells at 4 weeks post-αGalCer versus steady state. A sample of the overlapping genes between splenic and adipose iNKT cells is shown below the Venn diagrams. B. Lollipop plots showing the results from over-representation analysis of the overlapping genes detected in the analysis from Figure 4.9.2.A (i.e. the genes in the intersection of the Venn diagrams), performed against the KEGG pathway database.

A.


4 weeks post-αGC vs Steady State
Spleen
Adipose
4100
345
280
Ccr5, Ctla4, Gzma, Itga4, Itgb1,
Jund, Klrd1, Klre1, Lag3, Ly6a,
Maf, Serpina3g, Spry2, Tgfb1, Zeb2
Steady State vs 4 weeks post-αGC
Spleen
Adipose
477
341
2482
Atp5b, Acadm, Acadvl, Bzw2, Echs1,
Il2rb, Il7r, Jun, Junb, Nfkbia,
Rpl11, Rps11, Cox7a2l, mt-Atp6, mt-Co1

B.


Pathway Enrichment
4 weeks post-αGalCer
NK Cell Mediated
Cytoxcity
T cell receptor
signaling
0.0
0.5
1.0
1.5
2.0
-Log10(Adj. P Value)
Pathway Enrichment
Steady State
Ribosome
Oxidative
phosphorylation
Fatty Acid
Metabolism
0
5
10
15
20
25
-Log10(Adj. P Value)

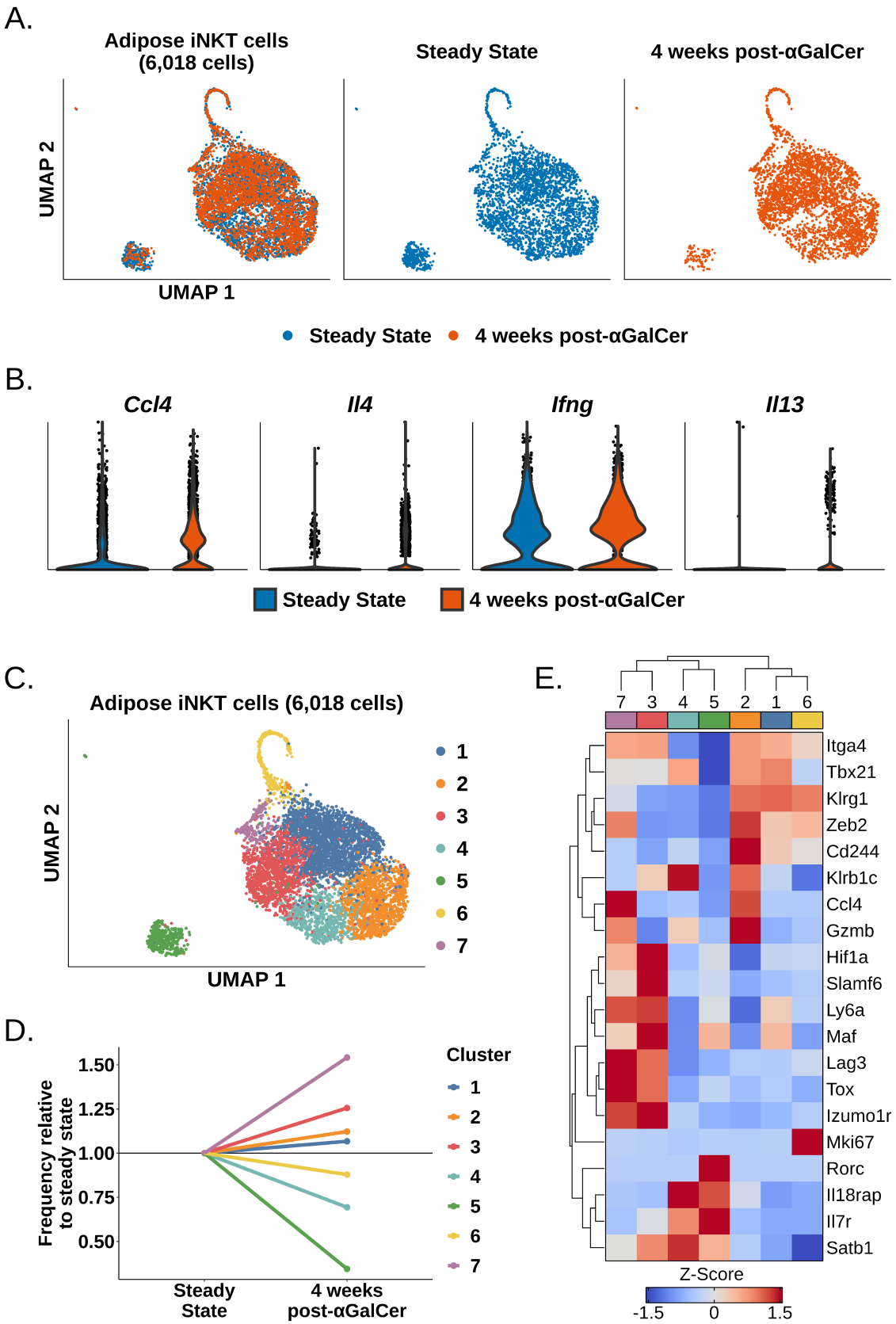
### 4.10 Granular analysis of adipose iNKT cells at 4 weeks post-αGalCer

We next decided to perform granular analysis of adipose iNKT cells at 4 weeks post-αGalCer, and to perform a more detailed comparison of adipose iNKT cells at steady state and 4 weeks post-αGalCer. Combined UMAP of both adipose data revealed extensive overlap (Figure 4.10.1.A), suggestive of broad transcriptional similarity between adipose iNKT cells at steady state and at 4 weeks post-αGalCer. We next performed gene expression analysis. Interestingly, adipose iNKT cells at 4 weeks post-αGalCer demonstrated significant enrichment of several different cytokines, including *Ccl4*, *Il4*, *Il13*, and *Ifng* (Figure 4.10.1.B). However, aside from *Ccl4*, which associated with specific iNKT cell populations (Figure 4.10.1.C, Figure 4.10.1.D), this increased cytokine expression was not linked to any particular population of adipose iNKT cells, and we also did not identify co-enrichment of typical iNKT cell activation markers. Therefore, the significance of this increased cytokine expression at 4 weeks post-αGalCer remains unclear. Other genes enriched at 4 weeks post-αGalCer included *Ly6a*, *Itga4*, *Maf*, *Klrk1*, and *Izumo1r*, while expression of NKT17 cell markers such as *Tmem176a*, *Tmem176b*, and *S100a4* was reduced.

We next performed cluster-based analysis to track changes in individual populations between steady state and 4 weeks post-αGalCer. UMAP and graph-based clustering identified a total of 7 different clusters among adipose iNKT cells (Figure 4.10.1.C). We then calculated the percentage of total iNKT cells comprised by each cluster at both steady state and 4 weeks post-αGalCer, allowing us to identify relative changes in the frequency of clusters at 4 weeks post-αGalCer (Figure 4.10.1.D). We also performed gene expression analysis to phenotype each cluster (Figure 4.10.1.E). We found that the frequency of NKT17 cells (Cluster 5) was significantly reduced at 4 weeks post-αGalCer (Figure 4.10.1.D, Figure 4.10.1.E), and constituted the largest shift in the proportion of any single cluster. Other clusters/populations which were reduced in frequency at 4 weeks post-αGalCer included a population of

NK1.1$^{+}$ NKT1 cells which lacked expression of *Itga4* (Cluster 4) and cycling cells (Cluster 6) (Figure 4.10.1.D, Figure 4.10.1.E). Notably, both of the adipose iNKT cell populations lacking expression of the memory-like iNKT cell marker *Itag4* (Cluster 4 and the NKT17 cell cluster, Cluster 6) were reduced in frequency at 4 weeks post-αGalCer, suggesting that memory-like iNKT cells accumulate in adipose tissue after αGalCer challenge. Two clusters of iNKT cells co-expressing *Maf*, *Tox*, *Itga4*, *Slamf6*, *Hif1a*, *Ly6a*, and *Lag3* (Cluster 3 and Cluster 7) represented the most enriched populations/clusters at 4 weeks post-αGalCer, followed by a cluster of iNKT cells co-expressing *Klrg1*, *Zeb2*, *Klrb1c*, *Cd244*, *Gzmb*, *Ccl4*, *Itga4*, and *Klf2* (Figure 4.10.1.D, Figure 4.10.1.E). *Ccl4* was also expressed by some cMAF$^{+}$ iNKT cells. Overall, these data suggest that memory-like cMAF$^{+}$ and KLRG1$^{+}$ iNKT cells accumulate in adipose tissue after αGalCer challenge, similar to the spleen.

**Figure 4.10.1: Granular analysis of adipose iNKT cells at 4 weeks post-αGalCer (overleaf).** A. UMAP plots of adipose iNKT cells at steady state and 4 weeks post-αGalCer. B. Violin plots showing increased expression of cytokine genes in adipose iNKT cells at 4 weeks post-αGalCer versus steady state. C. UMAP of adipose iNKT cells at steady state and 4 weeks post-αGalCer, with graph-based clustering applied. D. Line plot showing changes in the relative frequency of each of the clusters from Figure 4.10.1.A at 4 weeks post-αGalCer versus steady state iNKT cells. Cluster frequencies were calculated by taking the number of cells in each individual cluster as a percentage of total adipose iNKT cells at either steady state or 4 weeks post-αGalCer, and then calculating changes in the frequency of each cluster at 4 weeks post-αGalCer relative to steady state. E. Scaled average heatmap with hierarchical clustering of gene expression in the cell clusters from Figure 4.10.1.C.


A.
Adipose iNKT cells (6,018 cells)
Steady State
4 weeks post-αGalCer
UMAP 2
UMAP 1
Steady State
4 weeks post-αGalCer
B.
Ccl4
Il4
Ifng
Il13
Steady State
4 weeks post-αGalCer
C.
Adipose iNKT cells (6,018 cells)
UMAP 2
UMAP 1
1
2
3
4
5
6
7
D.
Frequency relative to steady state
1.50
1.25
1.00
0.75
0.50
Steady State
4 weeks post-αGalCer
Cluster
1
2
3
4
5
6
7
E.
7 3 4 5 2 1 6
Itga4
Tbx21
Klrg1
Zeb2
Cd244
Klrb1c
Ccl4
Gzmb
Hif1a
Slamf6
Ly6a
Maf
Lag3
Tox
Izumo1r
Mki67
Rorc
Il18rap
Il7r
Satb1
Z-Score
-1.5
0
1.5

Having identified changes in the adipose iNKT cell repertoire at 4 weeks post-αGalCer, we next performed individual granular analysis of these data, to examine iNKT cell heterogeneity in more detail. UMAP and graph-based clustering of adipose iNKT cells at 4 weeks post-αGalCer identified a total of 6 different clusters (Figure 4.10.2.A). As indicated by our combined analysis of steady state and 4 week adipose iNKT cells, we identified several populations of NKT1 cells, a minor population of NKT17 cells, and a population of cycling cells (4.10.2.A, 4.10.2.B, 4.10.2.C). Overall, adipose iNKT cells separated by differences between cycling, NKT1, and NKT17 cells first (i.e. along UMAP 1), and by differences between Cluster 5 and Cluster 2 versus Cluster 6 (i.e. along UMAP 2; Figure 4.10.2.A). Unlike adipose iNKT cells at steady state (Figure 3.2), we found that enrichment of *Klrb1c* and *Klrg1* was not mutually exclusive, and we were able to identify distinct *Klrg1*$^{pos}$ *Klrb1c*$^{high}$ (Cluster 6), *Klrg1*$^{neg}$ *Klrb1c*$^{high}$ (Cluster 2), *Klrg1*$^{pos}$ *Klrb1c*$^{low}$ (Cluster 1), and *Klrg1*$^{neg}$ *Klrb1c*$^{low}$ (Cluster 5) NKT1 cell populations (Figure 4.10.2.A, Figure 4.10.2.B). Gene expression analysis of these clusters revealed that Cluster 5 cells displayed enrichment of genes associated with splenic cMAF$^{+}$ iNKT cells and adipose NK1.1$^{-}$ iNKT cells (Figure 3.2.2) and expressed the memory-like iNKT cell markers *Itgb1* and *Itga4* (Figure 4.10.2.C). Cluster 6 iNKT cells displayed enrichment of gene signatures associated with splenic KLRG1$^{+}$ iNKT cells, and also expressed the memory-like markers *Itgb1* and *Itga4* (Figure 4.10.2.C). Therefore, our data suggest that although adipose iNKT cells constitutively express markers associated with memory-like or “trained” iNKT cells, and there are already iNKT cells expressing *Maf* and *Klrg1* in adipose tissue at steady state (Figure 3.2), stimulation of adipose iNKT cells with αGalCer may enhance the memory-like or “trained” phenotype of adipose iNKT cells and promote the accumulation of cMAF$^{+}$ and KLRG1$^{+}$ iNKT cells in adipose tissue.

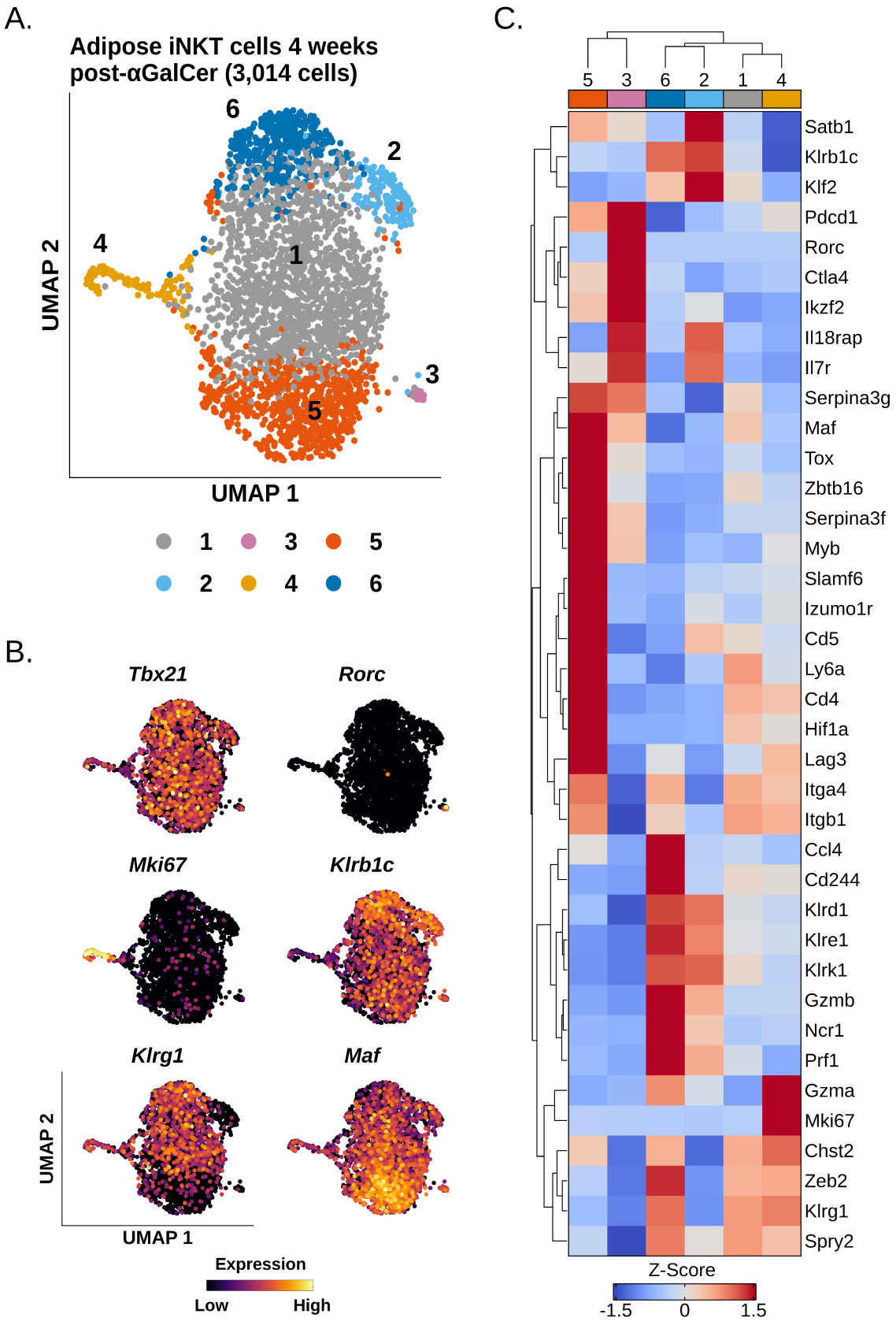

A.
Adipose iNKT cells 4 weeks post-αGalCer (3,014 cells)
6
2
4
1
3
5
UMAP 2
UMAP 1
1 3 5
2 4 6
B.
Tbx21
Rorc
Mki67
Klrb1c
Klrg1
Maf
UMAP 2
UMAP 1
Expression
Low
High
C.
5 3 6 2 1 4
Satb1
Klrb1c
Klf2
Pdcd1
Rorc
Ctla4
Ikzf2
Il18rap
Il7r
Serpina3g
Maf
Tox
Zbtb16
Serpina3f
Myb
Slamf6
Izumo1r
Cd5
Ly6a
Cd4
Hif1a
Lag3
Itga4
Itgb1
Ccl4
Cd244
Klrd1
Klre1
Klrk1
Gzmb
Ncr1
Prf1
Gzma
Mki67
Chst2
Zeb2
Klrg1
Spry2
Z-Score
-1.5
0
1.5

**Figure 4.10.2: Granular analysis of adipose iNKT cells at 4 weeks post-αGalCer (continued; previous page).** A. UMAP of adipose iNKT cells at 4 weeks post-αGalCer. B. Feature plots of gene expression in the data from Figure 4.10.2.A. C. Scaled average heatmap with hierarchical clustering of gene expression in the cell clusters from Figure 4.10.2.A.

### 4.11 Characterization of the transcriptional phenotype of NKT10 cells

One defining characteristic of both adipose iNKT cells and αGCPT splenic iNKT cells is that these populations are enriched for NKT10 cells, a unique and distinct subset of regulatory iNKT cells[49,91]. However, at the time of starting my PhD, the transcriptional signatures associated with NKT10 cells remained relatively uncharacterized. It was also unclear whether the NKT10 cells constitutively present in adipose tissue were similar to the iNKT10 cells that appear in other organs such as the spleen after activation with αGalCer. To address these questions, we used our scRNA-Seq data to characterize adipose NKT10 cells and splenic iNKT10 cells, and gain insight into the transcriptional phenotype of NKT10 cells.

Analysis of adipose iNKT cells had revealed intermediate enrichment of *Il10* at 4 hours post-αGalCer, and more significant enrichment of *Il10* at 72 hours post-αGalCer (Figure 4.4.3), indicating that these two activation states could be used to study adipose NKT10 cells. We first analyzed adipose NKT10 cells at 4 hours post-αGalCer. Our previous analysis of adipose iNKT cells at 4 hours post-αGalCer had demonstrated that expression of *Il10* was restricted to cytokine producing adipose NKT1 cells (Cytokine$^+$ NKT1 cells, Figure 4.11.1.A). Therefore, we performed granular analysis of adipose Cytokine$^+$ NKT1 cells to compare expression of *Il10* versus other NKT1 cell cytokines. Density plot mapping revealed that iNKT cells expressing *Il10* clustered distinctly to iNKT cells expressing other cytokines and secreted factors, such as *Ifng*, *Il4*, *Il13*, *Ccl4*, and *Il2* (Figure 4.11.1.B). This suggested that adipose NKT10 cells might be transcriptionally distinct to other adipose NKT1 cells. However, our ability to do gene expression and correlation analysis was limited by the low number (28) of adipose NKT10 cells at 4 hours post-αGalCer.

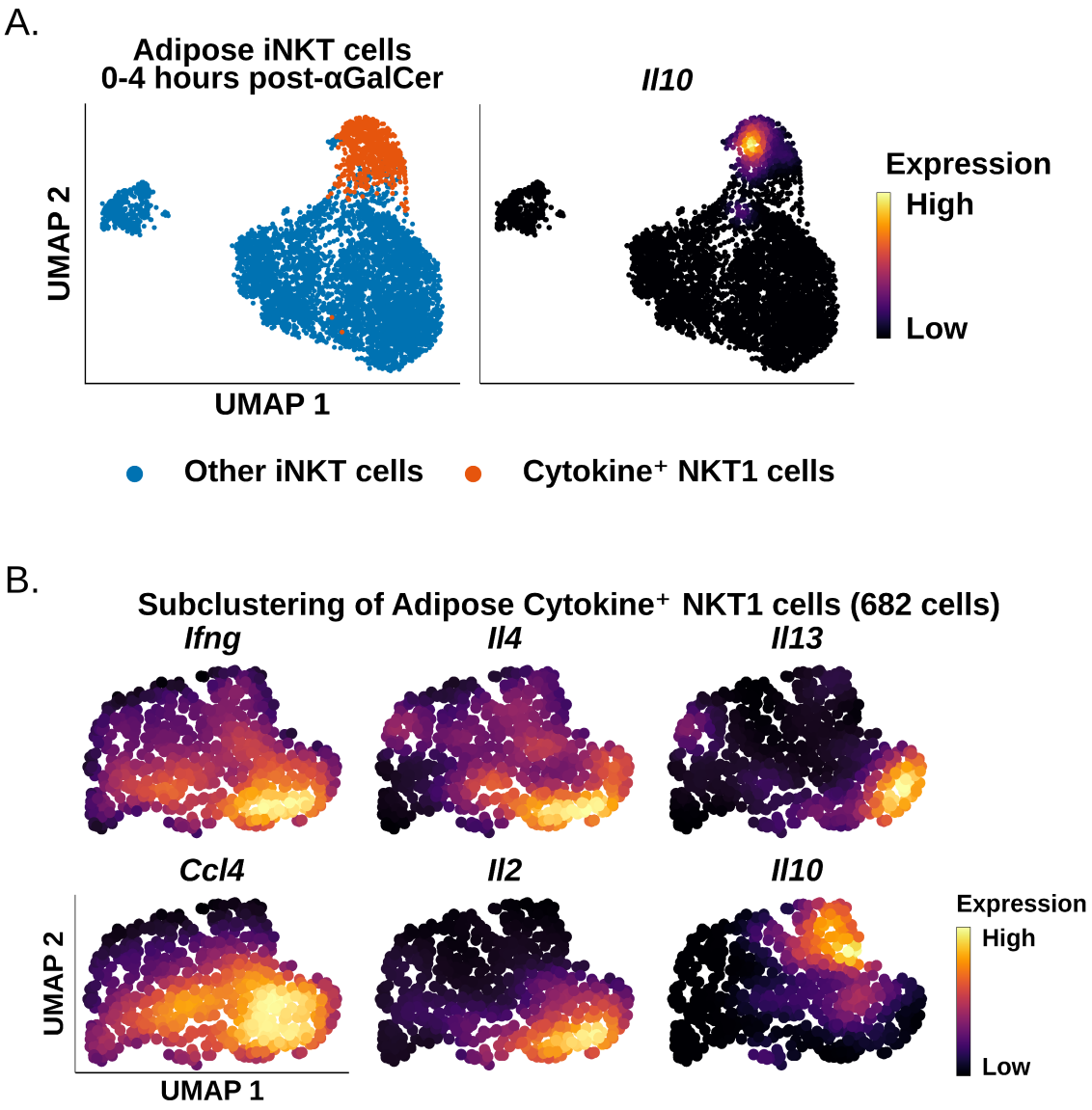
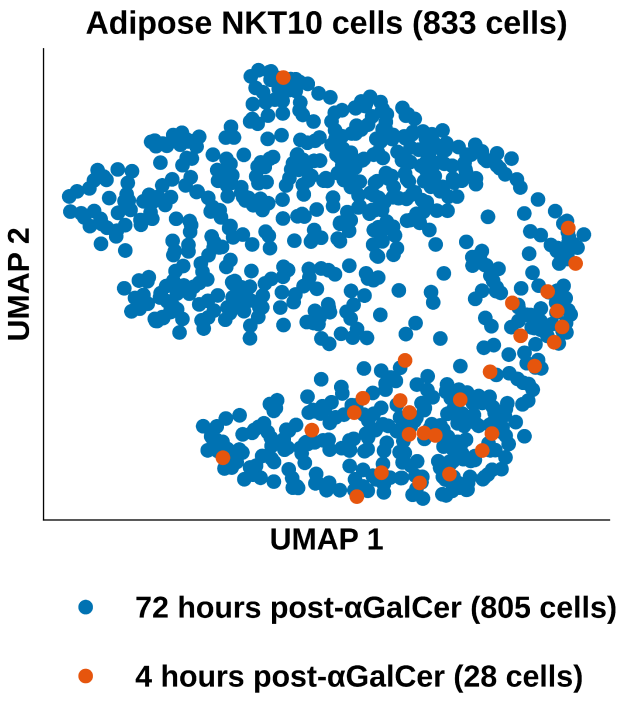



**Figure 4.11.1: Transcriptional analysis of NKT10 cells (part I).** A. UMAP plot of adipose iNKT cells at steady state and 4 hours post-αGalCer (left) and density plot of *Il10* gene expression in the same data (right). Cycling cells were excluded from the analysis. Cytokine$^{+}$ NKT1 cells, corresponding to Cluster 6 in the original clustering analysis (see Figure 3.11.2.A), are highlighted in orange, whereas all other iNKT cells are colored blue. B. Granular density plots of cytokine gene expression in Cytokine$^{+}$ NKT1 cells from Figure 4.11.1.A.

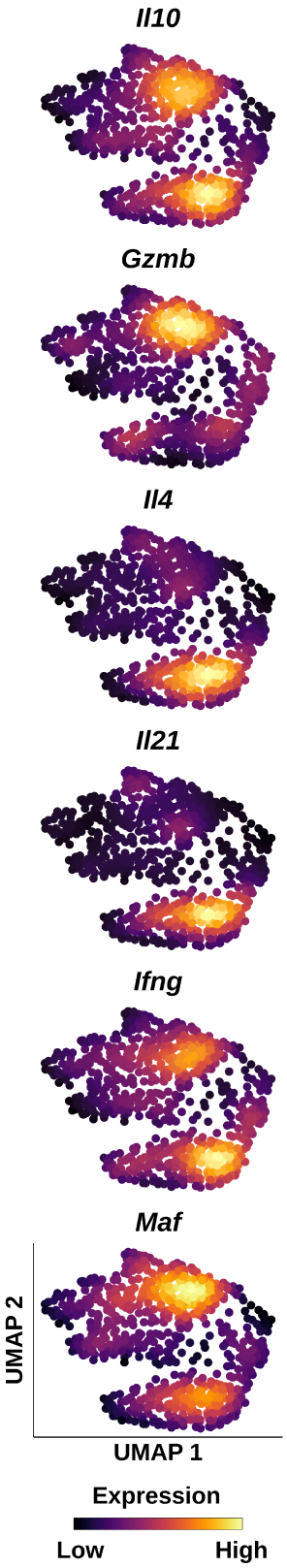
We next decided to perform combined analysis of adipose NKT10 cells at 4 and 72 hours post-αGalCer, to leverage the increased number of cells expressing *Il10* at 72 hours post-αGalCer. To do this, we isolated all adipose iNKT cells with non-zero expression of *Il10* at 4 and 72 hours post-αGalCer, identifying a total of 833 cells (Figure 4.11.2.A). This included 28 NKT10 cells at 4 hour post-αGalCer, and 805 cells at 72 hour post-αGalCer. Interestingly, we found that adipose NKT10 cells were heterogeneous, as some NKT10 cells displayed enrichment of *Il4* and *Il21*, while other NKT10 cells demonstrated increased expression of *Gzmb* (Figure 4.11.2.B). Notably, both NKT10 cell populations showed enrichment for *Ifng*, which correlated with our identification of *Il10* expression among adipose NKT1 cells at 4 hours post-αGalCer (Figure 4.11.1.A), and *Maf*, correlating with our αGCPT splenic iNKT cell analysis (Figure 4.7-4.8). We also found that NKT10 cells at 4 hour post-αGalCer clustered more closely with NKT10 cells expressing *Il4* and *Il21*, but not with NKT10 cells expressing *Gzmb* (Figure 4.11.2.A), suggesting that adipose NKT10 cells could be more homogeneous at 4 hours post-αGalCer, and more heterogeneous at 72 hours post-αGalCer. We next performed gene expression analysis comparing adipose NKT10 cells versus adipose non-NKT10 cells at 4 and 72 hours post-αGalCer. We found that adipose NKT10 cells displayed enrichment of *Gzmb*, *Maf*, *Hif1a*, *Il21*, and *Ccr5*, the immunoregulatory receptors *Ctla4*, *Lag3*, and *Pdcd1*, the Treg markers *Izumo1r* and *Tnfrsf18* (encoding GITR), the transcription factor *Hivep3*, *Tnfrsf9*, *Tnfrsf4*, and the polyamine synthesis enzyme *Odc1* (Figure 4.11.2.C). Interestingly, many of these genes have previously been associated with adaptive Tr1 cells[358,359,362–365], suggesting that adipose NKT10 cells might display a Tr1 cell-like phenotype.

**Figure 4.11.2: Transcriptional analysis of NKT10 cells (part II; overleaf).** A. UMAP plot of adipose NKT10 cells (normalized expression of *Il10* > 0) at 4 and 72 hours post-αGalCer. Cell cycle regression was performed during dimensionality reduction. B. Radar chart showing selected genes enriched in the adipose NKT10 cells from Figure 4.11.2.A after gene expression analysis versus all other adipose iNKT cells at 4 and 72 hours post-αGalCer. C. Density plots showing gene expression in the adipose NKT10 cells from Figure 4.11.2.A.

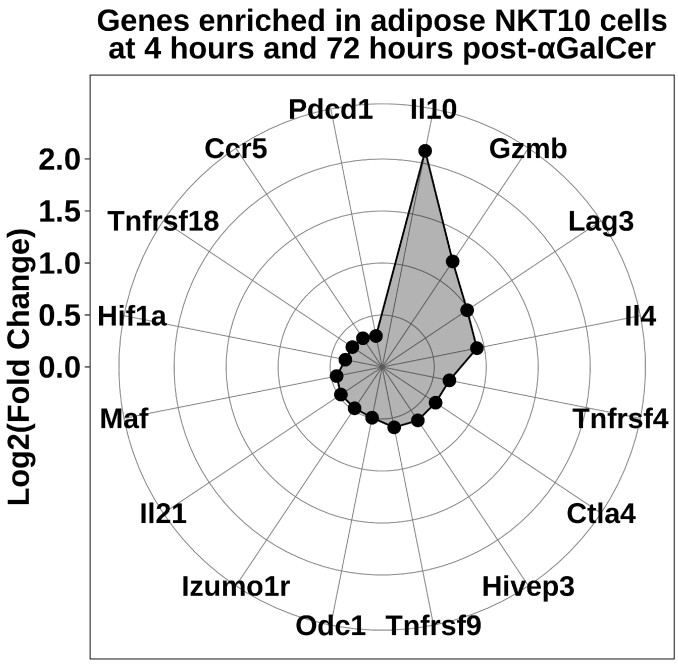
A.


Adipose NKT10 cells (833 cells)
UMAP 2
UMAP 1
72 hours post-αGalCer (805 cells)
4 hours post-αGalCer (28 cells)

B.


Il10
Gzmb
Il4
Il21
Ifng
Maf
UMAP 2
UMAP 1
Expression
Low
High

C.


Genes enriched in adipose NKT10 cells
at 4 hours and 72 hours post-αGalCer
Log2(Fold Change)
2.0
1.5
1.0
0.5
0.0
Pdcd1
Il10
Ccr5
Gzmb
Tnfrsf18
Lag3
Hif1a
Il4
Maf
Tnfrsf4
Il21
Ctla4
Izumo1r
Hivep3
Odc1
Tnfrsf9

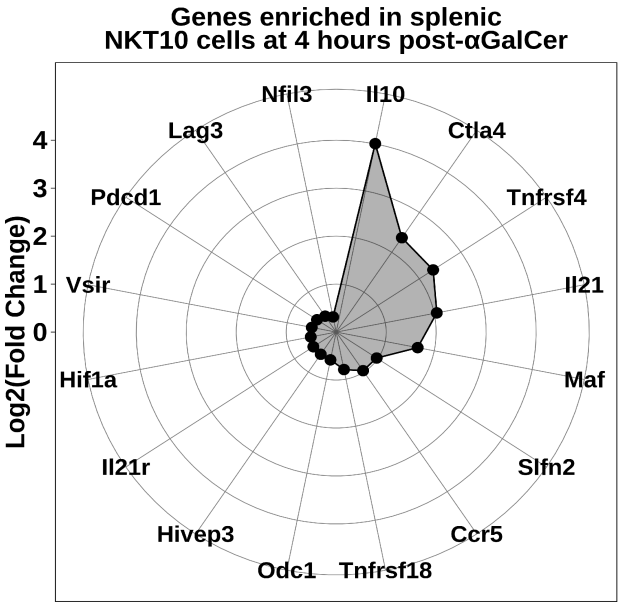
Having profiled the gene signature of adipose NKT10 cells, we next sought to identify genes shared between adipose and splenic NKT10 cells. To do this, we performed gene expression analysis of splenic NKT10 cells, leveraging both our activated and reactivated splenic iNKT cell data (Figure 4.6.1.A). We found that splenic NKT10 cells showed enrichment of many of the same genes as adipose NKT10 cells, including the Tr1 cell markers *Maf*, *Il21*, *Ccr5*, and *Hif1a*, the immunoregulatory receptors *Ctla4*, *Lag3*, and *Pdcd1*, the transcription factor *Hivep3*, *Tnfrsf18*, *Tnfrsf4*, and *Odc1* (Figure 4.11.3.A). Overlap analysis of adipose and splenic NKT10 cell DEGs identified a total of 39 genes that were constitutively enriched among NKT10 cells from both tissues (Figure 4.11.3.B) including *Maf*, *Il21*, *Slfn2*, *Vsir*, *Pdcd1*, *Ctla4*, *Lag3*, *Ccr5*, *Hif1a*, *Hivep3*, *Tnfrsf18*, and *Odc1*. Notably the conserved enrichment of many Tr1 cell markers among adipose and splenic NKT10 cells, such as *Maf*, *Il21*, *Ccr5*, and *Hif1a*, suggests that NKT10 cells may be functionally and phenotypically similar to Tr1 cells. Moreover, enrichment of *Il21*, an $NKT_{FH}$ cytokine, and other genes associated with $T_{FH}$ and $NKT_{FH}$ cells, such as *Maf*, *Lag3*, *Hi1fa* and *Pdcd1* (Figure 4.5), also suggests that NKT10 cells could be similar to $NKT_{FH}$ cells.

Interestingly, we identified enrichment of *Nfil3* (E4BP4) among splenic NKT10 cells. Since work by Lynch *et al.* (2015) and LaMarche *et al.* (2020) has shown that E4BP4 is a regulator of *Il10* among adipose iNKT cells, we wondered whether it might regulate expression of *Il10* among all NKT10 cells. To investigate this, we performed gene regulatory network (GRN) correlation analysis of *Il10* against *Nfil3* and all other transcription factors which were enriched among adipose and splenic NKT10 cells (Figure 4.11.3.C). We found that *Maf* was the most correlated transcription factor with *Il10*, and not *Nfil3* (Figure 4.11.3.C). Since we previously found that expression of *Maf* closely correlated with expression of *Il10* among both adipose and splenic iNKT cells (Figure 4.8.4, Figure 4.11.2), and cMAF is known to regulate production of IL-10 in other immune populations, such as Tr1 cells, B cells and

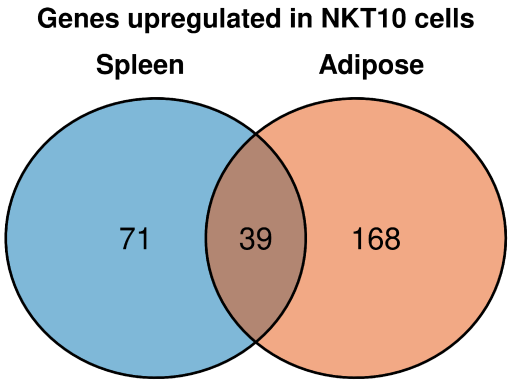
macrophages[361,370,371], our data therefore suggest that *Maf* is a major candidate regulator of NKT10 cells. To validate our analysis, and confirm that NKT10 cells expressed cMAF, we stimulated splenic iNKT cells at 4 weeks post-αGalCer with PMA and Ionomycin and stained for cMAF and IL-10. We found that $cMAF^+$ splenic iNKT cells produced significantly more IL-10 than $cMAF^-$ splenic iNKT cells (Figure 4.11.3.D, Figure 4.11.3.E), confirming that $cMAF^+$ iNKT cells are enriched for regulatory NKT10 cells, and demonstrating that cMAF is a novel marker for NKT10 cells. Notably, our data also validate our earlier hypothesis that memory-like $cMAF^+$ iNKT cells are an NKT10-like population or are enriched for NKT10 cells. Overall, our analysis suggests that NKT10 cells are an NKT1-like population of cells similar to adaptive Tr1 cells and $NKT_{FH}$ cells, and we identify cMAF as a novel marker and candidate regulator of NKT10 cells.

**Figure 4.11.3: Transcriptional analysis of NKT10 cells (part III; overleaf).** A. Radar chart showing selected genes enriched in activated and reactivated splenic NKT10 cells (normalized expression of *Il10* > 0), referenced from Figure 4.6.1.A after gene expression analysis versus all other activated and reactivated splenic iNKT cells. B. Venn diagram showing cross-analysis of genes enriched in splenic and adipose NKT10 cells. A sample of the overlapping genes between splenic and adipose iNKT cells is shown below the Venn diagram. C. Lollipop plot showing correlation values from GENIE3 analysis of *Il10* expression versus expression of *Nfil3* and transcription factors enriched in both adipose and splenic NKT10 cells. GENIE3 analysis was performed on all NKT10 cells (adipose and spleen) in a single normalized file. D. Representative contour plots of IL-10 expression in $cMAF^-$ or $cMAF^+$ resting splenic iNKT cells after 4 hours of stimulation with 50ng PMA and 1µg Ionomycin (*ex vivo*). iNKT cells were defined as live, single $CD19^-$ $CD8^-$ $CD11b^-$ $CD3^{low}$ CD1d $Tetramer^+$ cells. E. Box plots quantifying the data in Figure 4.11.2.D. N = 5 biological replicates from one experiment. Experiment performed once. Student's t-test. Asterisks denote significance, * $P < 0.05$; ** $P < 0.01$; *** $P < 0.001$. Horizontal lines represent median values.

A.

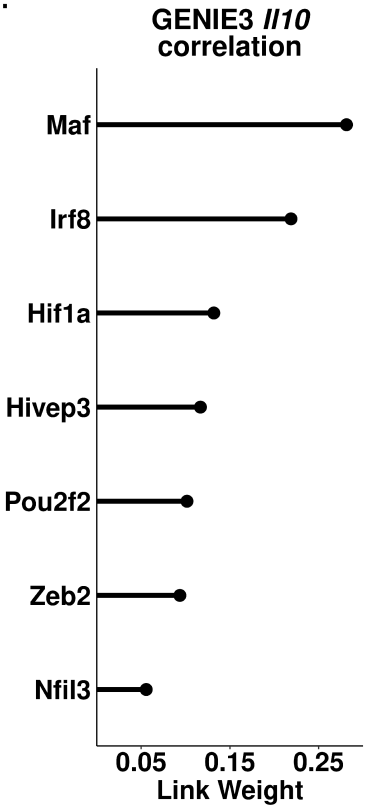



B.

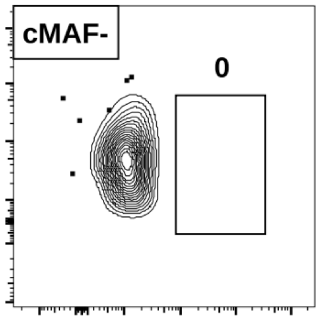


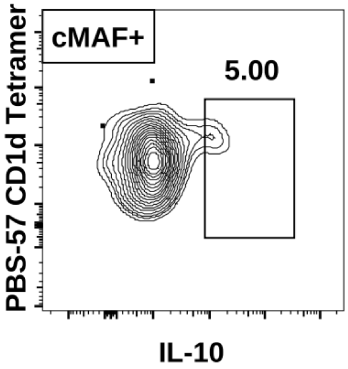

*Agpat4, Casp3, Ccr5, Ctla4, Hif1a, Hivep3, Il10, Il21, Lag3, Maf, Odc1, Pdcd1, Slfn2, Tgfb1, Tnfrsf18, Tnfrsf4, Vsir*

C.

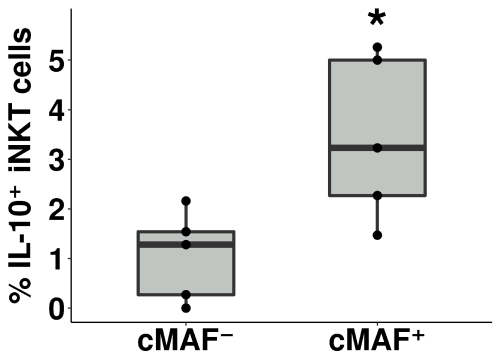



D.




E.



## Discussion

iNKT cells, like other innate immune cells, can rapidly respond to antigen and cytokine stimuli, and, upon activation, mount potent effector responses, especially cytokine production[352]. This enables iNKT cells to direct and potentiate downstream immune responses[115,183,185]. Similar to adaptive T cells, activated iNKT cells also proliferate and expand, forming an enlarged pool of cytokine competent cells that can participate in downstream effector responses[93,198,200]. Moreover, iNKT cell activation can induce the formation of long-lived memory-like iNKT cells, analogous to the formation of adaptive memory T cells[91,201,206]. Therefore, iNKT cell activation, and the response of iNKT cells to antigen, is multifaceted, and has hallmarks of both innate and adaptive immune responses[45]. In the first chapter of this thesis, we analyzed our scRNA-Seq data to profile early iNKT cell activation and gained insight into the different genes and transcriptional programs that underpin the rapid and potent response of iNKT cells to the prototypical glycolipid antigen, αGalCer[10]. In this second chapter, we sought to extend our scRNA-Seq analysis to downstream iNKT cell activation, including the expanded pool of iNKT cells at 72 hours post-αGalCer, and the contracted population of iNKT cells at 4 weeks post-αGalCer, when the iNKT cell response has subsided[91,198,200]. Our study also aimed to investigate the phenomenon of iNKT cell anergy, which has been reported after prior activation of iNKT cells with αGalCer[208], and to analyze the increased production of IL-10 by iNKT cells in response to secondary activation with αGalCer[16], similar to primary activation of adipose iNKT cells with αGalCer[49,91].

Comparative analysis of iNKT cells at steady state, 4 hours post-αGalCer, and 72 hours post-αGalCer revealed that iNKT cells undergo multiple rounds of transcriptional remodeling. Activation of iNKT cells with αGalCer induced an initial burst of rapid transcriptional reprogramming from 0-4 hours post-αGalCer, which coincided with acute cytokine production. iNKT cells then underwent a second round of transcriptional remodeling that coincided with

proliferation and expansion of iNKT cells over 2-3 days. We found that this first phase of transcriptional remodeling was characterized by increased expression of genes associated with iNKT cell and T cell activation, such as *Il2*, *Il2ra*, and *Myc*, upregulation of *Zbtb16* expression, and metabolic remodeling, including increased expression of genes associated with glycolysis, amino acid metabolism, and polyamine synthesis, while oxidative signatures were decreased. Notably, recent work by Fu *et al*. (2019) and Kumar *et al*. (2019) has shown that glucose is an important fuel for iNKT cell cytokine production[94,304], corroborating our transcriptional analysis. By contrast, we found that the second round of iNKT cell transcriptional remodeling was characterized by enrichment of transcripts associated with proliferation and the cell cycle, increased expression of genes linked to stem-like memory T cells and NKT2 cells, and the acquisition of features associated with memory-like iNKT cells. We also identified further remodeling of metabolic gene signatures, including downregulation of gene expression associated with amino acid metabolism and polyamine synthesis, while the expression of genes associated with oxidative metabolism was increased compared to iNKT cells at 4 hours post-αGalCer. Therefore, our data associate two distinct patterns of metabolic gene expression with different phases of iNKT cell activation, whereby iNKT cells may use aerobic glycolysis, amino acid metabolism and polyamine synthesis to fuel cytokine production and acute effector function, while oxidative metabolism may be used to support growth and proliferation of iNKT cells in tandem with glycolysis[156,160].

We also found that iNKT cells at 72 hours post-αGalCer were heterogeneous, and we identified differences between 72 hour adipose and splenic iNKT cells. Overall, cycling and G0/G1 iNKT cells were transcriptionally distinct, and we found that stem-like and memory-like gene expression was mostly associated with iNKT cells that were not actively proliferating. Among splenic iNKT cells, we found that expression of *Zbtb16* demarcated G0/G1 iNKT cell heterogeneity, with *Zbtb16*$^{high}$ NKT2 or stem-like iNKT cells and $NKT_{FH}$ cells

clustering together, and *Zbtb16*$^{low}$ NKT1-like cells and KLRG1$^{+}$ iNKT cells clustering together. Notably, previous work by Murray *et al*. (2021) has shown that NKT$_{FH}$ cells are transcriptionally similar to NKT2 cells, and that ~96% of KLRG1$^{+}$ iNKT cells are descended from T-bet$^{+}$ NKT1 cells[92], correlating with our scRNA-Seq analysis. Among adipose iNKT cells, we found that there was increased variation associated with NKT1-like cells expressing either *Klrg1* or *Klrb1c*, mirroring adipose iNKT cell heterogeneity at steady state[115]. Strikingly, we found that a subset of adipose iNKT cells were actively expressing markers of acute activation and cytokine production at 72 hours post-αGalCer, which was not the case for splenic iNKT cells. Notably, we previously demonstrated that adipose iNKT cells express markers of chronic endogenous activation at steady state, suggesting that the sustained activation of adipose iNKT cells at 72 hours post-αGalCer could be due to chronic endogenous stimulation of adipose iNKT cells. Alternatively, this finding could suggest that adipose iNKT cell activation is delayed compared to activation of iNKT cells in the spleen. 72 hours post-αGalCer also represented the peak of the regulatory response among adipose iNKT cells, with 72 hour adipose iNKT cells displaying enrichment of *Il10, Ctla4*, *Pdcd1*, and *Lag3*. This indicates that the regulatory response of adipose iNKT cells is delayed compared to the acute cytokine burst produced by splenic iNKT cells at ~4 hours post-αGalCer. Interestingly, enrichment of regulatory genes among adipose iNKT cells at 72 hours was associated with co-expression of genes linked to adaptive Tr1 cells, including *Maf*, *Il21*, *Gzmb*, *Ccr5*, and *Hi1fa*, suggesting that regulatory adipose iNKT cells may be similar to Tr1 cells.

After characterizing expanded iNKT cells at 72 hours post-αGalCer, we next turned our attention to long term transcriptional remodeling, iNKT cell anergy, and “trained” or memory-like iNKT cells, including KLRG1$^{+}$ iNKT cells, NKT$_{FH}$ cells, and iNKT10 cells. Analysis of splenic iNKT cells at 4 weeks post-αGalCer, when the iNKT cell response has subsided, identified preservation of steady state iNKT cell heterogeneity, including distinct NKT1, NKT2, and

NKT17 cell populations. Since past work by Murray *et al*. (2020) has shown that NKT1, NKT2, and NKT17 cells are not detectable at 6 days post-αGalCer[92], during the peak of the memory-like iNKT cell response, our analysis therefore suggests that steady state iNKT cell heterogeneity is reconstituted during late downstream iNKT cell activation, or possibly after the iNKT cell response has subsided. However, we also identified two memory-like iNKT cell populations that were not present at steady state, which we termed KLRG1$^+$ and cMAF$^+$ iNKT cells based on their respective enrichment of *Klrg1* and *Maf*. We found that KLRG1$^+$ and cMAF$^+$ iNKT cells were both broadly similar to NKT1 cells, displaying expression of NKT1 cell markers such as *Ccl5*, *Nkg7*, and *Slamf7*, but were otherwise highly transcriptionally distinct. KLRG1$^+$ iNKT cells showed enrichment of many genes previously associated with memory-like KLRG1$^+$ or NKT$_{eff}$ cells[92,206], including *Gzma*, *Gzmb*, *Cx3cr1*, *Spry2*, and *Klrk1*, and markers associated with terminally differentiated T$_{EM}$ and T$_{CM}$ cells, such as *Zeb2* and *S1pr5*[349,369]. Since *Zeb2* was the most highly enriched unique transcription factor associated with KLRG1$^+$ iNKT cells and was also expressed by the KLRG1$^{high}$ NKT$_{eff}$ cells previously analyzed by Murray *et al*. (2021)[92], we propose that ZEB2 could be a key regulator of memory-like KLRG1$^+$ iNKT cells. Functionally, we found that progressive enrichment of KLRG1$^+$ iNKT cells was correlated with progressively more blunted activation of splenic iNKT cells, while profiling of activated KLRG1$^+$ iNKT cells revealed enrichment of cytotoxic secreted factors such as *Gzma*, *Gzmb*, and *Prf1*.

By contrast, we found that cMAF$^+$ iNKT cells demonstrated increased expression of genes associated with NKT2 and NKT$_{FH}$ cells[46,61,92,173], including *Maf*, *Hif1a*, *Pdcd1*, *Cd4*, *Tox*, *Slamf6*, and *Tcf7*, and lacked expression of *Klrb1c*. Moreover, although we did not detect enrichment of *bona fide* NKT$_{FH}$ markers such as *Bcl6* or *Cxcr5*[201], we did find that cMAF$^+$ iNKT cells showed enrichment of a broad range of 19 NKT$_{FH}$ and T$_{FH}$ cell-associated genes compared to other iNKT cells, suggesting that cMAF$^+$ iNKT cells are

transcriptionally similar to $NKT_{FH}$ cells. $cMAF^+$ iNKT cells also displayed increased expression of genes associated with adipose $NK1.1^-$ NKT1 cells, including *Serpina3g*, *Serpina3f*, and *Chst2*, and Tregs[329,372], such as *Ctla4*, *Lag3*, *Pdcd1*, and *Izumo1r*, raising the possibility that $cMAF^+$ iNKT cells might constitute a regulatory population of iNKT cells. In agreement with this finding, we found that expression of *Il10* was highly correlated with expression of *Maf* among reactivated splenic iNKT cells, suggesting that $cMAF^+$ cells are a regulatory population of memory-like iNKT cells, similar to iNKT10 cells[16,91]. Moreover, we found that expression of *Il10* and *Maf* was highly correlated with expression of *Il21*, a flagship $NKT_{FH}$ cell cytokine[202], underscoring the relatedness of $cMAF^+$ and $NKT_{FH}$ cells. Co-expression of *Il21*, *Maf*, and *Il10* is also associated with Tr1 cells[361,365], suggesting that $cMAF^+$ iNKT cells might be similar to adaptive Tr1 cells. Like $KLRG1^+$ iNKT cells, we found that progressive enrichment of $cMAF^+$ iNKT cells was correlated with progressively more blunted activation of splenic iNKT cells. Therefore, our analysis links the anergic phenotype of antigen experienced iNKT cells to enrichment of memory-like $KLRG1^+$ and $cMAF^+$ iNKT cells. Interestingly, both $KLRG1^+$ and $cMAF^+$ iNKT cells displayed enrichment of the integrin subunits *Itga4* and *Itgb1*; since integrins are known to modulate TCR signaling[373], and we specifically linked $KLRG1^+$ and $cMAF^+$ iNKT cells with reduced iNKT cell activation, it is possible that integrins could modulate the response of $KLRG1^+$ and $cMAF^+$ iNKT cells to TCR stimulation.

We also analyzed the phenotype of adipose iNKT cells at 4 week post-αGalCer. Strikingly, we found that adipose iNKT cells demonstrated enrichment of many of the same markers as splenic iNKT cells at 4 weeks post-αGalCer, including the $cMAF^+$ and $KLRG1^+$ iNKT cell markers *Maf* and *Zeb2*. We also found that adipose and splenic iNKT cells were more transcriptionally similar at 4 weeks post-αGalCer than at steady state, suggesting that activation with αGalCer induces similar long term transcriptional remodeling among both adipose and splenic iNKT cells. Overall,

however, we found that the magnitude of transcriptional remodeling was reduced among adipose versus splenic iNKT cells at 4 weeks post-αGalCer, suggesting that adipose iNKT cells are less changed following activation with αGalCer. Notably, we previously found that steady state adipose iNKT cells constitutively express markers associated with antigen experience, such as *Maf*, *Klrg1*, *Itgb1*, and *Itga4*[49,115], suggesting that adipose iNKT cells are already antigen experienced at steady state. Granular analysis revealed that the frequency of adipose NKT17 cells was greatly reduced at 4 weeks post-αGalCer, and this loss of NKT17 cells constituted the single largest change in any individual adipose iNKT cell population. Notably, the frequency of NKT17 cells was also reduced at 72 hours post-αGalCer, suggesting that adipose NKT17 cells either do not proliferate and expand to the same extent as adipose NKT1 cells, or that αGalCer does not induce a proliferative response among adipose NKT17 cells. Aside from NKT17 cells, adipose iNKT cells at 4 weeks post-αGalCer also demonstrated enrichment of populations similar to memory-like splenic cMAF$^{+}$ and KLRG1$^{+}$ iNKT cells. This indicates that while there are already iNKT cells expressing *Klrg1* and *Maf* in the adipose tissue at steady state[49,115], activation of adipose iNKT cells with αGalCer may promote the accumulation of memory-like cMAF$^{+}$ and KLRG1$^{+}$ iNKT cells in adipose tissue, as it does in the spleen.

Our last major question to address as part of this thesis was the phenotype of NKT10 cells, and the relationship between NKT10 cells constitutively present in adipose tissue versus iNKT10 cells induced in organs such as the spleen after prior activation with αGalCer[16,49,91,115]. Interestingly, we found that adipose NKT10 cells were heterogeneous, particularly at 72 hours post-αGalCer, with some adipose NKT10 cells displaying co-expression of *Il10*, *Il21*, and *Il4*, while other adipose NKT10 cells co-expressed *Il10* and *Gzmb*. Notably, this heterogeneity is reminiscent of the phenotype of Tr1 cells[359,365], and we also found that adipose NKT10 cells displayed enrichment of many different Tr1 cell markers, including *Maf*, *Il21*, *Hif1a*, and *Ccr5* [358,361,363,365], suggesting that

adipose NKT10 cells may be phenotypically and functionally similar to Tr1 cells. We also found that adipose NKT10 cells expressed *Ifng*, a marker of NKT1 cells, and expression of *Il10* at 4 hours post-αGalCer was specific to adipose NKT1 cells. Therefore, our data suggest that adipose NKT10 cells are a subset of NKT1 cells or are an NKT1 cell-like population. Moreover, the enrichment of *Il21* among adipose NKT10 cells suggests that NKT10 cells might be similar to $NKT_{FH}$ or $T_{FH}$ cells.

We also analyzed the phenotype of splenic NKT10 cells. Intriguingly, we found that splenic iNKT cells expressed many of the same top DEGs as adipose NKT10 cells, including *Maf*, *Il21*, the immunoregulatory receptors *Ctla4*, *Pdcd1*, and *Lag3*, the tolerogenic factors *Slfn2* and *Vsir*[374,375], and Tr1 cell markers such as *Ccr5* and *Hif1a*. Using overlap analysis, we identified a core set of 39 genes that were constitutively enriched in NKT10 cells, regardless of tissue localization, indicating that diverse NKT10 cell populations share expression of a core network of genes. Importantly, correlation of *Il10* expression against these 39 genes identified cMAF as the most highly associated transcription factor with *Il10*, and we found that $cMAF^+$ splenic cells displayed increased production of IL-10 compared to $cMAF^-$ iNKT cells at 4 weeks post-αGalCer. Therefore, our data collectively identify cMAF as a candidate regulator and marker of NKT10 cells. This finding also retroactively identifies $cMAF^+$ iNKT cells in the adipose tissue and the spleen as NKT10 cell populations, or populations that are highly enriched for NKT10 cells, providing new insights into the biology of NKT10 cells across different tissues and activation states. Overall, our work identifies a conserved gene signature associated with NKT10 cells and suggests that NKT10 cells are a population of $cMAF^+$ iNKT cells that are transcriptionally similar to adaptive Tr1 cells, NKT1 cells, and $NKT_{FH}$ cells.

# Chapter 5: General Discussion

From simple beginnings with the identification of a $CD4^+$ $NK1.1^+$ population of Vα14-Jα18-restricted T cells[3,4,376], the study of iNKT cells has greatly expanded over the last 20-25 years, and it is now clear that there are multiple layers of heterogeneity within the iNKT cell repertoire. Not only does a branching developmental pathway in the thymus give rise to functionally distinct NKT1, NKT2, and NKT17 iNKT cell subsets[46,61,64,65], but iNKT cells also differentially localize to and become resident in a diverse array of tissues, where they can acquire highly unique and tissue-specific phenotypes[33,49,50,115,138]. Furthermore, beyond this steady state diversity, there are dramatic temporal changes in the phenotype of iNKT cells during effector responses. iNKT cells rapidly undergo activation in response to TCR and cytokine stimuli[13,247], and can mount potent innate-like cytokine responses, allowing this relatively small cohort of T cells to orchestrate and potentiate downstream immune responses[49,115,183,185,242]. Like adaptive T cells, activated iNKT cells also proliferate, leading to a massive increase in the number of iNKT cells over several days[198,200], and the formation of an expanded pool of effector cells[93]. Thereafter, this expanded population of iNKT cells contracts, typically returning to baseline frequencies within 1-2 weeks[198,200].

However, activation can also promote long term changes in iNKT cell phenotype and function. For example, novel populations of “trained” or memory-like iNKT cells have been shown to appear as early as 3 days post-activation[203]. These memory-like cells, including $NKT_{FH}$ cells and $KLRG1^+$ iNKT cells, become greatly expanded during iNKT cell activation, typically after ~5-7 days, but can also persist for weeks to months after activation subsides[92,202,206]. Curiously, antigen experienced iNKT cells can also become hyporesponsive to secondary activation[91,195,208], similar to how adaptive T cells can become exhausted or anergic[170,377]. It should be noted that this phenotype appears to be linked to changes in TCR signaling, or to changes in the responsiveness of iNKT cells to TCR stimulation, as the bypass of proximal TCR signaling events during secondary activation is sufficient to overcome iNKT cell anergy[208].

Another interesting phenomenon associated with antigen experienced iNKT cells is the regulatory polarization of cytokine responses. Secondary activation of antigen experienced iNKT cells results in increased production of IL-10[16,91], a cytokine which is not typically produced by most iNKT cells[17]. Notably, increased production of IL-10 during iNKT cell reactivation has been linked to the expansion of a dedicated population of IL-10-producing iNKT cells, known as NKT10 cells[91], which may be memory-like. Intriguingly, a similar regulatory phenotype has also been described for iNKT cells resident in the lipid rich environment of adipose tissue. Primary activation of adipose iNKT cells with αGalCer produces a muted cytokine response, similar to anergic antigen experienced iNKT cells, and increased production of IL-10[33,49,115]. Many adipose iNKT cells also express markers associated with “trained” or memory-like iNKT cells, such as CD49d (*Itga4*) and KLRG1, suggesting that adipose iNKT cells might already be antigen experienced or memory-like at steady state.

Against this backdrop of multifaceted iNKT cell heterogeneity, we sought to perform transcriptional characterization of iNKT cells, especially activated and memory-like iNKT cells. The transcriptional signatures underpinning adaptive $CD8^+$ and $CD4^+$ T cell activation and memory formation have been extensively studied in recent years, and there are numerous transcriptomic resources available for interrogation of different T cell activation states[153,154,156,173,329,378]. However, there are markedly fewer transcriptomic resources available for the investigation of iNKT cell activation, and the transcriptional profiles of some iNKT cell activation states, such as the expanded pool of iNKT cells at 72 hours post-αGalCer, have not previously been characterized, to the best of our knowledge. Therefore, to address this issue, we took advantage of modern high-throughput technology, and performed scRNA-Seq of 48,813 iNKT cells, the largest number of iNKT cells analyzed using scRNA-Seq to date, To assay as broad a range of iNKT cell activation states and subsets as possible, we performed sequencing of sorted whole iNKT cells after *in vivo* activation with

αGalCer, and isolated iNKT cells at steady state, 4 hours post-αGalCer, 72 hours post-αGalCer, and 4 weeks post-αGalCer, and we sequenced iNKT cells from two different organs, spleen and adipose tissue. To complement our scRNA-Seq analysis, we also reanalyzed several different published iNKT cell transcriptomic resources, including recent scRNA-Seq of human iNKT cells by Erkers *et al*. (2020), Zhou *et al*. (2020), and Gutierrez-Arcelus *et al*. (2019)[133–135], and bulk RNA-Seq and microarray resources published by Murray *et al*. (2021) and Sag *et al*. (2014)[91,92]. Collectively, this data enabled us to construct a transcriptomic atlas of iNKT cell activation, and gain insight into this highly dynamic and heterogeneous population. While it should be noted that iNKT cells can be activated by a multitude of ligands, many of which induce responses that are substantially different to the response induced by αGalCer, such as the response induced by OCH[15,379] for example, we chose to use αGalCer in our study as αGalCer is the most widely used ligand in the field of iNKT cell biology. Therefore, by using αGalCer, we hope that our study and findings will be as widely applicable and useful as possible for other researchers in the field, even if αGalCer itself is not representative of the entire spectrum of iNKT different cell ligands.

The first major finding of this study is that adipose iNKT cells are heterogeneous. Numerous previous studies have shown that murine iNKT cells can be separated into functionally distinct NKT1, NKT2, and NKT17 cells subsets across most organs[55–57,59,60,67]. However, at the time of starting my PhD, it was unknown if this was also the case for adipose iNKT cells. Past work by Lynch *et al*. (2015) has shown that adipose iNKT cells are an unusual regulatory population of iNKT cells that display increased production of IL-10, reduced expression of the master iNKT cell transcription factor PLZF (*Zbtb16*), and unique expression of the bZIP transcription factor E4BP4 (*Nfil3*)[49]. Therefore, it was unclear whether adipose iNKT cells would exhibit heterogeneity, and, if so, whether adipose iNKT cell heterogeneity would mirror the NKT1, NKT2, and NKT17 cell diversity described for iNKT cells in other

tissues. We identified three main adipose iNKT cell subsets, including two populations of NKT1 cells, and a population of NKT17 cells. Surprisingly, we found that NKT2 cells were not present in the adipose tissue of adult mice, and work by LaMarche *et al*. (2020) demonstrated that PLZF$^{high}$ NKT2-like cells were only detectable in the adipose tissue of neonatal mice[115]. We found that the two different NKT1 cell populations could be separated by expression of NK1.1 (*Klrb1c*), which has historically been an important marker for delineation of functional iNKT cell heterogeneity[56,107]. Transcriptionally, we found that NK1.1$^{+}$ iNKT cells displayed enrichment of cytotoxic gene signatures, whereas NK1.1$^{-}$ NKT1 cells showed enrichment of many of the markers previously associated with the adipose iNKT cell phenotype[49,91], such as *Il2*, and the "trained" or memory-like markers *Klrg1* and *Itga4*. Notably, work by LaMarche *et al*. (2020) showed that this transcriptional diversity also translated to functional diversity, as NK1.1$^{-}$ adipose iNKT cells were found to be the main producers of IL-10, IL-2, IL-4 and IL-13, whereas NK1.1$^{+}$ iNKT cells were more biased towards production of IFNγ[59,60,67,93,115]. Therefore, our work demonstrates that adipose NK1.1$^{-}$ NKT1 cells may be representative of the flagship regulatory adipose iNKT cell phenotype identified from bulk characterization of iNKT cells[49], whereas adipose NK1.1$^{+}$ NKT1 and NKT17 cells exemplify newfound heterogeneity within the adipose iNKT cell repertoire.

We also utilized our scRNA-Seq data to profile the transcriptional differences between adipose and splenic iNKT cells, building off previous work by Lynch *et al*. (2015)[49]. We found that steady state adipose iNKT cells showed increased expression of genes associated with ER stress, proliferation, apoptosis, targeted cytotoxicity, senescence, the actin cytoskeleton, and adhesion, while subsequent analysis of activated and antigen experienced adipose iNKT cells also revealed enrichment of many signaling pathways, including TCR signaling, chemokine signaling, IL-17 signaling, HIF-1 signaling, and PI3K-AKT signaling. By contrast, splenic iNKT cells displayed increased expression of ribosomal genes, and genes associated with oxidative

phosphorylation. Interestingly, profiling of transcription factor enrichment among adipose iNKT cells identified many factors associated with chronic activation and T cell exhaustion[170,172], including *Nr4a1*, *Nr4a2*, *Nr4a3*, *Nfatc1*, *Nfatc2*, and *Tox*. We also found that adipose iNKT cells demonstrated blunted activation and cytokine gene expression at 4 hours post-αGalCer, and we observed that adipose iNKT cells maintained expression of cytokine and activation markers at 72 hours post-αGalCer, even though activation and cytokine expression had already largely subsided among splenic iNKT cells. Overall, our data suggest that adipose iNKT cells may be constitutively chronically activated, possibly as a result of the lipid rich environment that they inhabit, and we hypothesize that chronic activation could blunt their ability to undergo further rapid activation after stimulation with strong lipid antigens such as αGalCer. Furthermore, our chronic activation hypothesis provides a possible explanation for many of the unusual features associated with adipose iNKT cells, including increased proliferation and increased expression of activation markers such as IL-2 and Nur77 at steady state[49], and constitutive enrichment of the memory-like markers KLRG1 and CD49d[49,91].

After profiling murine iNKT cell heterogeneity in the spleen and adipose tissue, we also assayed human iNKT cell heterogeneity by reanalyzing scRNA-Seq data from three recent publications, Erkers *et al*. (2020), Zhou *et al*. (2020), and Gutierrez-Arcelus *et al*. (2019). Most previous studies of human iNKT cell heterogeneity have focused on phenotypic and functional differences between $CD4^+$, $CD8^+$, and $CD4^-$ $CD8^-$ iNKT cells[91,122,125–127,182,183,284], as there are not thought to be human iNKT cell subsets equivalent to murine NKT1, NKT2, and NKT17 cells. Surprisingly, when we performed meta-analysis of human iNKT cells we did not identify differential expression of CD4 and CD8 at steady state, and instead we found that human iNKT cells separated on the basis of *GMZB*, *GZMK*, and *LEF1* expression. $GZMB^+$ iNKT cells displayed enrichment of many genes associated with cytotoxicity, while $LEF1^+$ iNKT cells co-expressed CCR7, suggesting that $LEF1^+$ iNKT cells might represent an

immature precursor population, similar to the LEF1$^{+}$ CCR7$^{+}$ progenitor iNKT cells found in mice[66]. However, analysis of activated human iNKT cells revealed that enrichment of *CD8* correlated with increased expression of granzymes and cytotoxic genes, including *GZMB*, and the chemokines *CCL4* and *CCL3*, aligning with previous reports indicating that CD8$^{+}$ human iNKT cells are similar to NK cells, Th1 cells, and murine NKT1 cells[122,125,128]. Conversely, enrichment of *CD4* correlated with increased expression of *TNF*, *IL2*, *IL4*, and *IL13*, suggesting that CD4$^{+}$ iNKT cells are similar to T helper cells, and produce more Th2 cytokines[122]. Aligning with the literature, we did not identify discrete human iNKT cell subsets equivalent to murine NKT1, NKT2, and NKT17 cells, and we noted that almost all human iNKT cells expressed *IFNG* in response to acute activation, indicating that most human iNKT cells may be similar to murine NKT1 cells. Overall, we did not identify the same degree of variation among human iNKT cells as we had found for murine iNKT cells.

One of the primary goals of this study was to characterize the transcriptional programs and gene signatures underpinning iNKT cell activation, including the transcriptional remodeling undergone by iNKT cells across different activation states. Therefore, we performed *in vivo* activation of iNKT cells with αGalCer, and sequenced iNKT cells at two key stages of activation: during acute activation at 4 hours post-αGalCer[17], and during downstream activation at 72 hours post-αGalCer, when iNKT cells are greatly expanded[93,198,200]. Acutely activated iNKT cells at 4 hours post-αGalCer were enriched for T cell activation markers and cytokines and showed increased expression of a suite of different transcription factors, including *Zbtb16*, *Irf4*, *Irf8*, EGR, NR4A, and NF-κB family members, *Bzw1*, and *Bhlhe40*. Acute iNKT cell activation also induced metabolic gene remodeling, and we identified increased expression of gene signatures associated with glycolysis, amino acid uptake and metabolism, and polyamine synthesis, while gene expression associated with oxidative metabolism was reduced. This suggests that acutely activated iNKT

cells may become less reliant on oxidative metabolism, upregulate glycolysis, and increase their uptake and production of metabolites to support different biosynthetic pathways, such as transcription and translation for cytokine production. Interestingly, this metabolic phenotype is similar to that of activated adaptive T cells, as aerobic glycolysis, amino acid metabolism, and polyamine synthesis have been documented to fuel and regulate T cell growth, proliferation, differentiation, and effector function[152,155,160–162]. However, while adaptive T cells undergo metabolic remodeling over the course of several days[152,156,160], iNKT cells displayed complete remodeling of metabolic gene signatures after just a few hours, in concert with innate-like cytokine production. This temporal difference may be reflective of the “poised” phenotype of iNKT cells, whereby iNKT cells emerge from the thymus as memory/effector cells already capable of rapidly responding to antigen[42,43]. Notably, we found that acutely activated human iNKT cells displayed an almost identical pattern of transcriptional remodeling to acutely activated murine iNKT cells, suggesting that a conserved transcriptional framework underpins acute iNKT cell activation.

We also found identified similar patterns of gene expression among acutely activated NKT1, NKT2 and NKT17 cells, in both spleen and adipose tissue, although as we had found with bulk adipose iNKT cells, adipose NKT1 and NKT17 cell activation was blunted compared to that of splenic iNKT cells. Therefore, our analysis demonstrates that conserved transcriptional motifs underpin the activation and effector function of phenotypically and functionally diverse iNKT cell subsets. This finding is supported by recent work from Kumar *et al*. (2019), who demonstrated that production of Th1, Th2, and Th17 cell cytokines by iNKT cells is dependent on glucose uptake[304], suggesting that glucose is used by all iNKT cell subsets to support effector cytokine production. Notably, activated NKT1, NKT2, and NKT17 cells also displayed differential gene expression, and we found that activated NKT2 and NKT17 cells displayed enrichment of genes associated with oxidative phosphorylation.

This finding correlated with an enhanced mitochondrial phenotype among NKT2 and NKT17 cells, and we found that production of IL-4, IL-13, and IL-17 by thymic NKT2 and NKT17 cells was significantly more dependent on oxidative phosphorylation than production of IFNγ by thymic NKT1 cells. Recent work by Zhao *et al*. (2021) and Raynor *et al*. (2020) has shown that mitochondrial or oxidative metabolism is enriched among NKT2 and NKT17 cells versus NKT1 cells in the thymus and during thymic development, and downregulation of oxidative metabolism is required for NKT1 cell differentiation[302,303]. Here we suggest that this bias towards oxidative metabolism persists among NKT2 and NKT17 cells after development, and, crucially, may regulate their function. Interestingly, we also identified increased expression of oxidative metabolic signatures among adipose NKT17 cells, and a recent study by Lopes *et al*. (2021) has shown that oxidative metabolism is enriched among γδ17 cells versus γδ1 cells[109]. Therefore, we hypothesize that oxidative metabolic enrichment may be a conserved feature of IL-17-producing innate T cells.

After an initial phase of transcriptional remodeling during acute iNKT cell activation, we found that iNKT cells underwent a second round of transcriptional reprogramming from 4 hours post-αGalCer to 72 hours post-αGalCer. This period of downstream activation was characterized by enrichment of genes associated with proliferation and the cell cycle, increased expression of stem-like memory T cell and NKT2 or NKTp cell markers, and the acquisition of gene signatures associated with memory-like $NKT_{FH}$ cell and $KLRG1^{+}$ iNKT cells. We also identified further remodeling of cellular metabolic programs. Gene expression associated with glycolysis remained elevated from 4 hours post-αGalCer, but amino acid metabolism and polyamine synthesis signatures were downregulated, and we instead identified enrichment of oxidative metabolism. This suggests that iNKT cells modify their metabolic profile throughout different stages of activation, possibly in response to changing metabolic requirements. Functionally, our data also specifically link

amino acid and polyamine metabolism to acute iNKT cell activation and effector cytokine production, whereas co-enrichment of glycolytic and oxidative metabolism may support iNKT cell proliferation. Interestingly, we found that the phenotype of splenic and adipose iNKT cells was distinct at 72 hours post-αGalCer. While cytokine production was largely diminished among splenic iNKT cells after 72 hours, adipose iNKT cells continued to produce cytokines, and we found that the expression of regulatory genes, such as *Il10*, *Pdcd1*, *Ctla4*, and *Lag3*, was highest among adipose iNKT cells at 72 hours post-αGalCer. This demonstrates that the peak of the regulatory response mounted by activated adipose iNKT cells is significantly delayed compared to the rapid, inflammatory cytokine burst among activated splenic iNKT cells. Other differences between adipose and splenic iNKT cells at 72 hours post-αGalCer included enrichment of promigratory genes in the KLF2 regulon among splenic iNKT cells, and increased expression of markers associated with adaptive Tr1 cells among adipose iNKT cells, including *Maf*, *Ccr5*, *Hif1a*, *Il21*, *Gzmb*, and *Gzma*, suggesting that regulatory adipose iNKT cells may be phenotypically and functionally similar to adaptive Tr1 cells[358,361,363–365].

After characterizing activated iNKT cells at 72 hours post-αGalCer, we next turned our attention to memory-like and antigen experienced iNKT cells. Analysis of splenic iNKT cells at 4 weeks post-αGalCer revealed blunted activation in response to secondary αGalCer stimulation, matching previous reports of anergy among antigen experienced iNKT cells[91,195,208], and we found that this blunted response was linked to the appearance of two memory-like iNKT cell populations, KLRG1$^+$ and cMAF$^+$ iNKT cells. KLRG1$^+$ iNKT cells displayed enrichment of many genes previously associated with “trained” $NKT_{eff}$ and KLRG1$^+$ iNKT cell populations[92,206], including *Gzma*, *Klrk1*, *Spry2*, and *Cx3cr1*, and also expressed the transcription factor *Zeb2*. ZEB2 is a known marker of terminally differentiated KLRG1$^+$ CD8$^+$ $T_{CM}$ and $T_{EM}$ cells[349,369], suggesting that KLRG1$^+$ iNKT cells are phenotypically similar to effector memory CD8$^+$ T cells. By contrast, cMAF$^+$ iNKT cells demonstrated enrichment

of many genes associated with adipose NK1.1$^-$ NKT1 cells and $NKT_{FH}$ cells, and we found that expression of *Maf* was highly correlated with expression of both *Il10* and *Il21* among reactivated splenic iNKT cells, indicative of a regulatory or follicular-like phenotype[92,115,201,202]. cMAF$^+$ iNKT cells also expressed the stem-like memory T cell markers *Slamf6* and *Tcf7*[100], and the precursor exhausted T (TPEX) cell markers *Pdcd1*, *Ctla4*, and *Lag3*[174].

Intriguingly, this finding suggests that memory-like or “trained” iNKT cell differentiation could follow a bifurcating trajectory, similar to the established memory precursor effector (MPEC) and short-lived effector (SLEC) cell model for CD8$^+$ T cell differentiation[167], whereby activated iNKT cells may undergo differentiation along either an effector-like (KLRG1$^+$, $NKT_{eff}$) or a regulatory/follicular/stem-like (cMAF$^+$, $NKT_{FH}$) pathway. In support of our hypothesis, we also identified memory-like cMAF$^+$ and KLRG1$^+$ iNKT cells in adipose tissue at 4 weeks post-αGalCer, suggesting that these two memory-like iNKT cell populations are a conserved component of the antigen experienced iNKT cell repertoire. Notably, although it has been reported that NKT1, NKT2, and NKT17 cells are not detectable during downstream iNKT cell activation[92], we were able to identify distinct NKT1, NKT2, and NKT17 cell populations at 4 weeks post-αGalCer, indicating that these iNKT cell subsets reappear as the iNKT cell response subsides. NKT1, NKT2, and NKT17 cells were also independent of cMAF$^+$ and KLRG1$^+$ iNKT cells, which could indicate that not all activated iNKT cells undergo differentiation into a memory-like iNKT cell state. Further analysis of late iNKT cell activation will be required to identify the stage at which NKT1, NKT2, and NKT17 cells become re-established, and how this process occurs.

Our analysis of adipose and antigen experienced iNKT cells also enabled us to assay the transcriptional phenotype of NKT10 cells. In the recent study by LaMarche *et al*. (2020), we showed that lipid-induced ER stress activates the IRE1a-XBP1s arm of the unfolded protein response (UPR), which in turn drives expression of the transcription factor E4BP4 (*Nifl3*)[115]. Work by Lynch *et*

*al*. (2015) has demonstrated that E4BP4 is a key regulator of IL-10 expression among adipose iNKT cells[49], indicating that the lipid rich environment of adipose tissue plays an important role in establishing the distinctive regulatory phenotype of its resident iNKT cell population. However, during our analysis of activated adipose iNKT cells, we noted that IL-10 is only expressed by a subset of cells[115], whereas E4BP4 is expressed by most adipose iNKT cells. This suggested that one or more additional factors might co-regulate IL-10 among adipose iNKT cells. Work by Motomura *et al*. (2011) has also shown that E4BP4 binds to an intronic, non-coding region of the IL-10 promoter[380], suggesting that one or more additional factors might be required to induce *Il10* transcription.

In this study we identified the transcription factor cMAF as candidate regulator of IL-10 in iNKT cells, correlating with previous studies demonstrating that cMAF regulates the expression of IL-10 in diverse immune population such as macrophages, B cells, and adaptive T cells[361,370,371]. While NKT17 cells are known to express cMAF, we did not identify co-expression of *Il10* and *Il17a* or *Il17f* within our data, and most NKT10 cells expressed *Ifng*, suggesting that NKT10 cells may arise from an NKT1 cell lineage, rather than an NKT17 cell lineage, at least among iNKT cells in the spleen and adipose tissue. Interestingly, cMAF is also expressed by adaptive Tr1 cells, and we identified conserved enrichment of many Tr1 cell markers among both splenic and adipose NKT10 cells, including *Maf*, *Il21*, *Hif1a*, and *Ccr5*[358,363,365]. This suggests that NKT10 cells may be functionally and phenotypically similar to adaptive Tr1 cells. Other conserved genes from our NKT10 cell analysis included the tolerogenic factors *Slfn2* and *Vsir*, the polyamine enzyme *Odc1*, the immunoregulatory receptors *Pdcd1*, *Lag3*, and *Ctla4*, *Tnfrsf18*, encoding GITR, *Tnfrsf4*, *Casp3*, and the acyltransferase *Agpat4*. Overall, we identified a core network of 39 genes which were enriched among adipose and splenic NKT10 cells, providing new insight into the phenotype and function of this elusive, unusual iNKT cell population.

Our use of scRNA-Seq in this study enabled us to survey the transcriptional landscape of iNKT cells in unparalleled detail, and assay the phenotype of heterogeneous iNKT cell subsets, such as NKT1, NKT2, NKT17, and NKT10 cells. However, scRNA-Seq is known to display a high incidence of dropout values, especially 10x scRNA-Seq[381,382], and sequencing depth is limited compared to bulk methods. Since our study was primarily based on scRNA-Seq data, therefore, we acknowledge that further work at the protein level will be required to fully validate and expand upon many of the findings in this study. However, we sought to mitigate this as much as possible by reanalyzing bulk sequencing data, where available, and we used flow cytometry to validate key findings such as adipose iNKT cell heterogeneity[115], oxidative metabolic enrichment among NKT2 and NKT17 cells, and enrichment of "trained" cMAF$^{+}$ and KLRG1$^{+}$ iNKT cells after prior activation with αGalCer. Some of the follow-up experiments that could be performed to extend the findings in this thesis include further analysis of the metabolic phenotype of iNKT cells, further exploration of the relationship between NKT10 and $NKT_{FH}$ cells at the protein level, and analysis of the role of cMAF in iNKT cells, especially NKT10 cells. We attempted to breed mice specifically lacking expression of cMAF among all cells that previously expressed CD4, including iNKT cells, but we were not able to obtain enough mice for experiments in time for the submission of this thesis. As of the writing of this thesis, we have received reviewer comments on our submitted manuscript Kane *et al*. (2021), and further experiments may be performed as part of the re-submission of this manuscript[383].

We believe that the findings from this study are significant in the field of innate T cells, and may also be informative or useful in several other fields, such as adipose tissue biology, and tumor immunology. Understanding which factors control the phenotype, function, and generation of NKT10 cells has several possible applications. For example, NKT10 cells have been shown to emerge in tumors, where they can promote tumor growth and enhance the function of other regulatory immune cells, such as Tregs[261]. However, our work suggests

that NKT10 cells can co-express *Ifng* and *Il10*. Skewing NKT10 cells towards a less regulatory phenotype by enhancing IFNγ and inhibiting IL-10 might have a therapeutic benefit in tumors where NKT10 cells are present. With respect to adipose tissue, work by Lynch *et al*. (2015; 2016) and LaMarche *et al*. (2020) has shown that adipose iNKT cells can induce weight loss through induction of FGF21 production by adipocytes and suppress inflammation in the adipose tissue through production of regulatory cytokines and trans-activation of adipose Tregs[49,115,138]. Moreover, although iNKT cells are typically rarer in humans than in mice, research by Lynch *et al*. (2009) has shown that iNKT cells are specifically enriched in human adipose tissue[33]. This suggests that modulation of adipose iNKT cells might be beneficial during obesity and metabolic syndrome, although a detailed understanding of adipose iNKT cells will be required in order to potentially harness these cells for therapeutic benefit. More generally, our insights into the factors and transcriptional signatures governing iNKT cell activation may be relevant to other innate T cells, as γδ T cells and MAIT cells respond similarly to iNKT cells after activation[1]. Therefore, the transcriptomic atlas of different iNKT cell activation states that we present here may assist other studies investigating innate T cell responses. In conclusion, our study reveals new insights into iNKT cell heterogeneity, phenotype, and function, and provides a collection of new transcriptomic resources for the analysis and interrogation of iNKT cell biology.

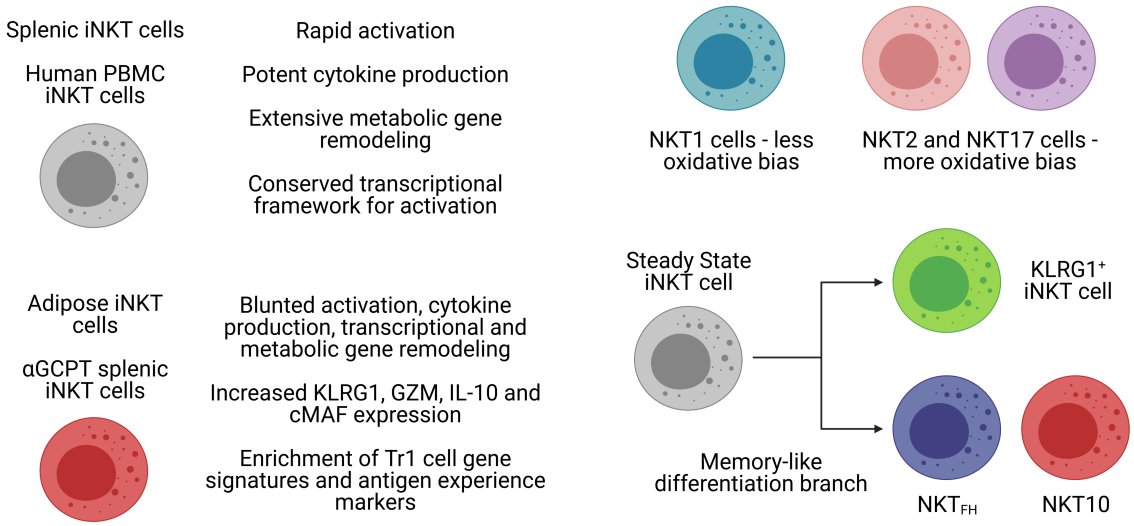



**Figure 5.1: Graphical summary of key findings**

# References


1. Godfrey, D. I., Uldrich, A. P., McCluskey, J., Rossjohn, J. & Moody, D. B. The burgeoning family of unconventional T cells. *Nat. Immunol.* **16**, 1114–1123 (2015).
2. Godfrey, D. I., MacDonald, H. R., Kronenberg, M., Smyth, M. J. & Kaer, L. Van. NKT cells: what's in a name? *Nat. Rev. Immunol.* **4**, 231–237 (2004).
3. Taniguchi, M., Harada, M., Dashtsoodol, N. & Kojo, S. Discovery of NKT cells and development of NKT cell-targeted anti-tumor immunotherapy. *Proceedings of the Japan Academy Series B: Physical and Biological Sciences* vol. 91 292–304 (2015).
4. Yoshimoto, T. & Paul, W. E. CD4pos NK1.1pos t cells promptly produce interleukin 4 in response to in vivo challenge with anti-cd3. *J. Exp. Med.* **179**, 1285–1295 (1994).
5. Benlagha, K., Weiss, A., Beavis, A., Teyton, L. & Bendelac, A. In vivo identification of glycolipid antigen-specific T cells using fluorescent CD1d tetramers. *J. Exp. Med.* **191**, 1895–903 (2000).
6. Matsuda, J. L. *et al.* Tracking the response of natural killer T cells to a glycolipid antigen using CD1d tetramers. *J. Exp. Med.* **192**, 741–54 (2000).
7. Singh, A. K., Tripathi, P. & Cardell, S. L. Type II NKT Cells: An Elusive Population With Immunoregulatory Properties. *Front. Immunol.* **0**, 1969 (2018).
8. Miceli, M. C. & Parnes, J. R. The roles of CD4 and CD8 in T cell activation. *Semin. Immunol.* **3**, 133–141 (1991).
9. Pei, B., Vela, J. L., Zajonc, D. & Kronenberg, M. Interplay between carbohydrate and lipid in recognition of glycolipid antigens by natural killer T cells. *Ann. N. Y. Acad. Sci.* **1253**, 68–79 (2012).
10. Kobayashi, E., Motoki, K., Uchida, T., Fukushima, H. & Koezuka, Y. KRN7000, a novel immunomodulator, and its antitumor activities. *Oncol. Res.* **7**, 529–34 (1995).

11. Morita, M. *et al.* Structure-Activity Relationship of α-Galactosylceramides against B16-Bearing Mice. *J. Med. Chem.* **38**, 2176–2187 (1995).

12. Anderson, C. K. & Brossay, L. The role of MHC class Ib-restricted T cells during infection. *Immunogenetics* **68**, 677 (2016).

13. Kawano, T. *et al.* CD1d-restricted and TCR-mediated activation of V(α)14 NKT cells by glycosylceramides. *Science (80-. ).* **278**, 1626–1629 (1997).

14. Kitamura, H. *et al.* α-galactosylceramide induces early B-cell activation through IL-4 production by NKT cells. *Cell. Immunol.* **199**, 37–42 (2000).

15. Parekh, V. V. *et al.* Quantitative and Qualitative Differences in the In Vivo Response of NKT Cells to Distinct α- and β-Anomeric Glycolipids. *J. Immunol.* **173**, 3693–3706 (2004).

16. Burdin, N., Brossay, L. & Kronenberg, M. Immunization with α-galactosylceramide polarizes CD1-reactive NK T cells towards Th2 cytokine synthesis. *Eur. J. Immunol.* **29**, 2014–2025 (1999).

17. Sag, D., Özkan, M., Kronenberg, M. & Wingender, G. Improved Detection of Cytokines Produced by Invariant NKT Cells. *Sci. Rep.* **7**, 16607 (2017).

18. Brennan, P. J. *et al.* Activation of iNKT cells by a distinct constituent of the endogenous glucosylceramide fraction. *Proc. Natl. Acad. Sci. U. S. A.* **111**, 13433–8 (2014).

19. Wieland Brown, L. C. *et al.* Production of α-Galactosylceramide by a Prominent Member of the Human Gut Microbiota. *PLoS Biol.* **11**, e1001610 (2013).

20. Kumar, A. *et al.* Natural Killer T Cells: An Ecological Evolutionary Developmental Biology Perspective. *Front. Immunol.* **8**, 1858 (2017).

21. Jukes, J. P., Wood, K. J. & Jones, N. D. Bystander activation of iNKT cells occurs during conventional T-cell alloresponses. *Am. J. Transplant.* **12**, 590–599 (2012).

22. Lin, S. J. *et al.* Interleukin-15 enhances the expansion and function of natural killer T cells from adult peripheral and umbilical cord blood. *Cytokine* **76**, 348–355 (2015).

23. Rhost, S. *et al.* Identification of novel glycolipid ligands activating a sulfatide-reactive, CD1d-restricted, type II natural killer T lymphocyte. *Eur. J. Immunol.* **42**, 2851–2860 (2012).

24. Shen, H. *et al.* Unveiling the heterogeneity of NKT cells in the liver through single cell RNA sequencing. *Sci. Reports 2020 101* **10**, 1–13 (2020).

25. Chang, D. H. *et al.* Inflammation-associated lysophospholipids as ligands for CD1d-restricted T cells in human cancer. *Blood* **112**, 1308–1316 (2008).

26. Jahng, A. *et al.* Prevention of Autoimmunity by Targeting a Distinct, Noninvariant CD1d-reactive T Cell Population Reactive to Sulfatide. *J. Exp. Med.* **199**, 947–957 (2004).

27. Zhao, J., Weng, X., Bagchi, S. & Wang, C.-R. Polyclonal type II natural killer T cells require PLZF and SAP for their development and contribute to CpG-mediated antitumor response. *Proc. Natl. Acad. Sci.* **111**, 2674–2679 (2014).

28. Chandra, S. *et al.* A new mouse strain for the analysis of invariant NKT cell function. *Nat. Immunol.* **16**, 799–800 (2015).

29. Dasgupta, S. & Kumar, V. Type II NKT cells: a distinct CD1d-restricted immune regulatory NKT cell subset. *Immunogenetics* **68**, 665–76 (2016).

30. Nowak, M. & Schmidt-Wolf, I. G. H. Natural killer T cells subsets in cancer, functional defects in prostate cancer and implications for immunotherapy. *Cancers* vol. 3 3661–3675 (2011).

31. Koay, H. F., Godfrey, D. I. & Pellicci, D. G. Development of mucosal-associated invariant T cells. *Immunology and Cell Biology* vol. 96 598–606 (2018).

32. Pistoia, V. *et al.* Human γδ T-Cells: From surface receptors to the therapy of high-risk leukemias. *Frontiers in Immunology* vol. 9 984 (2018).

33. Lynch, L. *et al.* Invariant NKT cells and CD1d+cells amass in human omentum and are depleted in patients with cancer and obesity. *Eur. J. Immunol.* **39**, 1893–1901 (2009).

34. Gapin, L. Development of invariant natural killer T cells. *Curr. Opin. Immunol.* **39**, 68–74 (2016).

35. Wang, H. & Hogquist, K. A. How Lipid-Specific T Cells Become Effectors: The Differentiation of iNKT Subsets. *Front. Immunol.* **0**, 1450 (2018).

36. Dashtsoodol, N. *et al.* Alternative pathway for the development of Vα 14+ NKT cells directly from CD4-CD8- thymocytes that bypasses the CD4+ CD8+ stage. *Nat. Immunol.* **18**, 274–282 (2017).

37. Kim, E. Y., Lynch, L., Brennan, P. J., Cohen, N. R. & Brenner, M. B. The transcriptional programs of iNKT cells. *Semin. Immunol.* **27**, 26–32 (2015).

38. Kimura, M. Y. *et al.* CD69 prevents PLZFhi innate precursors from prematurely exiting the thymus and aborting NKT2 cell differentiation. *Nat. Commun. 2018 91* **9**, 1–12 (2018).

39. Bennstein, S. B. Unraveling Natural Killer T-Cells Development. *Front. Immunol.* **8**, 1950 (2018).

40. Seiler, M. P. *et al.* Elevated and sustained expression of the transcription factors Egr1 and Egr2 controls NKT lineage differentiation in response to TCR signaling. *Nat. Immunol.* **13**, 264–271 (2012).

41. Kovalovsky, D. *et al.* The BTB-zinc finger transcriptional regulator PLZF controls the development of invariant natural killer T cell effector functions. *Nat. Immunol.* **9**, 1055–1064 (2008).

42. Savage, A. K. *et al.* The Transcription Factor PLZF Directs the Effector Program of the NKT Cell Lineage. *Immunity* **29**, 391–403 (2008).

43. Kovalovsky, D. *et al.* PLZF induces the spontaneous acquisition of memory/effector functions in T cells independently of NKT cell-related signals. *J. Immunol.* **184**, 6746–55 (2010).

44. Mao, A.-P. *et al.* Multiple layers of transcriptional regulation by PLZF in NKT-cell development. *Proc. Natl. Acad. Sci. U. S. A.* **113**, 7602–7 (2016).

45. Cohen, N. R. *et al.* Shared and distinct transcriptional programs underlie the hybrid nature of iNKT cells. *Nat. Immunol.* **14**, 90–9 (2013).

46. Engel, I. *et al.* Innate-like functions of natural killer T cell subsets result from highly divergent gene programs. *Nat. Immunol.* **17**, 728–39 (2016).

47. Bendelac, A., Killeen, N., Littman, D. R., Schwartz, R. H. & Bendelac, A. A subset of CD4+ thymocytes selected by MHC class I molecules. *Science* **263**, 1774–8 (1994).

48. Pellicci, D. G. *et al.* A natural killer T (NKT) cell developmental pathway iInvolving a thymus-dependent NK1.1(-)CD4(+) CD1d-dependent precursor stage. *J. Exp. Med.* **195**, 835–44 (2002).

49. Lynch, L. *et al.* Regulatory iNKT cells lack expression of the transcription factor PLZF and control the homeostasis of Treg cells and macrophages in adipose tissue. *Nat. Immunol.* **16**, 85–95 (2015).

50. Thomas, S. Y. *et al.* PLZF induces an intravascular surveillance program mediated by long-lived LFA-1–ICAM-1 interactions. *J. Exp. Med.* **208**, 1179–1188 (2011).

51. Milpied, P. *et al.* IL-17-producing invariant NKT cells in lymphoid organs are recent thymic emigrants identified by neuropilin-1 expression. *Blood* **118**, 2993–3002 (2011).

52. Clancy-Thompson, E. *et al.* Transnuclear mice reveal Peyer's patch iNKT cells that regulate B-cell class switching to IgG1. *EMBO J.* **38**, (2019).

53. Berzins, S. P., McNab, F. W., Jones, C. M., Smyth, M. J. & Godfrey, D. I. Long-term retention of mature NK1.1+ NKT cells in the thymus. *J. Immunol.* **176**, 4059–65 (2006).

54. Drennan, M. B. *et al.* Cutting Edge: The Chemokine Receptor CXCR3 Retains Invariant NK T Cells in the Thymus. *J. Immunol.* **183**, 2213–2216 (2009).

55. Doisne, J.-M. *et al.* Skin and peripheral lymph node invariant NKT cells are mainly retinoic acid receptor-related orphan receptor (gamma)t+ and respond preferentially under inflammatory conditions. *J. Immunol.* **183**, 2142–2149 (2009).

56. Michel, M. L. *et al.* Identification of an IL-17-producing NK1.1neg iNKT cell population involved in airway neutrophilia. *J. Exp. Med.* **204**, 995–1001 (2007).

57. Terashima, A. *et al.* A novel subset of mouse NKT cells bearing the IL-17 receptor B responds to IL-25 and contributes to airway hyperreactivity. *J. Exp. Med.* **205**, 2727–2733 (2008).

58. Crosby, C. M. & Kronenberg, M. Tissue-specific functions of invariant natural killer T cells. *Nat. Rev. Immunol.* **18**, 559–574 (2018).

59. Lee, Y. J. *et al.* Tissue-Specific Distribution of iNKT Cells Impacts Their Cytokine Response. *Immunity* **43**, 566–578 (2015).

60. Lee, Y. J., Holzapfel, K. L., Zhu, J., Jameson, S. C. & Hogquist, K. A. Steady-state production of IL-4 modulates immunity in mouse strains and is determined by lineage diversity of iNKT cells. *Nat. Immunol.* **14**, 1146–1154 (2013).

61. Lee, Y. J. *et al.* Lineage specific effector signatures of iNKT cells are shared amongst γδ T, innate lymphoid, and T helper cells. *J. Immunol.* **197**, 1460 (2016).

62. Kwon, D.-I. & Lee, Y. J. Lineage Differentiation Program of Invariant Natural Killer T Cells. *Immune Netw.* **17**, 365–377 (2017).

63. O'Brien, T. F. *et al.* Cytokine expression by invariant natural killer T cells is tightly regulated throughout development and settings of type-2 inflammation. *Mucosal Immunol.* **9**, 597–609 (2016).

64. Harsha Krovi, S. *et al.* Thymic iNKT single cell analyses unmask the common developmental program of mouse innate T cells. *Nat. Commun.* **11**, 1–15 (2020).

65. Baranek, T. *et al.* High Dimensional Single-Cell Analysis Reveals iNKT Cell Developmental Trajectories and Effector Fate Decision. *Cell Rep.* **32**, (2020).

66. Wang, H. & Hogquist, K. A. CCR7 defines a precursor for murine iNKT cells in thymus and periphery. *Elife* **7**, (2018).

67. Georgiev, H., Ravens, I., Benarafa, C., Förster, R. & Bernhardt, G. Distinct gene expression patterns correlate with developmental and functional traits of iNKT subsets. *Nat. Commun.* **7**, 13116 (2016).

68. Hogquist, K. & Georgiev, H. Recent advances in iNKT cell development. *F1000Research* vol. 9 (2020).

69. Tuttle, K. D. *et al.* TCR signal strength controls thymic differentiation of iNKT cell subsets. *Nat. Commun.* **9**, 2650 (2018).

70. Zhao, M. *et al.* Altered thymic differentiation and modulation of arthritis by invariant NKT cells expressing mutant ZAP70. *Nat. Commun.* **9**, 1–17 (2018).

71. Hsu, L. Y., Tan, Y. X., Xiao, Z., Malissen, M. & Weiss, A. A hypomorphic allele of ZAP-70 reveals a distinct thymic threshold for autoimmune disease versus autoimmune reactivity. *J. Exp. Med.* **206**, 2527–2541 (2009).

72. Sakaguchi, N. *et al.* Altered thymic T-cell selection due to a mutation of the ZAP-70 gene causes autoimmune arthritis in mice. *Nature* **426**, 454–460 (2003).

73. Park, J.-Y., Dipalma, D. T., Kwon, J., Fink, J. & Correspondence, J.-H. P. Quantitative Difference in PLZF Protein Expression Determines iNKT Lineage Fate and Controls Innate CD8 T Cell Generation. (2019) doi:10.1016/j.celrep.2019.05.012.

74. Oleinika, K. *et al.* CD1d-dependent immune suppression mediated by regulatory B cells through modulations of iNKT cells. *Nat. Commun.* **9**, 1–17 (2018).

75. Uddin, M. N. *et al.* Transcription factor Bcl11b sustains iNKT1 and iNKT2 cell programs, restricts iNKT17 cell program, and governs iNKT cell survival. *Proc. Natl. Acad. Sci.* **113**, 7608–7613 (2016).

76. Yu, J. S. *et al.* Differentiation of IL-17-producing invariant natural killer T cells requires expression of the transcription factor c-Maf. *Front. Immunol.* **8**, (2017).

77. Thapa, P. *et al.* NKAP Regulates Invariant NKT Cell Proliferation and Differentiation into ROR-γt–Expressing NKT17 Cells. *J. Immunol.* **196**, 4987–4998 (2016).

78. Thapa, P. *et al.* The differentiation of ROR-γt expressing iNKT17 cells is orchestrated by Runx1. *Sci. Rep.* **7**, 7018 (2017).

79. Engel, I., Zhao, M., Kappes, D., Taniuchi, I. & Kronenberg, M. The transcription factor Th-POK negatively regulates Th17 differentiation in Vα14i NKT cells. *Blood* **120**, 4524–4532 (2012).

80. Malhotra, N. *et al.* SOX4 controls invariant NKT cell differentiation by tuning TCR signaling. *J. Exp. Med.* **215**, 2887–2900 (2018).

81. Salmond, R. J. mTOR regulation of glycolytic metabolism in T cells. *Frontiers in Cell and Developmental Biology* vol. 6 122 (2018).

82. Donnelly, R. P. *et al.* mTORC1-Dependent Metabolic Reprogramming Is a Prerequisite for NK Cell Effector Function. *J. Immunol.* **193**, 4477–4484 (2014).

83. O'Brien, A. *et al.* Obesity Reduces mTORC1 Activity in Mucosal-Associated Invariant T Cells, Driving Defective Metabolic and Functional Responses. *J. Immunol.* **202**, 3404–3411 (2019).

84. Zhang, L. *et al.* Mammalian Target of Rapamycin Complex 1 Orchestrates Invariant NKT Cell Differentiation and Effector Function. *J. Immunol.* **193**, 1759–1765 (2014).

85. Wei, J., Yang, K. & Chi, H. Cutting edge: Discrete functions of mTOR signaling in invariant NKT cell development and NKT17 fate decision. *J. Immunol.* **193**, 4297–4301 (2014).

86. Sklarz, T. *et al.* mTORC2 regulates multiple aspects of NKT-cell development and function. *Eur. J. Immunol.* **47**, 516–526 (2017).

87. Carlson, C. M. *et al.* Kruppel-like factor 2 regulates thymocyte and T-cell migration. *Nature* **442**, 299–302 (2006).

88. Gordy, L. E. *et al.* IL-15 Regulates Homeostasis and Terminal Maturation of NKT Cells. *J. Immunol.* **187**, 6335–6345 (2011).

89. Webster, K. E. *et al.* IL-17-producing NKT cells depend exclusively on IL-7 for homeostasis and survival. *Mucosal Immunol.* **7**, 1058–1067 (2014).

90. Lynch, L. *et al.* Adipose Tissue Invariant NKT Cells Protect against Diet-Induced Obesity and Metabolic Disorder through Regulatory Cytokine Production. *Immunity* **37**, 574–587 (2012).

91. Sag, D., Krause, P., Hedrick, C. C., Kronenberg, M. & Wingender, G. IL-10–producing NKT10 cells are a distinct regulatory invariant NKT cell subset. *J. Clin. Invest.* **124**, 3725–3740 (2014).

92. Murray, M. P. *et al.* Transcriptome and chromatin landscape of iNKT cells are shaped by subset differentiation and antigen exposure. *Nat. Commun.* **12**, 1–14 (2021).

93. Cameron, G. & Godfrey, D. I. Differential surface phenotype and context-dependent reactivity of functionally diverse NKT cells. *Immunol. Cell Biol.* **96**, 759–771 (2018).

94. Fu, S. *et al.* Immunometabolism regulates TCR recycling and iNKT cell functions. *Sci. Signal.* **12**, eaau1788 (2019).

95. Díaz-Basabe, A., Strati, F. & Facciotti, F. License to Kill: When iNKT Cells Are Granted the Use of Lethal Cytotoxicity. *Int. J. Mol. Sci.* **21**, 1–17 (2020).

96. Crowe, N. Y. *et al.* Differential antitumor immunity mediated by NKT cell subsets in vivo. *J. Exp. Med.* **202**, 1279–1288 (2005).

97. Zhu, L. *et al.* TBK-binding protein 1 regulates IL-15-induced autophagy and NKT cell survival. *Nat. Commun. 2018 91* **9**, 1–14 (2018).

98. Watarai, H. *et al.* Development and function of invariant natural killer T cells producing T H2- and T H17-cytokines. *PLoS Biol.* **10**, (2012).

99. Drennan, M. B. *et al.* NKT sublineage specification and survival requires the ubiquitin-modifying enzyme TNFAIP3/A20. *J. Exp. Med.* **213**, 1973–81 (2016).

100. Jadhav, R. R. *et al.* Epigenetic signature of PD-1+ TCF1+ CD8 T cells that act as resource cells during chronic viral infection and respond to PD-1 blockade. *Proc. Natl. Acad. Sci. U. S. A.* **116**, 14113–14118 (2019).

101. Utzschneider, D. T. *et al.* T Cell Factor 1-Expressing Memory-like CD8+ T Cells Sustain the Immune Response to Chronic Viral Infections. *Immunity* **45**, 415–427 (2016).

102. Crawford, A. *et al.* Molecular and Transcriptional Basis of CD4+ T Cell Dysfunction during Chronic Infection. *Immunity* **40**, 289–302 (2014).

103. Yoshie, O. & Matsushima, K. CCR4 and its ligands: From bench to bedside. *Int. Immunol.* **27**, 11–20 (2015).

104. Cosorich, I., McGuire, H. M., Warren, J., Danta, M. & King, C. CCR9 Expressing T Helper and T Follicular Helper Cells Exhibit Site-Specific Identities During Inflammatory Disease. *Front. Immunol.* **0**, 2899 (2019).

105. Diehl, S. *et al.* Induction of NFATc2 Expression by Interleukin 6 Promotes T Helper Type 2 Differentiation. *J. Exp. Med.* **196**, 39 (2002).

106. Zhang, X. *et al.* TRAF3IP3 at the trans-Golgi network regulates NKT2 maturation via the MEK/ERK signaling pathway. *Cell. Mol. Immunol. 2019 174* **17**, 395–406 (2019).

107. Coquet, J. M. *et al.* Diverse cytokine production by NKT cell subsets and identification of an IL-17-producing CD4-NK1.1- NKT cell population. *Proc. Natl. Acad. Sci. U. S. A.* **105**, 11287–11292 (2008).

108. Doisne, J.-M. *et al.* Cutting Edge: Crucial Role of IL-1 and IL-23 in the Innate IL-17 Response of Peripheral Lymph Node NK1.1 − Invariant NKT Cells to Bacteria . *J. Immunol.* **186**, 662–666 (2011).

109. Lopes, N. *et al.* Distinct metabolic programs established in the thymus control effector functions of γδ T cell subsets in tumor microenvironments. *Nat. Immunol.* **22**, 179–192 (2021).

110. Kohlgruber, A. C. *et al.* γδ T cells producing interleukin-17A regulate adipose regulatory T cell homeostasis and thermogenesis. *Nat. Immunol.* **19**, 464–474 (2018).

111. Hedrick, M. N. *et al.* CCR6 is required for IL-23-induced psoriasis-like inflammation in mice. *J. Clin. Invest.* **119**, 2317–2329 (2009).

112. Wang, C., Kang, S. G., Lee, J., Sun, Z. & Kim, C. H. The roles of CCR6 in migration of Th17 cells and regulation of effector T-cell balance in the gut. *Mucosal Immunol.* **2**, 173–183 (2009).

113. Jung, C., Hugot, J.-P. & Barreau, F. Peyer's Patches: The Immune Sensors of the Intestine. *Int. J. Inflam.* **2010**, 1–12 (2010).

114. Vieth, J. A. *et al.* TCRα-TCRβ pairing controls recognition of CD1d and directs the development of adipose NKT cells. *Nat. Immunol.* **18**, 36–44 (2017).

115. LaMarche, N. M. *et al.* Distinct iNKT Cell Populations Use IFNγ or ER Stress-Induced IL-10 to Control Adipose Tissue Homeostasis. *Cell Metab.* **32**, 243-258.e6 (2020).

116. Huh, J. Y. *et al.* A Novel Function of Adipocytes in Lipid Antigen Presentation to iNKT Cells. *Mol. Cell. Biol.* **33**, 328–339 (2013).

117. Huh, J. Y. *et al.* Deletion of CD1d in Adipocytes Aggravates Adipose Tissue Inflammation and Insulin Resistance in Obesity. *Diabetes* **66**, 835–847 (2017).

118. Wu, J. *et al.* Tunicamycin specifically aggravates ER stress and overcomes chemoresistance in multidrug-resistant gastric cancer cells by inhibiting N-glycosylation. *J. Exp. Clin. Cancer Res.* **37**, 1–12 (2018).

119. Lee, H. *et al.* The presence of CD8+ invariant NKT cells in mice. *Exp. Mol. Med.* **41**, 866 (2009).

120. Wang, C. *et al.* CD8+NKT-like cells regulate the immune response by killing antigen-bearing DCs. *Sci. Reports 2015 51* **5**, 1–13 (2015).

121. Loh, L., Ivarsson, M. A., Michaëlsson, J., Sandberg, J. K. & Nixon, D. F. Invariant natural killer T cells developing in the human fetus accumulate and mature in the small intestine. *Mucosal Immunol. 2014 75* **7**, 1233–1243 (2014).

122. Gumperz, J. E., Miyake, S., Yamamura, T. & Brenner, M. B. Functionally Distinct Subsets of CD1d-restricted Natural Killer T Cells Revealed by CD1d Tetramer Staining. *J. Exp. Med.* **195**, 625 (2002).

123. Kim, C. H., Johnston, B. & Butcher, E. C. Trafficking machinery of NKT cells: shared and differential chemokine receptor expression among Vα24+Vβ11+ NKT cell subsets with distinct cytokine-producing capacity. *Blood* **100**, 11–16 (2002).

124. Andrews, K. *et al.* Expansion and CD2/CD3/CD28 stimulation enhance Th2 cytokine secretion of human invariant NKT cells with retained anti-tumor cytotoxicity. *Cytotherapy* **22**, (2020).

125. O'Reilly, V. *et al.* Distinct and overlapping effector functions of expanded human CD4 +, cd8α + and CD4 -CD8α - invariant natural killer T cells. *PLoS One* **6**, (2011).

126. Montoya, C. J. *et al.* Characterization of human invariant natural killer T subsets in health and disease using a novel invariant natural killer T cell-clonotypic monoclonal antibody, 6B11. *Immunology* vol. 122 1–14 (2007).

127. Trujillo-Ocampo, A. *et al.* IL-7 During Antigenic Stimulation Using Allogeneic Dendritic Cells Promotes Expansion of CD45RA-CD62L+CD4+ Invariant NKT Cells With Th-2 Biased Cytokine Production Profile. *Front. Immunol.* **11**, (2020).

128. Lee, P. T., Benlagha, K., Teyton, L. & Bendelac, A. Distinct Functional Lineages of Human Vα24 Natural Killer T Cells. *J. Exp. Med.* **195**, 637 (2002).

129. Monteiro, M. *et al.* Identification of Regulatory Foxp3+ Invariant NKT Cells Induced by TGF-β. *J. Immunol.* **185**, 2157–2163 (2010).

130. Park, J. E. *et al.* A cell atlas of human thymic development defines T cell repertoire formation. *Science (80-. ).* **367**, (2020).

131. Shimizu, K. *et al.* Eomes transcription factor is required for the development and differentiation of invariant NKT cells. *Commun. Biol.* **2**, (2019).

132. Aizarani, N. *et al.* A human liver cell atlas reveals heterogeneity and epithelial progenitors. *Nature* **572**, 199–204 (2019).

133. Gutierrez-Arcelus, M. *et al.* Lymphocyte innateness defined by transcriptional states reflects a balance between proliferation and effector functions. *Nat. Commun.* **10**, 1–15 (2019).

134. Erkers, T. *et al.* High-parametric evaluation of human invariant natural killer T cells to delineate heterogeneity in allo- And autoimmunity. *Blood* **135**, 814–825 (2020).

135. Zhou, L. *et al.* Single-Cell RNA-Seq Analysis Uncovers Distinct Functional Human NKT Cell Sub-Populations in Peripheral Blood. *Front. Cell Dev. Biol.* **8**, 384 (2020).

136. Ji, Y. *et al.* Short term high fat diet challenge promotes alternative macrophage polarization in adipose tissue via natural killer T cells and interleukin-4. *J. Biol. Chem.* **287**, 24378–86 (2012).

137. Schipper, H. S. *et al.* Natural killer T cells in adipose tissue prevent insulin resistance. *J. Clin. Invest.* **122**, 3343–3354 (2012).

138. Lynch, L. *et al.* iNKT Cells Induce FGF21 for Thermogenesis and Are Required for Maximal Weight Loss in GLP1 Therapy. *Cell Metab.* **24**, 510–519 (2016).

139. Arora, S. *et al.* Invariant natural killer T cells coordinate removal of senescent cells. *Med* **2**, 938-950.e8 (2021).

140. Wu, L. *et al.* Activation of invariant natural killer T cells by lipid excess promotes tissue inflammation, insulin resistance, and hepatic steatosis in obese mice. *Proc. Natl. Acad. Sci.* **109**, E1143–E1152 (2012).

141. Satoh, M. *et al.* Adipocyte-specific CD1d-deficiency mitigates diet-induced obesity and insulin resistance in mice. *Sci. Rep.* **6**, (2016).

142. Liew, P. X., Lee, W. Y. & Kubes, P. iNKT Cells Orchestrate a Switch from Inflammation to Resolution of Sterile Liver Injury. *Immunity* **47**, 752-765.e5 (2017).

143. Bénézech, C. *et al.* Inflammation-induced formation of fat-associated lymphoid clusters. *Nat. Immunol.* **16**, 819–828 (2015).

144. Guinoa, J. S. de *et al.* CD1d-mediated lipid presentation by CD11c+ cells regulates intestinal homeostasis. *EMBO J.* **37**, e97537 (2018).

145. Wen, X., Yang, J. Q., Kim, P. J. & Singh, R. R. Homeostatic regulation of marginal zone B cells by invariant natural killer T cells. *PLoS One* **6**, e26536 (2011).

146. Van Kaer, L. α-galactosylceramide therapy for autoimmune diseases: Prospects and obstacles. *Nat. Rev. Immunol.* **5**, 31–42 (2005).

147. Kumar, B. V., Connors, T. & Farber, D. L. Human T cell development, localization, and function throughout life. *Immunity* **48**, 202 (2018).

148. Smith-Garvin, J. E., Koretzky, G. A. & Jordan, M. S. T Cell Activation. *Annu. Rev. Immunol.* **27**, 591 (2009).

149. Li, P. & Leonard, W. J. Chromatin accessibility and interactions in the transcriptional regulation of T cells. *Front. Immunol.* **9**, (2018).

150. Hesterberg, R., Cleveland, J. & Epling-Burnette, P. Role of Polyamines in Immune Cell Functions. *Med. Sci.* **6**, 22 (2018).

151. Bevington, S. L. *et al.* IL-2/IL-7-inducible factors pioneer the path to T cell differentiation in advance of lineage-defining factors. *EMBO J.* **39**, (2020).

152. Marchingo, J. M., Sinclair, L. V., Howden, A. J. & Cantrell, D. A. Quantitative analysis of how myc controls t cell proteomes and metabolic pathways during t cell activation. *Elife* **9**, (2020).

153. Szabo, P. A. *et al.* Single-cell transcriptomics of human T cells reveals tissue and activation signatures in health and disease. **10**, 1–16 (2019).

154. Cano-Gamez, E. *et al.* Single-cell transcriptomics identifies an effectorness gradient shaping the response of CD4+ T cells to cytokines. **11**, 1–15 (2020).

155. Sinclair, L. V. *et al.* Antigen receptor control of methionine metabolism in T cells. *Elife* **8**, (2019).

156. Hartmann, F. J. *et al.* Single-cell metabolic profiling of human cytotoxic T cells. *Nat. Biotechnol.* **39**, 186 (2021).

157. Chaudhry, A. & Rudensky, A. Y. Control of inflammation by integration of environmental cues by regulatory T cells. *J. Clin. Invest.* **123**, 939–944 (2013).

158. Joshi, N. S. *et al.* Inflammation Directs Memory Precursor and Short-Lived Effector CD8(+) T Cell Fates via the Graded Expression of T-bet Transcription Factor. *Immunity* **27**, 281 (2007).

159. Plumlee, C. R. *et al.* Early Effector CD8 T Cells Display Plasticity in Populating the Short-Lived Effector and Memory-Precursor Pools Following Bacterial or Viral Infection. *Sci. Rep.* **5**, 1–13 (2015).

160. Angiari, S. *et al.* Pharmacological Activation of Pyruvate Kinase M2 Inhibits CD4+ T Cell Pathogenicity and Suppresses Autoimmunity. *Cell Metab.* **31**, 391-405.e8 (2020).

161. Sinclair, L. V., Neyens, D., Ramsay, G., Taylor, P. M. & Cantrell, D. A. Single cell analysis of kynurenine and System L amino acid transport in T cells. *Nat. Commun.* **9**, 1981 (2018).

162. Wu, R. *et al.* De novo synthesis and salvage pathway coordinately regulate polyamine homeostasis and determine T cell proliferation and function. *Sci. Adv.* **6**, 4275–4291 (2020).

163. Wang, Z. *et al.* Iron Drives T Helper Cell Pathogenicity by Promoting RNA-Binding Protein PCBP1-Mediated Proinflammatory Cytokine Production. *Immunity* **49**, 80-92.e7 (2018).

164. Kaech, S. M. & Cui, W. Transcriptional control of effector and memory CD8+ T cell differentiation. *Nat. Rev. Immunol. 2012 1211* **12**, 749–761 (2012).

165. Sallusto, F. & Lanzavecchia, A. Exploring pathways for memory T cell generation. *J. Clin. Invest.* **108**, 805–806 (2001).

166. Ando, M., Ito, M., Srirat, T., Kondo, T. & Yoshimura, A. Memory T cell, exhaustion, and tumor immunity. (2019) doi:10.1080/25785826.2019.1698261.

167. Chen, Y., Zander, R., Khatun, A., Schauder, D. M. & Cui, W. Transcriptional and Epigenetic Regulation of Effector and Memory CD8 T Cell Differentiation. *Front. Immunol.* **9**, 2826 (2018).

168. Dunn, J., McCuaig, R., Tu, W. J., Hardy, K. & Rao, S. Multi-layered epigenetic mechanisms contribute to transcriptional memory in T lymphocytes. *BMC Immunol.* **16**, 1–11 (2015).

169. Franco, F., Jaccard, A., Romero, P., Yu, Y. R. & Ho, P. C. Metabolic and epigenetic regulation of T-cell exhaustion. *Nat. Metab. 2020 210* **2**, 1001–1012 (2020).

170. Seo, H. *et al.* TOX and TOX2 transcription factors cooperate with NR4A transcription factors to impose CD8+ T cell exhaustion. *Proc. Natl. Acad. Sci. U. S. A.* **116**, 12410–12415 (2019).

171. Man, K. *et al.* Transcription Factor IRF4 Promotes CD8 + T Cell Exhaustion and Limits the Development of Memory-like T Cells during Chronic Infection. *Immunity* **47**, 1129-1141.e5 (2017).

172. Liu, X. *et al.* Genome-wide analysis identifies NR4A1 as a key mediator of T cell dysfunction. *Nature* **567**, 525–529 (2019).

173. Andreatta, M. *et al.* Interpretation of T cell states from single-cell transcriptomics data using reference atlases. *Nat. Commun.* **12**, 1–19 (2021).

174. Kallies, A., Zehn, D. & Utzschneider, D. T. Precursor exhausted T cells: key to successful immunotherapy? *Nat. Rev. Immunol. 2019 202* **20**, 128–136 (2019).

175. Blank, C. U. *et al.* Defining ‘T cell exhaustion’. *Nat. Rev. Immunol. 2019 1911* **19**, 665–674 (2019).

176. Im, S. J. *et al.* Defining CD8+ T cells that provide the proliferative burst after PD-1 therapy. *Nature* **537**, 417–421 (2016).

177. He, R. *et al.* Follicular CXCR5-expressing CD8+ T cells curtail chronic viral infection. *Nat. 2016 5377620* **537**, 412–416 (2016).

178. Govindarajan, S. *et al.* Stabilization of cytokine mRNAs in iNKT cells requires the serine-threonine kinase IRE1alpha. *Nat. Commun.* **9**, 1–12 (2018).

179. Matsuda, J. L. *et al.* Mouse Vα14i natural killer T cells are resistant to cytokine polarization in vivo. *Proc. Natl. Acad. Sci. U. S. A.* **100**, 8395–8400 (2003).

180. Fujii, S. I., Shimizu, K., Kronenberg, M. & Steinman, R. M. Prolonged IFN-γ-producing NKT response induced with α-galactosylceramide-loaded DCs. *Nat. Immunol.* **3**, 867–874 (2002).

181. Nishimura, T. *et al.* The interface between innate and acquired immunity: Glycolipid antigen presentation by CD1d-expressing dendritic cells to NKT cells induces the differentiation of antigen-specific cytotoxic T lymphocytes. *Int. Immunol.* **12**, 987–994 (2000).

182. Zeng, S. G. *et al.* Human Invariant NKT Cell Subsets Differentially Promote Differentiation, Antibody Production, and T Cell Stimulation by B Cells In Vitro. *J. Immunol.* **191**, 1666–1676 (2013).

183. Doherty, D. G., Melo, A. M., Moreno-Olivera, A. & Solomos, A. C. Activation and regulation of B cell responses by invariant natural killer T cells. *Frontiers in Immunology* vol. 9 (2018).

184. Smyth, M. J. *et al.* Sequential activation of NKT cells and NK cells provides effective innate immunotherapy of cancer. *J. Exp. Med.* **201**, 1973–1985 (2005).

185. Reilly, E. C. *et al.* Activated iNKT Cells Promote Memory CD8+ T Cell Differentiation during Viral Infection. *PLoS One* **7**, e37991 (2012).

186. Diao, H. *et al.* Osteopontin as a mediator of NKT cell function in T cell-mediated liver diseases. *Immunity* **21**, 539–550 (2004).

187. Nakagawa, R. *et al.* Antitumor activity of α-galactosylceramide, KRN7000, in mice with the melanoma B16 hepatic metastasis and immunohistological study of tumor infiltrating cells. *Oncol. Res.* **12**, 51–58 (2000).

188. Kitamura, H. *et al.* The natural killer T (NKT) cell ligand α-galactosylceramide demonstrates its immunopotentiating effect by inducing interleukin (IL)-12 production by dendritic cells and IL-12 receptor expression on NKT cells. *J. Exp. Med.* **189**, 1121–1127 (1999).

189. Naumov, Y. N. *et al.* Activation of CD1d-restricted T cells protects NOD mice from developing diabetes by regulating dendritic cell subsets. *Proc. Natl. Acad. Sci. U. S. A.* **98**, 13838–13843 (2001).

190. Chen, Y.-G. *et al.* Activated NKT Cells Inhibit Autoimmune Diabetes through Tolerogenic Recruitment of Dendritic Cells to Pancreatic Lymph Nodes. *J. Immunol.* **174**, 1196–1204 (2005).

191. Singh, N. *et al.* Cutting edge: activation of NK T cells by CD1d and alpha-galactosylceramide directs conventional T cells to the acquisition of a Th2 phenotype. *J. Immunol.* **163**, 2373–7 (1999).

192. Smith, E. *et al.* Cross-talk between iNKT cells and monocytes triggers an atheroprotective immune response in SLE patients with asymptomatic plaque. *Sci. Immunol.* **1**, (2016).

193. Valente, M. *et al.* Cross-talk between iNKT cells and CD8 T cells in the spleen requires the IL-4/CCL17 axis for the generation of short-lived effector cells. *Proc. Natl. Acad. Sci. U. S. A.* **116**, 25816–25827 (2019).

194. Wang, L. *et al.* Spatial distribution of IL4 controls iNKT cell-DC crosstalk in tumors. *Cell. Mol. Immunol.* **17**, 496–506 (2020).

195. Iyoda, T. *et al.* Invariant NKT cell anergy is induced by a strong TCR-mediated signal plus co-stimulation. *Int. Immunol.* **22**, 905–913 (2010).

196. Kaneda, H. *et al.* ICOS costimulates invariant NKT cell activation. *Biochem. Biophys. Res. Commun.* **327**, 201–207 (2005).

197. Kim, Y.-H., Kumar, A., Chang, C.-H. & Pyaram, K. Reactive Oxygen Species Regulate the Inflammatory Function of NKT Cells through Promyelocytic Leukemia Zinc Finger. *J. Immunol.* **199**, 3478–3487 (2017).

198. Wilson, M. T. *et al.* The response of natural killer T cells to glycolipid antigens is characterized by surface receptor down-modulation and expansion. *Proc. Natl. Acad. Sci. U. S. A.* **100**, 10913–10918 (2003).

199. Harada, M. *et al.* Down-regulation of the invariant Vα14 antigen receptor in NKT cells upon activation. *Int. Immunol.* **16**, 241–247 (2004).

200. Crowe, N. Y. *et al.* Glycolipid Antigen Drives Rapid Expansion and Sustained Cytokine Production by NK T Cells. *J. Immunol.* **171**, 4020–4027 (2003).

201. Chang, P.-P. P. *et al.* Identification of Bcl-6-dependent follicular helper NKT cells that provide cognate help for B cell responses. *Nat. Immunol. 2011 131* **13**, 35–43 (2011).

202. Rampuria, P. & Lang, M. L. CD1d-dependent expansion of NKT follicular helper cells in vivo and in vitro is a product of cellular proliferation and differentiation. *Int. Immunol.* **27**, (2015).

203. Chen, Z. *et al.* Memory Follicular Helper Invariant NKT Cells Recognize Lipid Antigens on Memory B Cells and Elicit Antibody Recall Responses. *J. Immunol.* **200**, 3117–3127 (2018).

204. Bai, L. *et al.* Natural killer T (NKT)–B-cell interactions promote prolonged antibody responses and long-term memory to pneumococcal capsular polysaccharides. *Proc. Natl. Acad. Sci.* **110**, 16097–16102 (2013).

205. Chang, P. P. & Vinuesa, C. G. Detection of mouse natural killer T follicular helper (NKTFH) cells by flow cytometry. in *T Follicular Helper Cells: Methods and Protocols* vol. 1291 135–141 (Humana Press, New York, NY, 2015).

206. Shimizu, K. *et al.* KLRG+ invariant natural killer T cells are long-lived effectors. *Proc. Natl. Acad. Sci. U. S. A.* **111**, 12474–12479 (2014).

207. Netea, M. G. *et al.* Defining trained immunity and its role in health and disease. *Nat. Rev. Immunol.* **20**, 375 (2020).

208. Parekh, V. V. *et al.* Glycolipid antigen induces long-term natural killer T cell anergy in mice. *J. Clin. Invest.* **115**, 2572 (2005).

209. Sullivan, B. A. & Kronenberg, M. Activation or anergy: NKT cells are stunned by α-galactosylceramide. *J. Clin. Invest.* **115**, 2328 (2005).

210. Kawakami, K. *et al.* Critical role of Vα14+ natural killer T cells in the innate phase of host protection against Streptococcus pneumoniae infection. *Eur. J. Immunol.* **33**, 3322–3330 (2003).

211. Nakamatsu, M. *et al.* Role of interferon-γ in Vα14+ natural killer T cell-mediated host defense against Streptococcus pneumoniae infection in murine lungs. *Microbes Infect.* **9**, 364–374 (2007).

212. Kinjo, Y. *et al.* Invariant natural killer T cells recognize glycolipids from pathogenic Gram-positive bacteria. *Nat. Immunol.* **12**, 966–974 (2011).

213. Girardi, E. *et al.* Unique Interplay between Sugar and Lipid in Determining the Antigenic Potency of Bacterial Antigens for NKT Cells. *PLOS Biol.* **9**, e1001189 (2011).

214. Brigl, M. *et al.* Innate and cytokine-driven signals, rather than microbial antigens, dominate in natural killer T cell activation during microbial infection. *J. Exp. Med.* **208**, 1163–1177 (2011).

215. Cavallari, M. *et al.* A semisynthetic carbohydrate-lipid vaccine that protects against S. pneumoniae in mice. *Nat. Chem. Biol. 2014 1011* **10**, 950–956 (2014).

216. Choi, H.-J. *et al.* Bacterial infection alters the kinetics and function of iNKT cell responses. *J. Leukoc. Biol.* **84**, 1462–1471 (2008).

217. Kim, S. *et al.* Impact of bacteria on the phenotype, functions, and therapeutic activities of invariant NKT cells in mice. *J. Clin. Invest.* **118**, 2301 (2008).

218. Cohen, N. R. *et al.* Innate recognition of cell wall β-Glucans drives invariant natural killer T cell responses against fungi. *Cell Host Microbe* **10**, 437–450 (2011).

219. Singh, D., Ghate, M., Godbole, S., Kulkarni, S. & Thakar, M. Functional invariant natural killer t cells secreting cytokines are associated with non-progressive human immunodeficiency virus-1 infection but not with suppressive anti-retroviral treatment. *Front. Immunol.* **9**, (2018).

220. Kakimi, K., Guidotti, L. G., Koezuka, Y. & Chisari, F. V. Natural killer T cell activation inhibits hepatitis B virus replication in vivo. *J. Exp. Med.* **192**, 921–930 (2000).

221. De Santo, C. *et al.* Invariant NKT cells reduce the immunosuppressive activity of influenza A virus-induced myeloid-derived suppressor cells in mice and humans. *J. Clin. Invest.* **118**, 4036–4048 (2008).

222. Jiang, X. *et al.* Restored circulating invariant NKT cells are associated with viral control in patients with chronic hepatitis B. *PLoS One* **6**, e28871 (2011).

223. Liu, J., Glosson, N. L., Du, W., Gervay-Hague, J. & Brutkiewicz, R. R. A Thr/Ser dual residue motif in the cytoplasmic tail of human CD1d is important for the down-regulation of antigen presentation following a herpes simplex virus 1 infection. *Immunology* **140**, 191–201 (2013).

224. Exley, M. A. *et al.* CD1d-reactive T-cell activation leads to amelioration of disease caused by diabetogenic encephalomyocarditis virus. *J. Leukoc. Biol.* **69**, 713–8 (2001).

225. Diana, J. *et al.* NKT Cell-Plasmacytoid Dendritic Cell Cooperation via OX40 Controls Viral Infection in a Tissue-Specific Manner. *Immunity* **30**, 289–299 (2009).

226. Paget, C. *et al.* Potential Role of Invariant NKT Cells in the Control of Pulmonary Inflammation and CD8 + T Cell Response during Acute Influenza A Virus H3N2 Pneumonia . *J. Immunol.* **186**, 5590–5602 (2011).

227. Ho, L. P. *et al.* Activation of invariant NKT cells enhances the innate immune response and improves the disease course in influenza A virus infection. *Eur. J. Immunol.* **38**, 1913–1922 (2008).

228. Dwivedi, V. *et al.* Adjuvant effects of invariant NKT cell ligand potentiates the innate and adaptive immunity to an inactivated H1N1 swine influenza virus vaccine in pigs. *Vet. Microbiol.* **186**, 157–163 (2016).

229. Ghazarian, L. *et al.* Protection against type 1 diabetes upon coxsackievirus B4 infection and iNKT-cell stimulation: Role of suppressive macrophages. *Diabetes* **62**, 3785–3796 (2013).

230. van Dommelen, S. L. H., Tabarias, H. A., Smyth, M. J. & Degli-Esposti, M. A. Activation of Natural Killer (NK) T Cells during Murine Cytomegalovirus Infection Enhances the Antiviral Response Mediated by NK Cells. *J. Virol.* **77**, 1877–1884 (2003).

231. Littwitz-Salomon, E., Schimmer, S. & Dittmer, U. Natural killer T cells contribute to the control of acute retroviral infection. *Retrovirology 2017 141* **14**, 1–10 (2017).

232. Nichols, K. E. *et al.* Regulation of NKT cell development by SAP, the protein defective in XLP. *Nat. Med. 2005 113* **11**, 340–345 (2005).

233. Rigaud, S. *et al.* XIAP deficiency in humans causes an X-linked lymphoproliferative syndrome. *Nature* **444**, 110–114 (2006).

234. Waldowska, M., Bojarska-Junak, A. & Roliński, J. A brief review of clinical trials involving manipulation of invariant NKT cells as a promising approach in future cancer therapies. *Central European Journal of Immunology* vol. 42 181–195 (2017).

235. Zhang, Y. *et al.* α-GalCer and iNKT Cell-Based Cancer Immunotherapy: Realizing the Therapeutic Potentials. *Front. Immunol.* **10**, 1126 (2019).

236. Giaccone, G. *et al.* A phase I study of the natural killer T-cell ligand α-galactosylceramide (KRN7000) in patients with solid tumors. *Clin. Cancer Res.* **8**, 3702–3709 (2002).

237. Poels, R. *et al.* Preclinical evaluation of invariant natural killer t cells modified with cd38 or bcma chimeric antigen receptors for multiple myeloma. *Int. J. Mol. Sci.* **22**, 1–16 (2021).

238. Zhu, Y. *et al.* Development of Hematopoietic Stem Cell-Engineered Invariant Natural Killer T Cell Therapy for Cancer. *Cell Stem Cell* **25**, 542-557.e9 (2019).

239. Nakagawa, R. *et al.* Mechanisms of the Antimetastatic Effect in the Liver and of the Hepatocyte Injury Induced by α-Galactosylceramide in Mice. *J. Immunol.* **166**, 6578–6584 (2001).

240. Smyth, M. J. *et al.* Sequential production of interferon-γ by NK1.1+ T cells and natural killer cells is essential for the antimetastatic effect of α-galactosylceramide. *Blood* **99**, 1259–1266 (2002).

241. Paget, C., Chow, M. T., Duret, H., Mattarollo, S. R. & Smyth, M. J. Role of γδ T Cells in α-Galactosylceramide–Mediated Immunity. *J. Immunol.* **188**, 3928–3939 (2012).

242. Hayakawa, Y. *et al.* Critical contribution of IFN-γ and NK cells, but not perforin-mediated cytotoxicity, to anti-metastatic effect of α-galactosylceramide. *Eur. J. Immunol.* **31**, 1720–1727 (2001).

243. Swann, J. B. *et al.* Type I natural killer T cells suppress tumors caused by p53 loss in mice. *Blood* **113**, 6382–6385 (2009).

244. Bellone, M. *et al.* iNKT cells control mouse spontaneous carcinoma independently of tumor-specific cytotoxic T cells. *PLoS One* **5**, e8646 (2010).

245. Moreno, M. *et al.* IFN-γ-Producing Human Invariant NKT Cells Promote Tumor-Associated Antigen-Specific Cytotoxic T Cell Responses. *J. Immunol.* **181**, 2446–2454 (2008).

246. Smyth, M. J. *et al.* Differential tumor surveillance by natural killer (NK) and NKT cells. *J. Exp. Med.* **191**, 661–668 (2000).

247. Cui, J. *et al.* Requirement for V(α)14 NKT cells in IL-12-mediated rejection of tumors. *Science (80-. ).* **278**, 1623–1626 (1997).

248. Kawano, T. *et al.* Natural killer-like nonspecific tumor cell lysis mediated by specific ligand-activated Vα14 NKT cells. *Proc. Natl. Acad. Sci. U. S. A.* **95**, 5690–5693 (1998).

249. Crowe, N. Y., Smyth, M. J. & Godfrey, D. I. A critical role for natural killer T cells in immunosurveillance of methylcholanthrene-induced sarcomas. *J. Exp. Med.* **196**, 119–127 (2002).

250. Shimizu, K., Kurosawa, Y., Taniguchi, M., Steinman, R. M. & Fujii, S. I. Cross-presentation of glycolipid from tumor cells loaded with α-galactosylceramide leads to potent and long-lived T cell-mediated immunity via dendritic cells. *J. Exp. Med.* **204**, 2641–2653 (2007).

251. Ambrosino, E. *et al.* Cross-Regulation between Type I and Type II NKT Cells in Regulating Tumor Immunity: A New Immunoregulatory Axis. *J. Immunol.* **179**, 5126–5136 (2007).

252. Hayakawa, Y., Rovero, S., Forni, G. & Smyth, M. J. α-galactosylceramide (KRN7000) suppression of chemical- and oncogene-dependent carcinogenesis. *Proc. Natl. Acad. Sci. U. S. A.* **100**, 9464–9469 (2003).

253. Fallarini, S., Paoletti, T., Orsi Battaglini, N. & Lombardi, G. Invariant NKT cells increase drug-induced osteosarcoma cell death. *Br. J. Pharmacol.* **167**, 1533–1549 (2012).

254. Nicol, A. *et al.* Human invariant Vα24+ natural killer T cells activated by a-galactosylceramide (KRN7000) have cytotoxic anti-tumour activity through mechanisms distinct from T cells and natural killer cells. *Immunology* **99**, 229–234 (2000).

255. Metelitsa, L. S. *et al.* Human NKT Cells Mediate Antitumor Cytotoxicity Directly by Recognizing Target Cell CD1d with Bound Ligand or Indirectly by Producing IL-2 to Activate NK Cells. *J. Immunol.* **167**, 3114–3122 (2001).

256. Molling, J. W. *et al.* Low levels of circulating invariant natural killer T cells predict poor clinical outcome in patients with head and neck squamous cell carcinoma. *J. Clin. Oncol.* **25**, 862–868 (2007).

257. Najera Chuc, A. E., Cervantes, L. A. M., Retiguin, F. P., Ojeda, J. V. & Maldonado, E. R. Low number of invariant NKT cells is associated with poor survival in acute myeloid leukemia. *J. Cancer Res. Clin. Oncol.* **138**, 1427–1432 (2012).

258. Tachibana, T. *et al.* Increased intratumor Vα24-positive natural killer T cells: A prognostic factor for primary colorectal carcinomas. *Clin. Cancer Res.* **11**, 7322–7327 (2005).

259. Coca, S. *et al.* The prognostic significance of intratumoral natural killer cells in patients with colerectal carcinoma. *Cancer* **79**, 2320–2328 (1997).

260. Moser, A. R. *et al.* ApcMin: A mouse model for intestinal and mammary tumorigenesis. *Eur. J. Cancer* **31**, 1061–1064 (1995).

261. Wang, Y. *et al.* Unique invariant natural killer T cells promote intestinal polyps by suppressing TH1 immunity and promoting regulatory T cells. *Mucosal Immunol. 2018 111* **11**, 131–143 (2017).

262. Wang, Y., Bhave, M. S., Yagita, H. & Cardell, S. L. Natural Killer T-Cell Agonist α-Galactosylceramide and PD-1 Blockade Synergize to Reduce Tumor Development in a Preclinical Model of Colon Cancer. *Front. Immunol.* **0**, 2715 (2020).

263. Tang, B. *et al.* Activation of Glioma Cells Generates Immune Tolerant NKT Cells. *J. Biol. Chem.* **289**, 34595 (2014).

264. Yu, F., Sharma, S., Edwards, J., Feigenbaum, L. & Zhu, J. Dynamic expression of T-bet and GATA3 by regulatory T cells maintains immune tolerance. *Nat. Immunol.* **16**, 197 (2015).

265. Subramanian, A. *et al.* Gene set enrichment analysis: A knowledge-based approach for interpreting genome-wide expression profiles. *Proc. Natl. Acad. Sci. U. S. A.* **102**, 15545–15550 (2005).

266. Tonti, E. *et al.* Follicular Helper NKT Cells Induce Limited B Cell Responses and Germinal Center Formation in the Absence of CD4+ T Cell Help. *J. Immunol.* **188**, 3217 (2012).

267. Coquet, J. M. *et al.* IL-21 Is Produced by NKT Cells and Modulates NKT Cell Activation and Cytokine Production. *J. Immunol.* **178**, 2827–2834 (2007).

268. Crotty, S. T follicular helper cell differentiation, function, and roles in disease. *Immunity* **41**, 529 (2014).

269. King, I. L. *et al.* Invariant natural killer T cells direct B cell responses to cognate lipid antigen in an IL-21-dependent manner. *Nat. Immunol.* **13**, 44–50 (2012).

270. Hong, S. *et al.* The natural killer T-cell ligand alpha-galactosylceramide prevents autoimmune diabetes in non-obese diabetic mice. *Nat. Med.* **7**, 1052–1056 (2001).

271. Sharif, S. *et al.* Activation of natural killer T cells by alpha-galactosylceramide treatment prevents the onset and recurrence of autoimmune Type 1 diabetes. *Nat. Med.* **7**, 1057–1062 (2001).

272. Wang, B., Geng, Y. B. & Wang, C. R. CD1-restricted NK T cells protect nonobese diabetic mice from developing diabetes. *J. Exp. Med.* **194**, 313–319 (2001).

273. Singh, A. K. *et al.* Natural Killer T Cell Activation Protects Mice Against Experimental Autoimmune Encephalomyelitis. *J. Exp. Med.* **194**, 1801–1811 (2001).

274. Jahng, A. W. *et al.* Activation of Natural Killer T Cells Potentiates or Prevents Experimental Autoimmune Encephalomyelitis. **194**, (2001).

275. Miyamoto, K., Miyake, S. & Yamamura, T. A synthetic glycolipid prevents autoimmune encephalomyelitis by inducing TH2 bias of natural killer T cells. *Nature* **413**, 531–534 (2001).

276. Chang, W.-S. *et al.* Cutting Edge: Programmed Death-1/Programmed Death Ligand 1 Interaction Regulates the Induction and Maintenance of Invariant NKT Cell Anergy. *J. Immunol.* **181**, 6707–6710 (2008).

277. Wingender, G., Krebs, P., Beutler, B. & Kronenberg, M. Antigen-specific cytotoxicity by invariant NKT cells in vivo is CD95/CD178-dependent and is correlated with antigenic potency. *J. Immunol.* **185**, 2721–2729 (2010).

278. Braun, N. A. *et al.* Development of spontaneous anergy in invariant natural killer T cells in a mouse model of dyslipidemia. *Arterioscler. Thromb. Vasc. Biol.* **30**, 1758–1765 (2010).

279. Wu, J. *et al.* TSC1 promotes iNKT cell anergy and inhibits iNKT cell-mediated anti-tumor immunity. *J. Immunol.* **192**, 2643 (2014).

280. Kumar, A. *et al.* Nur77 controls tolerance induction, terminal differentiation, and effector functions in semi-invariant natural killer T cells. *Proc. Natl. Acad. Sci.* **117**, 17156–17165 (2020).

281. Darcy, P. W., Denzin, L. K. & Sant'Angelo, D. B. YY1lo NKT cells are dedicated IL-10 producers. *Sci. Reports 2020 101* **10**, 1–15 (2020).

282. Oh, S. J. & Chung, D. H. Invariant NKT cells producing IL-4 or IL-10, but not IFN-gamma, inhibit the Th1 response in experimental autoimmune encephalomyelitis, whereas none of these cells inhibits the Th17 response. *J. Immunol.* **186**, 6815–6821 (2011).

283. Cui, K. *et al.* Suppression of natural killer cell activity by regulatory NKT10 cells aggravates alcoholic hepatosteatosis. *Front. Immunol.* **8**, 1414 (2017).

284. Engelmann, P. *et al.* Characterization of human invariant natural killer T cells expressing FoxP3. *Int. Immunol.* **23**, 473–484 (2011).

285. O'Neill, L. A. J. J., Kishton, R. J. & Rathmell, J. A guide to immunometabolism for immunologists. *Nat. Rev. Immunol.* **16**, 553–565 (2016).

286. Michelet, X. *et al.* Metabolic reprogramming of natural killer cells in obesity limits antitumor responses. *Nat. Immunol.* **19**, 1330–1340 (2018).

287. Keating, S. E. *et al.* Metabolic Reprogramming Supports IFN-γ Production by CD56 bright NK Cells . *J. Immunol.* **196**, 2552–2560 (2016).

288. Loftus, R. M. *et al.* Amino acid-dependent cMyc expression is essential for NK cell metabolic and functional responses in mice. *Nat. Commun.* **9**, 1–15 (2018).

289. Assmann, N. *et al.* Srebp-controlled glucose metabolism is essential for NK cell functional responses. *Nat. Immunol.* **18**, 1197–1206 (2017).

290. Zinser, M. E. *et al.* Human MAIT cells show metabolic quiescence with rapid glucose-dependent upregulation of granzyme B upon stimulation. *Immunol. Cell Biol.* **96**, 666–674 (2018).

291. Finlay, D. K. *et al.* PDK1 regulation of mTOR and hypoxia-inducible factor 1 integrate metabolism and migration of CD8+ T cells. *J. Exp. Med.* **209**, 2441–2453 (2012).

292. Zhang, L. & Romero, P. Metabolic Control of CD8+ T Cell Fate Decisions and Antitumor Immunity. *Trends Mol. Med.* **24**, 30–48 (2018).

293. Weinberg, S. & Chandel, N. S. Futility sustains memory T cells. *Immunity* **41**, 1 (2014).

294. O'Sullivan, D. The metabolic spectrum of memory T cells. *Immunol. Cell Biol.* **97**, 636–646 (2019).

295. Kouidhi, S., Noman, M. Z., Kieda, C., Elgaaied, A. B. & Chouaib, S. Intrinsic and tumor microenvironment-induced metabolism adaptations of

T cells and impact on their differentiation and function. *Front. Immunol.* **7**, (2016).

296. Patsoukis, N. *et al.* PD-1 alters T-cell metabolic reprogramming by inhibiting glycolysis and promoting lipolysis and fatty acid oxidation. *Nat. Commun. 2015 61* **6**, 1–13 (2015).
297. Bengsch, B. *et al.* Bioenergetic insufficiencies due to metabolic alterations regulated by PD-1 are an early driver of CD8+ T cell exhaustion. *Immunity* **45**, 358 (2016).
298. Shin, J. *et al.* Mechanistic target of rapamycin complex 1 is critical for invariant natural killer T-cell development and effector function. *Proc. Natl. Acad. Sci. U. S. A.* **111**, E776-83 (2014).
299. Mycko, M. P. *et al.* Selective Requirement for c-Myc at an Early Stage of Vα14i NKT Cell Development. *J. Immunol.* **182**, 4641–4648 (2009).
300. Finlay, D. K. *et al.* Temporal differences in the dependency on phosphoinositide-dependent kinase 1 distinguish the development of invariant Valpha14 NKT cells and conventional T cells. *J. Immunol.* **185**, 5973–82 (2010).
301. Park, H., Tsang, M., Iritani, B. M. & Bevan, M. J. Metabolic regulator Fnip1 is crucial for iNKT lymphocyte development. *Proc. Natl. Acad. Sci. U. S. A.* **111**, 7066–71 (2014).
302. Raynor, J. L. *et al.* Hippo/Mst signaling coordinates cellular quiescence with terminal maturation in iNKT cell development and fate decisions. *J. Exp. Med.* **217**, (2020).
303. Zhao, M. *et al.* Calcium signals regulate the functional differentiation of thymic iNKT cells. *EMBO J.* **40**, (2021).
304. Kumar, A. *et al.* Enhanced oxidative phosphorylation in NKT cells is essential for their survival and function. *Proc. Natl. Acad. Sci.* **116**, 201901376 (2019).
305. Schieber, M. & Chandel, N. S. ROS function in redox signaling and oxidative stress. *Current Biology* vol. 24 (2014).
306. Khurana, P. *et al.* Distinct Bioenergetic Features of Human Invariant Natural Killer T Cells Enable Retained Functions in Nutrient-Deprived States. *Article* **12**, 1 (2021).

307. Fu, S. *et al.* Impaired lipid biosynthesis hinders anti-tumor efficacy of intratumoral iNKT cells. *Nat. Commun. 2020 111* **11**, 1–15 (2020).

308. Hao, Y. *et al.* Integrated analysis of multimodal single-cell data. *Cell* **184**, 3573-3587.e29 (2021).

309. Hafemeister, C. & Satija, R. Normalization and variance stabilization of single-cell RNA-seq data using regularized negative binomial regression. *Genome Biol.* **20**, 1–15 (2019).

310. McInnes, L., Healy, J. & Melville, J. UMAP: Uniform Manifold Approximation and Projection for Dimension Reduction. *arXiv* (2018).

311. Korsunsky, I. *et al.* Fast, sensitive and accurate integration of single-cell data with Harmony. *Nat. Methods* **16**, 1289–1296 (2019).

312. Korotkevich, G. *et al.* Fast gene set enrichment analysis. *bioRxiv* 060012 (2016) doi:10.1101/060012.

313. Yu, G., Wang, L. G., Han, Y. & He, Q. Y. ClusterProfiler: An R package for comparing biological themes among gene clusters. *Omi. A J. Integr. Biol.* **16**, 284–287 (2012).

314. Kanehisa, M., Furumichi, M., Sato, Y., Ishiguro-Watanabe, M. & Tanabe, M. KEGG: Integrating viruses and cellular organisms. *Nucleic Acids Res.* **49**, D545–D551 (2021).

315. Liberzon, A. *et al.* Molecular signatures database (MSigDB) 3.0. *Bioinformatics* **27**, 1739–1740 (2011).

316. Raudvere, U. *et al.* G:Profiler: A web server for functional enrichment analysis and conversions of gene lists (2019 update). *Nucleic Acids Res.* **47**, W191–W198 (2019).

317. Gu, Z., Eils, R. & Schlesner, M. Complex heatmaps reveal patterns and correlations in multidimensional genomic data. *Bioinformatics* **32**, 2847–2849 (2016).

318. Alquicira-Hernandez, J. & Powell, J. E. Nebulosa recovers single-cell gene expression signals by kernel density estimation. *Bioinformatics* **37**, 2485–2487 (2021).

319. Huynh-Thu, V. A., Irrthum, A., Wehenkel, L. & Geurts, P. Inferring Regulatory Networks from Expression Data Using Tree-Based Methods. *PLoS One* **5**, e12776 (2010).

320. Robinson, M. D., McCarthy, D. J. & Smyth, G. K. edgeR: A Bioconductor package for differential expression analysis of digital gene expression data. *Bioinformatics* **26**, 139–140 (2009).

321. Smyth, G. K. limma: Linear Models for Microarray Data. *Bioinforma. Comput. Biol. Solut. Using R Bioconductor* 397–420 (2005) doi:10.1007/0-387-29362-0_23.

322. Law, C. W., Chen, Y., Shi, W. & Smyth, G. K. Voom: Precision weights unlock linear model analysis tools for RNA-seq read counts. *Genome Biol.* **15**, 1–17 (2014).

323. Smyth, G. K. *et al.* RNA-seq analysis is easy as 1-2-3 with limma, Glimma and edgeR. *F1000Research* **5**, 1408 (2018).

324. Tirosh, I. *et al.* Dissecting the multicellular ecosystem of metastatic melanoma by single-cell RNA-seq. *Science* **352**, 189–196 (2016).

325. Blondel, V. D., Guillaume, J. L., Lambiotte, R. & Lefebvre, E. Fast unfolding of communities in large networks. *J. Stat. Mech. Theory Exp.* **2008**, P10008 (2008).

326. Love, M. I., Huber, W. & Anders, S. Moderated estimation of fold change and dispersion for RNA-seq data with DESeq2. *Genome Biol.* **15**, (2014).

327. Gillespie, M. *et al.* The reactome pathway knowledgebase 2022. *Nucleic Acids Res.* **50**, D687–D692 (2022).

328. Krovi, S. H. & Gapin, L. Invariant Natural Killer T Cell Subsets—More Than Just Developmental Intermediates. *Front. Immunol.* **9**, (2018).

329. Ricardo Miragaia, A. J. *et al.* Single-Cell Transcriptomics of Regulatory T Cells Reveals Trajectories of Tissue Adaptation. (2019) doi:10.1016/j.immuni.2019.01.001.

330. D'Cruz, L. M., Stradner, M. H., Yang, C. Y. & Goldrath, A. W. E and Id Proteins Influence Invariant NKT Cell Sublineage Differentiation and Proliferation. *J. Immunol.* **192**, 2227–2236 (2014).

331. Papac-Milicevic, N. *et al.* The interferon stimulated gene 12 inactivates vasculoprotective functions of NR4A nuclear receptors. *Circ. Res.* **110**, (2012).

332. Drujont, L. *et al.* RORγt + cells selectively express redundant cation channels linked to the Golgi apparatus. *Sci. Rep.* **6**, 1–13 (2016).

333. Millward, J. M., Løbner, M., Wheeler, R. D. & Owens, T. Inflammation in the Central Nervous System and Th17 Responses Are Inhibited by IFN-γ–Induced IL-18 Binding Protein. *J. Immunol.* **185**, 2458–2466 (2010).

334. Harrison, O. J. *et al.* Epithelial-derived IL-18 regulates Th17 cell differentiation and Foxp3+ Treg cell function in the intestine. *Mucosal Immunol.* **8**, 1226–1236 (2015).

335. Christiaansen, A. F. *et al.* CD11a and CD49d enhance the detection of antigen-specific T cells following human vaccination. *Vaccine* **35**, 4255–4261 (2017).

336. Grau, M. *et al.* Antigen-Induced but Not Innate Memory CD8 T Cells Express NKG2D and Are Recruited to the Lung Parenchyma upon Viral Infection. *J. Immunol.* **200**, 3635–3646 (2018).

337. Pereira, B. I. *et al.* Sestrins induce natural killer function in senescent-like CD8+ T cells. *Nat. Immunol.* **21**, 684–694 (2020).

338. Covre, L. P., De Maeyer, R. P. H., Gomes, D. C. O. & Akbar, A. N. The role of senescent T cells in immunopathology. *Aging Cell* vol. 19 (2020).

339. Sano, R. & Reed, J. C. ER stress-induced cell death mechanisms. *Biochimica et Biophysica Acta - Molecular Cell Research* vol. 1833 3460–3470 (2013).

340. Stradner, M. H., Cheung, K. P., Lasorella, A., Goldrath, A. W. & D'Cruz, L. M. Id2 regulates hyporesponsive invariant natural killer T cells. *Immunol. Cell Biol.* **94**, 640–645 (2016).

341. Stephen, T. L. *et al.* SATB1 Expression Governs Epigenetic Repression of PD-1 in Tumor-Reactive T Cells. *Immunity* **46**, 51–64 (2017).

342. Jennings, E. *et al.* Nr4a1 and Nr4a3 Reporter Mice Are Differentially Sensitive to T Cell Receptor Signal Strength and Duration. *Cell Rep.* **33**, (2020).

343. Miyagawa, F. *et al.* Interferon regulatory factor 8 integrates T-cell receptor and cytokine-signaling pathways and drives effector differentiation of CD8 T cells. *Proc. Natl. Acad. Sci. U. S. A.* **109**, 12123–12128 (2012).

344. Long, X., Lin, Y., Ortiz-Vega, S., Yonezawa, K. & Avruch, J. Rheb binds and regulates the mTOR kinase. *Curr. Biol.* **15**, 702–713 (2005).

345. Carbon, S. *et al.* The Gene Ontology resource: Enriching a GOld mine. *Nucleic Acids Res.* **49**, D325–D334 (2021).

346. Lochner, M., Berod, L. & Sparwasser, T. Fatty acid metabolism in the regulation of T cell function. *Trends in Immunology* vol. 36 81–91 (2015).

347. Hong, J. W. & Wu, L. C. ZAS3 represses NFκB-dependent transcription by direct competition for DNA binding. *BMB Rep.* **43**, 807–812 (2010).

348. Stopfer, P., Männel, D. N. & Hehlgans, T. Lymphotoxin-β Receptor Activation by Activated T Cells Induces Cytokine Release from Mouse Bone Marrow-Derived Mast Cells. *J. Immunol.* **172**, 7459–7465 (2004).

349. Omilusik, K. D. *et al.* Transcriptional repressor ZEB2 promotes terminal differentiation of CD8+ effector and memory T cell populations during infection. *J. Exp. Med.* **212**, 2027–2039 (2015).

350. Yang, S., Liu, F., Wang, Q. J., Rosenberg, S. A. & Morgan, R. A. The shedding of CD62L (L-selectin) regulates the acquisition of lytic activity in human tumor reactive T lymphocytes. *PLoS One* **6**, 22560 (2011).

351. Stankovic, S. *et al.* Distinct roles in NKT cell maturation and function for the different transcription factors in the classical NF-κB pathway. *Immunol. Cell Biol.* **89**, 294–303 (2011).

352. Brennan, P. J., Brigl, M. & Brenner, M. B. Invariant natural killer T cells: an innate activation scheme linked to diverse effector functions. *Nat. Rev. Immunol.* **13**, 101–117 (2013).

353. Lee, J., Hyeon, D. Y. & Hwang, D. Single-cell multiomics: technologies and data analysis methods. *Experimental and Molecular Medicine* vol. 52 1428–1442 (2020).

354. Adams, N. M., Grassmann, S. & Sun, J. C. Clonal expansion of innate and adaptive lymphocytes. *Nature Reviews Immunology* vol. 20 694–707 (2020).

355. Geissmann, F. *et al.* Intravascular immune surveillance by CXCR6+ NKT cells patrolling liver sinusoids. *PLoS Biol.* **3**, 0650–0661 (2005).

356. Velázquez, P. *et al.* Cutting Edge: Activation by Innate Cytokines or Microbial Antigens Can Cause Arrest of Natural Killer T Cell Patrolling of Liver Sinusoids. *J. Immunol.* **180**, 2024–2028 (2008).

357. Lee, W. Y. *et al.* An intravascular immune response to Borrelia burgdorferi involves Kupffer cells and iNKT cells. *Nat. Immunol.* **11**, 295–302 (2010).

358. Alfen, J. S. *et al.* Intestinal IFN-γ–producing type 1 regulatory T cells coexpress CCR5 and programmed cell death protein 1 and downregulate IL-10 in the inflamed guts of patients with inflammatory bowel disease. *J. Allergy Clin. Immunol.* **142**, 1537-1547.e8 (2018).

359. Grossman, W. J. *et al.* Differential expression of granzymes A and B in human cytotoxic lymphocyte subsets and T regulatory cells. *Blood* **104**, 2840–2848 (2004).

360. Karwacz, K. *et al.* Critical role of IRF1 and BATF in forming chromatin landscape during type 1 regulatory cell differentiation. *Nat. Immunol.* **18**, 412–421 (2017).

361. Apetoh, L. *et al.* The aryl hydrocarbon receptor interacts with c-Maf to promote the differentiation of type 1 regulatory T cells induced by IL-27. *Nat. Immunol.* **11**, 854–861 (2010).

362. Gruarin, P. *et al.* Eomesodermin controls a unique differentiation program in human IL-10 and IFN-γ coproducing regulatory T cells. *Eur. J. Immunol.* **49**, 96–111 (2019).

363. Mascanfroni, I. D. *et al.* Metabolic control of type 1 regulatory (Tr1) cell differentiation by AHR and HIF1-α. *Nat. Med.* **21**, 638 (2015).

364. Yan, H. *et al.* Primary Tr1 cells from metastatic melanoma eliminate tumor-promoting macrophages through granzyme B- and perforin-dependent mechanisms. *Tumor Biol.* **39**, (2017).

365. Chihara, N., Madi, A., Karwacz, K., Awasthi, A. & Kuchroo, V. K. Differentiation and characterization of Tr1 cells. *Curr. Protoc. Immunol.* **2016**, 3.27.1-3.27.10 (2016).

366. Wu, Y., Tao, B., Zhang, T., Fan, Y. & Mao, R. Pan-cancer analysis reveals disrupted circadian clock associates with t cell exhaustion. *Front. Immunol.* **10**, 2451 (2019).

367. Andris, F. *et al.* The transcription factor c-Maf promotes the differentiation of follicular helper T cells. *Front. Immunol.* **8**, (2017).

368. Xu, W. *et al.* The Transcription Factor Tox2 Drives T Follicular Helper Cell Development via Regulating Chromatin Accessibility. *Immunity* **51**, 826-839.e5 (2019).

369. Evrard, M. *et al.* Sphingosine 1-phosphate receptor 5 (S1PR5) regulates the peripheral retention of tissue-resident lymphocytes. *J. Exp. Med.* **219**, (2021).

370. Liu, M. *et al.* Transcription factor c-Maf is essential for IL-10 gene expression in B cells. *Scand. J. Immunol.* **88**, (2018).

371. Cao, S., Liu, J., Song, L. & Ma, X. The Protooncogene c-Maf Is an Essential Transcription Factor for IL-10 Gene Expression in Macrophages. *J. Immunol.* **174**, 3484 (2005).

372. Ephrem, A. *et al.* Modulation of Treg cells/T effector function by GITR signaling is context-dependent. *Eur. J. Immunol.* **43**, 2421–2429 (2013).

373. Jankowska, K. I. *et al.* Integrins modulate T cell receptor signaling by constraining actin flow at the immunological synapse. *Front. Immunol.* **9**, 25 (2018).

374. Berger, M. *et al.* An Slfn2 mutation causes lymphoid and myeloid immunodeficiency due to loss of immune cell quiescence. *Nat. Immunol. 2010 114* **11**, 335–343 (2010).

375. ElTanbouly, M. A. *et al.* VISTA is a checkpoint regulator for naïve T cell quiescence and peripheral tolerance. *Science (80-. ).* **367**, (2020).

376. Chen, H. & Paul, W. E. Cultured NK1.1+ CD4+ T cells produce large amounts of IL-4 and IFN-gamma upon activation by anti-CD3 or CD1. *J. Immunol.* **159**, 2240–9 (1997).

377. Martinez, G. J. *et al.* The Transcription Factor NFAT Promotes Exhaustion of Activated CD8+ T Cells. *Immunity* **42**, 265–278 (2015).

378. Galletti, G. *et al.* Two subsets of stem-like CD8+ memory T cell progenitors with distinct fate commitments in humans. *Nat. Immunol.* **21**, 1552–1562 (2020).

379. Choi, J., Mele, T. S., Porcelli, S. A., Savage, P. B. & Haeryfar, S. M. M. Harnessing the Versatility of Invariant NKT Cells in a Stepwise Approach to Sepsis Immunotherapy. *J. Immunol.* **206**, 386–397 (2021).

380. Motomura, Y. *et al.* The transcription factor E4BP4 regulates the production of IL-10 and IL-13 in CD4+ T cells. *Nat. Immunol.* **12**, 450–459 (2011).

381. Kim, T. H., Zhou, X. & Chen, M. Demystifying ‘drop-outs’ in single-cell UMI data. *Genome Biol.* **21**, 1–19 (2020).

382. Wang, X., He, Y., Zhang, Q., Ren, X. & Zhang, Z. Direct Comparative Analyses of 10X Genomics Chromium and Smart-seq2. *Genomics, Proteomics Bioinforma.* **19**, 253–266 (2021).

383. Kane, H., LaMarche, N. M., Scannail, Á. N., Brenner, M. B. & Lynch, L. Longitudinal analysis of invariant natural killer T cell activation reveals a cMAF-associated transcriptional state of NKT10 cells. *bioRxiv* 2021.12.29.474454 (2021) doi:10.1101/2021.12.29.474454.